Supramolecular biomaterials in action

Please check the document version of this publication:

• A submitted manuscript is the version of the article upon submission and before peer-review. There can be important differences between the submitted version and the official published version of record. People interested in the research are advised to contact the author for the final version of the publication, or visit the DOI to the publisher's website.
• The final author version and the galley proof are versions of the publication after peer review.
• The final published version features the final layout of the paper including the volume, issue and page numbers.

Link to publication

Supramolecular Biomaterials in Action
Bioactivation through Surface Modifications

Supramolecular Biomaterials in Action

Olga Goor

Olga Goor

Uitnodiging

tot het bijwonen van de openbare verdediging van mijn proefschrift

Supramolecular Biomaterials in Action

Bioactivation through Surface Modifications

op dinsdag 19 september 2017 om 16:00 uur in de Senaatszaal in het Auditorium van de Technische Universiteit Eindhoven

Olga Goor
o.j.g.m.goor@tue.nl

ICMS Animation Studio, TU/e, 2017

Supramolecular Biomaterials in Action
Bioactivation through surface modifications

PROEFSCHRIFT

ter verkrijging van de graad van doctor aan de Technische Universiteit Eindhoven, op gezag van de rector magnificus prof.dr.ir. F.P.T. Baaijens, voor een commissie aangewezen door het College voor Promoties, in het openbaar te verdedigen op dinsdag 19 september 2017 om 16:00 uur

door

Olga Joseph Gertrudis Maria Goor

geboren te Geleen

Dit proefschrift is goedgekeurd door de promotoren en de samenstelling van de promotiecommissie is als volgt:

voorzitter: prof.dr. P.A.J. Hilbers
1^e promotor: prof.dr. E.W. Meijer
copromotor: dr.dr. P.Y.W. Dankers
leden: prof.dr. B.J. Ravoo (Universität Münster)
                     prof.dr. R.M.A. Heeren (Maastricht University)
                     prof.dr. P. Habibović (Maastricht University)
                     prof.dr. C.V.C. Bouten
adviseur(s):   prof.dr.ir. J.C.M van Hest

Het onderzoek of ontwerp dat in dit proefschrift wordt beschreven is uitgevoerd in overeenstemming met de TU/e Gedragscode Wetenschapsbeoefening.

Table of Contents

CHAPTER 1

The importance of surface functionalization of supramolecular biomaterials

1.1 Introduction

The advancement of biomaterials can greatly contribute to the multidisciplinary field of regenerative medicine. Biomaterials can be applied as scaffolds or delivery depots in a variety of biomedical applications and therapies. New generation biomaterials are developed that are well-defined and highly controlled, both in terms of their chemical composition as well as their performance. To date, biomaterials have found multiple applications in the fields of tissue engineering and regenerative medicine, ranging from dental implants to vascular grafts, stents and contact lenses. In general, it is the material surface which dictates the biological reaction *in vivo*. A cascade of reactions takes place upon implantation, where first proteins from the blood adsorb to the surface, followed by cell interrogation. Subsequently, these cells release biochemical factors and upon tissue formation ECM is produced whereby the biomaterial is encapsulated and isolated, or degraded and resolved in case of degradable materials. Ideally, the biomaterial instructs the *in vivo* environment to induce regeneration and the material degrades in time without the formation of scar tissue or fibrous tissue. Although many materials have been developed in order to meet all the properties as they are present in the highly ordered, dynamic and organized *in vivo* environment, no material is yet able to meet all of these characteristics. [1] Therefore, a challenge in the development of new generation biomaterials that find their application in the field of regenerative medicine, is to introduce structural and functional properties into these materials that closely mimic the natural environment. In order to meet these requirements, supramolecular biomaterials are envisioned to be suitable. [2]

1.2 Supramolecular polymers

Supramolecular chemistry, which is defined as the chemistry beyond the covalent bond, deals with molecular building blocks that are held together *via* non-covalent interactions, i.e. hydrogen bonds, electrostatic interactions, van der Waals interactions, host-guest assemblies and π-π stacking. [3,4] *Via* these secondary interactions, a multitude of complex structures with varying functions can be assembled. Due to the reversibility of the supramolecular interactions, these systems are inherently dynamic and to some extent show similarity with living systems found in nature. [5] Many natural systems are comprised of supramolecular components that *via* association and dissociation are engaged in a specific function and are able to respond to environmental changes (i.e. temperature and pH).

Supramolecular polymers can be formed by an array of non-covalently interacting building blocks using highly-directional interactions, which provides them with polymeric properties both in solution and in the solid state, yet with a dynamic character. [6] These types of supramolecular polymers hold promise as a class of novel biomaterials that can be applied in the field of tissue engineering and regenerative medicine, especially due to the controllable material properties in a dynamic, tunable and reversible way. [2]

A multitude of materials have been developed with a varying degree of dynamics, ranging

from soluble assemblies that are highly dynamic, *via* hydrogels with tunable yet less dynamic assembly kinetics to more robust solid-like materials that possess rather slow assembly kinetics. Structural parameters in the design and synthesis of functional supramolecular polymers for biomedical applications involve non-covalent interactions and topological structures. The non-covalent interactions greatly determine the secondary structure that is adapted by the supramolecular polymer. Moreover, as a result of the association constant and the concentration of the non-covalent interactions, the final structure and related function of the aggregates is determined. Topological structures depend on the degree of functionalization of the building blocks and thereby determine greatly the macroscopic performance of the supramolecular material. Additionally, it is important to control the degree of dynamics in these supramolecular ensembles. Particularly, the dynamics that are allowed in the design of robust solid-like supramolecular materials are rather low to ensure desired material properties. Although these classes of materials are highly promising and have shown applicability already in many areas, a major challenge in the formulation of supramolecular biomaterials is to provide both control over surface composition and surface functionality.

1.3 Supramolecular thermoplastic elastomers

Thermoplastic elastomers are a class of materials that are composed of both hard and soft segments. Phase separation between the hard and soft segments in thermoplastic elastomers can result in many different types of morphologies, i.e. nanofibers and rod-like assemblies. When the hard segments are monodisperse and well-defined, nano-scale fibers are formed, which have mechanical properties that are superior compared to less well defined analogues. Phase separation behavior is long known in block copolymers where the blocks are mutually immiscible. When introducing hydrogen bonding motifs to telechelic oligomers block copolymer mimics are obtained in which the hydrogen bonding end motifs phase separate from the bulk oligomers. Moreover, the strength of the hydrogen bonding motif has an influence on the mechanical properties of the telechelic supramolecular polymers.

Phase separation of telechelic supramolecular polymers with hydrogen bonding end groups can be induced by the introduction of additional lateral interactions, i.e. based on ureido-pyrimidinone motifs (UPy). Functionalization telechelic poly(ethylene butylene) with the UPy motif results in supramolecular polymers which display an increase in macroscopic properties yielding a supramolecular thermoplastic elastomer. [7] Supramolecular thermoplastic elastomers are noncovalent analogues of block copolymers, composed of high molecular weight, low polarity segments (soft blocks) and low molecular weight, high polarity segments (hard blocks). The hard segments are composed of self-assembling motifs that are able to form (semi)-crystalline domains upon assembly, resulting in phase separation and endowing thermoplastic material properties. [8]

Above the glass transition temperature, a temperature increase leads to dissociation of the noncovalent interactions and thus disassembly, resulting in a reduced viscosity and mechanical strength, which allows for ease in processability of the materials. Supramolecular

thermoplastic elastomeric materials make use of the reversible interactions in the main chain of the polymer and thereby the mechanical properties are a direct result of these secondary interactions. Thermal properties such as glass transition temperature and melt temperature determine macroscopic properties of supramolecular thermoplastic elastomers. Mobility of hydrogen bonds is limited when the glass transition temperature is above room temperature, which hinders the rearrangement of hydrogen bonds and thereby limits the self-healing capacity of the materials. On the other hand, a glass transition temperature or a melt temperature above room temperature improves the mechanical properties of the materials since the hydrogen bonds act as crosslinks. When designing biomaterials for regenerative medicine applications, these material properties should be taken into account. Thermoplastic elastomers with glass transition temperatures well above 37 °C would ideally facilitate mechanical support at the site of implantation.

1.4 Ureido-pyrimidinone (UPy) based supramolecular thermoplastic biomaterials

The reversible nature of the supramolecular self-complementary quadruple hydrogen bonding UPy motif allows for the development of supramolecular thermoplastic elastomer materials. The UPy moiety contemplates a modular character and thereby enables responsive material properties. Depending on the dynamics of the reversible hydrogen bonds determined by the polymers that are applied, different supramolecular materials can be obtained, i.e. supramolecular hydrogels, supramolecular thermoplastic elastomers and supramolecular nanoparticles. The supramolecular materials that are described in this thesis are based on the solid, elastic materials that exhibit excellent properties in bulk and are easy to process as a result of the low melt viscosity. Regardless of the reversible nature, these materials show mechanical properties similar to conventional macromolecules. By using the UPy-UPy interactions in a modular approach, it has already been shown that these materials can be bioactivated by the incorporation of UPy-biomolecules, thereby creating supramolecular thermoplastic elastomeric biomaterial. [9] The incorporation of UPy-modified peptides into a UPy-polymer scaffold has been reported, *via* a multi-step noncovalent synthesis method, whereby the UPy-peptides are simply mixed with the UPy-polymer and then processed into material films exhibiting bioactive properties. This modular approach holds great promise in the development of biomaterials for a variety of applications, since the bioactive modules (i.e. peptides mimics for proteins and growth factors) can be synthesized and coupled to a UPy-moiety prior to incorporation into the UPy-polymer materials. Moreover, the material formulation of the scaffold can be tuned into different morphologies, i.e. spin coated films, drop cast films and electrospun meshes, depending on the processing method.

The modular concept has been demonstrated by the mixing of UPy-functionalized oligocaprolactones (UPy-PCL) with UPy-modified cell adhesion promotion Gly-Arg-Gly-Asp-Ser (UPy-GRGDS) and synergistic Pro-His-Ser-Arg-Asn (UPy-PHSRN) peptide sequences. *In vitro* results showed strong and specific cell binding of fibroblasts to the bioactivated supramolecular materials, containing both the UPy-GRGDS and UPy-PHSRN. Strikingly, the

bioactive materials containing the UPy-peptides demonstrated *in vivo* the formation of single giant cells at the interface between the bioactive material and tissue. [9]

In the advance of the supramolecular materials based on the modular approach, applications in renal regenerative medicine, [10–13] cardiovascular tissue engineering [14–16] field and drug delivery applications [17–19] were explored. The development of a supramolecular bilayered scaffold with tailorable properties has been reported (Figure 1.1 B). By a mix and match approach, UPy-PCL and UPy-modified poly(ethylene glycol) (UPy-PEG) polymers were mixed and processed into electrospun fibers (Figure 1.1 A,C). The UPy-PEG resulted in anti-fouling behavior of the materials, thereby preventing cell attachment and spreading. Upon the introduction of 4 mol% UPy-RGD bioactive peptide (Figure 1.1 A), surfaces that were initially anti-fouling could be reactivated and cell attachment as well as cell spreading were observed. [12] Supramolecular biomaterials based on the UPy-motif showed great potential in a variety of applications as a result of the reversible supramolecular interactions, the modular character of the materials and the tunability of the bioactivity that can be incorporated.
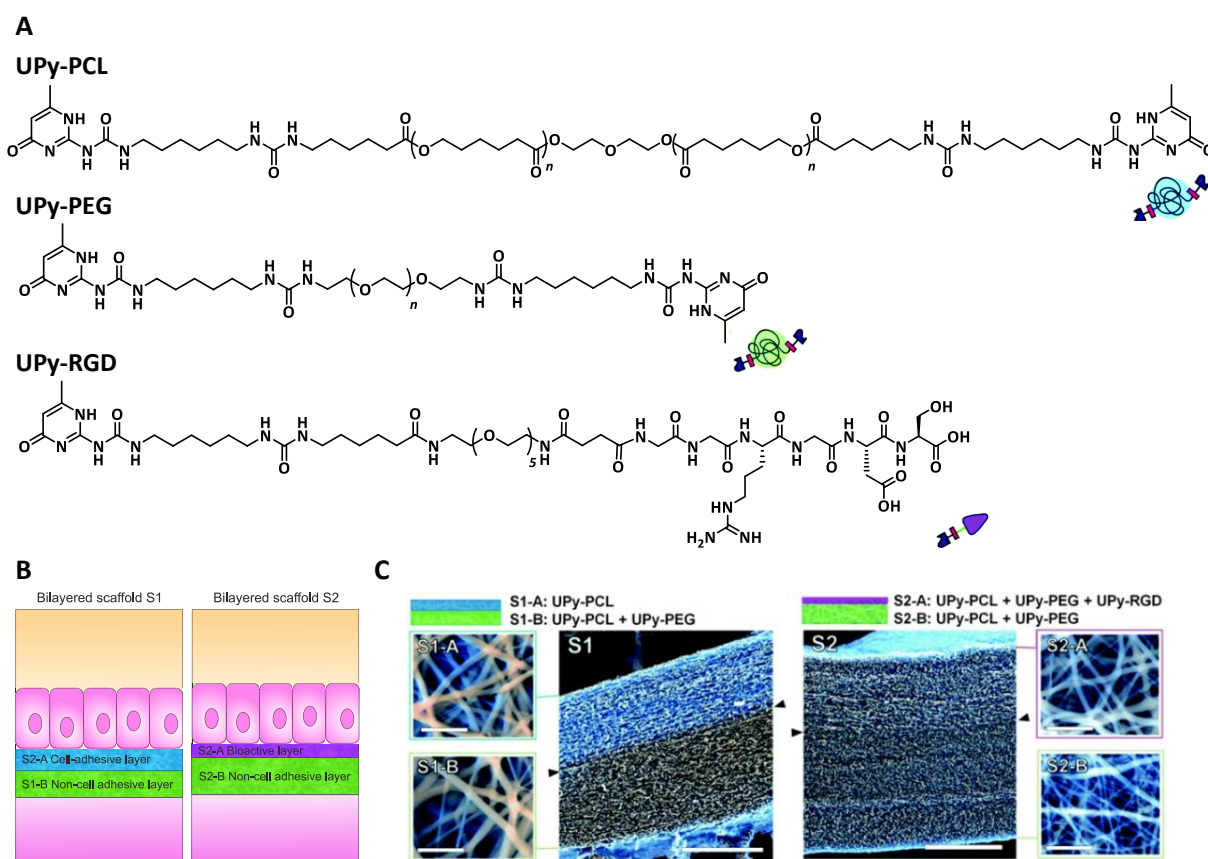
Figure 1.1. Supramolecular bilayered scaffolds with tailorable properties, A) Chemical structures of the building blocks in this study, UPy-PCL (M_n = 2 kg·mol^{-1}), UPy-PEG (M_n = 2 kg·mol^{-1}) and UPy-RGD bioactive peptide, B) Schematic representation of the bilayered scaffolds S1 and S2 that are electrospun using the different building blocks, where top layer A should facilitate cell adhesion and bottom layer B should prevent cell adhesion and C) SEM micrographs of the electrospun bilayered scaffolds S1 and S2, in the cross-section of the scaffolds the layer transition is indicated by the arrows (scale bars represent 200 μm). Top and bottom views show fiber diameters and pore sizes of the scaffolds (scale bars represent 5 μm), average fiber diameters ± standard deviation: S1-A: 576 ± 215 nm, S1-B: 636 ± 359 nm, S2-A: 428 ± 226 nm, S2-B: 283 ± 139. Adapted and reprinted from [[12]], published by the Royal Society for Chemistry.

1.5 Aim and outline of this thesis

Control of material functionalization *via* additives is important to fully control the materials properties and function. In the development of biomaterials, the surface functionality that is required is frequently provided by complex bioactive modules, which in general are highly incompatible with the material processing conditions. It would therefore be of great interest to investigate the concept of decoupling the material processing strategies and the functionalization strategies of the surface. This would offer flexibility in the choice of processing method and at the same time allows for exclusive surface modification.

As a result of the modular character to introduce functionality and the broad scope of processing possibilities, supramolecular thermoplastic elastomers define a class of biomaterials with high potential. Depending on the application, the material characteristics and behavior can be tuned based on the molecular building blocks. In future biomaterials, the modular combination of different supramolecular building blocks might result in the introduction of specific bioactivity, while at the same time anti-fouling properties at the surface can be guaranteed and bulk material properties are retained.

The research question that covers the work described in this thesis is based on how these UPy-additives can be designed and applied in order to activate supramolecular biomaterials *via* post-modification. Three different approaches are investigated:

- Based on natural interaction *via* heparin chemistry
- Host-guest chemistry based on cucurbit[8]uril
- Covalent chemistry *via* inverse electron demand Diels-Alder cycloaddition

Four different approaches based on UPy-additives to facilitate surface modifications that cover a broad scope of dynamics, ranging from truly supramolecular systems to the introduction of selective covalent modifications are disclosed. Systems based on UPy-peptide incorporation (Figure 1.2 A, Scheme 1.1 A), heparin chemistry (Figure 1.2 B, Scheme 1.1 B), supramolecular assembly *via* cucurbit[8]uril complexation (Figure 1.2 C, Scheme 1.1 C) and covalent click chemistry (Figure 1.2 D, Scheme 1.1 D) are investigated.

Supramolecular systems based on UPy-additives
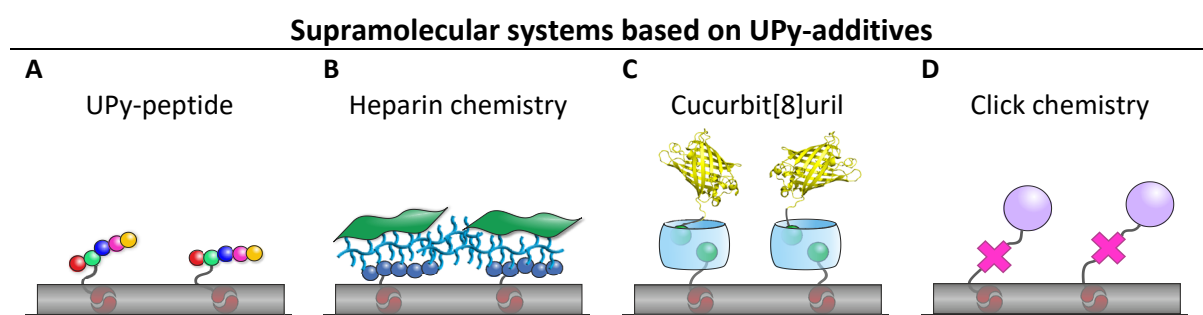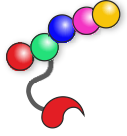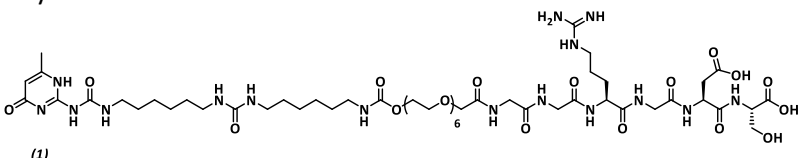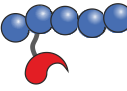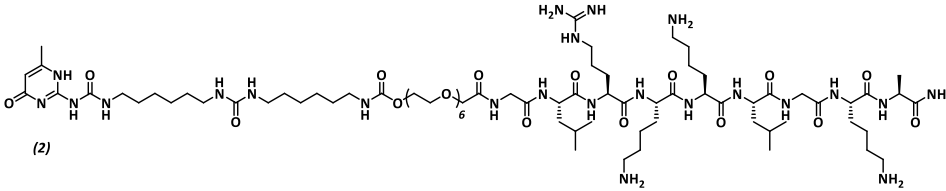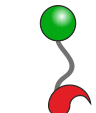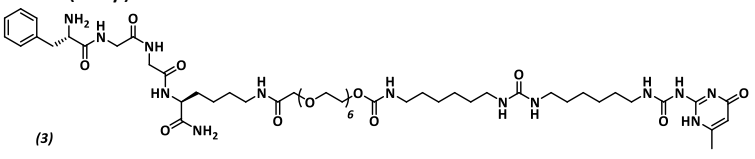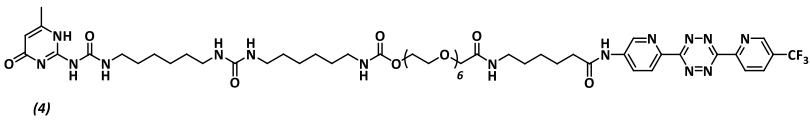
Figure 1.2. Surface functionalization approaches established on supramolecular UPy-based materials using UPy-additives, A) Modular incorporation of UPy-functionalized peptides, B) Protein immobilization based on heparin complexation onto UPy-functionalized heparin binding peptides, C) Supramolecular ternary complex formation based on cucurbit[8]uril chemistry and D) Covalent surface functionalization *via* click chemistry.

Table 1.1. Overview of the supramolecular UPy-additives that are explored in different systems, A) The UPy-peptide approach exemplified by a UPy-GGRGDS (**1**) additive, B) Heparin chemistry approach, *via* UPy-heparin binding peptide (**2**) additive incorporation, C) Cucurbit[8]uril approach using an FGGK(UPy) (**3**) additive and D) Click chemistry approach *via* a reactive UPy-Tetrazine (**4**) additive.

	UPy Additive design	
A	UPy-peptide	UPy-GGRGDS *(1)*
B	Heparin chemistry	UPy-Heparin binding peptide *(2)*
C	Cucurbit[8]uril chemistry	FGGK(UPy) *(3)*
D	Click chemistry	UPy-Tetrazine *(4)*

Chapter 2 provides a comprehensive overview of the scientific background in the field of supramolecular biomaterials. Recent strategies that have been reported to generate bioactive supramolecular materials as well as different strategies to functionalize the surface of these materials to introduce desirable characteristics are highlighted. Moreover, various solid supramolecular polymeric materials and respective characterization strategies of the material surfaces are discussed.

The synthesis of UPy-modified peptides as bioactive additives that can be incorporated into UPy-based supramolecular polymer materials is described in **Chapter 3**. As a proof-of-concept study the bioactivation of supramolecular biomaterials *via* heparin chemistry is demonstrated. To this end, UPy-functionalized heparin binding peptides are incorporated into the materials and subsequently the materials are modified with heparin and complexation is confirmed using fluorescence spectroscopy. Upon TGF-β3 complexation, the endothelial to mesenchymal transition of mouse embryonic endothelial cells is monitored and evaluated based on morphology as well as gene expression levels.

Chapter 4 introduces a more complex supramolecular material modification strategy, where the surface functionalization is introduced *via* supramolecular host-guest complexation of a cucurbit[8]uril (Q8) assembly at the polymer material interface. The ability of Q8 to simultaneously host two N-terminal phenylalanine guests in its cavity is used to synthesize an FGG-modified UPy-peptide (FGGK(UPy)) that can modularly be incorporated into the supramolecular UPy-based polymer. Yellow fluorescent protein with an N-terminal FGG-motif is expressed to facilitate Q8-mediated surface immobilization. Ternary complex formation is confirmed by MALDI-ToF MS, fluorescent spectroscopy and quartz crystal microbalance with dissipation monitoring (QCM-D) measurements.

In **Chapter 5** a new approach based on covalent surface modification is introduced. The ultrafast inverse electron demand Diels-Alder (iEDDA) cycloaddition based on tetrazine and *trans*-cyclooctene (TCO) is employed to functionalize the supramolecular UPy-based materials both with small molecules and proteins. A UPy-modified tetrazine (UPy-Tz) with a CF_3 group is synthesized and modularly incorporated into the supramolecular material. Additionally, a small TCO molecule with an iodine atom is synthesized. Both the fluorine and the iodine enable detection with X-ray photoelectron spectroscopy (XPS) and time-of-flight secondary ion mass spectrometry (ToF-SIMS) to confirm whether the cycloaddition occurs at the supramolecular material surface.

The system that is analyzed in Chapter 5 is utilized in **Chapter 6** to introduce an anti-fouling coating at the surface of these materials. Bicyclononyne (BCN) functionalized poly(ethylene glycol) (PEG) polymers are synthesized to modify the supramolecular polymer material, in which a UPy-Tz additive is incorporated, specifically at the surface. QCM-D studies reveal protein adhesion resistance of the modified surfaces. Additionally, cell adhesion can be assessed to investigate the ability of the functionalized materials to prevent cellular adhesion. Moreover, from a fundamental point of view, the influence of the molecular design of UPy-modified additives is investigated. UPy-Tz moieties with different hydrophilic spacers are designed and synthesized and modularly incorporated into the supramolecular polymer materials. The surface morphology is assessed by atomic force microscopy (AFM) and the surface composition is investigated using XPS. Solid state UV-Vis measurements are performed in order to relate the molecular design of the UPy-Tz additives to its reactivity at the supramolecular material surface.

The **epilogue** discusses how to develop supramolecular polymers into advanced biomaterials. Challenges that come along and design criteria in the synthesis and development of these materials for future regenerative medicine applications are addressed.

1.6 References

1. Bouten, C. V. C. *et al.* Substrates for cardiovascular tissue engineering. *Adv. Drug Deliv. Rev.* **63,** 221–241 (2011).
2. Webber, M. J., Appel, E. A., Meijer, E. W. & Langer, R. Supramolecular biomaterials. *Nat. Mater.* **15,** 13–26 (2016).
3. Lehn, J.M. in *Supramolecular Chemistry* 1–9 (Wiley-VCH Verlag GmbH & Co. KGaA, 1995).
4. Lehn, J.M. From supramolecular chemistry towards constitutional dynamic chemistry and adaptive chemistry. *Chem. Soc. Rev.* **36,** 151–160 (2007).
5. Epstein, R. J. *Human Molecular Biology: An Introduction to the Molecular Basis of Health and Disease.* (Cambridge University Press, 2003).
6. Brunsveld, L., Folmer, B. J., Meijer, E. W. & Sijbesma, R. P. Supramolecular polymers. *Chem. Rev.* **101,** 4071–4098 (2001).
7. Folmer, B. J. B., Sijbesma, R. P., Versteegen, R. M., van der Rijt, J. a. J. & Meijer, E. W. Supramolecular Polymer Materials: Chain Extension of Telechelic Polymers Using a Reactive Hydrogen-Bonding Synthon. *Adv. Mater.* **12,** 874–878 (2000).
8. Houton, K. A. & Wilson, A. J. Hydrogen-bonded supramolecular polyurethanes. *Polym. Int.* **64,** 165–173 (2015).
9. Dankers, P. Y. W., Harmsen, M. C., Brouwer, L. A., Van Luyn, M. J. A. & Meijer, E. W. A modular and supramolecular approach to bioactive scaffolds for tissue engineering. *Nat. Mater.* **4,** 568–574 (2005).
10. Dankers, P. Y. W. *et al.* The Use of Fibrous, Supramolecular Membranes and Human Tubular Cells for Renal Epithelial Tissue Engineering: Towards a Suitable Membrane for a Bioartificial Kidney. *Macromol. Biosci.* **10,** 1345–1354 (2010).
11. Dankers, P. Y. W. *et al.* Bioengineering of living renal membranes consisting of hierarchical, bioactive supramolecular meshes and human tubular cells. *Biomaterials* **32,** 723–733 (2011).
12. Mollet, B. B. *et al.* A modular approach to easily processable supramolecular bilayered scaffolds with tailorable properties. *J. Mater. Chem. B* **2,** 2483–2493 (2014).
13. Mollet, B. B., Bogaerts, I. L. J., van Almen, G. C. & Dankers, P. Y. W. A bioartificial environment for kidney epithelial cells based on a supramolecular polymer basement membrane mimic and an organotypical culture system. *J. Tissue Eng. Regen. Med.* **11,** 1820-1834 (2017).
14. Muylaert, D. E., Fledderus, J. O., Bouten, C. V., Dankers, P. Y. & Verhaar, M. C. Combining tissue repair and tissue engineering; bioactivating implantable cell-free vascular scaffolds. *Heart* **100,** 1825–1830 (2014).
15. van Almen, G. C. *et al.* Development of Non-Cell Adhesive Vascular Grafts Using Supramolecular Building Blocks. *Macromol. Biosci.* **16,** 350-362 (2016).
16. Muylaert, D. E. P. *et al.* Early in-situ cellularization of a supramolecular vascular graft is modified by synthetic stromal cell-derived factor-1α derived peptides. *Biomaterials* **76,** 187–195 (2016).
17. Dankers, P. Y. W. *et al.* Development and in-vivo characterization of supramolecular hydrogels for intrarenal drug delivery. *Biomaterials* **33,** 5144–5155 (2012).
18. Dankers, P. Y. W. *et al.* Hierarchical Formation of Supramolecular Transient Networks in Water: A Modular Injectable Delivery System. *Adv. Mater.* **24,** 2703–2709 (2012).
19. Bastings, M. M. C. *et al.* A Fast pH-Switchable and Self-Healing Supramolecular Hydrogel Carrier for Guided, Local Catheter Injection in the Infarcted Myocardium. *Adv. Healthc. Mater.* **3,** 70–78 (2014).

Advances in the development of supramolecular biomaterials

Abstract

Regenerative medicine applications aim to recreate or repair the living functional environment of the human body. Many biomaterials that are designed and synthesized in recent years are inspired by the extracellular matrix (ECM) that is responsible for mechanical, structural and biochemical support to cells. In order to synthetically mimic the materials properties of the ECM, it is essential to introduce specific bioactive cues to guide the body to regenerate. Upon implantation of a material, inevitably the material surface comes into contact with the *in vivo* environment and therefore it is of utmost importance that the material surface is functionalized in a desirable fashion. We propose that supramolecular materials that are composed of macromers and oligomers which are held together *via* noncovalent interactions are perfectly suitable to meet requirements to closely mimic the ECM in a synthetic fashion. In this chapter, we disclose recent strategies that have been reported to generate bioactive supramolecular materials as well as different strategies to functionalize the surface of these materials to introduce desirable characteristics. Various solid supramolecular polymeric materials and respective characterization strategies of the material surfaces are discussed.

2.1 Introduction

In the 1960-1970s, first generation biomaterials were designed to be used in the body. They were developed in a way that they comprised physical properties that match those of the replaced tissue and to induce a minimal toxic response. [1] In the 1980-1990s second generation biomaterials were developed with a strong emphasis on bioactivation, biocompatibility and controlled action-reaction in the physiological environment. Although minor improvements were made, synthetic materials were still unable to respond to changes in the physiological environment. Therefore, third generation biomaterials were designed to stimulate specific cellular responses at the molecular level. Molecular modifications of biodegradable polymers were aimed to direct specific interactions with cells and tissues, i.e. differentiation, extracellular matrix (ECM) production and organization. [2]

The design, synthesis and characteristics of truly mimetic biomaterials based on synthetic materials that are capable of recapitulating the structural and functional complexity of tissues is an intriguing challenge. This is due to the exceptionally complex nature of biological systems such as tissues. In this chapter, supramolecular polymeric biomaterials are highlighted, based on the self-assembly behavior and the introduction of functionality, i.e. bioactivity. The first part focuses on pristine macromolecular assemblies that are inspired by nature or exhibit natural building blocks and thereby show intrinsic functionality. The synthetic assemblies that are disclosed discuss materials that are inspired by proteins and growth factors, peptides and carbohydrates, nucleobases as well as hydrogen bonding motifs to direct the self-assembly behavior (Figure 2.1 BI). In the second part, materials that contain functionality as a result of host-guest assemblies based on cyclodextrins, cucurbit[n]urils, crown ethers and calix[n]arenes are discussed. These systems are particularly interesting as their dynamic assembly behavior can be tuned by the choice of the building block (Figure 2.1 BII). In the third part, the introduction of bioactivity into supramolecular thermoplastic elastomers is described, where materials based on polyurethanes, benzene tricarboxamide, bisurea and ureido-pyrimidinone (UPy) motifs are highlighted. Thermoplastic elastomeric materials
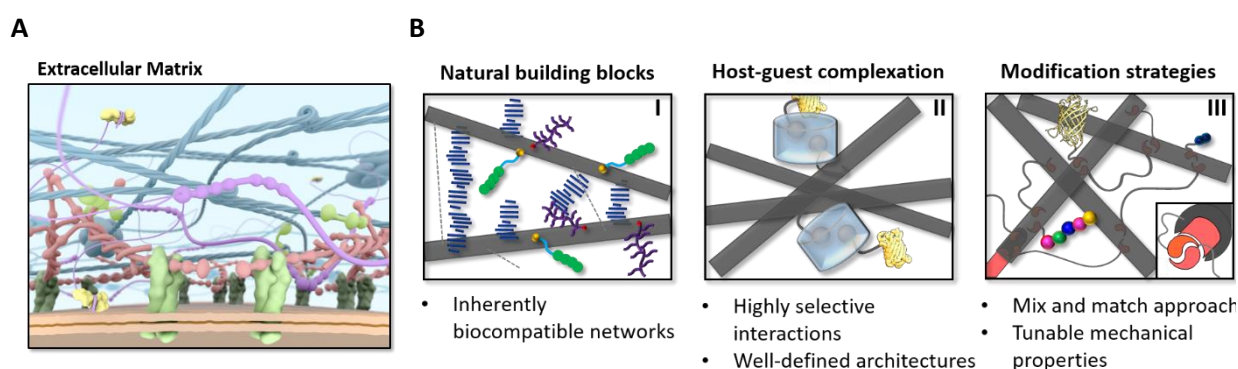
Figure 2.1. The extracellular matrix (ECM) serves as a source of inspiration for the design and development of synthetic biomaterials based on supramolecular interactions, A) Schematic representation of the ECM, Copyright Institute for Complex Molecular Systems Animation Studio and B) Three approaches in synthetic supramolecular polymeric materials that aim to mimic parts of the natural ECM which will be covered in this account; I based on natural interactions, II based on host-guest complexation and III thermoplastic elastomer modification strategies.

exhibit mechanical properties that can easily be tuned as a function of the base polymer. The design of the supramolecular motifs facilitates a modular approach towards the introduction of functionality in these classes of materials. Moreover, clinical translation and *in vivo* applications of these materials are disclosed (Figure 2.1 BIII).

2.2   Synthetic supramolecular polymeric materials inspired by natural building blocks

The field of supramolecular chemistry takes inspiration from design principles that are found in natural systems, in order to develop new synthetic materials that mimic these complex molecular assemblies. The design principles can be engineered according to specific requirements that are needed for the material, i.e. bioactivity or biocompatibility. The hierarchical self-assembled order and the ensemble of material properties, i.e. mechanical, structural and bioactive properties, found in the ECM is the main source of inspiration in the development of new generation biomaterials.

2.2.1   Supramolecular biomaterials inspired by proteins and growth factors

Many reports describe bioactivation of materials through the introduction of bioactive peptide sequences or the non-covalent and covalent conjugation of proteins onto the biomaterial. It is proposed that the natural protein interface is responsible for the stabilization of supramolecular protein structure. [3] Proteins self-assemble into well-defined hierarchical structures, which serves as a source of inspiration in the development and synthesis of synthetic analogues that can mimic this dynamic and reversible self-assembly process. Biological biopolymers consist of repetitive sequences and domains that are stabilized by noncovalent interactions that contribute to mechanical properties of the final structure they form, which enables assembly in hierarchical aggregates that ultimately determines their function. These characteristics and principles should be taken into account in the design of functional self-assembled polymeric biomaterials.

Maynard *et al.* focus on the design and synthesis of polymer-protein conjugates and develop polymers that mimic natural proteins. Besides that, materials surfaces and structures are designed through nanopatterning. Many of these strategies rely on covalent modification strategies to introduce bioactivity and are thus beyond the scope of this chapter, however there are a few beautiful examples which are disclosed here. Using photolithography, micron and submicron-scale features were fabricated in polymer films in order to develop a platform for protein immobilization and assembly. This approach gives rise to highly controlled surface functionalization with bioactive compounds. [4]

As a special class of proteins, growth factors, have grown interest in recent years, since they are involved in many processes and the therapeutic potential of growth factors holds great potential for applications in regenerative medicine. However the translation into clinical treatments is rather limited which might be a result of the poor stability of these proteins, a short circulation half-life and a rapid cell internalization rate. Growth factor proteins are essential factors in the regeneration process which are secreted by cells and are able to

directly interact with or are sequestered by the surrounding ECM for presentation to cell surface receptors.

In the field of biomaterials, there are a few strategies to present growth factors at the surface of the material, i.e. through natural affinity binding and adsorption, binding to ECM upon the introduction of a specific domain in the growth factor (heparin binding domain, collagen binding domain or other ECM binding domains) or covalent attachment through a chemical or enzymatic crosslink. [5] Due to the short lifetime of growth factors, the requirement of high and frequent use and the high costs, the biomaterials that have been developed either physically entrap growth factors in a polymer of supramolecular network or graft them onto supramolecular structures *via* non-covalent electrostatic interactions, whereby a sustained and controlled release could be realized. Peptide cues that mimic the active site of the growth factor could also be introduced into the supramolecular material, thereby eliminating the need to use full length growth factors. Many reports and review articles cover biomaterials presenting or incorporating growth factors based on hydrogels, which is beyond the scope of this chapter. [6,7]

Hubbell and Maynard reported on the discovery of a sulfated tetrapeptide that binds to vascular endothelial growth factor. Molecules that mimic the sulfated glycosaminoglycan heparin and have the property to bind growth factors with a heparin binding domain are important building blocks for synthetic biomaterials. Due to the ease of synthesis and modification, peptide-based heparin mimics are of interest and a sulfated tetrapeptide library that binds to vascular endothelial growth factor (VEGF) was synthesized using split-tool combinatorial chemistry. *Via* this combinatorial approach they were able to design a small peptide with only two sulfate groups that binds with higher affinity to the $VEGF_{165}$ than well-known heparin mimics. This concept may be applicable for other heparin-binding growth factors as well and might elucidate high binding affinity small sulfated peptides. [8]

Lee *et al.* reported on the local delivery of insulin-like growth factor (IGF-1) delivery in the myocardium. They designed self-assembling peptides composed of alternating hydrophilic and hydrophobic amino acids that assemble into nanofibers upon exposure to physiological conditions. The self-assembled nanofibers displayed the growth factor at the nanofiber surface. After *in vivo* injection into the rat myocardium, specific and controlled delivery of IGF-1 to local myocardial microenvironments was observed which improved cell therapy. [9]

An interesting study by Chmielewski *et al.* reported on mimicking the ECM by the design of collagen mimetic peptides that are able to assemble into a highly crosslinked 3D matrix upon a metal ion stimulus (Figure 2.2 A). Three collagen mimetic peptides were synthesized (HBN, HRGDSN and HBRGDS, Figure 2.2 B). Moreover, these assemblies can be functionalized with His-tag cargoes, in this case green fluorescent protein ($GFP-His_8$) and human epidermal growth factor ($hEGF-His_6$). The $hEGF-His_6$ is released gradually from the matrix and induces cell proliferation in an EGF-dependent cell line. The incorporation of RGDS in the collagen mimetic peptide facilitates encapsulation of the cells into the crosslinked 3D matrix (Figure 2.2 C). [10]
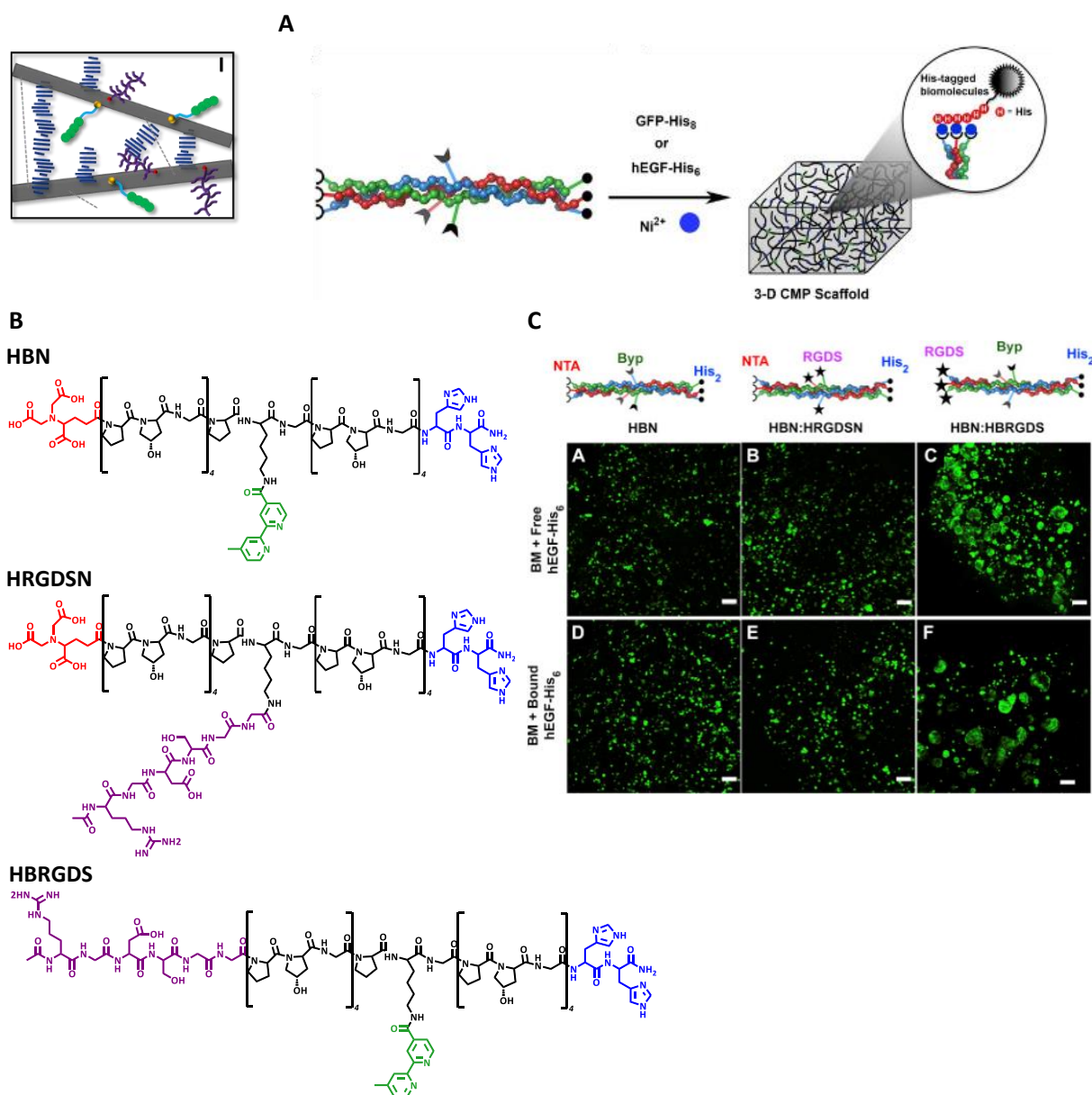
Figure 2.2. ECM mimic with functionalized metal-assembled collagen peptide scaffolds, A) Chemical structures of the HBN, HRGDSN and HBRGDS collagen mimetic peptides with (in blue) His$_2$ ligand for metal binding, (in green) bipyridine (Byp) for metal binding, (in red) NTA for metal binding and (in purple) the RGDS peptide sequence for cell attachment, B) Strategy for functionalization of the collagen mimetic peptide (CMP) scaffold with his-tagged biomolecules. Upon metal-ion promoted assembly metal ligands are able to incorporate His-tagged biomolecules and C) MCF 10A cell encapsulated in the CMP scaffold are viable and organize into spheroid structures in the HBN: HBRGDS scaffolds. Pictures were recorded after six days of encapsulation of soluble (top row) or bound (bottom row) hEGF-His$_6$, scale bars represent 100 μm. The stars in the triple helix cartoons indicate positions of the RGDS sequences. Reprinted from [10] with permission from Elsevier.

Inspiration taken from the assembly of proteins and higher ordered protein assemblies can be applied in the development of synthetic materials that are highly dynamic or functional. Proteins and growth factors are essential components that are abundant in the natural ECM. Natural materials based on these compounds are inherently biocompatible and bioactive, which makes them extremely suitable as biomaterials. Supramolecular polymeric

materials that mimic the intrinsic structure or function of the protein or growth factors are interesting alternatives towards new generation biomaterials.

2.2.2 Supramolecular biomaterials inspired by carbohydrates

Carbohydrates are involved in many biological processes and due to the ability to form hydrogen bonds they are interesting components in supramolecular chemistry. Carbohydrate-carbohydrate interactions and carbohydrate-protein interactions regulate biochemical processes in the human body, ranging from cell differentiation and proliferation to the immune response. [11] The ensemble of multiple carbohydrates in a multivalent complex ensures strength of the relatively weak noncovalent interactions of the single components. Glycosylated surfaces have been developed and used to study multivalent glycol-interfaces. [12] Many reports focus on the immobilization of host-guest responsive systems on gold or glass substrates,[13–16] as well as the use of supramolecular polysaccharide moieties in hydrogel development has grown interest in recent years, [17–22] which is not covered in this chapter. In this section focuses on a few literature examples in the development of supramolecular biomaterials that take inspiration from carbohydrate chemistry and their intriguing properties.

Seeberger *et al.* reported on the decoration of graphene sheet surfaces with multivalent sugar ligands in order to prepare a supramolecular carbohydrate-functionalized 2D surface. In the interest of investigating carbohydrate-protein interactions, adamantyl-functionalized graphene was supramolecularly assembled with mannose-β-CD. These self-assembled sensors can reversibly bind bacteria and upon IR-laser irradiation the bacteria are killed, which makes these types of materials feasible for disinfection applications. [23] Tran *et al.* reported a one-step recyclable method to synthesize a supramolecular polysaccharide composite material comprising cellulose, chitosan and crown ether (B15C5). The composite material demonstrated supramolecular properties, mechanical properties in the range of cellulose and adsorption capability of heavy metal ions and organic pollutants. The superior adsorption properties of the material are attributed to the presence of the crown ether. [24]

In order to develop protein resistant materials, Guan *et al.* studied the structure-property relationship of a carbohydrate-derived side-chain ether polymer. The results show that the molecular design of polymers can be tailored in order to aim for the desired material properties, which can be applied as various biomaterials. [25] A similar study based on polyethers was published a few years earlier where protein resistance behavior upon the introduction of a carbohydrate-derived side-chain polyether was also demonstrated. [26] More recently, Sun *et al*. reported on a layer-by-layer assembly approach to create healable antifouling films. They assemble the material by exponential layer-by-layer assembly of PEGylated branched poly(ethyleneimine) (bPEI) and hyaluronic acid (HA) followed by crosslinking *via* PEG diacid. The surface of these material films showed protein resistant behavior as well as inhibited cell attachment under physiological conditions. The antifouling properties of the surface are assigned to the synergic effect of the PEG-rich surface and the soft mechanical nature of the films. As a result of the high mobility of the bPEI-PEG and HA

polyelectrolytes and the noncovalent hydrogen bonding and electrostatic interactions, the material exhibits healing behavior. [27]

Materials inspired by or composed of carbohydrates are inherently biocompatible and bioactive as well as antifouling. These materials display interesting materials properties that on the one hand facilitate engagement into the human body while on the other hand prevent nonspecific adsorption of undesired compounds. Upon the introduction of additional, specific bioactivity it is hypothesized that these carbohydrate based materials can exhibit a specific function.

2.2.3 Supramolecular biomaterials inspired by peptides and peptide amphiphiles

In recent years, the use of peptides as building blocks in supramolecular architectures has been demonstrated. Oligo-peptide based self-assembled structures have been used to synthesize hybrid conjugates that are composed of peptides in combination with polymers, alkyl chains or phospholipids. [28–30] Peptides can serve to bring specific bioactivity into the material as well as due to electrostatic interactions dictate the self-assembly of the moieties into desired secondary structures, which makes them highly suitable to be applied in the field of tissue engineering and regenerative medicine. Due to their biocompatible properties they can be applied in aqueous environment directly or can act at the supramolecular polymer water interface.

2.2.3.1 Supramolecular biomaterials based on peptide building blocks

Collagen mimetic peptides that contain the triad amino acid sequence Gly-Hyp-X and Gly-X-Hyp, X frequently being Pro, have extensively been studied in order to reveal the triple-helix formation as well as the influence of the different amino acids on the assembly process. Self-assembling peptides have been synthesized that form collagen-like triple helices and are able to assemble into hydrogels, based on hierarchical assembly of natural collagen. [31–33]

Another class of ordered supramolecular polymers are based on the formation of β-sheet like structures, based on electrostatic interactions as a result of an alternating cationic-hydrophobic-anionic-hydrophobic peptide sequence, which is widely explored by Zhang *et al*. [34] B-sheet peptides have been applied as functional building blocks in the preparation of bioactive supramolecular nanofiber scaffolds, due to the inherent biocompatibility as well as the structural feature to adopt a secondary structure. [35,36]

Guan *et al*. focus on the synthesis of a polymeric β-sheet mimics that are able to assemble into hierarchical nanofibrils. Cu-catalyzed azide-alkyne cycloaddition was employed for the polymerization of a peptide monomer to induce high-order structure formation. These polymers further self-assemble intermolecularly into amyloid-like nanofibrils, induced by the folding and self-assembly of the resultant polymer. The polymerization thus leads to intramolecular folding to form a β-sheet (secondary structure) and further intermolecular organization into hierarchical nanostructures. [37]

Guan describes the current understanding of the molecular mechanisms that contribute to the exceptional mechanical properties of two biopolymers, one based on intermolecular weak forces between β-sheets to gain strength and toughness, and one where intramolecular modular design is used to achieve mechanical strength, toughness and elasticity. The mini review outlines on how supramolecular chemistry plays a critical role in the design of synthetic polymers that combine advanced mechanical and other functional properties. [38]

Another class of biomaterials described by Guan *et al*. is derived from natural saccharide and amino acid building blocks. Based on the abundancy of the natural monomers, the likelihood to generate biocompatible and biodegradable polymers, the convenient modification of these materials towards desired applications and the modularity of synthesis, these saccharide-peptide hybrid copolymers were designed as a new class of biomaterials. The materials were shown to be nontoxic, biodegradable and non-immunogenic and were tested for possible gene delivery applications and tissue engineering. [39]

Inspired by the intriguing properties of elastin, as an important ECM protein, a bioinspired modular synthesis approach to synthesize elastin-mimic polymers (EMPs) to probe the mechanism of elastin elasticity was reported by Guan *et al*. It was shown that the polymer conformation is not essential for the elasticity of EMPs. However, the hydrophobic hydration, as opposed to an organized secondary structure, turned out to play an important role for the elasticity. Moreover, the bioinspired EMPs show similarities with natural elastin in elasticity in bulk as well as LCST behavior. [40] In an effort to mimic the highly nonlinear elastic properties of human skin, a similar strategy *via* a bioinspired design of nanostructured elastomers with cross-linked soft matrix grafted rigid nanofibers was used. The synthetic material consists of cellulose and polyisoprene (PI), which differ in mechanical performance, semi-rigid and strong versus highly elastic, respectively, to mimic stiff collagen and elastin in the skin. The polymers are connected in order to allow for large deformation. Moreover, microphase separation into nanocomposites occurs which results in the nonlinear mechanical properties of skin. [41]

An interesting review by Guan reports about the structure and molecular mechanisms of natural polymeric materials and the progress towards synthetic mimics of these systems. [42]

Hubbell *et al.* reported on the development of a coating of surface-active copolymers that are RGD-grafted to induce specific cell attachment and spreading and contained poly(ethylene glycol) (PEG) to prevent nonspecific protein adsorption. A poly-L-lysine (PLL) backbone from which PEG was grafted with short and long chains was synthesized. The long chains of the PEG grafts were specifically conjugated with the RGD-containing peptide motif *via* the thiol of a cysteine in the peptide and a vinylsulfone terminus in the PEG chain, in order to facilitate cell binding. [43] Another report on the use of poly(ethylene glycol) (PEG) brushes in order to introduce non-fouling behavior into materials, was published by Klok and Hubbell *et al.* A non-biofouling coating is introduced following a two-step strategy that involves photobromination of a low density polyethylene (LDPE) substrate followed by surface-initiated atom transfer radical polymerization (SI-ATRP) of PEG-methacrylate (PEGMA) resulting in poly(poly(ethylene glycol)methacrylate) (PPEGMA) brushes. It was shown that

these coatings prevent non-specific adhesion of cells and hence could be functionalized with ECM derived peptides (GGGRGDS) to allow integrin-specific cell adhesion. [44]

2.2.3.2 Supramolecular biomaterials based on peptide amphiphiles

An elegant supramolecular system that is widely applied in the field of tissue engineering is based on peptide-based amphiphilic molecules that form three-dimensional nanofibers, which has been developed by Stupp *et al*. (Figure 2.3 B).[45] These peptide amphiphiles (PAs) are able to reversibly self-assemble into three-dimensional nanofibers and this nanofiber self-assembly process can be modulated either *via* pH, concentration and ionic composition (Figure 2.3 C). Furthermore, PAs are composed of three regions, a long aliphatic tail, a flexible peptide linker region and a bioactive region, which acts as specific bioactive cue (Figure 2.3 A). [46,47] In addition to these three regions, four cysteine residues were built in between the alkyl tail and the peptide linker, in order to facilitate oxidation to form disulfide bonds which can facilitate the polymerization of the nanofibrous structure. A phosphoserine residue was
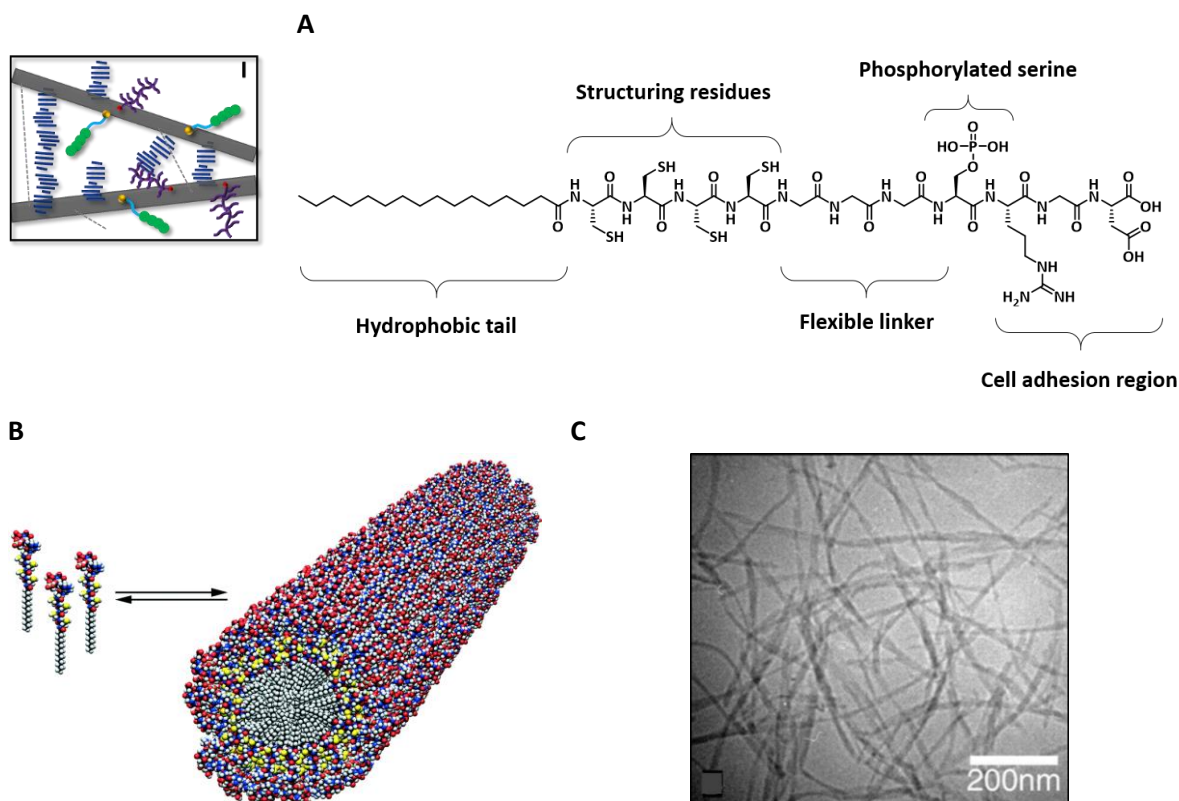
Figure 2.3. Supramolecular polymeric biomaterials based on peptide amphiphiles (PA), A) Chemical structure of PA with an aliphatic hydrophobic tail, cysteine residues as structuring motif to ensure disulfide bond formation to polymerize the self-assembled structure, a flexible linker of three glycine units, a phosphorylated serine residue to interact with calcium ions and direct mineralization of hydroxyapatite and a cell adhesion region which contains the RGD peptide ligand, B) Schematic representation of the self-assembly of the PA into cylindrical micelles and C) A cryo-TEM picture of the fibers formed by PA self-assembly that reveal the diameter of the fibers in the hydrated state to be 7.6 ± 1 nm. From [46]. Reprinted with permission from AAAS.

introduced to facilitate strong interaction with calcium ions (Figure 2.3 A). Lowering the pH below 4 induced the PAs self-assembly and the disulfide bond formation ensures fiber cross-linking resulting in a chemically robust fiber, which could be reversed by the reduction of the disulfide bonds (Figure 2.3B). The fibers are able to direct the mineralization of hydroxyapatite to create a composite material of which the *c* axis is aligned along the long axis of the supramolecular nanofibers. [46] The co-assembly of two bioactive PAs by electrostatic interactions at different pH has also been shown. At low pH, negatively charged PAs self-assemble, while at high pH positively charged PAs self-assemble and pairs of positively and negatively charged PA co-assemble at neutral pH. [48] Among others, the ability to bind complementary oligonucleotides was also explored *via* the synthesis of peptide nucleic acid/peptide amphiphile conjugates (PNA-PAs) that self-assemble into fiber-like nanostructures and are able to bind nucleotides with high affinity as well as specificity. [49] Heparin chemistry in combination with PA self-assembly was applied to develop nanomaterials for new blood vessel development. The PAs were equipped with the heparin binding peptide sequence LRKKLGKA. Heparin was used to nucleate the self-assembly of the PAs, yielding rigid nanofibers that display heparin and stimulated new blood vessel formation. [50] PA nanofibers with the neurite-promoting laminin derived IKVAV peptide sequence in high epitope density were studied for application for tissue engineering of nerves. The epitope density is thought to be the key factor for the rapid and selective differentiation into neurons. [47,51] The supramolecular structure in the natural ECM is related to the bioactive epitope density and dynamics and plays important roles in cell-matrix interactions as well as signaling. Stupp *et al.* probed the interactions of cells with supramolecular PA fibers that display cell adhesion RGD epitopes in various extremely high densities, i.e. branched and linear, in order to demonstrate the possibility of signaling cells using these supramolecular nanofibers. Branched architectures in the PA forming the nanofibers provides greater epitope accessibility to cells, due to the lower packing efficiency and thus additional space for epitope motion. When the supramolecular nanostructures display mobile epitopes at high density, improved signaling for cell adhesion, spreading and migration is observed. [52] This concept was explored for bladder tissue engineering, where PAs were coated onto the poly(glycolic acid) (PGA) fiber scaffolds and showed surface retention upon cell culture conditions and self-assembly into nanofibers. [53]

More recently, the order of PAs was investigated and it was shown that the anisotropic interactions of the peptide linker domain of PAs consisting of amino acids with a high β-sheet forming tendency directly connected to the hydrophobic tail ensure self-assembly into supramolecular nanofibers. [54] The attachment of VEGF mimetic peptide sequences to the PA have shown to improve the survival, proliferation and migration of human umbilical vein endothelial cells, compared to non-functionalized PA. [55] Stupp *et al.* continue their work on the development of stimuli-responsive dynamic materials. The ability of materials to respond to changes in physical structure and chemical composition could greatly improve the development of synthetic materials towards mimicking the dynamic features of the ECM. [56]

2.2.4   Supramolecular biomaterials inspired by nucleobase self-assembly

Inspired by the defined and selective self-assembly of nucleobases as found in nature, nucleobase supramolecular polymeric materials have gained attention in recent years. The use of nucleobases as recognition motifs to functionalize polymeric materials has been investigated by various research groups.

In the area of nucleobase supramolecular polymeric materials Long *et al.* have investigated the nucleobase self-assembly in supramolecular adhesives based on molecular recognition, with adenine and thymine. A flexible alkyl chain spacer for recognition sites was constructed, that was compared with a styrene analogue in order to investigate the structural modifications on the nucleobase self-assembly. These novel acrylic nucleobases were synthesized using an aza-Michael addition combined with copolymerization with *n*-butyl acrylate. It was shown that 7 mol% adenine-containing polymers self-assembled into needle-like microstructures within the polymer matrix, whereas thymine-containing polymers did not aggregate into distinct morphologies up to 32 mol%. Upon mixing, the thymine and adenine physically base pair together, resulting in thermodynamically stable complex formation. Moreover, these nucleobase functionalized polyacrylates exhibit tunable adhesive and cohesive strength, whereby the molar fractions of each nucleobase, their stacking interactions as well as the complementary hydrogen bonding are of influence on the self-assembly of these materials. [57] An approach to synthesize triblock copolymers with nucleobase, adenine and thymine, functionalized outer blocks was reported. These thermoplastic elastomeric block copolymers were synthesized and in blends of the complementary polymers, hydrogen-bonding interactions resulted in increased viscosity which can be attributed to association of the nucleobases in solution. Increased solution viscosity scaled with concentration, demonstrating the influence of the hydrogen-bonding equilibrium of the nucleobases. In solid state, hydrogen bonding resulted in compatibilization of the blends through the formation of associated adenosine-thymine hard phase upon annealing. Introducing complementary guest molecules resulted in selective uptake into the nucleobase-containing domains, which may potentially extrapolate towards use in drug delivery and biological applications. [58] The incorporation of nucleobases and other complementary hydrogen bonding interactions into a range of macromolecular structures generates complex tertiary and quaternary structures, which enables the supramolecular assembly and modification to adapt new properties.[59] Another elegant example reports on the use of RAFT polymerization to create self-complementary nucleobase-functionalized ABC triblock copolymers with fully acrylic backbones that self-assemble into well-defined lamellar microphase-separated morphologies (Figure 2.4 A,B). Moreover, complementary hydrogen bonding within the hard phase resulted in further enhanced mechanical performance of these materials. This class of thermoplastic elastomers are considered perfectly suitable for a wide variety of applications. [60] A feature article by Long and Anderson covers the use of imidazole derivatives and imidazolium-containing polymers in materials science and their potential use in biomedical applications. [61]

Materials based on nucleobase-grafted polycaprolactones as reversible networks were reported by Chang *et al.* The grafting resulted in retarded crystallization due to the supramolecular polymer formation. Molecular recognition experiments showed interactions between the adenine and uracil through strong cooperative hydrogen bonding. Morphology analysis revealed discrete nano-scale spherical aggregates upon self-assembly. *In vitro* cytotoxicity showed biocompatibility of these materials. [62]
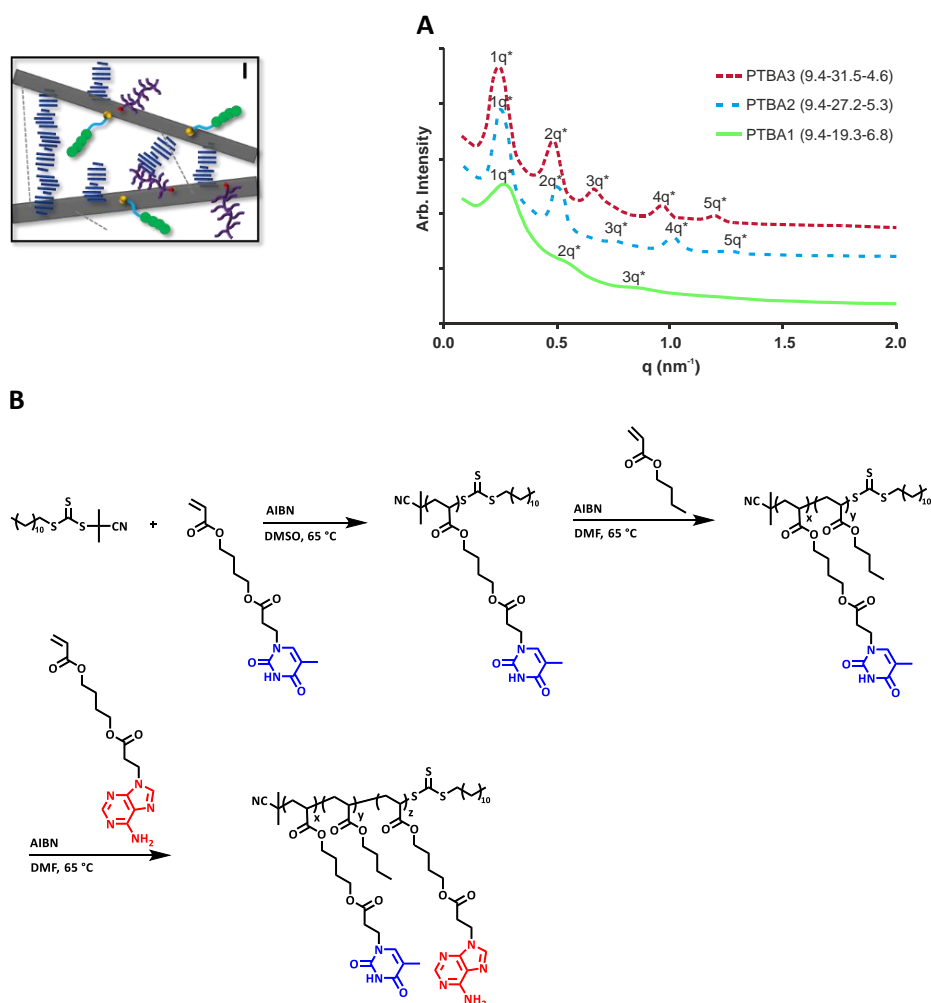
Figure 2.4. Nucleobase-functionalized ABC triblock copolymers that self-assemble into supramolecular architectures, A) SAXS profiles of PTBA triblock copolymers demonstrating ordered microphase separated morphology of the triblock copolymers of three different PTBA triblock copolymers with differences in block amount and B) RAFT polymerization of the preparation of poly(ThA-*b-n*BA-*b*-Ada) (PTBA) ABC triblock copolymers. Reprinted from [60], published by the Royal Society of Chemistry.

2.2.5   Supramolecular biomaterials inspired by synthetic hydrogen bonding motifs

Guan *et al.* reported on the design of a biomimetic modular polymer that consists of high modulus, toughness and resilience, and moreover possesses adaptive mechanical properties. The concept is based on the skeletal muscle protein titin, with a modular domain forming part that is composed of a 2-ureido-4[1H]-pyrimidinone (UPy) motif and a cyclic modular polymer using a peptidomimetic β-sheet dimer. These modular polymers exhibit unusual stress-strain behavior and unique shape-memory properties, giving rise to a material with a combination

of mechanical properties, including high modulus, toughness, large extensibility as well as intriguing adaptive behavior. The mechanism for these properties is explained by the fact that upon stretching, the polymer modules gradually unfold which result in a large extension and energy absorption. Upon cooling and stress removal, the unfolded UPy-moieties are in mutual proximity to other UPy-moieties of neighboring chains, resulting in the dimerization into another network, and thus another material shape. Upon temperature increase, in time the newly formed interchain formed UPy dimers become dynamic again and return to the original stable dimerized state. These materials give rise to the development of novel biomimetic polymeric materials with advanced properties. [63]

Guan *et al.* described the design of supramolecular block copolymers for new multiphase self-healing materials in bulk solid state. The soft block in the block copolymer consisted of poly(*n*-butyl acrylate) (PBA) and polystyrene (PS) as the hard block (PBA-*b*-PS), which exhibit microphase separation morphology and thermoplastic elastomer properties. To equip the polymers with self-healing behavior, the PBA-*b*-PS diblock copolymers were end-functionalized with UPy-motifs, resulting in the formation of an ABA triblock supramolecular polymer. The incorporation of UPy-moieties resulted in thermoplastic elastomers with dynamic and self-healing properties. Moreover, modularity of this system can facilitate the incorporation of bioactive motifs in order to develop functional biomaterials. [64] Another self-healing material was developed based on the multiphase design strategy to program dynamic healing motifs based on hydrogen bonds in the soft phase of a hard-soft multiphase system (Figure 2.5 A). Thereby, the unique properties of hybrid polymers (stiffness and toughness) are merged with those of dynamic supramolecular assemblies (autonomic healing). Here, a hydrogen-bonding brush polymer (HBP) that self-assembles into a two-phase morphology and behaves like a TPE, with a high Young's modulus and extensibility, was synthesized (Figure 2.5 B). These materials showed tunable mechanical properties *via* the molecular design (Figure 2.5 C). Moreover, the creep recovery behavior of these self-healing supramolecular thermoplastic elastomers showed creep recovery behavior at different stress levels similar to that of covalently linked elastomers (Figure 2.5 D). Microphase separated behavior of these materials was revealed by TEM (Figure 2.5 E). [65]

ABA block copolymers that are composed of a rigid poly(methyl methacrylate) (PMMA) middle block and two dynamic poly(acrylate amide) (PA-amide) terminal blocks that have hydrogen bonding capacity were synthesized to synthesize a multivalent hydrogen bonding block copolymer that can self-assemble into a strong and tough self-healing material. By adjusting the chain length of the blocks, the mechanical properties of the material could be tuned and the block copolymers self-assemble into spherical microphase-separated morphologies. These hydrogen bonding block copolymers exhibit improved mechanical properties as well as self-healing capability. [66] A single-component sticky polymer-grafted nanoparticle approach has been developed by the introduction of strong molecular interactions to the graft to increase the cohesive attraction in the self-assembled nanocomposites. Multivalent hydrogen bonding motifs were introduced onto the polymer grafts to facilitate self-assembly into 3D superlattice nanocomposites. The dynamic hydrogen
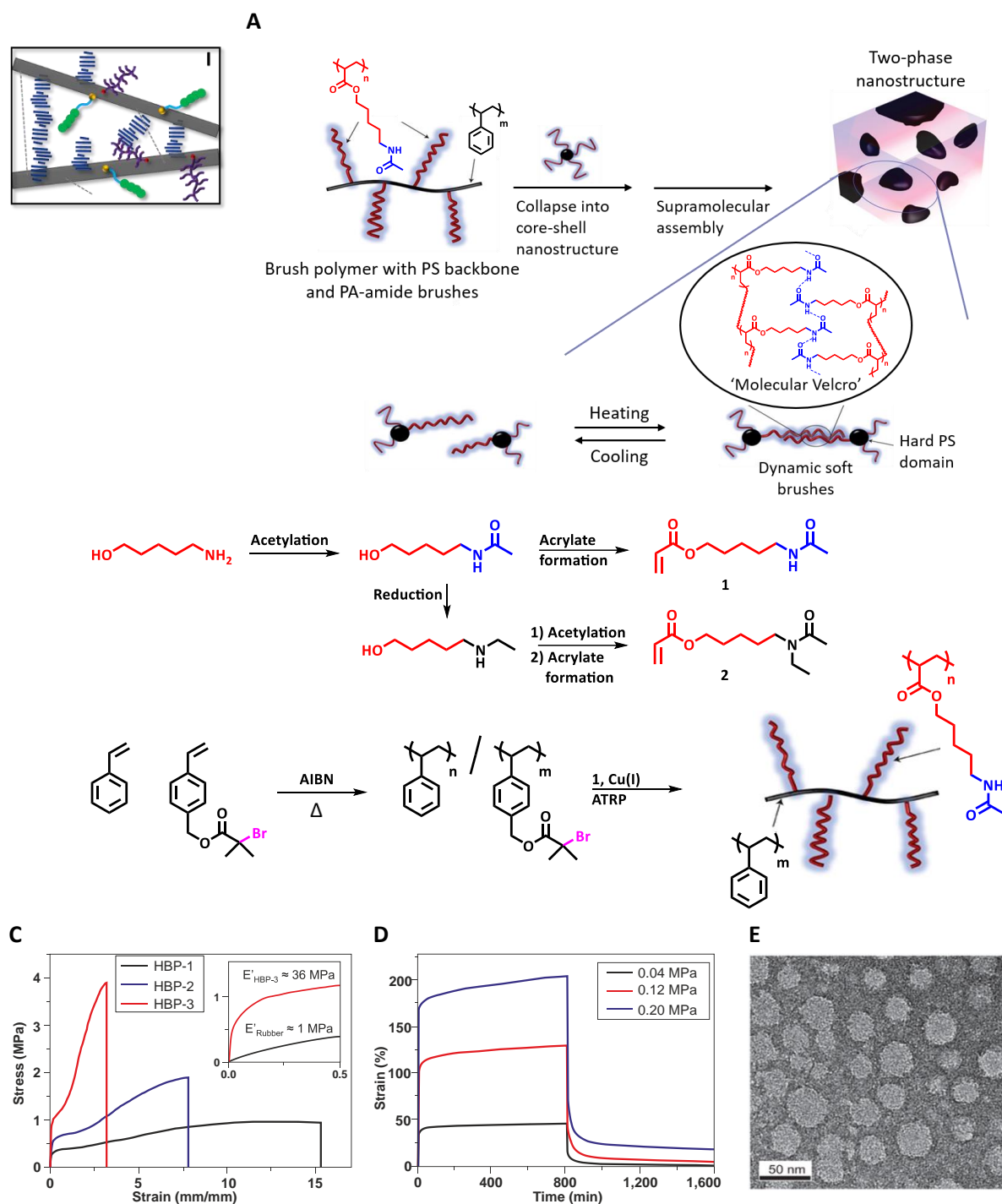
Figure 2.5. Multiphase design of autonomic self-healing thermoplastic elastomers, A) Hydrogen-bonding brush polymer self-assembles into a two-phase nanostructure morphology during processing (I) and the supramolecular connections between the soft brushes can rupture reversibly under stress in contrast to conventional TPE systems, where rupture of covalent connections is irreversible, B) Synthesis of hydrogen-bonding monomer **1** and hydrogen-bond blocked control monomer **2** (I) and synthesis of hydrogen-bonding brush polymer (HBP)s, by copolymerization of styrene with an ATRP co-monomer **4** *via* free-radical polymerization, followed by ATRP polymerization of monomer **1** to form the brushes (II). Control HBP was prepared similarly using monomer **2** in the brush formation, C) Static tensile tests of HBPs 1-3 illustrate TPE-like stress-strain behavior and tunability of mechanical properties *via* molecular design, inset: tensile behavior of HBP-3 compared with natural rubber, D) Creep recovery behavior at different stress levels follows that of covalently linked elastomers and E) TEM images provide clear evidence of microphase-separated structures with spherical polystyrene cores dispersed in a soft PA-amide matrix, which was selectively stained with uranyl acetate. Adapted by permission from Macmillan Publishers Ltd: Nature Chemistry [65], copyright 2012.

bonding facilitates the formation of tunable dynamic, self-healing materials and mechanochromic nanocomposite materials in bulk. [67] Along these lines, self-healing multiphase polymers were developed based on dynamic metal-ligand interactions. Polystyrene (PS) was used as the backbone from which multiple imidazole-containing brushes were grown. Imidazole is able to complex with Zn^{2+} thereby inducing the formation of a microphase separated material with a PS hard phase and a Zn^{2+}-imidazole soft phase. Mechanical properties could easily be tuned by varying several molecular parameters. The metal-ligand interactions offer advantages over hydrogen bonded systems as they are less sensitive to moisture and have a broad range of tunability both in terms of kinetics and thermodynamics. [68] A thermoplastic elastomer brush copolymer which is self-healing was synthesized *via* a two-step polymerization, with a PMMA backbone and a flexible polyacrylate-amide (PA-amide) brush that exhibits thermoplastic elastomer properties in bulk. The dynamic hydrogen bonds in the soft PA-amide matrix enable spontaneous self-healing properties after mechanical damage. [69]

Inspired by the nucleobase complementary hydrogen bonding capacity, Long *et al.* designed another class of materials, in which star-shaped poly(ethylene-*co*-propylene) (MW 12 – 90 kDa) was end-functionalized with the four-fold self-complementary hydrogen bonding UPy motif. It was found that UPy end-functionalized poly(ethylene-*co*-propylene) forms microphase separated morphologies. [70]

In conclusion, in the development of supramolecular polymeric biomaterials, nature and natural building blocks are a main source of inspiration. In particular, mimicking the natural ECM, which is composed of multiple supramolecular assemblies of both structural and functional compounds, with completely synthetic materials is a challenge. In the previous sections developments where either the supramolecular polymer assemblies consist of natural building blocks to introduce specific function and guide the self-assembly or the development of supramolecular polymers that are based on hydrogen bonding motifs were highlighted.

2.3 Host-guest complexation

Many elegant immobilization strategies have been employed in recent years to covalently attach proteins at the surface of solid supports, including chemo-selective covalent attachment of proteins *via* the amine functionality of lysines of proteins to *N*-hydroxysuccinimide (NHS) or aldehydes to form peptide or imine bonds. Native chemical ligation, split-intein mediated protein trans-splicing or enzyme mediated ligations are among others also explored in this field.[71–73] In order to maintain protein stability and allow for site-specific reversible immobilization using mild reaction conditions, supramolecular ligation strategies prove to be excellent candidates.

Supramolecular complexation based on host-guest interactions have grown interest in biomaterials science. One-dimensional linear supramolecular polymers can be formed through the engagement of complementary host and guest unimers, which can be associated *via* host-guest heteroditopic monomers or *via* two-component equimolar mixtures of hosts

and guests heterocomplementary complexes. Polyassociation of host-guest monomers yields supramolecular homopolymers, in which association and growth occur immediately after host-guest recognition. Host-guest complexes involve a cooperative effect of noncovalent interactions, i.e. hydrophobic interactions, hydrogen bonding and electrostatic interactions, and guest molecules are able to incorporate into the cavity of the host. The complexation of host and guest relies on complementarity in size and shape.[74] Many reports in the literature report on stimuli-responsive supramolecular polymers based on host-guest assemblies, in aqueous solution, which is beyond the scope of this chapter.[75]

Supramolecular polymers based on host-guest interaction exhibit interesting properties and therefore are perfectly suitable for various applications. Host-guest supramolecular polymers are able to form well-defined macromolecular architectures, and can be used to prepare responsive materials with properties that can be tuned upon changing environmental conditions. Complementarity in both shape and interaction with a host is a typical phenomenon of the guest, i.e. molecular recognition including hydrogen bonding, electrostatic interactions, van der Waals interactions and the hydrophobic effect. The dynamic behavior in complex biological systems can elegantly be mimicked by host-guest systems that rely on supramolecular complexation. The introduction of surface functionality through this approach has grown interest towards multifunctional biointerfaces that are stimuli-responsive, biocompatible and adaptable.[76]

2.3.1 Host guest complexes based on cyclodextrin

Cyclodextrin (CD) is composed of a hydrophilic exterior surface and a hydrophobic interior cavity, which is able to host multiple guest ligands. They are cyclic oligosaccharides composed of five or more α-D-glucopyranoside units in a ring linked through α-1,4-glycosidic bonds. Frequently used CD are composed of six (α-CD), seven (β-CD) or eight (γ-CD) glucopyranoside monomers. A widely used approach is the grafting of polymers with CD to provide a cationic surface charge which may reduce polymer toxicity as well as facilitate molecular stabilization. Most examples of successful application of CD host-guest assemblies report on their hydrogel formation capabilities. It has been shown that macroscopic self-assembly can take place based on the molecular recognition of the CD with the corresponding ligands.[77,78]

CD host-guest inclusion has also proven to be an efficient approach to functionalize surfaces of solid material films. Li *et al.* report on a strategy where first β-CDs were covalently grafted onto a cellulose fiber surface and subsequently adamantane end-capped oligomers were immobilized onto the fiber surface, thereby changing the properties of the cellulose materials as desired. PCL on both ends capped with adamantane (AD-PCL) was synthesized and supramolecularly assembled onto the CD-containing cellulose fibers. To synthesize bioactive supramolecular biomaterials, adamantane conjugated biomolecules can be assembled to introduce surface functionality.[79] In the development of functional supramolecular solid materials, Zhao *et al.* have developed a method to selectively functionalize poly(ε-caprolactone) (PCL) surfaces with both an antifouling coating as well as the introduction of a peptide to specifically bind endothelial progenitor cells (EPC) (Figure 2.6 A). *Via* the host-guest

assembly of *β*-CD and adamantine they realized surface functionalization of the PCL materials. The PCL films were surface grafted with *β*-CD and subsequently adamantane functionalized PEG and EPC binding peptides were immobilized on the PCL-CD surface (Figure 2.6 B). The materials were characterized by XPS, water contact angle and by means of a fluorescence assay with a FITC-labelled EPC-peptide. XPS revealed a difference in surface composition after assembly of the adamantane-compounds (Figure 2.6 C). Water contact angle measurements revealed a slight decrease in angle, indicative of surface functionalization. Moreover, PEG functionalization of the surface resulted in antifouling behavior, fibrinogen adhesion as well as platelet adhesion was reduced. Inclusion of the EPC binding peptide resulted in enhanced attachment of EPCs (Figure 2.6 D,E). The results indicate that the dual functionalization approach was applied successfully and is promising in the development of vascular grafts to induce *in situ* endothelialization.[80]

Ohya *et al.* reported on the synthesis of an amphiphilic biodegradable poly(l-lactide)-grafted *α*-CD copolymer (CD-*g*-PLLA) and determined thermal, mechanical, degradation and microphase separation properties of the materials. To develop drug-encapsulating materials, AD-functionalized drugs could be assembled onto the materials surface. [81] Another illustration of dynamic biomaterial surfaces is reported by Yui *et al*. They synthesized a tri-block copolymer containing hydrophilic polyrotaxane and hydrophobic poly(*iso-*
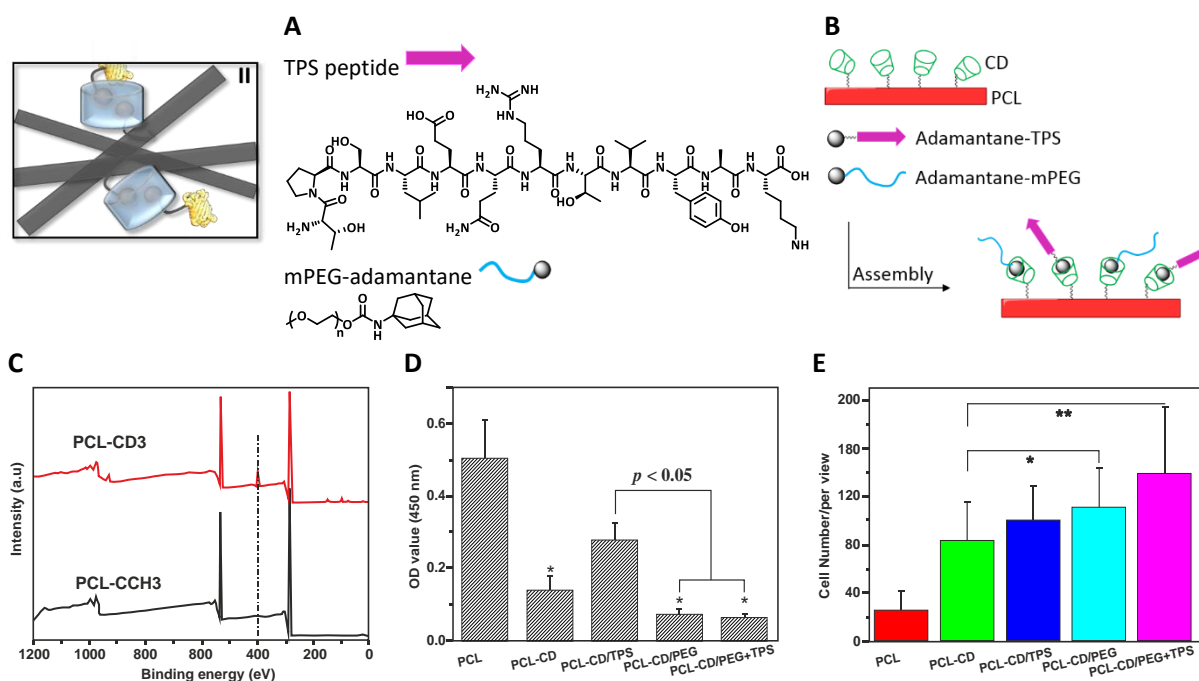
Figure 2.6. Development of both antifouling and bioactive coating as solid supramolecular scaffold based on cyclodextrin (CD) host-guest chemistry, A) Chemical structures of the bioactive TPS peptide (TPSLEQRTVYAK) and the antifouling mPEG-adamantane moieties, B) Surface functionalization based on CD host-guest chemistry. CD is covalently introduced at the PCL polymer surface and subsequently mPEG-adamantane and TPS-adamantane are assembled, C) XPS results of PCL film before (black) and after CD functionalization (red), D) Human plasma fibrinogen adsorption on different surfaces measured through an ELISA assay and e) Endothelial progenitor cell (EPC) adhesion on the different surfaces in the presence of 2% serum. Adapted with permission from [80]. Copyright 2013 American Chemical Society.

butylmethacrylate) (P*i*BMA) segments *via* atom transfer radical polymerization (ATRP). To prepare the polyrotaxane tri-block copolymer, the hydrophobic monomer *iso*-butyl methacrylate was synthesized using a pseudopolyrotaxane with a 2-bromoisobutyryl end-capped PEG and α-CD as a macro-initiator. Hydrophilicity was introduced *via* the methylation of the α-CD. The extraordinary protein adsorption behavior at the polyrotaxane surface would be derived from the high surface mobility of the methylated α-CD along the PEG backbone. [82]

The grafting of multi-walled carbon nanotubes (MWNTs) with biodegradable supramolecular polypseudorotaxane has been reported by Xie *et al.* They functionalized MWNTs with biodegradable supramolecular polypseudorotaxanes by combining ring-opening polymerization and supramolecular inclusion complexation between guest grafted-PCL and host α-CD. Upon the inclusion of α-CD, more bundles and entanglements of MWNTs were identified, indicative for supramolecular α-CD host-guest assembly at the surface of the MWNTs. [83] Another study performed by Amiel *et al.*, developed a supramolecular host-guest strategy based on β-CD to decorate polymer interfaces with PEG grafts. By Cu-catalyzed azide-alkyne cycloaddition, a series of bifunctional adamantyl with different PEG chains grafted CD chains were synthesized. The ability to form inclusion complexes with monomeric *β*-Cd, neutral poly-*β*-CD and cationic poly-*β*-CD strongly depends on the degree of substitution by the adamantyl functions, indicative for a cooperative binding effect. [84] Chen *et al.* reported on the regulation of protein binding capability of surfaces *via β*-CD host-guest interactions by varying the localized and average ligand density. It is long known that the ligand presentation at interfaces has a significant influence on their interaction with biomolecules and subsequent biological responses. Lysine-plasminogen (Lys-Plg) was chosen as a model to investigate specific protein binding capability of ligand-modified surfaces. *Via* surface-initiated atom transfer radical polymerization (SI-ATRP) a bioinert surface was generated by poly[2-hydroxyethyl methacrylate-*co*-(adamantan-1-yl)-methyl methacrylate] on a silicon wafer. Lysine-monosubstituted *β*-CD containing one lysine per *β*-CD moiety and lysine-persubstituted *β*-CD containing 7 lysines per *β*-CD moiety were integrated onto the surfaces *via* host-guest interactions between *β*-CD and adamantane. The average lysine density of the surface could be modulated by changing the lysine valency on the *β*-CD scaffold as well as by using pure *β*-CD to dilute the per-6-lysine-*β*-CD. [85]

The biocompatible nature and the self-assembling properties with multiple guest molecules in a variety of different applications yield CD perfectly suitable for the use in biomedical applications.

2.3.2   Host guest complexes based on cucurbit[n]uril

Host-guest systems based on the cucurbit[n]uril (CB) host have the ability to complex various guests in their cavity, depending on the corresponding ring size. Although CBs were first synthesized in the early 1900s, the structure was not revealed until 1981. CB[n]s can be obtained by condensation of glycoluril and formaldehyde giving rise to macrocyclic structures of glycoluril repeating units (typically n = 5 - 8) linked *via* methylene groups. [86] CBs have been explored in a multitude of applications, ranging from drug delivery, molecular recognition and

self-assembly and as multivalent scaffold.[87–89] Recent studies propose that the electrostatic positive outer surface of CB[n]s provides a balance in the various supramolecular driving forces for CB[n] assembly. [86] CB[5] has the ability to bind gases and small solvents (i.e. Ar, N_2O, CO_2, CH_3OH and CH_3CN), investigated both in solution state and in solid state. CB[6] can bind ω-amino acids, ω-amino alcohols, aliphatic alcohols, acids and nitriles, bipyridine derivatives, aromatic compounds, non-ionic surfactants and poly(ethylene glycols), cyclodextrins, diamides, and α-amino acids and dipeptides. CB[7]s have a somewhat larger cavity and are therefore able to bind a wider range of guests, among which positively charged aromatic compounds including adamantanes and bicyclooctanes, naphthalenes, stilbenes, viologens, o-carborane, ferrocene and cobaltocene derivatives and metal complexes. CB[8]s have a similar cavity size as γ-CD, with less conformational flexibility. CB[8] prefers to bind positively charged guests by ion-dipole interactions, where the guests either fill partly or completely fill the cavity. Moreover, CB[8] is able to host two aromatic rings, leading to the formation of termolecular complexes in a cooperative fashion. In biomedical applications, the aromatic amino acid phenylalanine is mostly used through homogeneous termolecular complex formation. Hetero-termolecular complexes with CB[8] have also been reported, i.e. methylviologen and tryptophan or naphthalene. [90,91]

Urbach *et al.* described the selective recognition and noncovalent dimerization of *N*-terminal aromatic peptides in aqueous solution by CB[8], showing cooperative binding with high affinity, $K = 10^{11}$ M^{-2} for the ternary complex in aqueous medium at neutral pH. [92] Moreover, Urbach reported on the charge-mediated recognition of *N*-terminal tryptophan and methylviologen in aqueous medium by CB[8], with affinities in the range of $K_a = 1.3 \times 10^5$ M^{-1}. [93]

Various examples have been reported where these strategies have been applied either on silicon, gold or glass substrates.[71] Jonkheijm *et al.* reported on highly ordered monolayers of *β*-CD on gold and glass surfaces to immobilize glycoconjugates *via* photoresponsive azobenzene moieties. Azobenzenes are able to bind in the CD and CB cavity in the stable *trans* form and can be released upon UV-irradiation and subsequent isomerization into the *cis*-azobenzene. [15] Moreover, nanostructured materials based on cucurbituril supramolecular chemistry approaches have grown interest in recent years.[94]

Scherman *et al.* applied the CB[8] host-guest chemistry extensively in order to develop supramolecular hydrogel formulations with many potential applications, which is beyond the scope of this chapter. [95–98]

Bilayer lipid membranes are of interest in the design of biofunctional coatings, controlled release technologies and biosensors. Recently, Brunsveld *et al*. reported on the controlled immobilization of proteins on DOPC lipid bilayers using supramolecular noncovalent interactions based on CB[8] (Figure 2.7 C). They relied on the formation of the ternary complex in two-steps where first the methylviologen binds, followed by the binding of an indole. Both binding events have individual binding constants in the range of $K_a = 10^5$ M^{-1}. An YFP model protein with an *N*-terminal tryptophan-glycine-glycine (WGG-YFP) motif was expressed and methylviologen guests anchored with a cholesterol moiety to enable
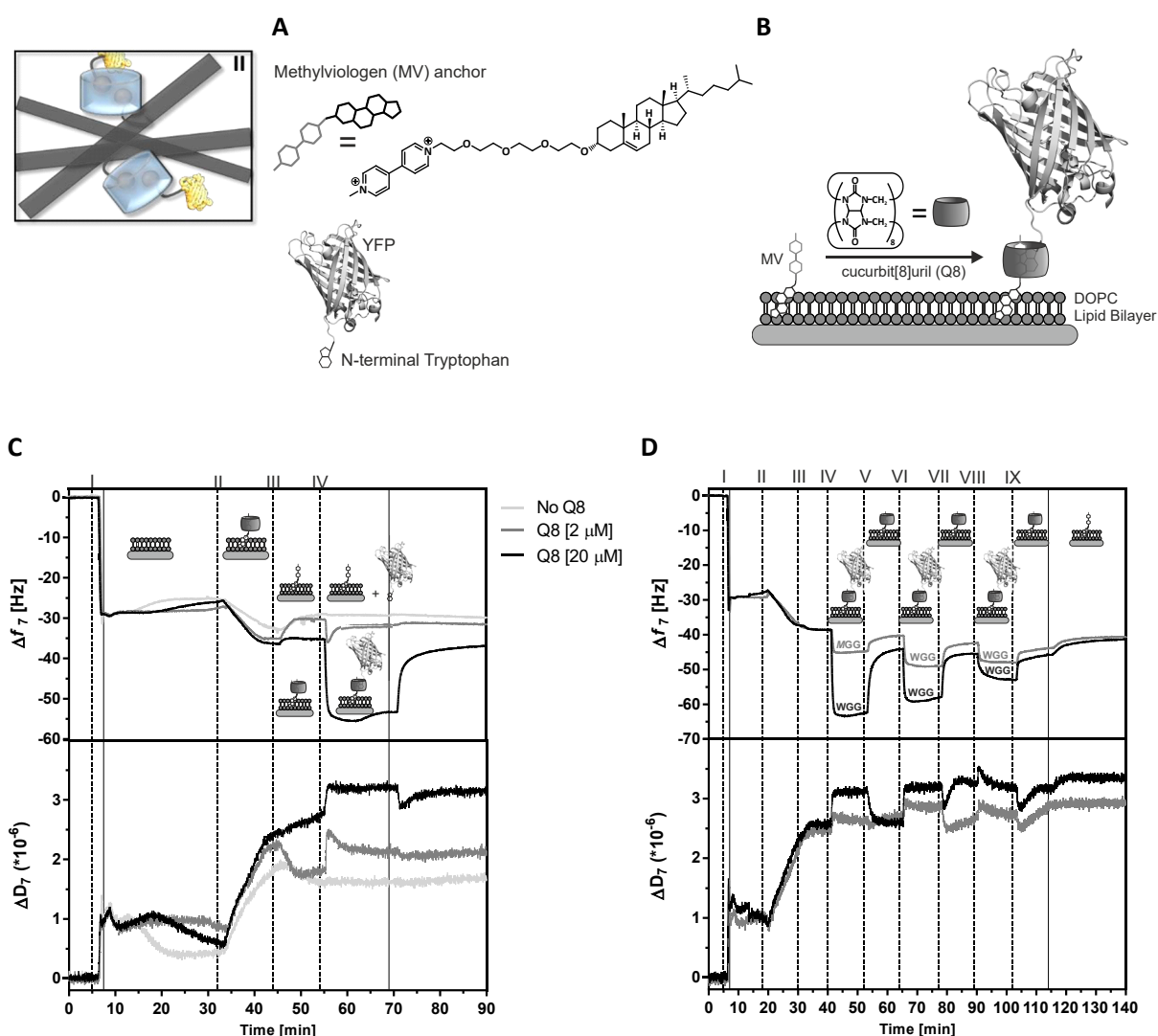
Figure 2.7. Supramolecular protein immobilization on lipid bilayers, A) Chemical structures of the methylviologen (MV) anchor and the WGG-functionalized YFP protein (WGG-YFP), B) Schematic overview of the supramolecular protein immobilization on a DOPC lipid bilayer using CB[8] macrocyclic host, which can host simultaneously an N-terminal tryptophan and a methylviologen, C) QCM-D sensogram with both the frequency response (Δf) (top) and dissipation response (ΔD) (bottom) demonstrating the influence of CB[8] concentration on the WGG-YFP binding on the bilayer and D) QCM-D sensogram that shows the stepwise assembly of the supramolecular complex with both the frequency response (Δf) (top) and dissipation response (ΔD) (bottom), I: formation of the lipid bilayer, II: incorporation of the MV anchor (5 µM) with CB[8] (50 µM) , IV: WGG-YFP (2 µM, black line) and MGG-YFP (2 µM, grey line) administration in the presence of CB[8], V: removal of protein off the surface by washing with CB[8] (50 µM), which was repeated twice afterwards (VI – IX). Reprinted with permission from [99]. Copyright Wiley-VCH Verlag GmbH & Co. KGaA, Weinheim.

incorporation into the lipid bilayer (Figure 2.7 A,B). The supramolecular complex formation in solution was studied using isothermal titration calorimetry (ITC) revealing an enthalpy driven process. Subsequent study of supramolecular protein immobilization was studied with quartz crystal microbalance with dissipation monitoring (QCM-D). They showed subsequently the immobilization of the lipid bilayer, the incorporation of the cholesterol-methylviologen anchor into the bilayer and the WGG-YFP assembly upon CB[8] administration (Figure 2.7 C). Moreover, the protein immobilization proved to be reversible by subsequently assembly and disassembly steps up to three times (Figure 2.7 D). The system provides a method for site-

selective reversible protein immobilization on supramolecular material surfaces. [99] The association constants and therefore the stability of the supramolecular complexes formed by CBs as well as solubility concerns at high concentrations are a drawback for these system in the development of new generation biomaterials. However, the high selectivity in host-guest interactions and the tunable ring sizes of CBs, affords this class of materials with high potential for future developments.

2.3.3   Crown ether based host-guest systems

Crown-ether based molecular recognition motifs have been widely explored to fabricate supramolecular polymers with interesting properties due to their good selectivity and convenient environmental responsiveness. The host-guest complex can be applied to afford rotaxanes, mechanically interlocked structures. Mechanical bonds can be an integral part of the polymer backbone and thereby introduce mobility elements such as rotation and elongation into the main chain, resulting in viscoelastic material properties. [100] Crown ethers are known as the first generation of supramolecular host moieties, explored by Stoddart *et al*. [101] Typically, crown ether based host-guest assemblies are a class of self-assembled structures in which cyclic species are associated onto rod-like molecules and are locked by two bulky moieties at the ends, preventing dissociation. [102] Crown ether hosts, such as bis(*p*-phenylene)-34-crown-10, bis(*m*-phenylene)-32-crown-10 and dibenzo-24-crown-8 are involved to afford host-guest complexes and create rotaxanes. The guest moiety is able to interlock into the crown ether, creating a *pseudo*-rotaxane in case there are no bulky stoppers present and upon the addition of a bulky moiety at the end of the guest a rotaxane is formed.

Stang *et al.* reported on the development of functionalizable supramolecular polymer networks based on hierarchical unification of coordination-driven self-assembly, hydrogen bonding and crown-ether based host-guest interactions. A Pt(II)-pyridine motif was used to assemble a metallohexagon bearing two different functional moieties, a UPy group and a benzo-21-crown-7 (B21C7) motif. The complementary hydrogen bonding interactions of the UPy-groups result in the formation of a hexagon-cored supramolecular polymer network with free B21C7 moieties. Orthogonal functionalization is obtained by crown ether-dialkylammonium salt-based host-guest interactions, which does not interfere with the structure of the supramolecular network. The combination of metal-ligand coordination, hydrogen bonding and host-guest interactions in a hierarchical fashion has proven to be an elegant approach to develop functionalizable supramolecular polymers. [103]

Huang *et al.* showed that supramolecular nanofibers and nanogels exhibit unique mechanical properties, which led to the development of a host-guest monomer containing a B21C7 group and a second ammonium salt moiety connected *via* a long alkyl chain. Upon self-assembly, linear high molecular weight supramolecular fibers form in solution, with a high viscosity. *Via* electrospinning, these polymers can form smooth nanofibers. This approach is unique considering the low molecular weight monomers and paves the way to post-functionalize these materials in order to introduce surface bioactivity. [104,105]

In order to prevent protein adhesion, non-adhesive surfaces can be developed as well as slow releasing agents can be incorporated into the material. Ratner *et al.* developed a surface treatment to prevent nonspecific protein adhesion and reduce or eliminate subsequent bacterial adhesion and biofilm formation by plasma deposition. The resistance to proteins and initial bacterial attachment in plasma deposited crown ether thin films were investigated. [106] In the interest of reduced bacterial biofilm deposition, Denes *et al.* report on the deposition of PEG-like structures onto stainless steel surfaces *via* a cold-plasma-enhanced process. *Via* the plasma treatment, a macromolecular network is deposited onto the stainless steel. The plasma treated surfaces were more hydrophilic, showed reduced surface roughness as compared to the untreated materials and significant reduced bacterial attachment and biofilm formation. [107]

Crown ethers have received considerable interest in materials science research. Their specific ligand binding and ion-specific interactions can be incorporated into material networks to confer specific design criteria.

2.3.4 Calix[n]arenes host-guest assemblies

Calix[n]arenes, a generic nomenclature for a class of macrocyclic compounds, are composed of phenolic units which are connected *via* methylene bridges. Baeyer *et al.* proposed the synthesis of these moieties *via* reaction of phenols and aldehydes under strong acidic conditions. The *n* in the nomenclature of the calixarenes denotes the number of phenolic units that are linked *via* methylene bridges, providing the cavity of the molecule. Among many applications of calixarenes, to date the immobilization of calixarenes on a solid support is a prominent applied process to construct various calixarene-based materials. [108] Moreover, calixarene-based supramolecular polymeric materials are equipped with interesting properties such as self-healing ability, and electrochemical-responsiveness. The structure enables calixarenes to feature 'molecular basket' properties for neutral and ionic guests.

Ertul *et al*. reported on a novel approach where calixamide nanofibers were produced by electrospinning and subsequently demonstrated toxic anion binding to the fiber structures. Polyacrylonitrile (PAN) nanofiber-based calixarene derivatives were electrospun to develop functional nanofibers. The fiber diameter of PAN electrospun fibers increased upon the addition of calixarenes. Toxic anion extraction of chromium (Cr(IV)) was studied from aqueous medium and revealed successful adsorption of the toxins on the nanofiber-based calixamide material. This system contributes to the development of functional nanofibers for a variety of applications, among which are controlled drug delivery, catalysis and filtration. [109]

Calixarenes are an interesting class of supramolecular host-guest assemblies, owing to their ease of modification with respect to shape and size. These properties give rise to an expanding array of guest molecules that can assess different biomedical applications, due to the ability to either expand or shrink depending on the flexibility in the upper-rim or lower-rim components of the calixarenes.

To conclude, supramolecular polymeric materials that are equipped with host-guest assemblies form an interesting class of materials. As a result of the specificity of the host-guest interactions, functionality can easily be introduced. Host-guest assemblies can improve the selectivity of biomolecule-ligand binding as a result of the recognition-directed interactions. The high selectivity, strong yet dynamic interactions and the reversible nature of these assemblies can be exploited to mimic complex molecular-recognition systems as they appear in nature that are able to adapt to changes in the environment.

2.4 Modification strategies to introduce bioactivity into supramolecular thermoplastic elastomer materials

An elegant approach to introduce functionality at materials surfaces is *via* the modular incorporation of additives that can easily be mixed and matched with the bulk supramolecular polymer material. The supramolecular motif, which is the driving force for self-assembly is introduced in the bioactive moiety as well, to facilitate modular incorporation.

Structural biomaterials that exhibit extraordinary properties that are specifically designed for a certain application, often require hierarchical structure formation on different length scales. Supramolecular polymers and networks based on molecular recognition units that guide the self-assembly give rise to elastomeric materials with tailorable mechanical properties. This class of materials show excellent processing and self-healing properties and in particular show a modular tunable nature. Incorporation of structuring components as well as the prevention of nonspecific surface reactions and the introduction of bioactivity can easily be achieved, while mechanical properties of the bulk remain unchanged. Supramolecular elastomeric materials based on different supramolecular motifs, i.e. polyurethanes, benzene tricarboxamides, bisurea and ureido-pyrimidinone (UPy) moieties are highlighted.

2.4.1 Design criteria for supramolecular thermoplastic elastomer based biomaterials

The design criteria of a synthetic biomaterial that is able to support both soft and mechanically active tissues, should meet a range of requirements including biodegradability, biocompatibility, elasticity, responsive mechanical properties, processability, adaptability, modularity and responsive behavior. Supramolecular thermoplastic elastomers combine good material properties with low-viscosity melt and thereby they are easy to process. Specifically, due to additional secondary interactions (i.e. lateral hydrogen bonding), polymers are perfectly suitable to be applied in a biological environment and thereby allow for cell attachment and tissue growth. Many processing methods have been reported in order to prepare porous scaffolds composed of small diameter fibers, including electrospinning, melt spinning, solvent casting, thermally induced phase separation and phase inversion methods. As a result of both the mechanical and physical strength as well as the elastomeric properties of supramolecular thermoplastic elastomers, these materials are applied in a broad range of biomaterial applications, including small-diameter vascular grafts, cardiac patches, blood

vessels, renal living membranes and scaffold materials in regenerative medicine. Generally, these materials are processed using harsh conditions (i.e. organic solvent or high temperatures) but act at the interface in aqueous environment.

2.4.2 Supramolecular thermoplastic elastomers based on polyurethanes

Thermoplastic polyurethanes (TPU) were first developed in the late 1930s and to date are widely used in industrial applications due to their interesting properties. In the late 1960s polyurethane elastomers were first considered as potential biomaterials by Boretos and coworkers. [110] They are thermoplastic elastomer materials composed of hard and soft segments that can be synthesized *via* reaction between diisocyanate and diol. The soft blocks are formed by a polyol and an isocyanate, and are responsible for the flexibility and elastomeric character of the materials. The hard block, constructed from a chain extender and an isocyanate results in the toughness and physical performance of the TPU material. High polarity segments in the hard phase result in crystalline domains whereas low polarity segments determine the soft flexible matrix phase. The elastic behavior of TPU arises from the crystalline domains that act as physical crosslinks in the materials, and the elongation behavior is determined by the flexible chains. These properties result in high elongation and tensile strength and the elastic behavior. Moreover, at elevated temperatures, TPU becomes soft and easily processable, and upon cooling the materials harden. Supramolecular TPU materials benefit from reversible and stimuli-responsive behavior as a result of the noncovalent links between the building blocks and rely on intermolecular recognition to form complex architectures. In contrast to covalent polymers, temperature elevation in supramolecular TPU leads to dissociation of the noncovalent interaction, resulting in a decrease in viscosity and mechanical properties allowing them to be easily processable and giving rise to self-healing and shape memory properties. [111]

The main classes of TPU materials that find their application in the biomedical field consist of polyester TPU, polyether TPU and polycaprolactone TPU. TPU biomaterials are of particular interest as materials for tissue engineering, where mechanical properties are very important design criteria.

In development of functional materials for biomedical applications, Wagner *et al.* explored thermoplastic elastomers exhibiting bioactive components. To improve thromboresistance in respiratory assist devices, they developed a hollow fiber membrane which was modified with functional zwitterionic macromolecules. These devices aim for optimized performance in terms of gas transfer efficiency and thromboresistance. They report on three zwitterionic macromolecules that were attached to the hollow fiber membrane surface in order to improve thromboresistance; carboxyl-functionalized zwitterionic phosphorylcholine (PC), sulfobetaine macromolecules through thiol-ene radical polymerization and low-molecular weight sulfobetaine –*co*-methacrylic acid block copolymer, respectively, prepared *via* reversible addition-fragmentation chain transfer (RAFT) polymerization and covalently immobilized onto the hollow fiber membrane. The zwitterionic surfaces showed an increase in phosphor and sulfur surface content and a significantly lower

platelet deposition as compared to unmodified and heparin-coated control surfaces. Also the CO_2 removal rate of the zwitterionic surfaces was increased as compared to the control surfaces. Zwitterionic coatings display a promising approach in the performance of artificial lung devices. [112]

In another study, Wagner *et al.* reported on a biodegradable, elastomeric polyurethane material containing a coating with an anti-proliferative agent released in a controlled fashion for cardiovascular stent applications. The degradation behavior, hemocompatibility and drug release were investigated for poly(carbonate urethane) urea (PCUU) and poly(ester urethane) urea (PEUU) coated magnesium alloy stents, with poly(lactic-co-glycolic acid) (PLGA) coated and bare stents as controls. PCUU showed significant decreased magnesium alloy erosion as compared to the PEUU and PLGA coated and bare magnesium alloy stents. The PCUU coatings also showed reduced platelet adhesion and inhibited proliferation was observed upon paclitaxel loading in the PCUU coatings. [113] To apply multilayer coatings of biodegradable PEUU embedded with anti-proliferation drug paclitaxel surface modified metallic biomaterials, a direct-inkjet technique was employed, which provides selective patterning capability to deposit multimaterial coatings on three-dimensional implant devices, such as cardiovascular stents. To study the influence of drug loading and coating thickness, drug release profiles were studied to obtain tunable release kinetics. Paclitaxel loaded coatings showed a significant reduction in platelet adhesion as well as decreased cell proliferation when compared to the unloaded control coatings. [114] Another elegant study reports on the prolonged effect of surface modification by the incorporation of pendant reactive groups in the bulk (Figure 2.8 B). Biodegradable PEUU polymers with variable amino content were developed, which could be functionalized with carboxylated phosphorylcholine in order to generate PEUU-phosphorylcholine polymers (Figure 2.8 A). Surfaces were characterized using XPS and FTIR in order to study the different functionalization steps. Moreover, mechanical, thermal and degradation properties were determined for the amine incorporation and the subsequent phosphorylcholine modifications. Upon amine incorporation the water absorption increased and further increased after phosphorycholine conjugation. In wet conditions the tensile strength and initial modulus decreased with increasing hydrophilicity, but remained in the range of 5-10 MPa and 10-20 MPa, respectively (Figure 2.8 C). As expected, phosphorylcholine conjugation resulted in reduced platelet adhesion and reduced cell proliferation (Figure 2.8 D). [115]

A nonthrombogenic biodegradable elastomeric polyurethane with variable sulfobetaine content was synthesized from a mixture containing PCL-diol and sulfobetaine-diol in various combinations, reacted with diisocyanatobutane and chain extended with putrescine. At higher sulfobetaine content, the wet tensile strength increased as well as breaking strain and moreover, thrombotic deposition was reduced. *Via* electrospinning these materials could be processed into vascular conduit formats. [116] Synthetic poly(ester urethane)urea (PEUU) electrospun (diameter 100-900 nm depending on the polymer concentration) scaffolds were prepared as an ECM mimic. Collagen was introduced into the PEUU by blending in order to increase cell adhesion and mechanical properties of the material. The results demonstrate an
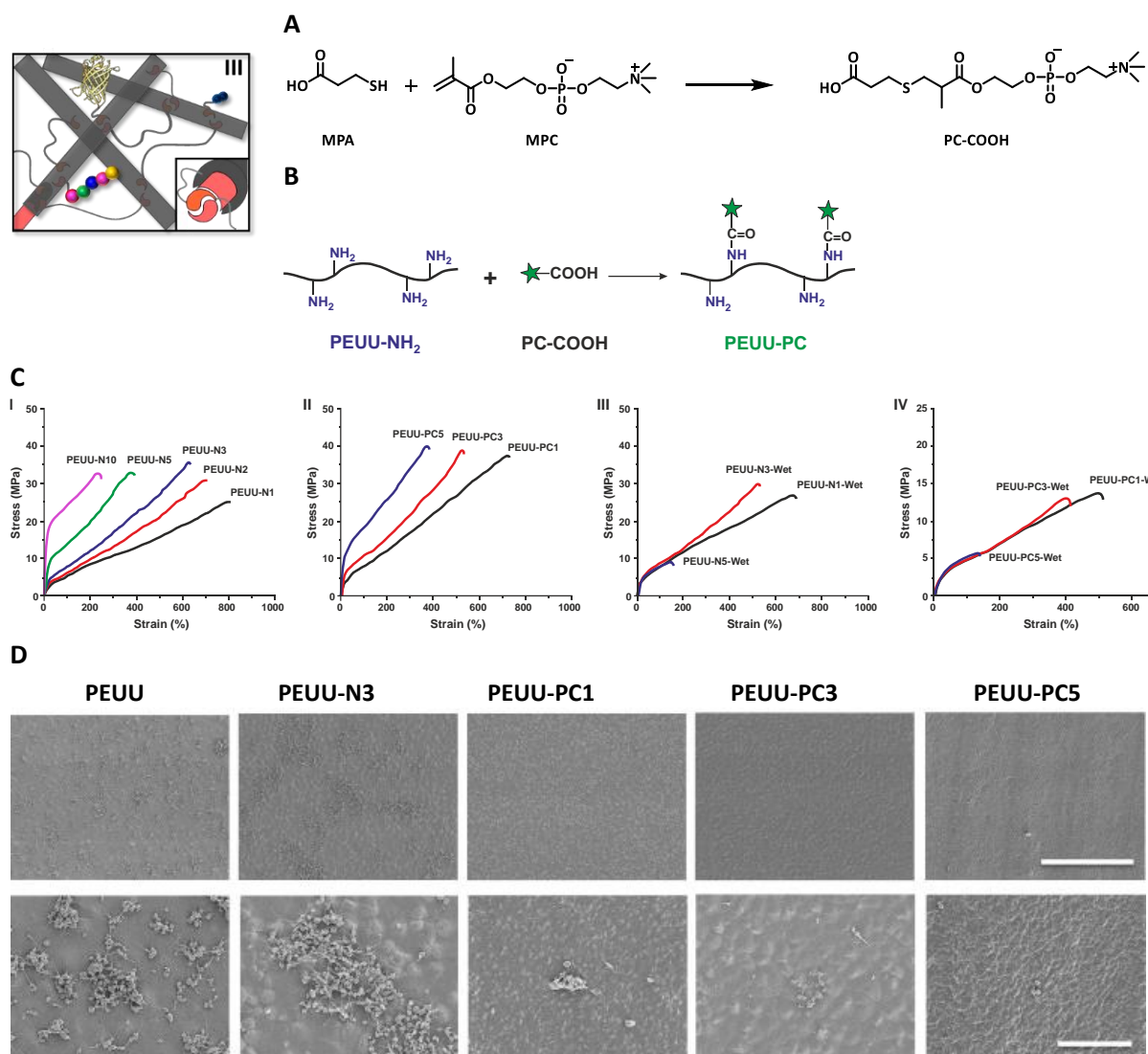
Figure 2.8. Prolonged effect of surface modifications is achieved by the incorporation of pendant reactive groups in the bulk, a) Synthesis of carboxylated phosphorylcholine (PC-COOH) that can be conjugated to the poly(ester urethane) urea (PEUU) elastomers for subsequent bulk modifications, b) Schematic representation of the bulk functionalization to generate PEUU-PC polymers, c) Stress-strain curves of cast polyurethane films under dry conditions: (I) PEUU-NH$_2$, (II) PEUU-PC, and wet conditions: (III) PEUU-NH$_s$-Wet, (IV) PEUU-PC-Wet, immersed in water (37 °C) for 24 h and d) Platelet adhesion after 3h contact with ovine blood on cast films of PEUU, PEUU-N$_3$, PEUU-PC1, PEUU-PC3, PEUU-PC5, scale bar = 50 µm top row, 10 µm bottom row. Reprinted from [115] with permission from Elsevier.

approach to mimic elastic ECM properties by relying on synthetic components that provide mechanical properties and function comparable to native matrix and proteins can provide the desired bioactivity. [117] To stimulate wound healing, the hollow fiber membrane could be administered at the wound to provide local and externally regulated controlled release of regenerative factors and after sufficient healing, these materials desirably degrade themselves. Therefore, an enzymatically biodegradable thermoplastic elastomer was synthesized consisting of polyurethane urea (PUU) based on polycaprolactone (PCL) as mechanically strong polymers and polyethylene glycol (PEG) as soft segments and a collagenase-sensitive peptide (GGGLGPAGGK) as a chain stopper. Electrospun fibers exhibited appropriate mechanical properties as a result of the PCL, showed sustained release of a model

protein as a result of the PEG incorporation and were susceptible to collagenase degradation as a result of the incorporation of the peptide. [118]

In conclusion, biomaterials exhibiting elastomeric material properties are very suitable candidates for a multitude of different biomedical applications due to the robust mechanical properties and the relatively easy modification strategies in order to either incorporate bioactivity or delivery capability.

2.4.3 Supramolecular polymers based on benzene-1,3,5-tricarboxamide nanorods

Supramolecular materials based on the triple hydrogen bonding motif benzene-1,3,5-tricarboxamide (BTA) have been extensively studied. This motif forms 1D columnar structures in solution as well as in the solid state as a result of a three-fold intermolecular hydrogen bonding in a helical type of arrangement. [119–121] However, the amount of publications where they are applied as solid supramolecular materials is limited. Mes *et al.* reported on the use of the BTA motif for a supramolecular material based on phase segregated nanorods in a polymer poly(ethylene butylene) (PEB) matrix. Telechelic polymers end-capped or copolymerized with BTAs both result in the formation of supramolecular material. As a result of the intrinsic phase segregation behavior of the BTA nanorods with the amorphous PEB, thermoplastic elastomeric behavior is obtained. The phase segregation results in strong multiple cross-linking anchoring points with dimensional order within the soft PEB polymer matrix, which in turn leads to materials exhibiting thermoplastic elastomeric properties. [122] This new class of supramolecular thermoplastic elastomer can find potential applications in the biomedical engineering field. However, processing as well as bioactivation and surface enhancement still remains unexplored.

2.4.4 Supramolecular thermoplastic elastomers based on the bisurea hydrogen bonding motif

The mechanical properties as well as the processability of the polyamides and polyurethanes have been an inspiration in the synthesis and development of new polymers where the amides and the urethanes were replaced with urea motifs, due to their stronger bifurcated hydrogen bonding. Although the N,N'-dimethylurea and N,N'-diethylurea motifs are well known and self-assemble in nonpolar solvents, introduction of branching increases solubility. Noncovalent cross-links of the supramolecular hydrogen bonding motifs between the polymer chains are able to crystallize. The thermoplastic elastomeric behavior of the materials is a result of breaking of the crosslinks upon heating and thereby a decrease in viscosity.

Leibler and coworkers developed a rubber-like system with recoverable extensibility. Network formation occurs after mixing ditopic and multitopic molecules with (amidoethyl)-imidazolidone, bis(amidoethyl)urea and diamidotetraethyltriurea side moieties which act as multiple-hydrogen-bonding crosslinkers. Upon fracturing, the materials will self-heal when bringing the two surfaces together at room temperature and the behavior turned out to be

reproducible many times. [123] The hydrogen bonded network does not crystallize. At low temperatures hydrogen bonds act as crosslinks and result in soft rubber like material properties, whereas at elevated temperatures these hydrogen bonds are broken and the material becomes a viscoelastic liquid.

Functionalization of poly(ε-caprolactone) (PCL) oligomers with urea motifs results in nanofiber morphology. [124] Due to synergistic aggregation of a second urea in the bisurea motif, these moieties aggregate in a cooperative fashion. Moreover, the bisurea motif is able to bundle together and crystallize into long nanofibers that can act as supramolecular crosslinks. The mechanical properties of these materials are perfectly suitable to be used in soft tissue engineering applications. Since there are only two urea groups involved in the hydrogen bonding, these segments stack exactly on top of each other, forming long nanofibers. Guest molecules can selectively be incorporated into these supramolecular polymers if they fit the supramolecular motif. The design of thermoplastic elastomers with monodisperse bisurea hard blocks allows for the incorporation of guest molecules with a matching bisurea moiety enabling molecular recognition and thereby selective modulation of mechanical properties. [125] This selective incorporation reinforces the material and provides good mechanical properties. It was shown that the supramolecular reinforcement fillers can be successfully incorporated into the bisurea polymers and thereby strengthen the materials from 12 to 20 MPa. [126,127] The concept of self-sorting in elastomeric matrices with bisurea polymers with only small differences in structure (i.e. variations of one or a few methylene units) between the urea groups has also been demonstrated. [128] Thermoplastic elastomers are proposed to have great potential to be used as biomaterials, as a result of their elasticity, toughness properties and modular character with regard to introducing specific bioactive functionality, i.e. peptides or growth factors. Biodegradable polyurethane(urea)s based on poly(ε-caprolactone) and 1,4-diisocyanatobutane have been shown to be biocompatible and fulfill mechanical requirements. [129,130] Upon the introduction of a bisurea motif, supramolecular additives can be introduced to provide the materials with a desired function, i.e. bioactivity or anti-fouling behavior. The mechanical properties of the materials can easily be tuned by the choice of polymer backbone in order to meet the requirements of the designated environment.

2.4.5   Ureido-pyrimidinone (UPy) based supramolecular thermoplastic elastomers

A range of supramolecular polymers have been developed based on a synthetically accessible quadruple hydrogen bonding unit with a high association constant, i.e. the UPy moiety. [131] *Via* a quadruple hydrogen bonding motif, the UPy-moiety is able to dimerize with an association constant exceeding 10^6 M^{-1} (K_{dim} $6 \cdot 10^7$ M^{-1} in chloroform, $1 \cdot 10^7$ M^{-1} in chloroform saturated with water and $6 \cdot 10^8$ M^{-1} in toluene). [131,132] The UPy-motif is present as a mixture of different tautomers, two keto tautomers that display an AADD hydrogen bonding array and an enol form that forms a DADA hydrogen bonding array (Figure 2.9). It has been shown that the keto tautomer bears less repulsive secondary interactions and concomitant higher dimerization constant than the enol tautomer. [133] The UPy-moieties can either be used

to end-functionalize short telechelic prepolymers, yielding bifunctional supramolecular oligomers or can be incorporated in the polymer main chain, forming a supramolecular chain-extended UPy-polymer (CE-UPy).

In order to obtain a high degree of supramolecular polymerization and thereby real polymer-like behavior, the association constants need to be sufficiently high. [131] The ease of UPy-moiety synthesis facilitates large scale production of supramolecular polymers, with interesting material properties. Many examples have been published, including telechelically UPy-functionalized polydimethylsilanes (PDMS), [131,134] PEB, [135–137] polyethers, [135,138,139] polycarbonates, [135,140] polystyrenes (PS) [141] and polyesters. [135,142–144]
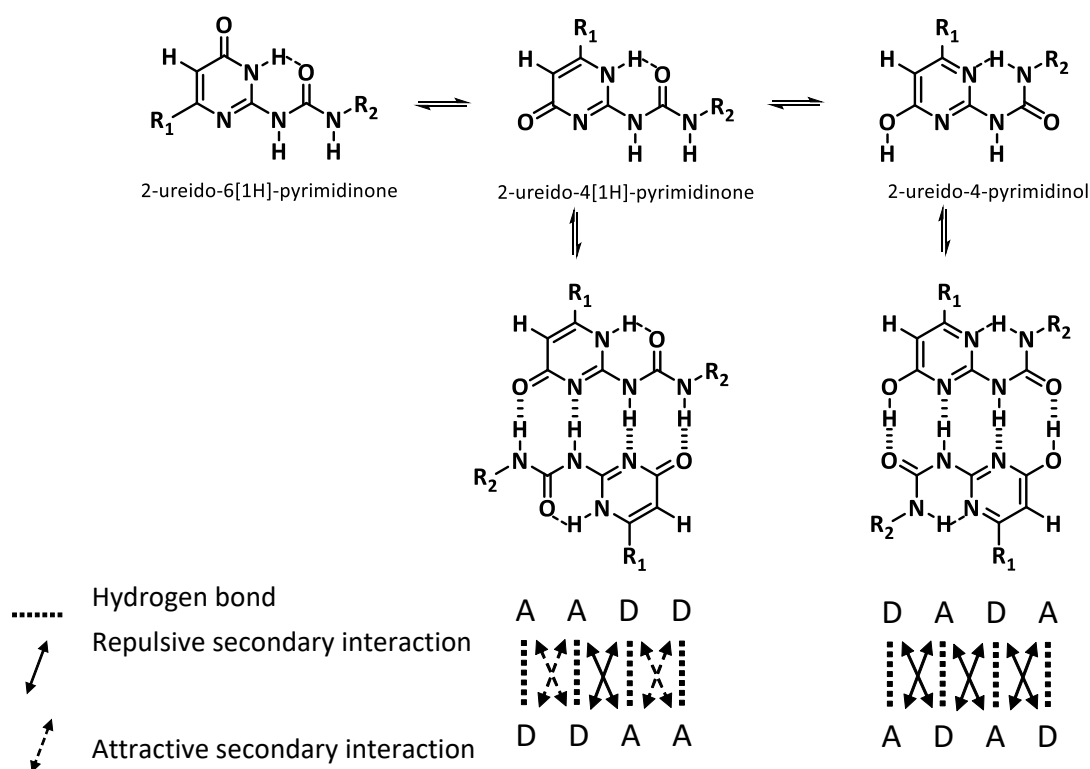
Figure 2.9. Tautomeric forms and dimers formed by the ureido-pyrimidinone moiety.

Upon UPy-functionalization, the material properties change drastically. As a result of the reversible hydrogen-bonding nature of the UPy, at high temperatures the non-covalent interactions are broken, which results in materials that exhibit properties similar to low molecular weight oligomers. The material properties can be controlled based on the oligomers that are introduced, i.e. amorphous or semi-crystalline oligomers. Phase separation behavior can be introduced by the incorporation of additional lateral interactions. As a results of these lateral interactions, the UPy-polymers not only polymerize in a linear fashion, but the dimers that are formed are also able to stack as a result of lateral hydrogen bonding of urethane or urea functionality. Reinforcement of the materials by the additional lateral interactions increases the mechanical properties and results in supramolecular thermoplastic elastomer materials. [137,145,146] Moreover, these material properties as a result of the strong

secondary interactions yield beneficial processing conditions for these materials as well. The reversible and highly directional secondary interactions result in polymeric material properties, in concentrated solutions and in bulk. Highly viscous amorphous PEB becomes a strong and flexible rubber-like material when UPy-moieties are introduced *via* a urethane linker [142,143,147] When UPy-moieties are incorporated into the main polymer chain, chain-extended UPy-polymers can be synthesized with improved material properties while the materials still benefit from the modular character. [143]

The ease of processing of these supramolecular polymers in the melt or in solution and excellent properties in the solid state, their compatibility with other systems and the reversibility of the supramolecular motif yields these materials perfectly suitable for application as supramolecular biomaterials, which were discussed in chapter 1.

2.4.6 Supramolecular biomaterials towards *in vivo* applications

Supramolecular biomaterials that consist of functionalized surfaces and that can be processed into a desirable format, have already found a few applications *in vivo*. [148,149] Tirrell *et al.* reported an approach to promote a protective immune response *in vivo* based on self-assembled PA micelles that contained a cytotoxic epitope. They synthesized PA with two C_{16} aliphatic tails conjugated to a peptide derived from a cytotoxic T-cell epitope from the model tumor antigen ovalbumin that self-assembled into cylindrical PA displaying a high density of the peptide. These constructs induced an immune response *in vivo* in mice, tumors showed a significantly slower growth which resulted in longer survival times. The PA system acts as an antigen depot, thereby concentrating the antigen peptides and protecting them from degradation which as a result prolongs antigen exposure to the immune system. [150]

In another study, Hess *et al.* developed a coating for polymer stents in order to prevent neointimal hyperplasia. Based on the assumption that platelet and inflammatory cell recruitment can induce neointimal proliferation, this coating was developed to reduce cell-stent interactions. The copolymer coating is composed of a poly(L-lysine) backbone, grafted with poly(ethyleneglycol) (PEG), developed by Hubbell *et al.*, that can nonspecifically adsorb to the stainless steel stent surface. *In vivo* studies were performed in which the coated and uncoated stents were implanted in an epicardial coronary. Histological examination revealed that the coated stents developed significantly less neointimal hyperplasia as compared to the uncoated controls. [151]

Wippermann *et al.* work on the investigation of bacterial cellulose (BC) as a potential scaffold for application as small-diameter vascular grafts. BC has been characterized as a biomaterial with high mechanical strength and high water retention values. They investigated the *in vivo* performance of BC small-diameter grafts with regard to technical feasibility, functional performance, the ability to provide a scaffold for neoformation of a vascular wall as well as the proinflammatory potential in sheep. The study showed that BC grafts provide a scaffold for cell ingrowth and support tissue engineering performed by the organism itself. [152]

Hollinger *et al.* reported on the synthesis, biodegradability and biocompatibility of lysine diisocyanate (LDI) and glucose-based polymer. The materials are synthesized *via*

polymerization of highly purified LDI with glucose and after subsequent hydration, a spongy matrix is spontaneously formed. In aqueous solution these materials degraded and yielded lysine and glucose degradation products. *In vivo* examination for 8 weeks revealed that subcutaneous implantation of hydrated matrix degraded three times faster than *in vitro*. No immunogenic response was observed, nor was an antibody response induced in the host. Histological analysis of the implanted polymer showed that a minimal foreign body response had occurred and the formation of a capsule around the degrading polymer. [153]

Both chemical and biological properties of supramolecular UPy-polymers based on oligocaprolactones were investigated in our group. The development of materials with different ratios of oligocaprolactones that were end-functionalized with UPy-moieties or chain-extended with UPy-moieties in the main chain have been reported. Due to the high crystallinity of the end-functionalized UPy-polymers, these polymers are more stiff and brittle, and subcutaneously implanted discs fractured. A low inflammatory response was observed, as well as fibrous capsule formation, demonstrating inertness of the material. On the other hand, the chain-extended UPy-polymers show less crystalline domains and bear more flexible properties. After *in vivo* implantation, deformation of the material was observed as well as cell infiltration. A mixture of the two different polymers (20% end-functionalized UPy-polymer and 80% chain-extended UPy-material) showed flexible material properties without visible deformation after *in vivo* implantation. A mild foreign body response observed upon implantation of the pristine polymer mixture. This study demonstrates the tunability of material properties based on a modular approach. [143] Recently, an *in-situ* approach for early cellularization of supramolecular vascular grafts substituted with supramolecular stromal cell-derived factor 1α derived peptides was presented. SDF1α is a powerful chemoattractant of lymphocytes, monocytes and progenitor cells, and, plays an important role in cellular signaling and tissue repair. The SDF1α-derived peptides were functionalized with a supramolecular UPy motif to facilitate modular incorporation into UPy-modified polymer scaffolds and facilitate bioactivation of the materials. As a proof of concept *in vivo* the bioactivated electrospun scaffolds were implanted as rat abdominal aorta interposition grafts. After 7 days an increased cellularity by CD68$^+$ cells was observed, indicating that a synthetic, bioactivated, cell-free supramolecular biomaterial can attract and stimulate leukocyte populations upon SDF1α incorporation. This is a first step towards *in situ* cardiovascular tissue engineering using electrospun supramolecular bioactive scaffolds. [154]

In a similar way, a non-cell adhesive vascular graft based on a modular supramolecular approach was developed. Here UPy-modified polycaprolactone (UPy-PCL) and UPy-modified poly(ethylene glycol) (UPy-PEG) or chain-extended PCL (CE-UPy-PCL) were used (Figure 2.10 A). Electrospun CE-UPy-PCL and CE-UPy-PCL:UPy-PEG (90:10) were evaluated as vascular grafts *in vivo* in a rat model and the non-cell adhesive grafts showed hardly any cell infiltration after 48 hours, demonstrating the non-fouling character of these materials (Figure 2.10 B,C,D). In current studies these non-cell adhesive materials are reactivated upon the incorporation of a small fraction of UPy-modified bioactive peptides. [155]

Although a few examples where supramolecular materials have been applied in *in vivo* evaluations were highlighted in this chapter, the number of clinical implementations of supramolecular biomaterials are very limited, which implies material design and performance still require considerable optimization. In future biomaterial design, the introduction of specific bioactivity on the one hand while addressing appropriate fouling behavior on the other hand, in conjunction with suitable mechanical properties for a specific application should be taken into account.
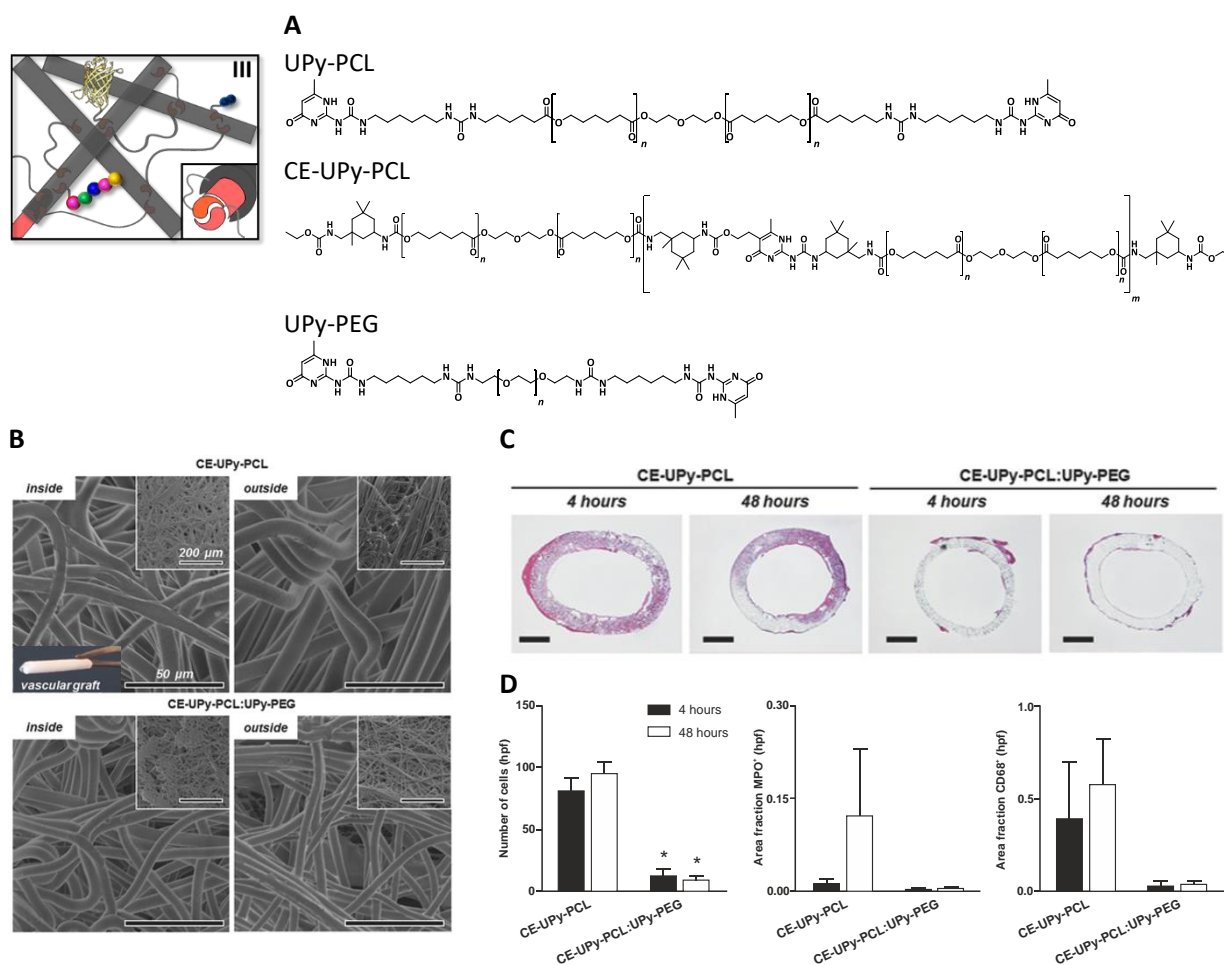
Figure 2.10. Development of a non-cell adhesive vascular graft, A) Chemical structures of the molecules in this report, UPy-PCL, chain-extended UPy-PCL (CE-UPy-PCL) and UPy-PEG, B) SEM images of the morphology of both the inside (lumen) and the outside of the electrospun vascular grafts of CE-UPy-PCL (top) and CE-UPy-PCL : UPy-PEG (90:10) (bottom) and an insert of the final construct (top left), scale bars represent 50 μm, C) Cross sectional slices of the grafts both 4 and 48 hours after implantation, scale bars represent 500 μm and D) Quantitative analysis of histological data showing reduced cellularity in CE-UPy-PCL : UPy-PEG vascular grafts (left), MPO positive granulocytes (middle) and CD68+ macrophages (right) relative to tissue area. Bar graphs represent infiltrating cell numbers from four representative high power fields (hpf) per tissue section analyzed at 400x magnification. The data is represented as mean ± S.E.M. Reprinted with permission from [155], copyright 2015 WILEY-VCH Verlag GmbH & Co. KGaA, Weinheim.

2.5 Conclusions

The strength and importance of bringing functionality into supramolecular biomaterials which ultimately find their application in the fields of tissue engineering and regenerative medicine is described in this chapter. Upon implantation in an *in vivo* environment, the surface of any material inevitably is exposed to the environment, which emphasizes the importance of proper surface functionalization. Strategies to functionalize material surfaces in order to generate desired material properties, i.e. bioactivity and nonfouling behavior have been disclosed in this chapter. Typically, surface functionality can be introduced upon changes in or adaptation of the different building blocks that formulate the biomaterial. Although a few materials that have been applied in *in vivo* studies were described, supramolecular materials have not yet made their way into many clinical applications. Although much progress has been made in the development of new biomaterials in order to meet nature's complexity in recent years, there is still a large gap between synthetic supramolecular materials and those found in nature. [156]

In order to be able to regenerate damaged tissues or organs, the challenges that are faced in biomaterials and medicine are immense. [157] It is envisioned that multidisciplinary research, ranging from cell biology to materials science and physics, is necessary in order to advance the field to translation of biomedical advances from bench to bedside. Moreover, the use of supramolecular biomaterials in this area plays an important role, due to the intrinsic dynamic character of these materials, the modularity in their formulation and the ease of material property tunability. The development of supramolecular biomaterials has established highly functional materials that can be easily controlled and therefore find broad utility in a multitude of biomedical applications.

2.6 References

1. Hench, L. L. Biomaterials. *Science* **208,** 826–831 (1980).
2. Hench, L. L. & Polak, J. M. Third-generation biomedical materials. *Science* **295,** 1014–1017 (2002).
3. Jones, S. & Thornton, J. M. Principles of protein-protein interactions. *Proc. Natl. Acad. Sci. USA.* **93,** 13–20 (1996).
4. Christman, K. L. *et al.* Submicron Streptavidin Patterns for Protein Assembly. *Langmuir* **22,** 7444–7450 (2006).
5. Mitchell, A. C., Briquez, P. S., Hubbell, J. A. & Cochran, J. R. Engineering growth factors for regenerative medicine applications. *Acta Biomater.* **30,** 1–12 (2016).
6. Zhu, J. & Marchant, R. E. Design properties of hydrogel tissue-engineering scaffolds. *Expert Rev. Med. Devices* **8,** 607–626 (2011).
7. Hirano, Y. & Mooney, D. J. Peptide and Protein Presenting Materials for Tissue Engineering. *Adv. Mater.* **16,** 17–25 (2004).
8. Maynard, H. D. & Hubbell, J. A. Discovery of a sulfated tetrapeptide that binds to vascular endothelial growth factor. *Acta Biomater.* **1,** 451–459 (2005).
9. Davis, M. E. *et al.* Local myocardial insulin-like growth factor 1 (IGF-1) delivery with biotinylated peptide nanofibers improves cell therapy for myocardial infarction. *Proc. Natl. Acad. Sci.* **103,** 8155–8160 (2006).
10. Hernandez-Gordillo, V. & Chmielewski, J. Mimicking the extracellular matrix with functionalized, metal-assembled collagen peptide scaffolds. *Biomaterials* **35,** 7363–7373 (2014).
11. *Essentials of Glycobiology*. (Cold Spring Harbor Laboratory Press, 2009).
12. Delbianco, M., Bharate, P., Varela-Aramburu, S. & Seeberger, P. H. Carbohydrates in Supramolecular Chemistry. *Chem. Rev.* **116,** 1693–1752 (2016).

13. Nachtigall, O., Kördel, C., Urner, L. H. & Haag, R. Photoresponsive switches at surfaces based on supramolecular functionalization with azobenzene-oligoglycerol conjugates. *Angew. Chem. Int. Ed.* **53,** 9669–9673 (2014).

14. Gade, M. *et al.* Supramolecular scaffolds on glass slides as sugar based rewritable sensors for bacteria. *Chem. Commun.* **51,** 6346–6349 (2015).

15. Voskuhl, J., Sankaran, S. & Jonkheijm, P. Optical control over bioactive ligands at supramolecular surfaces. *Chem. Commun.* **50,** 15144–15147 (2014).

16. Massia, S. P. & Stark, J. Immobilized RGD peptides on surface-grafted dextran promote biospecific cell attachment. *J. Biomed. Mater. Res.* **56,** 390–399 (2001).

17. Li, R. *et al.* Coassembled nanostructured bioscaffold reduces the expression of proinflammatory cytokines to induce apoptosis in epithelial cancer cells. *Nanomedicine Nanotechnol. Biol. Med.* **12,** 1397–1407 (2016).

18. Hou, X.-F., Chen, Y. & Liu, Y. Enzyme-responsive protein/polysaccharide supramolecular nanoparticles. *Soft Matter* **11,** 2488–2493 (2015).

19. Lee, S. S. *et al.* Bone regeneration with low dose BMP-2 amplified by biomimetic supramolecular nanofibers within collagen scaffolds. *Biomaterials* **34,** 452–459 (2013).

20. Clemente, M. J., Romero, P., Serrano, J. L., Fitremann, J. & Oriol, L. Supramolecular Hydrogels Based on Glycoamphiphiles: Effect of the Disaccharide Polar Head. *Chem. Mater.* **24,** 3847–3858 (2012).

21. Dumitriu, S. & Chornet, E. Inclusion and release of proteins from polysaccharide-based polyion complexes. *Adv. Drug Deliv. Rev.* **31,** 223–246 (1998).

22. Baldwin, A. D. & Kiick, K. L. Polysaccharide-modified synthetic polymeric biomaterials. *Pept. Sci.* **94,** 128–140 (2010).

23. Qi, Z. *et al.* Multivalency at Interfaces: Supramolecular Carbohydrate-Functionalized Graphene Derivatives for Bacterial Capture, Release, and Disinfection. *Nano Lett.* **15,** 6051–6057 (2015).

24. Mututuvari, T. M. & Tran, C. D. Synergistic adsorption of heavy metal ions and organic pollutants by supramolecular polysaccharide composite materials from cellulose, chitosan and crown ether. *J. Hazard. Mater.* **264,** 449–459 (2014).

25. Metzke, M. & Guan, Z. Structure–Property Studies on Carbohydrate-Derived Polymers for Use as Protein-Resistant Biomaterials. *Biomacromolecules* **9,** 208–215 (2008).

26. Metzke, M., Bai, J. Z. & Guan, Z. A Novel Carbohydrate-Derived Side-Chain Polyether with Excellent Protein Resistance. *J. Am. Chem. Soc.* **125,** 7760–7761 (2003).

27. Chen, D. *et al.* Layer-by-layer-assembled healable antifouling films. *Adv. Mater.* **27,** 5882–5888 (2015).

28. Ramakers, B. E. I., Hest, J. C. M. van & Löwik, D. W. P. M. Molecular tools for the construction of peptide-based materials. *Chem. Soc. Rev.* **43,** 2743–2756 (2014).

29. Hawker, C. J. & Wooley, K. L. The convergence of synthetic organic and polymer chemistries. *Science* **309,** 1200–1205 (2005).

30. Klok, H.-A. Biological–synthetic hybrid block copolymers: Combining the best from two worlds. *J. Polym. Sci. Part Polym. Chem.* **43,** 1–17 (2005).

31. Shoulders, M. D. & Raines, R. T. Collagen Structure and Stability. *Annu. Rev. Biochem.* **78,** 929–958 (2009).

32. Yu, S. M., Li, Y. & Kim, D. Collagen Mimetic Peptides: Progress Towards Functional Applications. *Soft Matter* **7,** 7927–7938 (2011).

33. Stephanopoulos, N., Ortony, J. H. & Stupp, S. I. Self-Assembly for the Synthesis of Functional Biomaterials. *Acta Mater.* **61,** 912–930 (2013).

34. Zhao, X. & Zhang, S. Molecular designer self-assembling peptides. *Chem. Soc. Rev.* **35,** 1105–1110 (2006).

35. Zhang, S. *et al.* Self-complementary oligopeptide matrices support mammalian cell attachment. *Biomaterials* **16,** 1385–1393 (1995).

36. Gelain, F., Horii, A. & Zhang, S. Designer Self-Assembling Peptide Scaffolds for 3-D Tissue Cell Cultures and Regenerative Medicine. *Macromol. Biosci.* **7,** 544–551 (2007).

37. Yu, T.-B., Bai, J. Z. & Guan, Z. Cycloaddition-Promoted Self-Assembly of a Polymer into Well-Defined β Sheets and Hierarchical Nanofibrils. *Angew. Chem. Int. Ed.* **48,** 1097–1101 (2009).

38. Guan, Z. Supramolecular design in biopolymers and biomimetic polymers for advanced mechanical properties. *Polym. Int.* **56,** 467–473 (2007).

39. Metzke, M., O'Connor, N., Maiti, S., Nelson, E. & Guan, Z. Saccharide–Peptide Hybrid Copolymers as Biomaterials. *Angew. Chem. Int. Ed.* **44,** 6529–6533 (2005).

40. Chen, Y. & Guan, Z. Bioinspired Modular Synthesis of Elastin-Mimic Polymers To Probe the Mechanism of Elastin Elasticity. *J. Am. Chem. Soc.* **132,** 4577–4579 (2010).

41. Wang, Z. *et al.* Bioinspired Design of Nanostructured Elastomers with Cross-Linked Soft Matrix Grafting on the Oriented Rigid Nanofibers To Mimic Mechanical Properties of Human Skin. *ACS Nano* **9,** 271–278 (2015).

42. Kushner, A. M. & Guan, Z. Modular Design in Natural and Biomimetic Soft Materials. *Angew. Chem. Int. Ed.* **50,** 9026–9057 (2011).

43. VandeVondele, S., Vörös, J. & Hubbell, J. A. RGD-grafted poly-l-lysine-graft-(polyethylene glycol) copolymers block non-specific protein adsorption while promoting cell adhesion. *Biotechnol. Bioeng.* **82,** 784–790 (2003).

44. Lavanant, L., Pullin, B., Hubbell, J. A. & Klok, H.-A. A Facile Strategy for the Modification of Polyethylene Substrates with Non-Fouling, Bioactive Poly(poly(ethylene glycol) methacrylate) Brushes. *Macromol. Biosci.* **10,** 101–108 (2010).

45. Hartgerink, J. D., Beniash, E. & Stupp, S. I. Peptide-amphiphile nanofibers: A versatile scaffold for the preparation of self-assembling materials. *Proc. Natl. Acad. Sci.* **99,** 5133–5138 (2002).

46. Hartgerink, J. D., Beniash, E. & Stupp, S. I. Self-assembly and mineralization of peptide-amphiphile nanofibers. *Science* **294,** 1684–1688 (2001).

47. Silva, G. A. *et al.* Selective differentiation of neural progenitor cells by high-epitope density nanofibers. *Science* **303,** 1352–1355 (2004).

48. Niece, K. L., Hartgerink, J. D., Donners, J. J. J. M. & Stupp, S. I. Self-Assembly Combining Two Bioactive Peptide-Amphiphile Molecules into Nanofibers by Electrostatic Attraction. *J. Am. Chem. Soc.* **125,** 7146–7147 (2003).

49. Guler, M. O., Pokorski, J. K., Appella, D. H. & Stupp, S. I. Enhanced Oligonucleotide Binding to Self-Assembled Nanofibers. *Bioconjug. Chem.* **16,** 501–503 (2005).

50. Rajangam, K. *et al.* Heparin binding nanostructures to promote growth of blood vessels. *Nano Lett.* **6,** 2086–2090 (2006).

51. Li, A. *et al.* A bioengineered peripheral nerve construct using aligned peptide amphiphile nanofibers. *Biomaterials* **35,** 8780–8790 (2014).

52. Storrie, H. *et al.* Supramolecular crafting of cell adhesion. *Biomaterials* **28,** 4608–4618 (2007).

53. Harrington, D. A. *et al.* Branched peptide-amphiphiles as self-assembling coatings for tissue engineering scaffolds. *J. Biomed. Mater. Res. A* **78,** 157–167 (2006).

54. Velichko, Y. S., Stupp, S. I. & de la Cruz, M. O. Molecular Simulation Study of Peptide Amphiphile Self-Assembly. *J. Phys. Chem. B* **112,** 2326–2334 (2008).

55. Webber, M. J. *et al.* Supramolecular nanostructures that mimic VEGF as a strategy for ischemic tissue repair. *Proc. Natl. Acad. Sci.* **108,** 13438–13443 (2011).

56. Freeman, R., Boekhoven, J., Dickerson, M. B., Naik, R. R. & Stupp, S. I. Biopolymers and supramolecular polymers as biomaterials for biomedical applications. *MRS Bull.* **40,** 1089–1101 (2015).

57. Cheng, S., Zhang, M., Dixit, N., Moore, R. B. & Long, T. E. Nucleobase Self-Assembly in Supramolecular Adhesives. *Macromolecules* **45,** 805–812 (2012).

58. Mather, B. D. *et al.* Supramolecular Triblock Copolymers Containing Complementary Nucleobase Molecular Recognition. *Macromolecules* **40,** 6834–6845 (2007).

59. Hemp, S. T. & Long, T. E. DNA-Inspired Hierarchical Polymer Design: Electrostatics and Hydrogen Bonding in Concert. *Macromol. Biosci.* **12,** 29–39 (2012).

60. Zhang, K., Fahs, G. B., Aiba, M., Moore, R. B. & Long, T. E. Nucleobase-functionalized ABC triblock copolymers: self-assembly of supramolecular architectures. *Chem. Commun.* **50,** 9145–9148 (2014).

61. Anderson, E. B. & Long, T. E. Imidazole- and imidazolium-containing polymers for biology and material science applications. *Polymer* **51,** 2447–2454 (2010).

62. Lin, I.-H. *et al.* Nucleobase-grafted polycaprolactones as reversible networks in a novel biocompatible material. *RSC Adv.* **3,** 12598–12603 (2013).

63. Kushner, A. M., Vossler, J. D., Williams, G. A. & Guan, Z. A Biomimetic Modular Polymer with Tough and Adaptive Properties. *J. Am. Chem. Soc.* **131,** 8766–8768 (2009).

64. Hentschel, J., Kushner, A. M., Ziller, J. & Guan, Z. Self-Healing Supramolecular Block Copolymers. *Angew. Chem. Int. Ed.* **51,** 10561–10565 (2012).

65. Chen, Y., Kushner, A. M., Williams, G. A. & Guan, Z. Multiphase design of autonomic self-healing thermoplastic elastomers. *Nat. Chem.* **4,** 467–472 (2012).

66. Chen, Y. & Guan, Z. Multivalent hydrogen bonding block copolymers self-assemble into strong and tough self-healing materials. *Chem. Commun.* **50,** 10868–10870 (2014).

67. Williams, G. A. *et al.* Mechanically Robust and Self-Healable Superlattice Nanocomposites by Self-Assembly of Single-Component 'Sticky' Polymer-Grafted Nanoparticles. *Adv. Mater.* **27,** 3934–3941 (2015).

68. Mozhdehi, D., Ayala, S., Cromwell, O. R. & Guan, Z. Self-Healing Multiphase Polymers via Dynamic Metal–Ligand Interactions. *J. Am. Chem. Soc.* **136,** 16128–16131 (2014).

69. Chen, Y. & Guan, Z. Self-healing thermoplastic elastomer brush copolymers having a glassy polymethylmethacrylate backbone and rubbery polyacrylate-amide brushes. *Polymer* **69,** 249–254 (2015).

70. Mather, B. D., Elkins, C. L., Beyer, F. L. & Long, T. E. Morphological Analysis of Telechelic Ureidopyrimidone Functional Hydrogen Bonding Linear and Star-Shaped Poly(ethylene-co-propylene)s. *Macromol. Rapid Commun.* **28,** 1601–1606 (2007).

71. Jonkheijm, P., Weinrich, D., Schröder, H., Niemeyer, C. M. & Waldmann, H. Chemical Strategies for Generating Protein Biochips. *Angew. Chem. Int. Ed.* **47,** 9618–9647 (2008).

72. Chen, Y.-X., Triola, G. & Waldmann, H. Bioorthogonal chemistry for site-specific labeling and surface immobilization of proteins. *Acc. Chem. Res.* **44,** 762–773 (2011).

73. Schmid, E. L., Keller, T. A., Dienes, Z. & Vogel, H. Reversible Oriented Surface Immobilization of Functional Proteins on Oxide Surfaces. *Anal. Chem.* **69,** 1979–1985 (1997).

74. Yang, L., Tan, X., Wang, Z. & Zhang, X. Supramolecular Polymers: Historical Development, Preparation, Characterization, and Functions. *Chem. Rev.* **115,** 7196–7239 (2015).

75. Ma, X. & Tian, H. Stimuli-responsive supramolecular polymers in aqueous solution. *Acc. Chem. Res.* **47,** 1971–1981 (2014).

76. Yang, H., Yuan, B., Zhang, X. & Scherman, O. A. Supramolecular Chemistry at Interfaces: Host–Guest Interactions for Fabricating Multifunctional Biointerfaces. *Acc. Chem. Res.* **47,** 2106–2115 (2014).

77. Harada, A., Kobayashi, R., Takashima, Y., Hashidzume, A. & Yamaguchi, H. Macroscopic self-assembly through molecular recognition. *Nat. Chem.* **3,** 34–37 (2011).

78. Yamaguchi, H. *et al.* Photoswitchable gel assembly based on molecular recognition. *Nat. Commun.* **3,** 603 (2012).

79. Zhao, Q. *et al.* Surface Modification of Cellulose Fiber via Supramolecular Assembly of Biodegradable Polyesters by the Aid of Host–Guest Inclusion Complexation. *Biomacromolecules* **11,** 1364–1369 (2010).

80. Ji, Q. *et al.* Dual functionalization of poly(ε-caprolactone) film surface through supramolecular assembly with the aim of promoting in situ endothelial progenitor cell attachment on vascular grafts. *Biomacromolecules* **14,** 4099–4107 (2013).

81. Nagahama, K., Shimizu, K., Ouchi, T. & Ohya, Y. Biodegradable poly(l-lactide)-grafted α-cyclodextrin copolymer displaying specific dye absorption by host–guest interactions. *React. Funct. Polym.* **69,** 891–897 (2009).

82. Inoue, Y., Ye, L., Ishihara, K. & Yui, N. Preparation and surface properties of polyrotaxane-containing tri-block copolymers as a design for dynamic biomaterials surfaces. *Colloids Surf. B Biointerfaces* **89,** 223–227 (2012).

83. Yang, Y. *et al.* Functionalization of carbon nanotubes with biodegradable supramolecular polypseudorotaxanes from grafted-poly(ε-caprolactone) and α-cyclodextrins. *Eur. Polym. J.* **46,** 145–155 (2010).

84. Antoniuk, I., Wintgens, V., Volet, G., Nielsen, T. T. & Amiel, C. Bifunctionalized dextrans for surface PEGylation via multivalent host–guest interactions. *Carbohydr. Polym.* **133,** 473–481 (2015).

85. Shi, X. *et al.* Regulation of Protein Binding Capability of Surfaces via Host–Guest Interactions: Effects of Localized and Average Ligand Density. *Langmuir* **31,** 6172–6178 (2015).

86. Ni, X.-L. *et al.* Self-Assemblies Based on the 'Outer-Surface Interactions' of Cucurbit[n]urils: New Opportunities for Supramolecular Architectures and Materials. *Acc. Chem. Res.* **47,** 1386–1395 (2014).

87. Masson, E., Ling, X., Joseph, R., Kyeremeh-Mensah, L. & Lu, X. Cucurbituril chemistry: a tale of supramolecular success. *RSC Adv.* **2,** 1213–1247 (2012).

88. Assaf, K. I. & Nau, W. M. Cucurbiturils: from synthesis to high-affinity binding and catalysis. *Chem. Soc. Rev.* **44,** 394–418 (2014).

89. Kim, K. *et al.* Functionalized cucurbiturils and their applications. *Chem. Soc. Rev.* **36,** 267–279 (2007).

90. Lee, J. W., Samal, S., Selvapalam, N., Kim, H.-J. & Kim, K. Cucurbituril Homologues and Derivatives: New Opportunities in Supramolecular Chemistry. *Acc. Chem. Res.* **36,** 621–630 (2003).

91. Lagona, J., Mukhopadhyay, P., Chakrabarti, S. & Isaacs, L. The Cucurbit[n]uril Family. *Angew. Chem. Int. Ed.* **44,** 4844–4870 (2005).

92. Heitmann, L. M., Taylor, A. B., Hart, P. J. & Urbach, A. R. Sequence-Specific Recognition and Cooperative Dimerization of N-Terminal Aromatic Peptides in Aqueous Solution by a Synthetic Host. *J. Am. Chem. Soc.* **128,** 12574–12581 (2006).

93. Bush, M. E., Bouley, N. D. & Urbach, A. R. Charge-Mediated Recognition of N-Terminal Tryptophan in Aqueous Solution by a Synthetic Host. *J. Am. Chem. Soc.* **127,** 14511–14517 (2005).

94. Gürbüz, S., Idris, M. & Tuncel, D. Cucurbituril-based supramolecular engineered nanostructured materials. *Org. Biomol. Chem.* **13,** 330–347 (2014).

95. Appel, E. A. *et al.* Supramolecular Cross-Linked Networks via Host–Guest Complexation with Cucurbit[8]uril. *J. Am. Chem. Soc.* **132,** 14251–14260 (2010).

96. Appel, E. A. *et al.* Ultrahigh-Water-Content Supramolecular Hydrogels Exhibiting Multistimuli Responsiveness. *J. Am. Chem. Soc.* **134,** 11767–11773 (2012).

97. Xu, X. *et al.* Formation of Cucurbit[8]uril-Based Supramolecular Hydrogel Beads Using Droplet-Based Microfluidics. *Biomacromolecules* **16,** 2743–2749 (2015).

98. Rowland, M. J., Atgie, M., Hoogland, D. & Scherman, O. A. Preparation and Supramolecular Recognition of Multivalent Peptide-Polysaccharide Conjugates by Cucurbit[8]uril in Hydrogel Formation. *Biomacromolecules* **16,** 2436–2443 (2015).

99. Bosmans, R. P. G. *et al.* Supramolecular Protein Immobilization on Lipid Bilayers. *Chem. Eur. J.* **21,** 18466–18473 (2015).

100. Fox, J. D. & Rowan, S. J. Supramolecular Polymerizations and Main-Chain Supramolecular Polymers. *Macromolecules* **42,** 6823–6835 (2009).

101. Rowan, S. J. & Stoddart, J. F. Surrogate-stoppered [2]rotaxanes: a new route to larger interlocked architectures. *Polym. Adv. Technol.* **13,** 777–787 (2002).

102. Zheng, B., Wang, F., Dong, S. & Huang, F. Supramolecular polymers constructed by crown ether-based molecular recognition. *Chem. Soc. Rev.* **41,** 1621–1636 (2012).

103. Zhou, Z., Yan, X., Cook, T. R., Saha, M. L. & Stang, P. J. Engineering Functionalization in a Supramolecular Polymer: Hierarchical Self-Organization of Triply Orthogonal Non-covalent Interactions on a Supramolecular Coordination Complex Platform. *J. Am. Chem. Soc.* **138,** 806–809 (2016).

104. Yan, X., Wang, F., Zheng, B. & Huang, F. Stimuli-responsive supramolecular polymeric materials. *Chem. Soc. Rev.* **41,** 6042–6065 (2012).

105. Yan, X. *et al.* Supramolecular polymer nanofibers viaelectrospinning of a heteroditopic monomer. *Chem. Commun.* **47,** 7086–7088 (2011).

106. Johnston, E. E., Bryers, J. D. & Ratner, B. D. Plasma Deposition and Surface Characterization of Oligoglyme, Dioxane, and Crown Ether Nonfouling Films. *Langmuir* **21,** 870–881 (2005).

107. Denes, A. R., Somers, E. B., Wong, A. C. L. & Denes, F. 12-crown-4–ether and tri(ethylene glycol) dimethyl–ether plasma-coated stainless steel surfaces and their ability to reduce bacterial biofilm deposition. *J. Appl. Polym. Sci.* **81,** 3425–3438 (2001).

108. Gezici, O. & Bayrakci, M. Calixarene-engineered surfaces and separation science. *J. Incl. Phenom. Macrocycl. Chem.* **83,** 1–18 (2015).

109. Bayrakcı, M., Özcan, F. & Ertul, Ş. Synthesis of calixamide nanofibers by electrospinning and toxic anion binding to the fiber structures. *Tetrahedron* **71,** 3404–3410 (2015).

110. Boretos, J. W. & Pierce, W. S. Segmented polyurethane: A polyether polymer. An initial evalution for biomedical applications. *J. Biomed. Mater. Res.* **2,** 121–130 (1968).

111. Houton, K. A. & Wilson, A. J. Hydrogen-bonded supramolecular polyurethanes. *Polym. Int.* **64,** 165–173 (2015).

112. Ye, S. H. *et al.* Hollow fiber membrane modification with functional zwitterionic macromolecules for improved thromboresistance in artificial lungs. *Langmuir* **31,** 2463–2471 (2015).

113. Gu, X. *et al.* Biodegradable, elastomeric coatings with controlled anti-proliferative agent release for magnesium-based cardiovascular stents. *Colloids Surf. B Biointerfaces* **144,** 170–179 (2016).

114. Perkins, J., Hong, Y., Ye, S.-H., Wagner, W. R. & Desai, S. Direct writing of bio-functional coatings for cardiovascular applications. *J. Biomed. Mater. Res. A* **102,** 4290–4300 (2014).

115. Fang, J. *et al.* Biodegradable poly(ester urethane)urea elastomers with variable amino content for subsequent functionalization with phosphorylcholine. *Acta Biomater.* **10,** 4639–4649 (2014).

116. Ye, S. H. *et al.* Nonthrombogenic, biodegradable elastomeric polyurethanes with variable sulfobetaine content. *ACS Appl. Mater. Interfaces* **6,** 22796–22806 (2014).

117. Stankus, J. J., Guan, J. & Wagner, W. R. Fabrication of biodegradable elastomeric scaffolds with sub-micron morphologies. *J. Biomed. Mater. Res. A* **70,** 603–614 (2004).

118. Fu, H. L., Hong, Y., Little, S. R. & Wagner, W. R. Collagenase-labile polyurethane urea synthesis and processing into hollow fiber membranes. *Biomacromolecules* **15,** 2924–2932 (2014).

119. Lightfoot, M. P., Mair, F. S., Pritchard, R. G. & Warren, J. E. New supramolecular packing motifs: π-stacked rods encased in triply-helical hydrogen bonded amide strands. *Chem. Commun.* **0,** 1945–1946 (1999).

120. Brunsveld, L. *et al.* Chiral Amplification in Columns of Self-Assembled N,N′,N″-Tris((S)-3,7-dimethyloctyl)benzene-1,3,5-tricarboxamide in Dilute Solution. *Chem. Lett.* **29,** 292–293 (2000).

121. Smulders, M. M. J., Schenning, A. P. H. J. & Meijer, E. W. Insight into the Mechanisms of Cooperative Self-Assembly: The 'Sergeants-and-Soldiers' Principle of Chiral and Achiral C3-Symmetrical Discotic Triamides. *J. Am. Chem. Soc.* **130,** 606–611 (2008).

122. Roosma, J., Mes, T., Leclère, P., Palmans, A. R. A. & Meijer, E. W. Supramolecular Materials from Benzene-1,3,5-tricarboxamide-Based Nanorods. *J. Am. Chem. Soc.* **130,** 1120–1121 (2008).

123. Cordier, P., Tournilhac, F., Soulié-Ziakovic, C. & Leibler, L. Self-healing and thermoreversible rubber from supramolecular assembly. *Nature* **451,** 977–980 (2008).

124. Wisse, E. *et al.* Molecular recognition in poly(epsilon-caprolactone)-based thermoplastic elastomers. *Biomacromolecules* **7,** 3385–3395 (2006).

125. Koevoets, R. A. *et al.* Molecular Recognition in a Thermoplastic Elastomer. *J. Am. Chem. Soc.* **127,** 2999–3003 (2005).

126. Wisse, E., Govaert, L. E., Meijer, H. E. H. & Meijer, E. W. Unusual Tuning of Mechanical Properties of Thermoplastic Elastomers Using Supramolecular Fillers. *Macromolecules* **39,** 7425–7432 (2006).

127. Wisse, E. *et al.* Segmental Orientation in Well-Defined Thermoplastic Elastomers Containing Supramolecular Fillers. *Macromolecules* **42,** 524–530 (2009).

128. Botterhuis, N. E., Karthikeyan, S., Spiering, A. J. H. & Sijbesma, R. P. Self-Sorting of Guests and Hard Blocks in Bisurea-Based Thermoplastic Elastomers. *Macromolecules* **43,** 745–751 (2010).

129. Spaans, C. J., Groot, J. H. de, Dekens, F. G. & Pennings, A. J. High molecular weight polyurethanes and a polyurethane urea based on 1,4-butanediisocyanate. *Polym. Bull.* **41,** 131–138 (1998).

130. Hong, Y. *et al.* Generating Elastic, Biodegradable Polyurethane/Poly(lactide-co-glycolide) Fibrous Sheets with Controlled Antibiotic Release via Two-Stream Electrospinning. *Biomacromolecules* **9,** 1200–1207 (2008).

131. Sijbesma, R. P. *et al.* Reversible polymers formed from self-complementary monomers using quadruple hydrogen bonding. *Science* **278,** 1601–1604 (1997).

132. Söntjens, S. H. M., Sijbesma, R. P., van Genderen, M. H. P. & Meijer, E. W. Stability and Lifetime of Quadruply Hydrogen Bonded 2-Ureido-4[1H]-pyrimidinone Dimers. *J. Am. Chem. Soc.* **122,** 7487–7493 (2000).

133. Beijer, F. H., Sijbesma, R. P., Kooijman, H., Spek, A. L. & Meijer, E. W. Strong Dimerization of Ureidopyrimidones via Quadruple Hydrogen Bonding. *J. Am. Chem. Soc.* **120,** 6761–6769 (1998).

134. Hirschberg, J. H. K. K. *et al.* Supramolecular Polymers from Linear Telechelic Siloxanes with Quadruple-Hydrogen-Bonded Units. *Macromolecules* **32,** 2696–2705 (1999).

135. Folmer, B. J. B., Sijbesma, R. P., Versteegen, R. M., van der Rijt, J. a. J. & Meijer, E. W. Supramolecular Polymer Materials: Chain Extension of Telechelic Polymers Using a Reactive Hydrogen-Bonding Synthon. *Adv. Mater.* **12,** 874–878 (2000).

136. Henk M Keizer, R. van K. Keizer HM , van Kessel R , Sijbesma RP , Meijer EW : Scale-up of the synthesis of ureidopyrimidinone functionalized telechelic poly(ethylenebutylene). *Polymer* **44,** 5505–5511 (2003).

137. Kautz, H., van Beek, D. J. M., Sijbesma, R. P. & Meijer, E. W. Cooperative End-to-End and Lateral Hydrogen-Bonding Motifs in Supramolecular Thermoplastic Elastomers. *Macromolecules* **39,** 4265–4267 (2006).

138. Keizer, H. M., Sijbesma, R. P., Jansen, J. F. G. A., Pasternack, G. & Meijer, E. W. Polymerization-Induced Phase Separation Using Hydrogen-Bonded Supramolecular Polymers. *Macromolecules* **36,** 5602–5606 (2003).

139. Lange, R. F. M., Van Gurp, M. & Meijer, E. W. Hydrogen-bonded supramolecular polymer networks. *J. Polym. Sci. Part Polym. Chem.* **37,** 3657–3670 (1999).

140. Dankers, P. Y. W. *et al.* Oligo(trimethylene carbonate)-Based Supramolecular Biomaterials. *Macromolecules* **39,** 8763–8771 (2006).

141. Yamauchi, K., Lizotte, J. R., Hercules, D. M., Vergne, M. J. & Long, T. E. Combinations of Microphase Separation and Terminal Multiple Hydrogen Bonding in Novel Macromolecules. *J. Am. Chem. Soc.* **124,** 8599–8604 (2002).

142. Dankers, P. Y. W., Harmsen, M. C., Brouwer, L. A., Van Luyn, M. J. A. & Meijer, E. W. A modular and supramolecular approach to bioactive scaffolds for tissue engineering. *Nat. Mater.* **4,** 568–574 (2005).

143. Dankers, P. Y. W. *et al.* Chemical and biological properties of supramolecular polymer systems based on oligocaprolactones. *Biomaterials* **27,** 5490–5501 (2006).

144. Yamauchi, K., Kanomata, A., Inoue, T. & Long, T. E. Thermoreversible Polyesters Consisting of Multiple Hydrogen Bonding (MHB). *Macromolecules* **37,** 3519–3522 (2004).

145. van Beek, D. J. M., Spiering, A. J. H., Peters, G. W. M., te Nijenhuis, K. & Sijbesma, R. P. Unidirectional Dimerization and Stacking of Ureidopyrimidinone End Groups in Polycaprolactone Supramolecular Polymers. *Macromolecules* **40,** 8464–8475 (2007).

146. Botterhuis, N. E., van Beek, D. J. M., van Gemert, G. M. L., Bosman, A. W. & Sijbesma, R. P. Self-assembly and morphology of polydimethylsiloxane supramolecular thermoplastic elastomers. *J. Polym. Sci. Part Polym. Chem.* **46,** 3877–3885 (2008).

147. Mollet, B. B. *et al.* A modular approach to easily processable supramolecular bilayered scaffolds with tailorable properties. *J. Mater. Chem. B* **2,** 2483–2493 (2014).

148. Martina, M. & Hutmacher, D. W. Biodegradable polymers applied in tissue engineering research: a review. *Polym. Int.* **56,** 145–157 (2007).

149. Dong, R. *et al.* Functional supramolecular polymers for biomedical applications. *Adv. Mater.* **27,** 498–526 (2015).

150. Black, M. *et al.* Self-Assembled Peptide Amphiphile Micelles Containing a Cytotoxic T-Cell Epitope Promote a Protective Immune Response In Vivo. *Adv. Mater.* **24,** 3845–3849 (2012).

151. Billinger, M. *et al.* Polymer stent coating for prevention of neointimal hyperplasia. *J. Invasive Cardiol.* **18,** 423–426 (2006).

152. Scherner, M. *et al.* In vivo application of tissue-engineered blood vessels of bacterial cellulose as small arterial substitutes: proof of concept? *J. Surg. Res.* **189,** 340–347 (2014).

153. Zhang, J.-Y. *et al.* Synthesis, biodegradability, and biocompatibility of lysine diisocyanate-glucose polymers. *Tissue Eng.* **8,** 771–785 (2002).

154. Muylaert, D. E. P. *et al.* Early in-situ cellularization of a supramolecular vascular graft is modified by synthetic stromal cell-derived factor-1α derived peptides. *Biomaterials* **76,** 187–195 (2016).

155. van Almen, G. C. *et al.* Development of Non-Cell Adhesive Vascular Grafts Using Supramolecular Building Blocks. *Macromol. Biosci.* **16,** 350-362 (2015).

156. Yang, Y.-W., Sun, Y.-L. & Song, N. Switchable host-guest systems on surfaces. *Acc. Chem. Res.* **47,** 1950–1960 (2014).

157. Pashuck, E. T. & Stevens, M. M. Designing regenerative biomaterial therapies for the clinic. *Sci. Transl. Med.* **4,** 160sr4 (2012).

Solid-phase based synthesis of UPy-peptide conjugates and their application in supramolecular biomaterials

Abstract

The introduction of bioactive functionality into supramolecular biomaterials greatly benefits from the modular character of these materials and hence gives rise to the synthesis of a broad scope of bioactive cues. In the first part of this chapter, the design and synthesis of ureido-pyrimidinone functionalized peptides (UPy-peptides) *via* a convergent solid-phase based approach is described. The second part shows the application of UPy-based heparin binding peptides, which facilitate the complexation of heparin onto the material surface. The surface bound heparin provides the immobilization of growth factors that exhibit a heparin binding domain. The consecutive bioactivation of cells by these immobilized growth factors is investigated based on cell morphology and gene expression levels.

3.1 Synthesis of UPy-functionalized peptide conjugates

The most convenient way of incorporating bioactive functionality into biomaterials is *via* short peptide sequences that mimic specific domains that are present in proteins or growth factors, since they are easy to synthesize to scale as well as easy to modify in a desired fashion, typically without the loss of function. Furthermore, peptides are generally more resistant to chemical processing than proteins, which also facilitates their integration into biomaterials. Polymer-based scaffolds of varying degrees of mechanical strength have been generated to meet the specific mechanical demands *in vivo*. For both classes – stiff and soft – a variety of covalent [5–8] and non-covalent [9–15] polymer networks have been explored. In contrast to covalently cross-linked scaffolds, the dynamic nature of supramolecular cross-linking provides a more straightforward way to functionalize polymers through introduction of biological cues and markers conjugated to complementary supramolecular monomers. [16–19] Furthermore, the use of specific interactions facilitates precise hierarchical self-organization and self-optimization, [20–22] and can be used to tune the rate of biodegradation. [23] Supramolecular biomaterials based on UPy-functionalized polymers, have shown promising results as scaffolds in cardiovascular [24] and renal [9,25] regenerative medicine. Extracellular matrix (ECM) derived biological cues can be introduced by the non-covalent incorporation of UPy-functionalized bioactive peptides. In this way, the properties of the supramolecular biomaterial can be rapidly optimized through straightforward mixing of different peptide combinations at different ratios.

3.1.1 Development of UPy-functionalized peptides

UPy-functionalization of peptides has previously been performed *via* reaction of the N-terminus of the peptide with a carbonyldiimidazole-activated methyl-isocytosine, yielding an UPy-peptide without spacer between the UPy and the first amino acid (e.g. UPy-peptide **1** in Figure 3.1 A), [18] or *via* a UPy-hexyl-isocyanate synthon (e.g. UPy-peptide **2** in Figure 3.1 B). [26,27] The introduction of an oligoethylene glycol (OEG)-based linker group *via* an oxime ligation strategy (UPy-peptide **3** in Figure 3.1 C) further increased the incorporation efficiency and
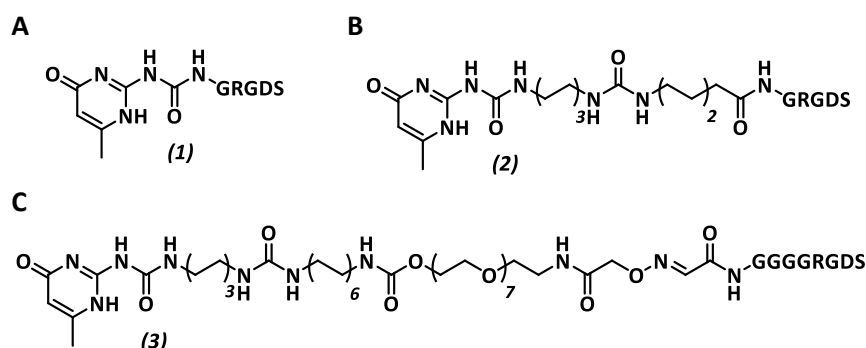

Figure 3.1. UPy-peptide designs, exemplified by the ECM derived (GGG)GRGDS sequence, previously used for the functionalization of UPy-based biomaterials. [18,27,28]

accessibility of the peptides within the biomaterial. [28] However, for the production of functional materials a fine-tuning of the amphiphilic properties of the materials is desirable, and can be achieved through the introduction of a mixture of hydrophobic and hydrophilic spacer groups within the UPy-peptide conjugates. In this chapter the efficient solid-phase synthesis of UPy-functionalized peptide conjugates with different lengths of hydrophobic and hydrophilic linkers for their use in supramolecular biomaterial applications is described. The synthesis of the UPy-peptide conjugates is explored using two convergent strategies. The data suggests that a convergent strategy, using amide coupling chemistry to introduce a suitable UPy-derived linker molecule at the N-terminus of the peptide, is the most suitable for the scaled-up synthesis of UPy-peptide conjugates. This convergent strategy in particular enables access to a broad range of conjugates and is envisioned to find extensive use in the preparation of supramolecular biomaterials. In the second part of this chapter, the applicability of this convergent UPy-peptide synthesis approach is demonstrated. UPy-functionalized heparin binding peptides (UPy-HBP) are modularly incorporated into the UPy-functionalized polycaprolactone (PCLdiUPy) material and subsequently heparin is complexed at the surface. *Via* a heparin chemistry approach, transforming growth factor beta (TGF-ß) is immobilized onto the bioactivated supramolecular biomaterial *via* its heparin binding domain. The bioactivation of the surface and is investigated by *in vitro* cell studies.

3.1.2   Results: Convergent synthesis

Two different convergent approaches were investigated in order to increase the overall yield and efficiency of the UPy-peptide synthesis. For both approaches, the peptides were first synthesized by standard Fmoc solid phase peptide synthesis (SPPS) on a Rink amide resin. The UPy building blocks **4, 5, 6** and **7** (Figure 3.2), were synthesized according to an efficient and scalable solution-phase protocol in yields ranging from 11-25% over 6-10 steps. The difference between these UPy building blocks lies in their chain length and in the composition of the hydrophilic and hydrophobic spacers.

Compounds **4-7** were then coupled to the resin-bound peptide using amide coupling chemistry at the step prior to resin cleavage. The two convergent approaches explored
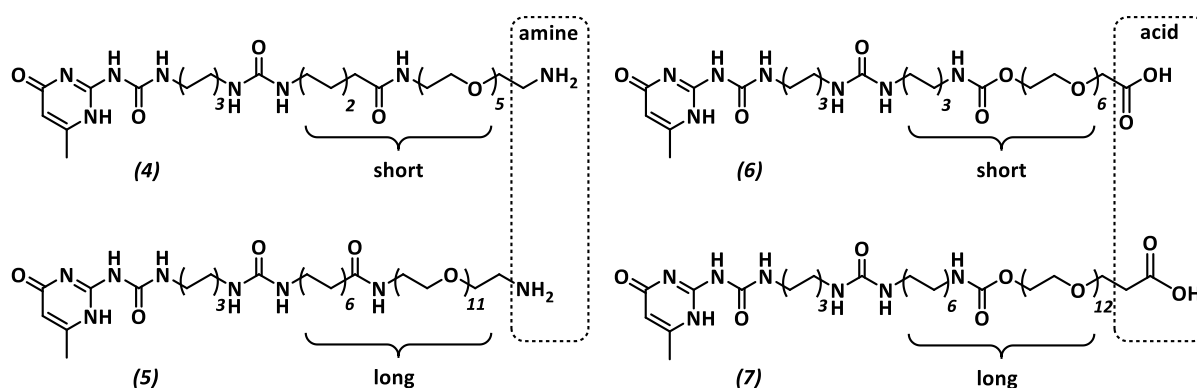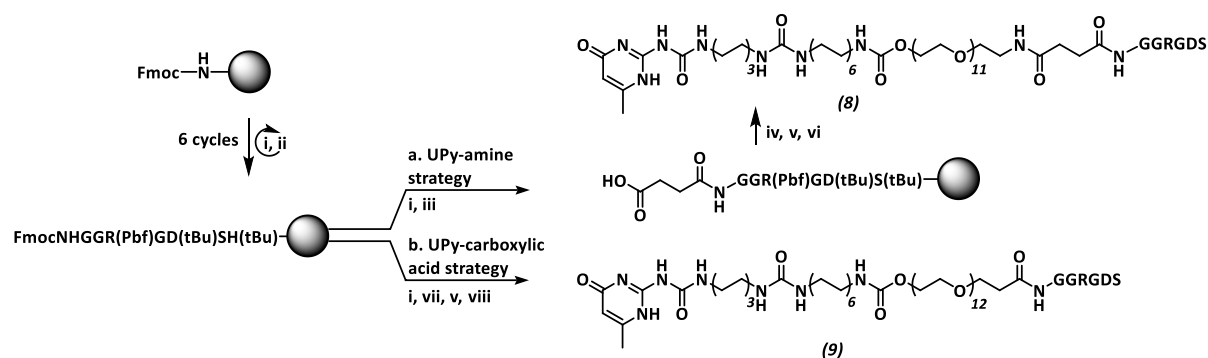

Figure 3.2. Chemical structures of the amine-terminated (**4**, **5**) and carboxylic-acid-terminated (**6**, **7**) UPy-building blocks bearing different spacer lengths for convergent UPy-peptide synthesis

Scheme 3.1. Convergent synthesis of UPy-peptide conjugates on a Rink amide resin, as exemplified by GGRGDS peptide conjugates **8** via UPy-amine strategy and **9** via carboxylic acid strategy. i) 20% (v/v %) piperidine/NMP, 2 x 5 min, RT; ii) Fmoc-protected amino acid, HBTU, DIPEA, NMP, 30 min, RT; iii) succinic anhydride, pyridine, DMF, 16 hours, RT; iv) UPy-building block **5**, PyBOP, DIPEA, DMF, 2x 16 hours, RT, v) TFA/H_2O/TIS (95/2.5/2.5 v/v %) 4 hours, RT; vi) RP-HPLC (H_2O/MeCN/0.1% TFA); vii) UPy-building block **7**, HATU, DIPEA, DMF, 2 hours, RT; viii) TFA/H_2O/TIS/EDT (94/2/2/2 v/v %) 4 hours, RT.

(Scheme 3.1), differ at the point of connection: while the first approach – UPy-amine strategy – introduced the UPy-building blocks **4** and **5** through activation of a resin-bound acid functionality, the second approach – UPy-carboxylic acid strategy – required preactivation of compounds **6** or **7** before coupling to the peptide N-terminus.

3.1.3   UPy-amine strategy

To enable coupling of UPy-amine building blocks **4** and **5**, a carboxylic acid group was installed at the peptide N-terminus by reacting the α-amino group with succinic anhydride. Coupling of the functionalized peptide to UPy-amine derivatives **4** or **5** (Figure 3.2) was achieved *via* the activated ester, formed upon treatment with benzotriazol-1-yloxytripyrrolidinophosphonium hexafluorophosphate (PyBOP) in the presence of N,N-diisopropylethylamine (DIPEA). In the final step, the UPy-peptide conjugate was deprotected and cleaved from the resin using a mixture of trifluoroacetic acid (TFA), triisopropylsilane (TIS) and H_2O (95/2.5/2.5 v/v %), and purified by preparative RP-HPLC. This resulted in the successful formation of fibronectin (GGRGDS, GGPHSRN and scrambled control peptide GSGDRG)[29] and collagen I (GGDGEA)[30] derived peptide conjugates **8a-d** in yields of 20-32% for building block **4**. Similar yields were obtained for UPy-peptide conjugates **9a** and **9b**, where the UPy-building block **5** was equipped with a longer OEG spacer. Furthermore, an irreversible side reaction was observed, which would contribute to the overall low yields (Scheme 3.2). Analogous to aspartyl and asparaginyl cyclization, presumably, the 1-hydroxybenzotriazol activated ester (**10**) undergoes an intramolecular ring closure reaction with the amide at the peptide N-terminus, forming the succinimide adduct of the peptide (**11**) on the resin while releasing the benzotriazolate (**12**) into solution.[31–33] Due to this side reaction as well as the limited yields that are obtained using this UPy-amine strategy, another convergent strategy is explored in order to improve the yields.
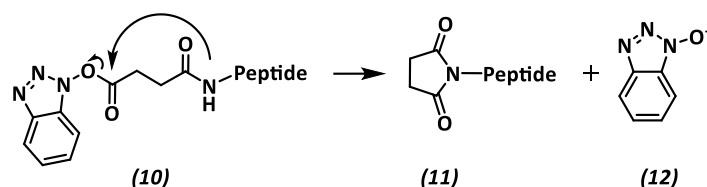
Scheme 3.2. Proposed mechanism for the side reaction yielding the succinimide adduct of the peptide (**11**) related to the use of compounds **4** and **5**.
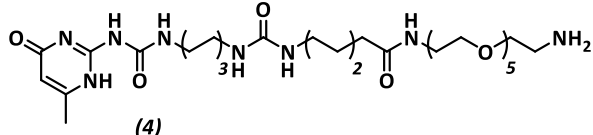
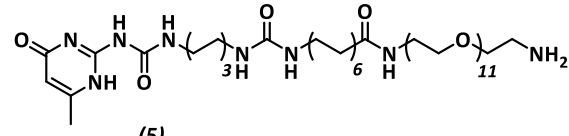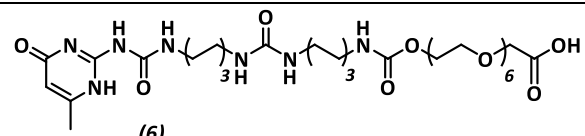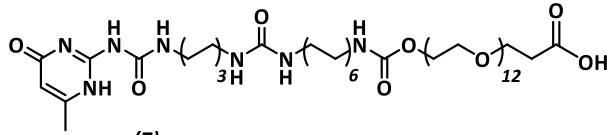### 3.1.4 UPy-carboxylic acid strategy

Final yields between 42-57% are achieved for the UPy-peptide conjugates using a similar convergent strategy that avoids the undesirable succinimide formation as was described in the previous section. To this end, carboxylic-acid-derived UPy building blocks **6** and **7** (Figure 3.2) are used for direct coupling to the peptide N-terminus. Amide coupling is performed using PyBOP in the presence of DIPEA in DMF. Subsequently the UPy-peptide constructs are deprotected and cleaved from the resin, followed by purification by preparative RP-HPLC yielding the UPy-peptide conjugates in yields up to 42% for **14a,b**. Lower molecular weight sequences (**13a**) resulted in yields of 50%. Pleasingly, the yield could be further improved to 57% for the UPy-GGRGDS conjugate (**13b**) using HATU (1-[bis(dimethylamino) methylene]-1H-1,2,3-triazolo-[4,5-b] pyridinium 3-oxid hexafluorophosphate) instead of PyBOP as activating agent. Furthermore, the use of HATU circumvents the formation of a benzotriazole PyBOP adduct at the UPy-enolate tautomer, [34,35] which could be readily converted to the desired product over the course of 15 days. [36]

In addition to peptides on solid support, the UPy-carboxylic acid building block **6** was also successfully coupled in solution to a cyclic RGD analogue using standard solution-phase chemistry conditions, to afford the UPy-peptide conjugate **13c** in a useful 56% yield. A summary of the peptides that were synthesized from the different UPy-building blocks *via* the different strategies is provided in table 3.1.

3.1.5 Conclusions

The development of two convergent strategies for the synthesis of UPy-peptide conjugates was described in this part of the chapter. The highest yields were obtained when utilizing carboxylic-acid-functionalized building blocks **6** and **7**, which were readily synthesized with high overall yields. The convergent strategy enables a fast optimization of the peptide sequence and an efficient coupling of the pre-prepared UPy-linker moiety, facilitating the access to diverse libraries of UPy-peptide conjugates. These can be readily mixed with the UPy-functionalized polymeric material in different compositions and at different ratios, which allows for the incorporation of bioactive functionality into these supramolecular materials.

Table 3.1. Summary of the UPy-peptide conjugates and yields obtained *via* divergent and convergent strategies.

Synthetic strategy	Compound	Peptide sequence (R)[d]	Yield (%)
Convergent	**8a**	GGRGDS	21
(4)	**8b**	GGPHSRN	20
	8c	GSGDRG	32
	8d	GGDGEA	20
(5)	**9a**	GGRGDS	19
	9b	GGGPHSRN	33
(6)	**13a**	GGRGDS	50
	13b	GGRGDS[a]	57
	13c	c(KRGDf)[a,b]	56[c]
(7)	**14a**	GGRGDS[a]	42
	14b	GGDGEA[a]	42

[a] coupled using HATU, [b] solution-phase chemistry, [c] yield of the protected UPy-peptide, [d] UPy-linker is attached to N-terminal amino group

3.2 Introduction of bioactivity *via* heparin chemistry

The immobilization of specific proteins and growth factors at the surface of the materials plays a crucial role in order to mimic the natural environment, which is greatly determined by the extracellular matrix (ECM) surrounding the tissue. A strategy by which proteins with a heparin binding domain can be introduced at the biomaterial surface is *via* the immobilization of heparin. This heparin chemistry approach to immobilize growth factors onto biomaterials has widely been explored, both in hydrogel materials [37–43] as well as on surfaces.[41,42,44,45] In a more controlled fashion, complexation of heparin and subsequently proteins can be induced by the introduction of a heparin binding peptide at the material surface. [42,46] A supramolecular approach was developed by Stupp and coworkers, where they immobilized heparin onto supramolecularly assembled peptide amphiphiles *via* a heparin binding peptide (LRKKLGKA) in order to effectively bind and activate angiogenic growth factors for cell signaling [47] and

ischemic tissue repair [48] The design of the heparin binding peptide sequence was based on a consensus sequence XBBBXXBX (where X is a hydrophobic amino acid and B is a basic amino acid). [49]

Endothelial to mesenchymal transition (EndoMT) is crucial in the development of valves in the embryonic heart and is driven by the activation of TGF-β signaling, which is recognized by the loss of endothelial phenotype and the gain of mesenchymal phenotype and delamination of the cells from the surface. [54] The mesenchymal transition is associated with the loss of tight junctions, reorganization of the cytoskeleton, acquisition of invasive and migratory properties and the production and deposition of extracellular matrix. [55]

TGF-ß immobilization is performed *via* supramolecular heparin chemistry to generate surface functionality. *Via* a convergent solid phase peptide synthesis approach using UPy-building block **6**, a UPy-heparin binding peptide (UPy-HBP, Figure 3.3b, **16**) is synthesized that can be modularly incorporated into the supramolecular UPy-based polymer material. Here, telechelically UPy-modified polycaprolactone (PCLdiUPy, **15**) is used as the base material (Figure 3.3a). The subsequent immobilization of heparin (Figure 3.3c) *via* specific electrostatic interactions allows the complexation of TGF-β3 to the heparin *via* its heparin binding domain (Figure 3.3d).

A PCLdiUPy

(15)

B UPy-HBP

(16)

C   **D**
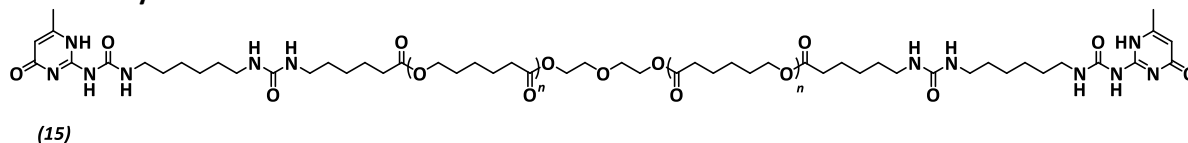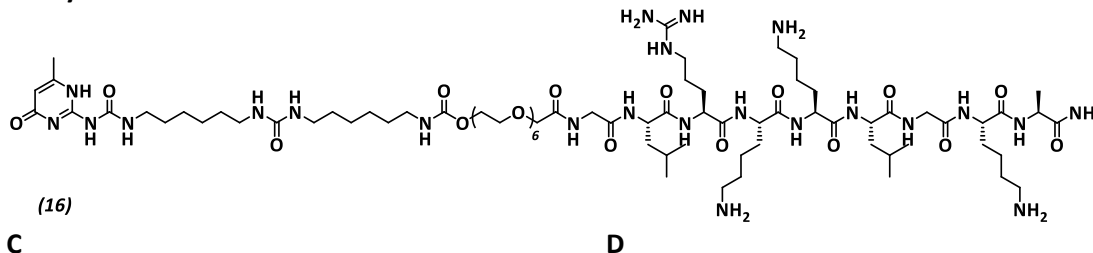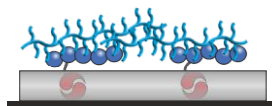
Heparin complexation   **Growth factor immobilization**
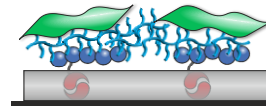
Figure 3.3. Chemical structures and corresponding cartoon representations of the molecules in this study, A) PCLdiUPy (**15**) polymer (M_n = 2000 Da) as the base polymer, B) UPy-Heparin binding peptide (UPy-HBP, **16**), C) Heparin complexation onto the supramolecular surface *via* UPy-HBP and D) Subsequent growth factor immobilization *via* the heparin complexation onto the supramolecular surface *via* UPy-HBP.

First, heparin immobilization onto the UPy-based supramolecular material was investigated. Next, the ability to complex transforming growth factor beta-3 (TGF-ß3) to this

heparin modified surfaces is illustrated by demonstrating EndoMT transdifferentiation of mouse embryonic endothelial cells (MEEC). The work described in this second part was performed in close collaboration with Dr. Geert van Almen and Rudie van der Velden, Msc, Eindhoven University of Technology, The Netherlands.

3.2.1 Synthesis of UPy-HBP and the supramolecular material formulation

The UPy-HBP (**16**) is synthesized *via* a convergent solid phase peptide synthesis approach in a final yield of 42%, 76 mg (Scheme 3.3). Acid functionalized UPy-building block **6** is coupled to the peptide sequence on the resin (GLR(Pbf)K(Boc)K(Boc)LGK(Boc)A, **17**) prior to cleavage and subsequent purification. The product (**16**) was isolated in 42% yield and was characterized.
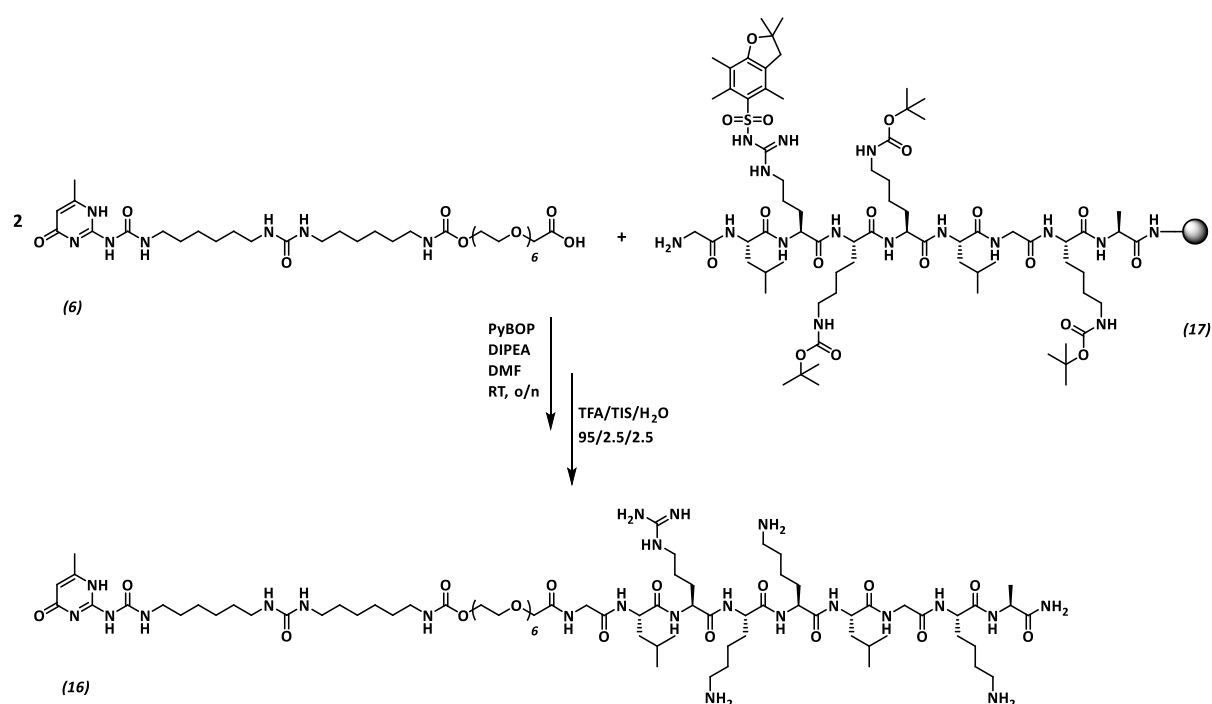
Scheme 3.3. Synthesis of UPy-HBP. After solid phase peptide synthesis and Fmoc-deprotection of the N-terminal Gly of the HBP (51), 2 equivalents of UPy-COOH synthon (**6**) in DMF were added, using PyBOP and DIPEA. The reaction was allowed to shake overnight at room temperature. After conjugation, the UPy-HBP (**16**) was cleaved from the resin and orthogonal deprotection groups were removed, using TFA/TIS/H_2O in a 95/2.5/2.5 ratio. The purified UPy-HBP was obtained at a yield of 42% and successful synthesis was confirmed using LC/MS (MW_{calc} = 1726.1 g·mol^{-1}, MW_{obs} = 576.8 g·mol^{-1} [M + 3H] $^{3+}$.

3.2.2 The immobilization of heparin

The ability to selectively immobilize heparin onto the supramolecular polymeric material was investigated. To this end, immobilization of fluorescein isothiocyanate labelled heparin (Heparin-FITC) was measured using fluorescence spectroscopy. Dropcast films of
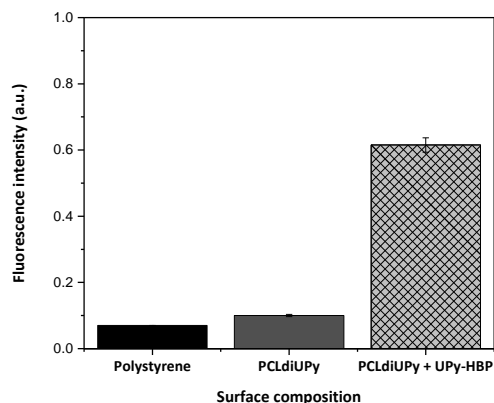
Figure 3.4. Fluorescence spectroscopy measurements of surface fluorescence after Heparin-FITC immobilization on polystyrene (PS, left), PCLdiUPy (middle) and PCLdiUPy with 4 mol% UPy-HBP (right) surfaces.

PCLdiUPy and PCLdiUPy with 4 mol% UPy-HBP were prepared and subsequently incubated with a solution of Heparin-FITC, followed by thorough surface washing, 5 times with milli-Q water. Incorporation of UPy-HBP results in a 6-fold increase in surface fluorescence (Figure 3.4), as compared to the pristine PCLdiUPy and the PS surfaces. These results indicate that UPy-HBP is incorporated into the PCLdiUPy polymer film and moreover is present at the materials surface to allow the immobilization of the heparin-FITC through the complexation with the UPy-HBP.

3.2.3   TGF-ß3 complexation onto heparin to induce EndoMT in MEEC

Investigation of endothelial to mesenchymal transition (EndoMT) on the UPy-HBP supramolecular polymer surface complexed with heparin was performed using TGF-β3 as active growth factor to induce EndoMT in MEEC. Dropcast material films were prepared from PCLdiUPy and PCLdiUPy with 4 mol% UPy-HBP. Subsequently, heparin sodium salt was incubated at the surface, followed by one washing step. Finally, 2 ng·mL^{-1} TGF-β3 was either added into the growth medium or immobilized at the surface in order to induce EndoMT. MEEC were cultured at the different surfaces for 48 hours and analyzed both with bright field microscopy (Figure 3.5) and gene expression levels indicative for the upregulation of mesenchymal markers (Figure 3.6). The immobilization of heparin *via* incorporation of UPy-HBP in the PCLdiUPy materials, results in both the surface immobilization of TGF-β3 and the addition of TGF-β3 in the culture medium to a change in morphology towards an elongated phenotype (Figure 3.5 F,G). These results show that in all cases the addition of TGF-β3 results in a different morphology. In contrast, cells cultured on a polystyrene or a PCLdiUPy surface without TGF-β3 stimulation, show cobble stone morphology (Figure 3.5 A,C) as expected. Upon introduction of TGF-β3 in the culture medium, a change in morphology towards a more elongated phenotype was observed (Figure 3.5 B,D). When TGF-ß3 is able to non-specifically adsorb at the PCLdiUPy material surface (Figure 3.5 E), the cells adapt an elongated morphology, indicative that TGF-β3 has an effect on these cells.
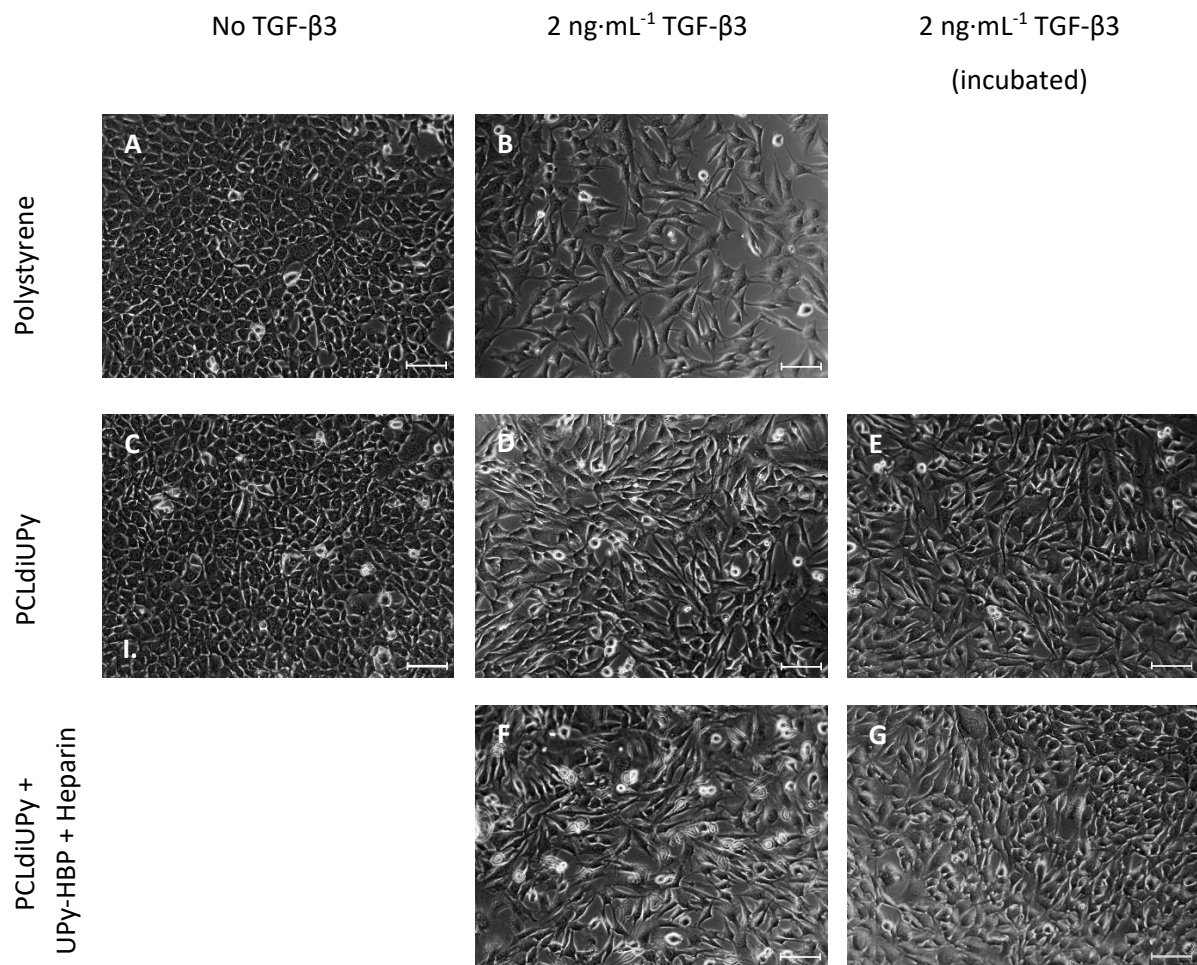
Figure 3.5. Bright-field microscopy images of MEEC cultured on polystyrene, stimulated with and without TGF-β3 for 48 hours, A) Control situation without TGF-β3 stimulation, B) Stimulation with 2 ng·mL^{-1} TGF-β3 in the culture medium, C) PCLdiUPy without TGF-β3 stimulation, D) PCLdiUPy stimulation with 2 ng·mL^{-1} TGF-β3 in the culture medium, E) PCLdiUPy with 2 ng·mL^{-1} TGF-β3 incubated at the surface, F) PCLdiUPy with 4 mol% UPy-HBP with heparin and subsequent 2 ng·mL^{-1} TGF-β3 in the culture medium and G) PCLdiUPy with 4 mol% UPy-HBP with heparin and subsequent 2 ng·mL^{-1} TGF-β3 incubated at the surface. Scale bars represent 100 μm, magnification 10x.

The gene expression levels of the mesenchymal marker α-SMA as well as the transcription factor Snail were investigated (Figure 3.6). Increase in α-SMA expression is observed in all TGF-β3 treated cases (Figure 3.6 A). Remarkably, a 12-fold increase is observed when TGF-β3 is added into the culture medium at the PCLdiUPy with UPy-HBP and heparin surface, whereas the direct immobilization at the surface results in a 3-6-fold increase. This effect is possibly explained by the ability of TGF-β3 to reversibly attach at the surface while at the same time retaining activity in the culture medium. This effect is less pronounced when TGF-β3 is pre-incubated at the surface prior to cell seeding. The effect of TGF-β3 on the transcription factor Snail displays less abundant differences. Upon the introduction of TGF-β3, either in the culture medium or incubated at the surface, a ~3-fold upregulation is observed, indicating that TGF-β3 results in EndoMT behavior of the MEEC.

A

B

Figure 3.6. Real time qPCR analysis of the mesenchymal marker α-SMA (A) and the transcription factor Snail (B). The data is corrected for GAPDH mRNA levels and error bars represent standard error of the mean (SEM).

3.2.4 Conclusions

The feasibility to introduce bioactive functionality at the surface of supramolecular biomaterials *via* UPy-peptide incorporation was explored. UPy-functionalized heparin binding peptide (UPy-HBP) was synthesized and incorporated into a PCLdiUPy thermoplastic elastomer material. Subsequent introduction of fluorescently labeled heparin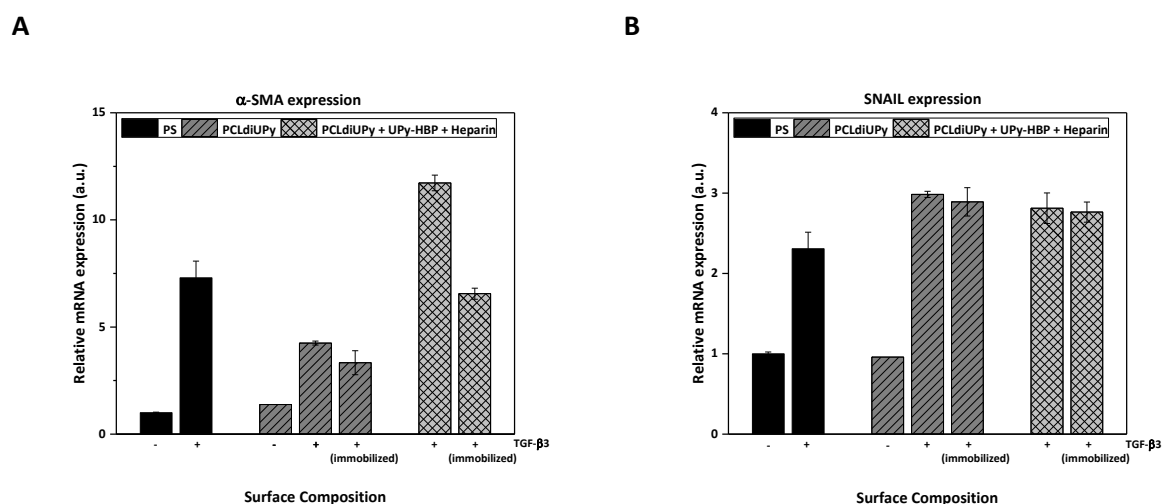 showed a 6-fold increase in surface fluorescence, suggesting UPy-HBP was properly incorporated and heparin was successfully immobilized at the surface.

During EndoMT, cells undergo morphological changes, i.e. tight junctions are lost, and gene expression levels of mesenchymal markers are upregulated whereas endothelial markers are downregulated influenced by TGF-β3 stimulation. Upon the introduction of TGF-β3 in MEEC, both morphological changes as well as an increase in mesenchymal markers were observed, indicative for EndoMT to take place. However, TGF-β3 nonspecifically adsorbed onto the PCLdiUPy surfaces, indicated by morphological changes as well as upregulation of mesenchymal markers in cells cultured on these surfaces. Based on gene expression levels, the surfaces comprised of PCLdiUPy with 4 mol% UPy-HBP and heparin immobilized and TGF-β3 administered into the culture medium outperform the surfaces where TGF-β3 is also pre-incubated at the material. This effect might result from the relative high concentration of TGF-β3 that is present in the culture medium, whereas TGF-β3 is also enhanced at the material surface as a result of the reversible interactions with heparin. At these surfaces the TGF-β3 concentration might not be as high as in the pre-incubated surfaces, however the ability to endogenously capture TGF-β3 from the medium might be beneficial to induce the EndoMT.

Bioactivation of supramolecular thermoplastic elastomer surfaces by heparin immobilization *via* the modular incorporation of UPy-HBP and subsequent growth factor immobilization was investigated. The results show the ability to induce EndoMT in MEEC upon stimulation with TGF-β3, giving rise to further optimization of this method towards the development of a functional supramolecular biomaterials for regenerative medicine applications.

3.3 Acknowledgements

Dr. Isja de Feijter and dr. Marta Comellas-Aragonès are acknowledged for their help on the UPy-peptide synthesis part of this chapter. Moreover, I would like to thank dr.ir. Serge Söntjens, dr.ir. Joris Peeters and dr.ir. Henk Janssen, SyMO-Chem BV, Eindhoven, the Netherlands, for providing the UPy-building blocks as well as their useful discussions and suggestions on the UPy-peptide synthesis part. Dr. Geert van Almen and Rudie van der Velden, Msc, are acknowledged for their collaboration on the heparin chemistry approach, more specifically the cell studies.

3.4 Materials and methods

Instrumentation

Preparative reversed phase high pressure liquid chromatography (prep-RP-HPLC) was performed on a system consisting of the following components: Shimadzu LC-8A preparative liquid chromatography pumps (with an Alltima C18 5u (125 x 20 mm) preparative reversed phase column and gradients of water-acetonitrile, supplemented with 0.1% trifluoro acetic acid), a Shimadzu CBM-20A prominence communications bus module and Shimadzu DGU 20A3 prominence degasser, Thermo Finnigan Surveyor photodiode detector array (PDA) detector, Finnigan LCQ Deca XP Max and Thermo Finnigan surveyor auto sampler. Or on a system consisting of the following components: Shimadzu SCL-10A VP system controller, equipped with an LC-8A injector and pump system, a SPD-10AV vp UV-VIS detector, FRC-10A fraction controller and a phenomenex mini 5μ 110A AXIA p ac column of 150 x 2.1 mm running with gradients of water-acetonitrile supplemented with 0.1% formic acid. Reversed phase high pressure liquid chromatography–mass spectrometry (RP-HPLC-MS) was performed on a system consisting of the following components: Shimadzu SCL-10A VP system controller with Shimadzu LC-10AD VP liquid chromatography pumps (with an Alltima C18 3u (50 mm x 2.1 mm) reversed phase column and gradients of water-acetonitrile supplemented with 0.1% formic acid, a Shimadzu DGU 20A3 prominence degasser, a Thermo Finnigan surveyor auto sampler, a Thermo Finnigan surveyor PDA detector and a Thermo Scientific LCQ Fleet. ^{1}H NMR and ^{13}C NMR spectra were recorded on a 400 MHz NMR (Varian Mercury Vx or Varian 400MR) operating at 400 MHz for ^{1}H NMR and 100 MHz for ^{13}C NMR. Proton chemical shifts are reported in ppm downfield from tetramethylsilane (TMS) and carbon chemical shifts in ppm downfield from TMS using the resonance of the deuterated solvent as internal standard. Abbreviations used are s: singlet, d: doublet, t: triplet, q: quartet, m: multiplet. IR spectra were acquired on a Perkin-Elmer spectrum Two equipped with a UATR Two sample stage.

Materials

Rink Amide 4-Methylbenzhydrylamine (MBHA) resin, Fmoc-protected amino acids, *o*-benzotriazole-*N*,*N*,*N'*,*N'*-tetramethyl-uronium-hexafluoro-phosphate (HBTU) and benzotriazol-1-yloxytripyrrolidino-phosphonium hexafluorophosphate (PyBOP) were purchased from Nova Biochem. O,O-Bis(2-aminoethyl)octadecaethylene glycol was obtained from Polypure. O,O-Bis(2-aminoethyl)pentaethylene glycol was kindly provided by Jolanda Spiering, Eindhoven university of technology, Eindhoven, the Netherlands. Unless stated otherwise, all other reagents and chemicals were obtained from commercial sources and used without further purification. 1,1,1,3,3,3-Hexafluoroisopropanol (HFIP) was purchased from Acros. PyBOP and amino acids for solid phase peptide synthesis were purchased from Novabiochem. The solvents dichloromethane (DCM), dimethylformamide (DMF), hexane, N-methylpyrrolidone (NMP) and N,N-diisopropylethylamine (DIPEA) were purchased from Biosolve and used as received, unless stated otherwise. 2(6-Isocyanatohexylaminocarbony-lamino)-6-methyl-4[1H]pyrimidinone (UPy-C6-NCO) was synthesized as described[26] and the PCLdiUPy polymer was synthesized by SyMO-Chem BV (Eindhoven, the Netherlands)[56].

Synthesis

Conversions of the UPy-peptide conjugates were determined by performing mini-cleavages and analysis by RP-HPLC-MS. Mini cleavages were done by drying the resin after every reaction and cleaving and deprotecting the peptide conjugates with trifluoroacetic acid (TFA) using water and triisopropyl silane (TIS) as scavengers (95:2.5:2.5 v/v %). The excess of TFA was removed *in vacuo* after which the product was precipitated with diethyl ether (-30 °C) and lyophilized. After the synthesis the conjugates were cleaved and deprotected using the same procedure. The crude products were purified using either preparative reversed phase liquid chromatography or reversed phase column chromatography.

Solid phase peptide synthesis

All peptides were made using automated or manual solid phase peptide synthesis on a 200 µmol scale using standard Fmoc-chemistry. Amino acids were coupled for 30 minutes. After synthesis the resin was washed with *N*-methyl-2-pyrrolidinone (NMP) and dichloromethane (DCM) and dried *in vacuo*. 5 mg of each peptide on resin was taken for a mini cleavage and was analyzed with RP-LCMS using a gradient of MeCN in water, both with 0.1% formic acid.

GGGGRGDS RP-HPLC-MS: calc. M_w = 660.6 g·mol^{-1}, found m/z: 661.7 [M+H]$^+$.
GGGPHSRN RP-HPLC-MS: calc. M_w = 779.8 g·mol^{-1}, found m/z: 780.8 [M+H]$^+$.
GGGYIGSR RP-HPLC-MS: calc. M_w = 764.8 g·mol^{-1}, found m/z: 765.8 [M+H]$^+$.
Fmoc-GGRGDS RP-HPLC-MS: calc. M_w = 768.3 g·mol^{-1}, found m/z: 769.5 [M+H]$^+$.
Fmoc-GGPHSRN RP-HPLC-MS: calc. M_w = 944.4 g·mol^{-1}, found m/z: 945.5 [M+H]$^+$.
Fmoc-GSGDRG RP-HPLC-MS: calc. M_w = 768.3 g·mol^{-1}, found m/z: 769.6 [M+H]$^+$.
Fmoc-GGDGEA RP-HPLC-MS: calc. M_w = 725.3 g·mol^{-1}, found m/z: 726.3 [M+H]$^+$.
Fmoc-c(KRGDf) RP-HPLC-MS: calc. M_w = 911.5 g·mol^{-1}, found m/z: 912.6 [M+H]$^+$.

Synthesis of UPy-building block 4

The full synthetic details can be found in Ref. [9]
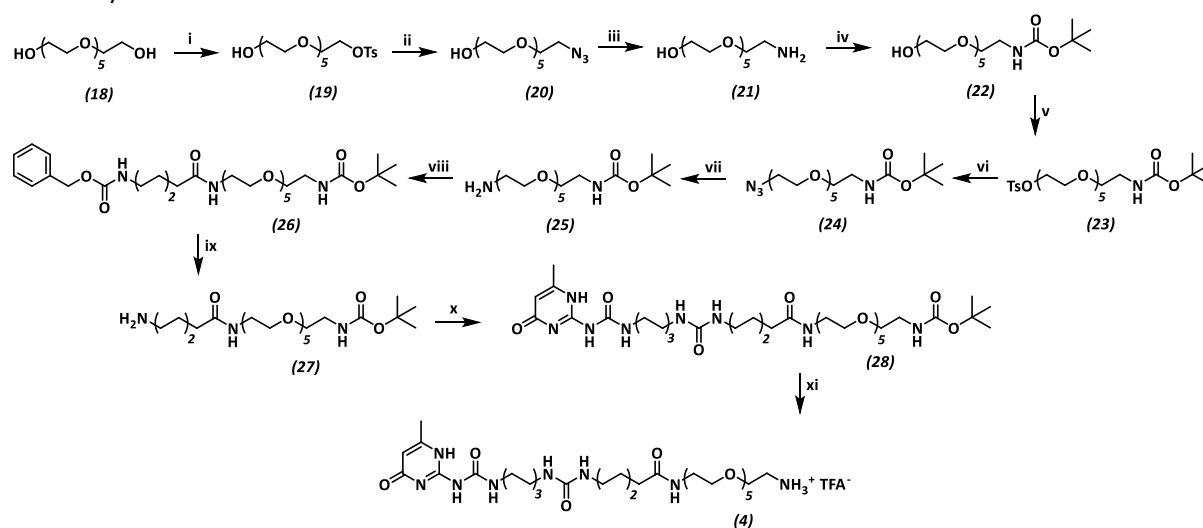
Scheme 3.4. Synthesis of UPy building block **4**. i) TsCl, KI/Ag$_2$O, DCM, 0°C, 3 h, 74%; ii) NaN$_3$, DMF, 50°C, 16 hours, 90%; iii) 10% wt Pd/C, H$_2$, MeOH, aq. NH$_3$, RT, 5 hours, 95%; iv) Boc$_2$O, Et$_3$N, MeOH, RT, o.n., 97%; v) TsCl, NaOH, THF/H$_2$O, RT, 16 hours , 94%; vi) NaN$_3$, DMF, 50°C, 16 hours, 95%; vii) 10% Pd/C, H$_2$, NaN$_3$, MeOH, RT, 3 hours, 90%; viii) CbzNHC$_5$H$_{10}$COOH, EDC, DMAP, Ar, RT, 16 hours, 64%; ix) 10% Pd/C, Et$_3$SiH, MeOH, Ar, RT, 2 hours; x) UPy-C6-NCO, CHCl$_3$, RT, 1.5 hours, 80%; xi) TFA, RT, 5 hours, quantitative.

Synthesis of UPy-building block 5
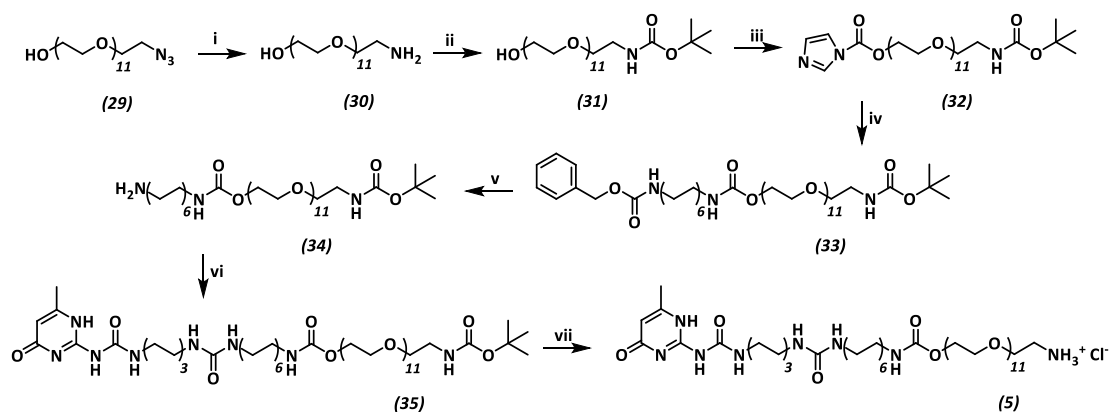
Scheme 3.5. Synthesis of UPy building block **5**. i) H$_2$, 10% wt Pd/C, MeOH, RT, 3 hours, 96%; ii) Boc$_2$O, DIPEA, CHCl$_3$, RT, 2 hours, quantitative; iii) CDI, CHCl$_3$, RT, 16 hours, quantitative; iv) CbzNHC$_{12}$H$_{24}$NH$_2$, DIPEA, CHCl$_3$, reflux, 18 hours 67%; v) Et$_3$SiH, 10% Pd/C, MeOH, RT, 88%; vi) UPy-C6-NCO, DIPEA, CHCl$_3$, RT, 3 hours, 72%; vii) HCl:dioxane (3:1), 0 °C, 18 hours, 95%.

*Synthesis of compound **30***

Undeca(ethylene glycol)azide **29** (4.29 g, 7.52 mmol) was dissolved in methanol (MeOH) (40 mL). 10% wt Pd/C (424 mg) was added and the solution was hydrogenated in a Parr low pressure reactor (50 psi) for 3 hours at room temperature. Product formation was confirmed by the disappearance of the IR 2103 (cm^{-1}) peak corresponding to the azide. The reaction mixture was filtrated using hyflo and the solvent was evaporated in vacuo yielding the undeca(ethylene glycol)amine **30** (4.10 g, 95.5%). ^{1}H NMR (400 MHz, CDCl$_3$): δ 2.6-2.8 (t, 2H), 3.5 (t, 2H), 3.6-3.8 (m, 44H), ppm.

*Synthesis of compound **31***

Undeca(ethylene glycol)amine **30** (4.10 g, 7.51 mmol) was dissolved in chloroform (150 mL). *N,N*-diisopropylethylamine (5.5 mL, 30.04 mmol) and di-*tert*-butyldicarbonate (3.29 g, 15.02 mmol) were added and the solution was allowed to stir for two hours under an argon atmosphere at room temperature. Conversion as determined by ^{1}H NMR was quantitative. ^{1}H NMR (400 MHz, CDCl$_3$): δ 1.4-1.5 (s, 9H), 3.3 (t, 2H), 3.6-3.8 (m, 44H), 5.1 (s, 1H) ppm. RP-HPLC-MS: calc. M$_w$ = 645.8 g·mol^{-1}, found m/z: 546.5 [M-Boc+H]$^+$.

*Synthesis of compound **32***

In situ, 1,1'-Carbonyldiimidazole (CDI) (1.85 g, 11.27 mmol) was added to the reaction mixture and the solution was stirred overnight under an argon atmosphere at room temperature. Conversion as determined by ^{1}H NMR was quantitative. ^{1}H NMR (400 MHz, CDCl$_3$): δ 1.4 (s, 9H), 3.3 (s, 2H), 3.4-3.6 (m, 44H), 3.8 (m, 2H), 4.6 (m, 2H), 5.2 (s, 1H), 7.1 (s, 1H), 7.4 (s, 1H), 8.3 (s, 1H) ppm. RP-HPLC-MS: calc. M$_w$ = 739.9 g·mol^{-1}, found m/z: 740.4 [M+H]$^+$.

*Synthesis of compound **33***

In situ, carboxybenzyl-dodecyl-diamine (3.77 g, 11.27 mmol) and *N,N*-Diisopropylethylamine (5.00 mL, 28.71 mmol) were added to the reaction mixture and the solution was refluxed overnight under an argon atmosphere. The product was purified using C18 column chromatography. A gradient from 5-100% CH$_3$CN/H$_2$O in one hour was used. The purified product was dried *in vacuo* at 40 °C overnight yielding an off-white film (2.88 g, 67.0%). ^{1}H NMR (400 MHz, CDCl$_3$): δ 1.2-1.6 (m, 25H), 1.8 (s, 4H), 3.1-3.4 (m, 6H), 3.4-3.8 (m, 44H), 4.2 (m, 2H), 4.7-4.9 (s, 2H), 5.1 (1, 1H), 5.1 (s, 2H), 7.3-7.4 (m, 5H) ppm. RP-HPLC-MS: calc. M$_w$ = 1006.3 g·mol^{-1}, found m/z: 906.7 [M-Boc+H]$^+$.

Synthesis of compound **34**

To product **33** (2.70 g, 2.86 mmol), 10% wt Pd/C (0.30 g, 0.29 mmol) and fresh methanol (100 mL) were added. While stirring, triethylsilane (4.57 mL, 28.6 mmol) was dropwise added and the reaction mixture was allowed to bubble under argon atmosphere at room temperature. After the bubbling had stopped, the suspension was filtrated over hyflo to remove the Pd/C catalyst, evaporated and dried *in vacuo* at 30 ˚C overnight yielding a white/yellow solid (2.37 g, 87.6%). RP-HPLC-MS: calc. M_w = 872.2 g·mol^{-1}, found m/z: 872.6 [M+H]$^+$.

Synthesis of compound **35**

Compound **34** (2.37 g, 2.71 mmol) was dissolved in dry chloroform (100 mL) and subsequently *N,N*-diisopropylethylamine (2.20 mL, 12.20 mmol) and ureido-pyrimidinone-hexyl-isocyanate (0.88 g, 2.98 mmol) were added. The reaction mixture was allowed to stir for three hours under an argon atmosphere at room temperature. The product was purified using C18 column chromatography. A gradient from 5-100% CH$_3$CN/H$_2$O in one hour was used. The purified product dried *in vacuo* at 40 ˚C overnight yielding an off-white film (2.27 g, 71.9%). ^{1}H NMR (400 MHz, CDCl$_3$): δ 1.2-1.6 (m, 37H), 2.2 (s, 3H), 3.0-3.4 (m, 10H), 3.4-3.8 (m, 44H), 4.1 (s, 2H), 4.5 (s, 1H), 4.7 (s, 1H), 4.9 (s, 1H), 5.1 (s, 1H), 5.8 (s, 1H), 10.1 (s, 1H), 11.8 (s, 1H), 13.1 (s, 1H) ppm. RP-HPLC-MS: calc. M_w = 1165.5 g·mol^{-1}, found m/z: 533.4 [M-Boc+2H]$^{2+}$.

Synthesis of compound **5**

Compound **35** (1.18 g, 1.03 mmol) was cooled on an ice bath, hydrochloride/dioxane (30 mL, 2 M) was added and the reaction mixture was allowed to stir overnight under argon atmosphere from 0 °C to room temperature. The suspension was evaporated and subsequently washed three times with dichloromethane (15 mL). The product was evaporated yielding a white/yellow film (1.038 g, 94.6%). ^{1}H NMR (400 MHz, CDCl$_3$): δ 1.2-1.7 (m, 28H), 2.4 (s, 3H), 3.1-3.4 (m, 10H), 3.4-3.8 (m, 44H), 4.2 (s, 2H), ppm. RP-HPLC-MS: calc. M_w = 1065.0 g·mol^{-1}, found m/z: 1066.00 [M+H]$^+$, 533.4 [M+2H]$^{2+}$.

Synthesis of UPy-building block 6
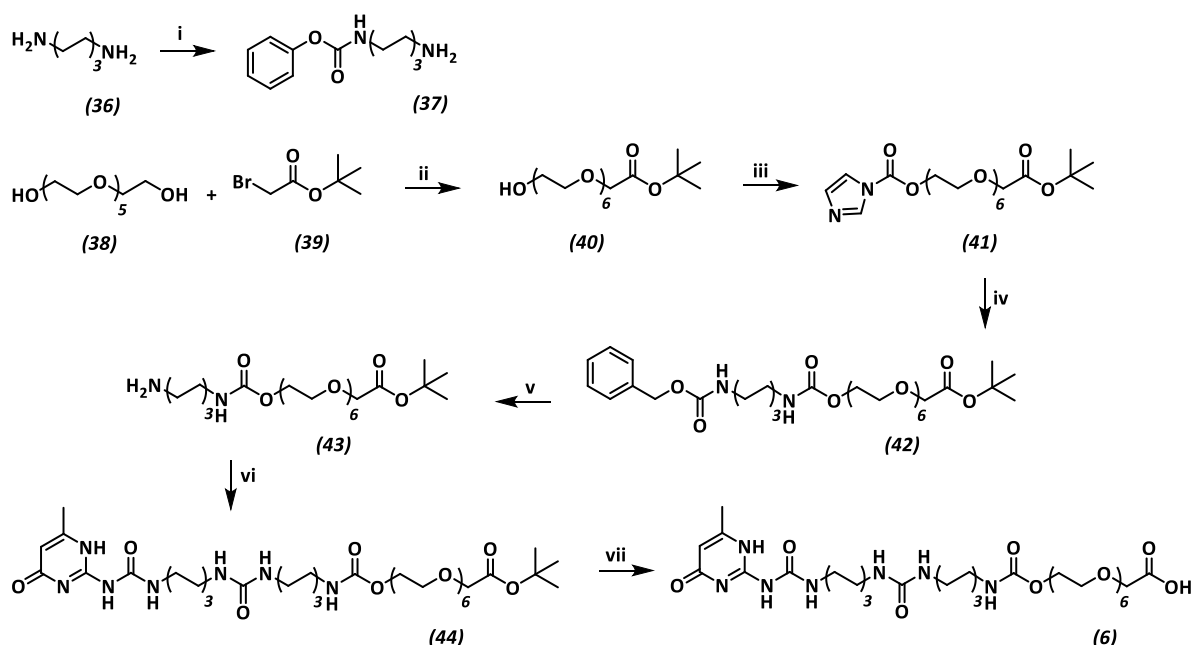
Scheme 3.6. synthesis of UPy building block **6** i) BPC, EtOH, RT, 2 hours, 31%; ii) t-BuOH, t-BuOK, 5 °C, 2 hours, 41%; iii) CDI, CHCl$_3$, RT, 16 hours, 94%; iv) CbzNHC$_{12}$H$_{24}$NH$_2$, CHCl$_3$, reflux at 65 °C, 16 hours, 98%; v) 5% Pd/C, H$_2$, EtOH, RT, 5 hours, 95%; vi) UPy-C6-NCO, DIPEA, CHCl$_3$, 65 °C, 2 hours, quantitative; vii) TFA, DCM, RT, 3 hours, 95%.

Synthesis of compound **37**

A mixture of 1,6-diaminohexane **36** (39.15 g, 0.338 mol) and benzyl phenyl carbonate (35.7 g, 0.156 mol) in ethanol (125 mL) was stirred for 2 hours at room temperature and subsequently heated for an additional hour at reflux to achieve full conversion. The reaction mixture was allowed to cool to room temperature, affording a white precipitate. After removing the precipitate by filtration, the supernatant was evaporated to dryness and dissolved in 330 mL 2 M aqueous HCl. The resulting solution was extracted with dichloromethane (DCM) (2 x 150 mL). The aqueous phase was subsequently adjusted to pH = 10 with 6 M aqueous NaOH and extracted with DCM (3 x 150 mL). All organic phases were combined, dried over Na_2SO_4, evaporated to dryness, and dissolved in 200 mL diethyl ether. The resulting solution was extracted with 1M aqueous NaOH (3 x 50 mL), dried over Na_2SO_4, and evaporated to dryness to afford crude **37**. The product was recrystallized from diethyl ether at −18ºC to afford white crystals (12.0 g, 31%). ^{1}H NMR (400 MHz, $CDCl_3$): δ 1.03 (br.s, 2H), 1.58-1.14 (m, 8H), 2.66 (t, J = 6.9 Hz, 2H), 3.18 (q, J = 6.7 Hz, 2H), 4.83 (br.s, 1H), 5.08 (s, 2H), 7.45 − 7.19 (m, 5H) ppm. ^{13}C NMR (400 MHz, $CDCl_3$): δ 26.63, 26.68, 30.07, 33.83, 41.12, 42.25, 66.67, 128.17, 128.21, 128.61, 136.78, 156.51 ppm. RP-LCMS: calc. M_w = 250.2 g·mol^{-1}, found m/z: 251.3 [M+H]$^+$.

Synthesis of compound **38**

Hexaethyleneglycol **38** (HEG, 18 g, 63.8 mmol) was dried under reduced pressure at 100 °C for 1 hour. After cooling to room temperature it was dissolved in 70 mL tert-butanol. Potassium *tert*-butoxide (6.5 g, 58 mmol) was added, and the solution was stirred for 2 hours after which it was cooled to 5 °C. *Tert*-butyl bromoacetate **39** (13 g, 66.7 mmol) was added while cooling with ice. Stirring at room temperature was continued overnight. The reaction mixture was concentrated and co-evaporated with toluene three times. The resulting material was diluted with 150 mL of water and extracted with diethyl ether (3 x 100 mL). The resulting aqueous phase was subsequently extracted with chloroform (3 x 100 mL). The combined chloroform layers were dried over $MgSO_4$ and evaporated to dryness yielding 17.8 g of the crude product. Eluting over silica with chloroform containing 1–5% methanol afforded the pure product (10.3 g, 41%). ^{1}H NMR (400 MHz, $CDCl_3$): δ 1.46 (s, 9H), 3.69 (m, 24H), 4,01 (s, 2H) ppm. ^{13}C NMR (400 MHz, $CDCl_3$): δ 28.04, 61.60, 68.95, 70.28, 70.48, 70.50, 70.52, 70.64, 72.47, 81.40, 169.60 ppm. RP-LCMS: calc. M_w = 396.5 g·mol^{-1}, found m/z: 419.0 [M+Na]$^+$.

Synthesis of compound **41**

tBuOAc-HEG **40** (7.58 g, 19 mmol) dissolved in 20 mL of chloroform was added slowly to a solution of 1,1'-carbonyldiimidazole (3.41 g, 21 mmol) in 20 mL of chloroform. After stirring for 16 hours the solution was diluted with 100 mL of chloroform and extracted twice with 70 mL 1 M aqueous citric acid. The combined water layers were extracted with 50 mL of chloroform, the combined chloroform layers were washed with a saturated sodium chloride solution, dried over $MgSO_4$, and concentrated to dryness yielding pure product (8.8 g, 94%). ^{1}H NMR (400 MHz, $CDCl_3$): δ 1.46 (s, 9H), 3.65 (m, 20H), 3.83 (t, 2H), 4,01 (s, 2H), 4.58 (t, 2H), 7,04 (s, 1H), 7,43 (s, 1H), 8.18 (s, 1H) ppm. ^{13}C NMR (400 MHz, $CDCl_3$): δ 28.07, 67.11, 68.57, 68.99, 70.53, 70.56, 70.61, 70.68, 81.47, 117.15, 130.62, 137.15, 148.67, 169.62 ppm.

Synthesis of compound **42**

The activated HEG **41** (8.83 g, 18 mmol) dissolved in 15 mL chloroform was added to mono-protected diamine **39** in 45 mL chloroform. The reaction mixture was stirred at reflux for 16 hours, cooled to room temperature and diluted with 200 mL chloroform. The solution was washed with 120 mL 1 M aqueous citric acid and with a 1:1 mixture of a saturated aqueous sodium chloride (60 mL) and 1 M aqueous citric acid (60 mL). The combined water layers were extracted with 60 mL chloroform. The combined chloroform layers were washed with a saturated sodium chloride solution, dried over $MgSO_4$ and concentrated to yield of the pure product (11.8 g, 98%). ^{1}H NMR (400 MHz, $CDCl_3$): δ 1.33 (m, 4H), 1.46 (m, 13H), 3.18 (m, 4H), 3.65 (m, 20H), 3.69 (t, 2H), 4,01 (s, 2H), 4.20 (t, 2H), 4.91 (s, 2 NH), 5.10 (s, 2H), 7.31 (m, 5H) ppm. ^{13}C NMR (400 MHz, $CDCl_3$): δ 26.22, 28.09, 029.82, 40.77, 40.85, 63.80, 66.53, 69.01, 69.64, 70.49, 70.53, 70.55, 70.59, 70.69, 81.51, 128.04, 128.08, 128.48, 136.66, 256.43, 169.66 ppm. RP-LCMS: calc. M_w = 672.8 g·mol^{-1}, found m/z: 673.2 [M+H]$^+$, 690.4 [M+NH$_4$]$^+$, 695.4 [M+Na]$^+$, 617.3 [M-tBu+H]$^+$.

Synthesis of compound **43**

tBuOAc-HEG-C6-diamine-Z **42** (8.8 g, 13.1 mmol) was dissolved in 80 mL ethanol and nitrogen gas was bubbled through for 10 minutes. After adding 0.9 g of Pd/C (5% Pd, Degussa type), the mixture was shaken in a Parr reactor at 55 psi H_2 for 5 hours. After adding additional Pd/C, the mixture was shaken overnight at 50 psi H_2. The reaction mixture was filtered over Celite and evaporated to dryness to afford the pure product (6.9 g, 98%) ^{1}H NMR (400 MHz, $CDCl_3$): δ 1.39 (m, 4H), 1.48 (s, 9H), 1.53 (m, 2H), 5.62 (m, 2H), 2.86 (t, 2H), 3.16 (q, 2H), 3.67 (m, 22H), 4.05 (s, 2H), 4.11 (t, 2H), 5.18 (s, 1NH, $1NH_2$), 5.54 (t, 1NH). ^{13}C NMR (400 MHz, $CDCl_3$): δ 26.08, 28.08, 29.48, 29.72, 40.59, 40.69, 63.62, 68.95, 69.75, 70.42, 70.44, 70.46, 70.61, 81.61, 156.50, 169.17, 169.70. RP-LCMS: calc. M_w = 538.7 g·mol^{-1}, found m/z: 539.5 [M+H]$^+$.

Synthesis of compound **44**

tBuOAc-HEG6-C6-NH_2 **43** (6.77 g, 12.6 mmol), UPy-C6-NCO (3.5 g, 11.9 mmol) and N,N-diisopropylethylamine (DIPEA, 1 mL, 6.3 mmol) were stirred in 100 mL chloroform at 65 °C. After 2 hours no isocyanate absorption was observed with FT-IR. 50 mL of chloroform and 20 mL of ethanol were added and the mixture was filtered over Celite. The filtrate was concentrated and dissolved in 140 mL chloroform and 10 mL ethanol and precipitated in 1500 mL pentane. The product was collected by filtration and washed with pentane. Drying yielded 9.95 g (101%) of the product contaminated with DIPEA. This crude product was used without further purification. ^{1}H NMR (400 MHz, $CDCl_3$) δ 1.38 (d, 7H), 1,5 (m, 27H), 2.21 (s, 3H), 3.1 (m, 7H), 3.23 (m, 2H), 3.63 (m, 24H), 4.01 (s, 2H), 4.21 (t, 2H), 4.71 (s, NH), 4.88 (s, NH), 5.06 (s, NH),5.82 (s, 1H), 10.02 (s, NH), 11.81 (s, NH), 13.12 (s, NH) ppm. ^{13}C NMR (400 MHz, $CDCl_3$): δ 18.94, 26.21, 26.29, 26.35, 28.09, 29.31, 29.79, 29.95, 30.19, 39.64, 39.99, 40.74, 41.94, 53.66, 63.77, 68.99, 69.63, 70.52, 70.68, 81.56, 106.52, 148.48, 154.64, 156.45, 156.52, 158.80, 169.68, 173.18 ppm. RP-LCMS: calc. M_w = 832.0 g·mol^{-1}, found m/z: 832.6 [M+H]$^+$, 854.5. [M+Na]$^+$.

Synthesis of compound **6**

tBuOAc-HEG-C6-C6-UPy **44** was dissolved in 150 mL dichloromethane with 50 mL trifluoro acetic acid. After stirring for 3 hours at room temperature the reaction was concentrated and co-evaporated three times with toluene. The crude product was dissolved in 60 mL chloroform and 12 mL ethanol and precipitated in 1000 mL diisopropyl ether. The product was collected by filtration and washed with diisopropyl ether. An addition wash step with 50 mL diisopropyl ether containing 50 mg BHT and drying yielded the pure product. (8 g, 95%). ^{1}H NMR (400 MHz, $CDCl_3$/CD_3OD) δ 1.20-1.55 (14H), 1.59 (t, 2H), 2.24 (s, 3H), 3.11 (m, 6H), 3.27 (m, 2H), 3.68 (m, 20H), 4.15 (s, 2H), 4.19 (t, 2H), 5.85 (s, 1H) ppm. ^{13}C NMR (400 MHz, DMSO-d_6): δ 18.52, 23.47, 26.47, 26.55, 29.54, 29.85, 30.44, 30.46, 30.86,, 396.43, 39.59, 39.62, 63.42, 68.02, 68.15, 69.35, 70.18, 70.22, 70.27, 70.42, 104.95, 151.87, 155.25, 156.58, 158.55, 172.08 ppm. RP-LCMS: calc. M_w = 775.9 g·mol^{-1}, found m/z: 776.5 [M+H]$^+$, 798.3 [M+Na]$^+$.

Synthesis of UPy-building block 7
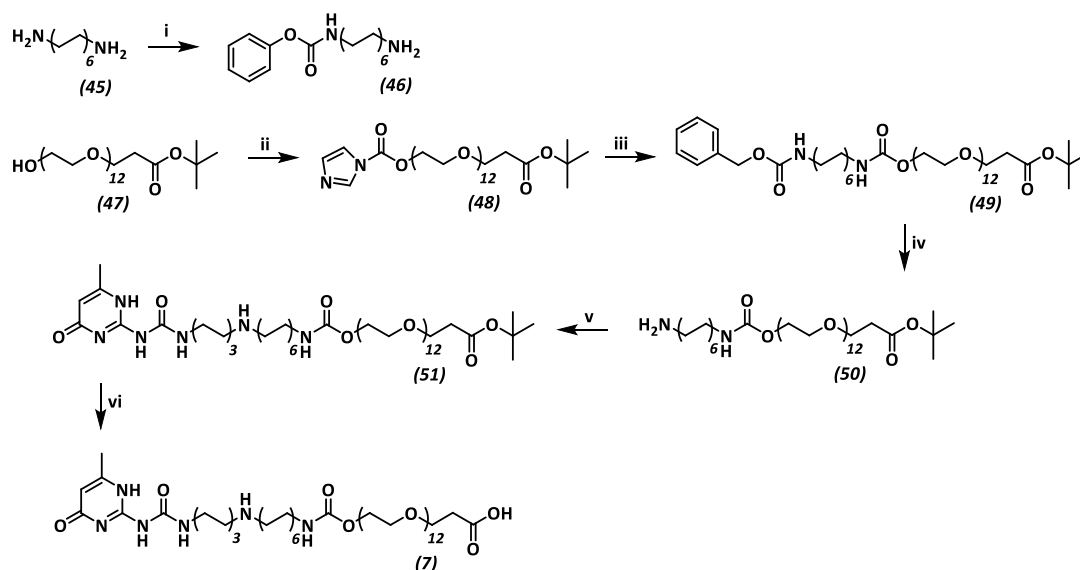
Scheme 3.7. Synthesis of UPy building block **7**. i) BPC, EtOH, reflux at 65 °C, o.n., 45%; ii) CDI, CHCl3, RT, 24 hours, quantitative; iii) CbzNHC$_{12}$H$_{24}$NH$_2$, CHCl$_3$, 65 °C, 24 hours, 67%; iv) 5% Pd/C, H$_2$, EtOH, RT, 20 hours, 94%; v) UPy-C$_6$-NCO, DIPEA, CHCl$_3$, 65 °C, 1 hour, 85%; vi) TFA, DCM, RT, 3 hours, 86%.

*Synthesis of compound **46***

Benzyl carbonate (5 g, 21.9 mmol) was dissolved in 10 mL ethanol and was added dropwise to a solution of 1,12-diaminododecane **45** (4.83 g, 24.1 mmol) in 25 mL ethanol. The resulting mixture was stirred overnight at reflux. After cooling to room temperature, 50 mL of ethanol was added, resulting in a precipitate that was removed by filtration and washed with 100 mL of ethanol. The ethanol was subsequently concentrated to approximately 10 mL and stirred with aqueous HCl (450 mL, 1M) for 30 minutes. The resulting salt was collected by filtration, washed with 1 M HCl, and stirred for 16 hours in aqueous HCl (250 mL, 1M). The solid was collected by filtration and washed with diethyl ether (2 x 100 mL) and dichloromethane (3 x 100 mL). The resulting residue was dissolved in 200 mL of dichloromethane and 50 mL of ethanol. This solution was washed twice with 50 mL of a 1 M solution of sodium hydroxide. The aqueous phase was extracted twice with 50 mL dichloromethane and once with 50 mL of chloroform containing 10% methanol. The combined organic layers were dried over Na$_2$SO$_4$ en concentrated *in vacuo* to afford the crude product, which was purified by column chromatography using silica, eluting with dichloromethane containing 10-15% methanol and 1-2% triethylamine yielding the pure product (3.33 g, 45%). ^{1}H NMR (400 MHz, CDCl$_3$): δ 1.15 (s, 2H), 1.26 (m, 16H), 1.45 (m, 4H), 2.65 (t, 2H), 3.18 (q, 2H), 5.08 (s, 2H), 7.37 (m, 5H) ppm. ^{13}C NMR (400 MHz, CDCl$_3$): δ 26.58, 26.68, 29.11, 29.64, 29.37, 29.40, 29.68, 32.95, 40.80, 41.84, 66.38, 75.60, 75.62, 127.79, 127.88, 128.32, 136.50, 156.77 ppm. RP-LCMS: calc. M$_w$ = 334.3 g·mol^{-1}, found m/z: 335.4 [M+H]$^+$.

*Synthesis of compound **49** via **48***

OEG12-tBu **47** (1 g, 1.48 mmol) was dissolved in 5 mL chloroform. The reaction mixture was stirred at room temperature for 24 hours. Amine **46** (0.545 g, 1.63 mmol) was added to this reaction mixture and stirring was continued for 2 hours at 65 °C, affording a turbid solution. The reaction mixture was cooled to room temperature and the precipitate was removed by filtration. Analysis by NMR revealed incomplete conversion to the carbamate. Additional amine **46** (0.21 g, 0.63 mmol) was added to the reaction mixture, which was heated at reflux for another 24 hours to afford full conversion. The reaction mixture was then diluted with 40 mL of chloroform and washed with a 0.5 M aqueous citric acid solution (2 x 20 mL) and a saturated sodium chloride

was added dropwise to a solution of N,N-carbonyldiimidazole (0.264 g, 1.63 solution (20 mL), drying over $MgSO_4$ and concentrated *in vacuo*. The crude product was purified by silica column chromatography using chloroform containing 2-5% of methanol to afford the pure product (1.03 g, 67%). ^{1}H NMR (400 MHz, $CDCl_3$): δ 1.26 (m, 16H), 1.47 (m, 13H), 2.51 (t, 2H), 3.18 (m, 4H), 3.65 (m, 48H), 4.21 (t, 2H), 5.08 (s, 2H), 7.37 (m, 5H) ppm. ^{13}C NMR (400 MHz, $CDCl_3$): δ 26.71, 28.08, 29.22, 29.47, 29.93, 36.24, 41.02, 41.09, 63.76, 66.51 66.87, 69.67, 70.33, 70.47, 70.48, 70.54, 80.46, 128.02, 128.07, 128.46, 136.66, 156.36, 170.86 ppm. RP-LCMS: calc. M_w = 1034.65 g·mol^{-1}, found m/z: 1035.1 $[M+H]^+$, 1052.4 $[M+NH_4]^+$, 1057.6 $[M+Na]^+$.

Synthesis of compound **50**
1.03 g of tBu-OEG12-C12-diamine-Z **49** was dissolved in 25 mL ethanol in a round bottom flask provided with one stopcock attached to an argon/vacuum line and one stopcock attached to a balloon filled with H_2 After addition of 90 mg Pd/C (5% Pd, Degussa type), the system was purged and brought to a hydrogen atmosphere. The reaction mixture was stirred for 20 hours at room temperature, purging and refilling the balloon as necessary, leading to full conversion. The reaction mixture was filtered over Celite and evaporated to dryness affording the pure product (0.84 g, 94%). ^{1}H NMR (400 MHz, $CDCl_3$): δ 1.31 (m, 16H), 1.45 (s, 9H), 1.50 (m, 4H), 1.76 (t, 2H), 2.51 (t, 2H), 2.94 (t, 2H), 3.18 (q, 4H), 3.65 (m, 48H), 4.21 (t, 2H), 5.40 (t, 1H) ppm. ^{13}C NMR (400 MHz, $CDCl_3$): δ 26.54, 26.64, 27.90, 28.06, 28.93, 29.09, 29.23, 29.27, 29.30, 29.83, 36.23, 40.13, 41.00, 63.60, 66.85, 69.81, 70.31, 70.48, 80.45, 156.38 ppm. RP-LCMS: calc. M_w = 900.61 g·mol^{-1}, found m/z: 901.6 $[M+H]^+$.

Synthesis of compound **51**
tBu-OEG12-C12-NH_2 **50** (0.83 g, 0.92 mmol), UPy-C6-NCO (0.27 g, 0.92 mmol) and N,N-diisopropylethylamine (0.18 mL, 1.01 mmol) were stirred in 15 mL chloroform at 65 °C. After 1 hour no isocyanate absorption was observed with FT-IR, 2 mL ethanol was added and the mixture was filtered over Celite. The filtrate was concentrated and dissolved in 8 mL chloroform and 2 mL of ethanol and precipitated in 100 mL pentane. The product was collected by filtration and washed with pentane. Drying yielded the pure product (0.95 g, 85%). ^{1}H NMR (400 MHz, $CDCl_3$): δ 1.4 (m, 37H), 2.22 (s, 3H), 2.51 (t, 2H), 3.20 (m, 8H), 3.65 (m, 48H), 4.21 (t, 2H), 4.63 (s, NH), 4.85 (s, NH), 4.95 (s, NH), 5.83 (s, 1H), 10.05 (s, NH), 11.85 (s, NH), 13.18 (s, NH). RP-LCMS: calc. M_w = 1193.8 g·mol^{-1}, found m/z: 608.8 $[M+H+Na]^{2+}$, 1194.3 $[M+H]^+$.

Synthesis of compound **7**
tBu-OEG12-C12-C6-UPy **51** was dissolved in 20 mL dichloromethane and 5 mL trifluoro acetic acid was added. After stirring for 3 hours at room temperature the reaction was concentrated and co-evaporated three times with toluene. The crude product was dissolved in 6 mL chloroform and 0.5 mL ethanol and precipitated in 100 mL diisopropyl ether. The product was collected by filtration and washed with diisopropyl ether. Drying yielded 0.78 g (86%) of the pure product. ^{1}H NMR (400 MHz, $CDCl_3$): δ 1.4 (m, 28H), 2.22 (s, 3H), 2.62 (t, 2H), 3.20 (m, 8H), 3.65 (m, 48H), 4.21 (t, 2H), 4.95 (s,3 NH), 5.83 (s, 1H), 10.05 (s, NH), 11.85 (s, NH), 13.18 (s, NH). ^{13}C NMR (400 MHz, $CDCl_3$): δ 18.95, 26.69, 26.87, 29.20, 29.28, 29.45, 29.90, 30.15, 35.05, 39.55, 40.59, 63.79, 66.70, 69.67, 70.29, 70.53, 75.60, 106.52, 139.45, 156.48, 187.24, 187.26 ppm. RP-LCMS: calc. M_w = 1137.70 g·mol^{-1}, found m/z: 1138.58 $[M+H]^+$, 570.1 $[M+2H]^{2+}$.

Convergent synthesis of UPy-peptide conjugates

Synthesis of UPy-peptide conjugates using UPy-building block 4

*Coupling of UPy building block **4** to the peptides*
The resin with the peptides (200 μmol) was allowed to swell in dry DMF (4 mL) for 30 min. Succinic anhydride (200 mg, 2 mmol) and pyridine (2 mL) were dissolved in 3 mL dry DMF. The resulting mixture was added to the peptides and shaken overnight at room temperature. The product was washed with dry DMF (6x). The acid-functionalized peptide (0.1 mmol) on the resin was set to swell in DMF (5 mL) for 2 hours. A stock solution of UPy building block was prepared by dissolving the compound **4** (200 mg, 0.25 mmol) in 4 mL DMF with DIPEA (174 μL, 1 mmol) and PyBOP (104 mg, 0.2 mmol). This mixture was added to the peptide on the resin and shaken

overnight at room temperature. The product was washed with DMF (6x) the next day. After washing, the peptide-containing resin was washed with 3 mL DCM (6x), allowed to dry under high vacuum and stored at -30 °C. Cleavage of the UPy-functionalized peptide and deprotection of the amino acid protecting groups was performed using a cleavage cocktail consisting of TFA, H_2O and TIS (95/2.5/2.5 v/v %) This mixture was added to the syringe and shaken for 3.5 hours at room temperature, the TFA was removed with a flow of N_2, followed by precipitation of the product in ice-cold diethylether (20 mL). The precipitate was pelleted by centrifugation at 20k rpm for 10 min, re-dissolved in 10% MeCN in H_2O, and lyophilized. The UPy-functionalized peptide was purified using preparative RP-HPLC-MS on a C18 column using a gradient of 18-22% MeCN in H_2O, containing 0.1% TFA. Lyophilizing yielded the pure products **8a** 21%, **8b**, 20% **8c**, 32%, **8d** 20%.

8a RP-LCMS: calc. M_w = 1315.6 g·mol^{-1}, found m/z: 1315.8 [M+H]$^+$, 648.7 [M+2H]$^{2+}$, 439.6 [M+3H]$^{3+}$.

8b RP-LCMS: calc. M_w = 1491.8 g·mol^{-1}, found m/z: 1491.7 [M+H]$^+$, 746.5 [M+2H]$^{2+}$, 498.0 [M+3H]$^{3+}$.

8c RP-LCMS: calc. M_w = 1314.6 g·mol^{-1}, found m/z: 1315.8 [M+H]$^+$, 658.4 [M+2H]$^{2+}$, 669.3 [M+H+Na]$^{2+}$.

8d RP-LCMS: calc. M_w = 1271.6 g·mol^{-1}, found m/z: 1272.5 [M+Na]$^+$, 636.9 [M+2H]$^{2+}$.

Synthesis of UPy-peptide conjugates using UPy-building block 5

*Coupling of UPy building block **5** to the peptides*

The resin with the peptides (200 µmol) was allowed to swell in dry DMF (2 mL). Succinic anhydride (200 mg, 2 mmol) and pyridine (2 mL) were dissolved in 3 mL dry DMF. The resulting mixture was added to the peptides (200 µmol) and shaken overnight at room temperature. The product was washed dry DMF (6x). A stock solution of UPy-building block **15** was prepared by dissolving the compound (266 mg, 250 µmol) in 8 mL DMF with PyBOP (104 mg, 200 µmol) and DIPEA (70 µL, 400 µmol). *Via* the syringe, 2 mL of the mixture was added to each of the peptides and shaken overnight at room temperature. This procedure was repeated after one day, and washing six times with DMF. The resin-bound product was washed six times with DMF. Cleavage of the UPy-peptide conjugates was performed using a cleavage cocktail of TFA/H_2O/TIS/EDT (92.5/2.5/2.5/2.5 v/v %) for four hours, the TFA was removed with a flow of N_2, followed by precipitation of the product in cold di-ethyl ether for 15 minutes. After spinning the precipitate for 15 minutes at 20k RPM and redissolving in 1:1 H_2O:MeCN with TFA the products were lyophilized. Purification by prep-RP-HPLC on a C18 column using a gradient of 15-40% MeCN in H_2O with 0.1% TFA yielded **9a** 19%, **9b** 33%.

9a RP-LCMS: calc. M_w = 1693.9 g·mol^{-1}, found m/z: 847.6 [M+2H]$^{2+}$, 565.5 [M+3H]$^{3+}$.

9b RP-LCMS: calc. M_w = 1927.1 g·mol^{-1}, found m/z: 964.5 [M+2H]$^{2+}$, 643.3 [M+3H]$^{3+}$, 482.7 [M+4H]$^{4+}$.

Synthesis of UPy-peptide conjugates using UPy-building block 6

*Coupling of UPy building block **6** to the peptide RGDS using PyBOP (solid phase)*

The dry peptide on Rink Amide MBHA resin (26 µmol) were suspended in NMP and allowed to swell for one hour, followed by deprotection two times with 20% piperidine in NMP (4 mL, 8.3 mmol) while shaken 5 min. The resin was washed with 3 mL NMP (6x). UPy building block **6** (58 mg, 51 µmol), PyBOP (26.6 mg, 51 µmol) and DIPEA (24.5 µl, 260 µmol) were dissolved in 3 mL DMF and added to the resin. The reaction mixture was shaken at room temperature for 16 hours, the resin was washed with 3 mL NMP (1x) and alternating with DCM and diethyl ether (5x). The peptide conjugate was deprotected and cleaved from the resin using a cleavage cocktail of TFA/H_2O/TIS/EDT (94/2/2/2 v/v %) for four hours. The resulting UPy-peptide conjugate was precipitated in ice-cold diethyl ether and incubated at -20 °C for 15 minutes. The precipitate was pelleted by centrifugation at 20k rpm for 10 minutes. The supernatant was re-dissolved in 10% MeCN in H_2O, and lyophilized. The products were purified using preparative RP-HPLC-MS on a C18 column using a gradient of 30-50% MeCN in H_2O, containing 0.1% TFA. Lyophilizing yielded the pure product **13a** 50%.

13a RP-LCMS: M_w = 1303.7 g·mol^{-1}l, found m/z: 1304.8 [M+H]$^+$, 653.3 [M+2H]$^{2+}$, 435.9 [M+3H]$^{3+}$.

Coupling of UPy-peptide building block 6 to the peptide RGDS using HATU (solid phase)

Rink Amide resin (~ 100 µmol) with the attached peptide was allowed to swell in N,N-Dimethylacetamide (DMAc) for 3 hours, rinsed with DMAc and combined with a solution of **6** (115 mg, 0.15 mmol), DIPEA (52 µL, 0.3 mmol), and HATU (49 mg, 0.13 mmol) in DMAc that was pre-activated for 30 minutes. The resin was agitated in the reaction mixture for 90 minutes, rinsed with DMAc (7 x 2 mL), rinsed with DCM (5 x 2 mL) and dried *in vacuo*. After a test-cleavage showed complete conversion to **13b** the resin was stirred in 5 mL cleavage mixture (TFA/H_2O/TIS 95/2.5/2.5 v/v %) for 2 hours. The resulting solution was collected and the resin was washed with cleavage mixture (2 x 2.5 mL) and DCM (2 x 2.5 mL). The collected organic phases were reduced to 4 mL by gently blowing argon over the solution. The resulting mixture was precipitated in 50 mL ice-cold diethyl ether resulting in a white precipitate that was collected by centrifugation, dried. The product was purified using preparative RP-HPLC-MS on a C18 column using a gradient of MeCN in H_2O, containing 0.1% formic acid to afford 74 mg **13b** (57%).

13b RP-LCMS: calc. M_w = 1303.7 g·mol^{-1}, found: 1304.4 [M+H]$^+$, 653.1 [M+2H]$^{2+}$.

Coupling of UPy-peptide building block 6 to cyclic RGD using PyBOP (solution phase)

A solution of **6** (54 mg, 70 µmol), c(KRGDf) amine (66 mg, 72 µmol), PyBOP (39 mg, 75 µmol), and DIPEA (35 µL, 200 µmol) was stirred in 4.5 mL DMF for 1 hour under argon. After confirmation of full conversion with LC-MS the reaction mixture was precipitated in 40 mL diethyl ether. The crude product was dried and purified using preparative RP-HPLC-MS on a C18 column using a gradient of MeCN in H_2O, containing 0.1% formic acid to afford 74 mg **13c** (56%).

13c RP-LCMS: calc. M_w = 1668.9 g·mol^{-1}, found m/z: 1669.5 [M+H]$^+$, 835.8 [M+2H]$^{2+}$.

Deprotection of 13c

Protected RGD derivative **13c** (105 mg) was stirred with TFA (9.5 mL), TIS (250 µL) and water (250 µL) for 90 minutes. The volume was subsequently reduced to approx. 5 mL at room temperature by gently blowing argon over the solution. The resulting mixture was precipitated in 45 mL ice-cold ether. The precipitate was collected by centrifugation, dried, purified by RP-HPLC-MS on a C18 column using a gradient of MeCN in H_2O, containing 0.1% formic acid and lyophilized to afford 94 mg **13c** as a white fluffy solid (109% containing TFA).

13c' RP-LCMS: calc. M_w = 1360.7 g·mol^{-1}, found m/z: 1361.6 [M+H]$^+$, 681.7 [M+2H]$^{2+}$, 454.8 [M+3H]$^{3+}$.

Synthesis of UPy-peptide conjugates using UPy-building block 7

Coupling of UPy-peptide building block 7 to the peptides

The dry peptides on Rink Amide MBHA resin (52 µmol for GGDGEA, 28 µmol for GGRGDS) were suspended in NMP and allowed to swell for one hour, followed by deprotection two times with 20% piperidine in NMP (4 mL, 8.3 mmol) while shaken 5 min. The resin was washed with 3 mL NMP (6x) and 3 mL DMF (6x). UPy building block **7** (100 mg, 87.8 µmol) was pre-activated using HATU (27.5 mg, 72.3 µmol) and DIPEA (27.0 µL, 155.0 µmol) in 10 mL DMF for 30 minutes at room temperature. The reaction mixture in DMF was added to the resin and shaken at room temperature for two hours, the resin was washed with 3 mL DMF (6x) and 3mL DCM (6x), deprotected and cleaved from the resin using a cleavage cocktail of TFA/H_2O/TIS/EDT (94/2/2/2 v/v %) for four hours. The resulting UPy-peptide conjugates were precipitated in ice-cold hexane/diethyl ether (20/80 v/v %) mixture, and incubated at -20 °C for 15 minutes. The precipitate was pelleted by centrifugation at 20k rpm for 10 minutes. The pellet was re-dissolved in 10% MeCN in H_2O, and lyophilized. The products were purified using preparative RP-HPLC-MS on a C18 column using a gradient of 30-50% MeCN in H_2O, containing 0.1% TFA. Lyophilizing yielded the pure products **14a** 42%, **14b** 42%.

14a RP-LCMS: calc. M_w = 1666.9 g·mol^{-1}, found m/z: 1666.8 [M+H]$^+$, 834.3 [M+2H]$^{2+}$, 556.7 [M+3H]$^{3+}$.
14b RP-LCMS: calc. M_w = 1622.9 g·mol^{-1}, found m/z: 1623.7 [M+H]$^+$, 812.5 [M+2H]$^{2+}$, 542.3 [M+3H]$^{3+}$.

Methods

Preparation of dropcast surfaces. Samples were prepared by dropcast of 30 µL of a solution of 50 mg·mL^{-1} PCLdiUPy with 0 or 4 mol% UPy-HBP from HFIP on glass cover slips with a diameter of 12 mm, yielding a thin solid material film with a thickness in the range of 4-6 µm as was determined by profilometry measurements. Fluorescence assay samples were prepared by dropcast of 25 µL of a solution of 50 mg·mL^{-1} of the PCLdiUPy with 0 or 4 mol% UPy-HBP from HFIP in a well of 96-wells plate. Subsequent solvent evaporation yielded a solid, impermeable dropcast film.

Solid Phase Peptide Synthesis. The UPy-HBP peptide was manually synthesized *via* Fmoc solid phase peptide synthesis (SPPS) on an Fmoc-Rink-Amide resin (Novabiochem) at a 400 µmol scale. The resin was allowed to swell for 15 minutes in N-methylpyrrolidone (NMP). Fmoc deprotection was done with 5 mL 20% (v/v) piperidine in NMP and incubated for 5 minutes, twice. Amino acids (4 eq.) (Novabiochem) were activated with 2-(1H-Benzotriazole-1-yl)-1,1,3,3-Tetramethyluronium hexafluorophosphate (HBTU) (3.9 eq.) in NMP and alkalized with N,N-diisopropylethylamine (DIPEA) (8 eq.) in a total volume of 12 mL. Amino acids were coupled once for 30 minutes. The final amino acid (Phe) was Boc-protected. All steps were performed under constant agitation and with washing steps with NMP (4 mL) in between. After the peptide coupling, UPy-COOH was coupled at the N-terminus while the peptide was still on the resin using PyBOP and DiPEA in DMF overnight. In a final step, the UPy-peptide was cleaved from the resin using 95% trifluoroacetic acid (TFA), 2.5% triisopropylsilane (TIS) and 2.5% H$_2$O for 3 hours at room temperature. The cleaved UPy-peptide was precipitated in ice cold diethylether, centrifuged (2000 rpm, 10 minutes) and dissolved in MeCN/H$_2$O (1:6, v/v %). The cleaved UPy-peptide was purified using a preparative LC-ESI-MS system, equipped with a reverse phase C18 column. After filtration, the UPy-peptide was purified using a linear gradient of 30-35% MeCN/H$_2$O with 0.1% TFA and a flow of 20 mL·min^{-1}. The final purity of the UPy-peptide was determined with an analytical LCMS using a 5-70 MeCN gradient in H$_2$O with 0.1% formic acid (FA) in a final yield of 42%. After lyophilization, the purified UPy-peptide was stored at -30 °C.

^{1}H NMR (400 MHz, DMSO-d$_6$): δ 11.56 (s, 1H), 9.70 (s, 1H), 8.17-7.00 (m, 15H), 5.75 (s, br, 2H), 4.34 – 4.30 (q, 1H), 4.24 – 4.14 (m, 6H), 4.04 – 4.02 (t, 2H), 3.93 (s, 2H), 3.85 – 3.65 (2d, 2H), 3.61 – 3.51 (m, 22H), 3.15 – 3.08 (m, 4H), 2.96 – 2.91 (m, 6H), 2.76 – 2.67 (m, 6H), 2.10 (S, 3H), 1.71 – 1.21 (m, 47H), 0.89 – 0.82 (m, 12H). ESI-MS (positive mode): *m/z* calcd. For [M+H]$^+$ 1164.4; found: 583.1 [M+2H]$^{2+}$. HPLC: 5.30 min, *m/z*: 583.08 [M+2H]$^{2+}$, 1164.67 [M+H]$^{1+}$, 1186.58 [M+Na]$^{1+}$.

Fluorescence spectroscopy. Fluorescence assays were performed on a Thermo Scientific Fluoroskan Ascent Microplate Fluorometer. Surfaces were excited at 488 nm and emission was recorded at 538 nm. Surfaces were prepared from 50 mg·mL^{-1} PCLdiUPy +/- 4 mol% UPy-HBP in HFIP dropcast into a 96-wells plate. After overnight drying of the surface, surfaces were incubated overnight with 100 µL heparin-FITC (Life Technologies) at 20 µg·mL^{-1} concentration at 37 °C. Fluorescence levels were determined after washing three times. (Fluoroskan Ascent FL).

Surface experiments. Heparin incubation was done using heparin sodium salt (Sigma Aldrich: Cat.# 3149-10ku, Lot.#SLBC9940v, 192 u·mg^{-1}) at a 20 µg·mL^{-1} concentration, 250 µL·well^{-1}, for 1 hour at 37 °C. Non heparin coated controls were incubated using PBS. Fluid was pipetted off and one washing step was performed, addition of 250 µL PBS in all wells, and pipetting fluid off all wells. Subsequently designated surfaces were incubated 1h with an effective dose of 2 ng TGF-β3 (250 µL at 8 ng·mL^{-1} concentration), other surfaces incubated with PBS at 37 °C. After incubation the fluids were pipetted off and were immediately seeded with MEEC (no washing step after TGF-β incubation).

Maintaining cell-lines. MEEC were maintained on tissue culture treated polystyrene using high glucose DMEM (Life Technologies #41966) + 10% FBS (no heat inactivation[†]) + 1% Penicillin/Streptomycin. Stimulation with either TGF-β1 or β3 in MEEC was performed with a reduced serum concentration (5%).

Cell seeding. In all experiments cells MEEC were seeded at a density of 15,000 cells·cm^{-2}. In all experiments including soluble growth factors or peptides 6 well plates were used, and 142,500 cells·well^{-1} were seeded. Surface experiments were performed in 24 well plates, where 28500 cells·mL^{-1} were seeded.

Cell stimulation. Approximately 2 hours after seeding, seeding medium was aspirated and replaced by stimulation medium containing additional TGF-β3 (Peprotech, Cat. #100-36E, Lot# 0513410) at the specified concentrations without intermediate washing steps. Medium was refreshed every 48 hours, thereby also refreshing the stimulus. Experiments were performed N=4 for soluble experiments and N=3 for surfaces.

mRNA isolation. After 48 hours or of culture, the cells were washed 3 times with PBS and trypsinized. Cells were resuspended and transferred to 1.5 mL Eppendorf tubes on a well per well basis. Eppendorf tubes were spun 5 min at 440 G and medium was aspirated. Cell pellets were then washed using 1 mL PBS (3 times, with 5 min, 440 G spin in between washing steps). mRNA was then extracted using High Pure RNA Isolation Kit (Roche, #11 828 665 001) according to manufacturer's protocol. With 15,000 G at 2nd time washing with wash buffer II and mRNA was eluted using 50 µL elution buffer. RNA purity and concentration were determined by fluorescence absorption using a nano-drop spectrophotometer.

cDNA synthesis. cDNA synthesis was performed using iScript cDNA synthesis kit (Biorad, #17-8891) according to manufacturer's protocol. Sample cDNA for RT-PCR was made by dilution of stock cDNA to a concentration of 1 ng·µL^{-1}.

RT-PCR. PCR reaction for all experiments was performed using a two-step protocol followed by a melting curve using Biorad CFX96 Real time system-C1000 touch thermal cycler. In all experiments a standard curve and N.T.C. was taken into account. Ideal temperatures for primers was determined by a gradient run and subsequently a std-curve and melt curve was determined to assess specific product formation. Primer master mixes per samples were prepared as follows: 6.9 µL mQ, 12.5 µL iQ SYBR Green Supermix (Biorad, #170-8886), 0.3 µL Fw (25 pmol concentration), and 0.3 µL Rev (25 pmol concentration). 96 well plates (Biorad, #HSP9645) were filled with 20 µL mastermix per well and subsequently 5.0 µL (5 ng) sample cDNA was added. Std curves were performed using a 10 ng·µL^{-1} starting concentration and a subsequent 5 times dilution for 5 concentrations. mRNA levels were corrected for GAPDH mRNA levels. The average of each group was determined as the standard deviations (= stdev). SEM was determined by dividing the stdev by sample size. Data and SEM were standardized by dividing the averages with the average of the control group. Statistical analyses were performed using a T-test. Assuming a two tailed distribution and assuming two-sample equal variance. All groups were N=4.

RT-PCR amplification protocol.

Step 1:	95 °C	3:00	Go to: Step 2
Step 2:	95 °C	0:10	
	63 °C	0:30	
	Plate read		Go to: Step 2, 39x, and then Step 3.
Step 3:	50 °C	0:05	
Step 4:	Increase temp 0.5 °C	0:05	
	Plate read		Go to: Step 4, till 95 °C.

[†] Heat inactivation can activate latent TGF-β present in FBS therefore maintain cells in non-heat inactivated culture media.

Cryopreservation of MEEC. To ensure the availability of the Mouse Embryonic Endothelial Cell-line at Eindhoven University of Technology for future work cells were cryopreserved. In the cryopreservation process cells are slowly cooled (-1°C·minute^{-1}) to -80 °C forcing the cells into a quiescent state and subsequently stored in liquid Nitrogen for long term viable storage. MEEC were expanded, collected and counted. The cells were then pre diluted in ice cold DMEM (Life Technologies #41966), containing 10% FBS to a concentration of $4·10^6$ cells·mL^{-1}. Subsequently an equal volume of DMEM, containing 10% FBS and 20% DMSO was added and the cell suspension was thoroughly mixed. Aliquots of 1 mL were added to cryogen vials (Nunc Cryotube Vials #2015-07) and these were then stored in Mr. Frosty Freezing Container's and stored at -80 °C for 3 days. The vials were then transferred to liquid nitrogen storage (Tower: Red, Box: 5)

Primers for mouse cell types:

GENE	FW	REV
GADPH	GCGACTTCAACAGCAACTCC	CCCTGTTGCTGTAGCCGTAT
A-SMA	GAAGGAGATCACAGCCCTCG	GAAGGTAGACAGCGAAGCCA
SNAIL	CCACACTGGTGAGAAGCCAT	CACATCCGAGTGGGTTTGGA
FLK-1	ACCAAGGCGACTATGTTTGC	GGGCAAGTCACTTCAATGGT
CD31	AGGTCGACCCTAAGAACGGA	CTCTTCTCGGGACATGGACG

3.5 References

1. Vacanti, C. A. History of tissue engineering and a glimpse into its future. *Tissue Eng.* **12,** 1137–1142 (2006).
2. Place, E. S., Evans, N. D. & Stevens, M. M. Complexity in biomaterials for tissue engineering. *Nat. Mater.* **8,** 457–470 (2009).
3. Lutolf, M. P. & Hubbell, J. A. Synthetic biomaterials as instructive extracellular microenvironments for morphogenesis in tissue engineering. *Nat. Biotechnol.* **23,** 47–55 (2005).
4. Shin, H., Jo, S. & Mikos, A. G. Biomimetic materials for tissue engineering. *Biomaterials* **24,** 4353–4364 (2003).
5. Nimmo, C. M. & Shoichet, M. S. Regenerative Biomaterials that 'Click': Simple, Aqueous-Based Protocols for Hydrogel Synthesis, Surface Immobilization, and 3D Patterning. *Bioconjug. Chem.* **22,** 2199–2209 (2011).
6. Teixeira, L. S. M., Feijen, J., van Blitterswijk, C. A., Dijkstra, P. J. & Karperien, M. Enzyme-catalyzed crosslinkable hydrogels: emerging strategies for tissue engineering. *Biomaterials* **33,** 1281–1290 (2012).
7. Balakrishnan, B. & Banerjee, R. Biopolymer-Based Hydrogels for Cartilage Tissue Engineering. *Chem. Rev.* **111,** 4453–4474 (2011).
8. Sun, J. Y. *et al.* Highly stretchable and tough hydrogels. *Nature* **489,** 133–136 (2012).
9. Mollet, B. B. *et al.* A modular approach to easily processable supramolecular bilayered scaffolds with tailorable properties. *J. Mater. Chem. B* **2,** 2483–2493 (2014).
10. van Bommel, K. J. C. *et al.* Responsive Cyclohexane-Based Low-Molecular-Weight Hydrogelators with Modular Architecture. *Angew. Chem. Int. Ed.* **43,** 1663–1667 (2004).
11. Li, J., Ni, X. & Leong, K. W. Injectable drug-delivery systems based on supramolecular hydrogels formed by poly(ethylene oxide)s and α-cyclodextrin. *J. Biomed. Mater. Res. A* **65,** 196–202 (2003).
12. Galler, K. M., Hartgerink, J. D., Cavender, A. C., Schmalz, G. & D'Souza, R. N. A customized self-assembling peptide hydrogel for dental pulp tissue engineering. *Tissue Eng. Part A* **18,** 176–184 (2012).
13. Zhou, M. *et al.* Self-assembled peptide-based hydrogels as scaffolds for anchorage-dependent cells. *Biomaterials* **30,** 2523–2530 (2009).
14. Hartgerink, J. D., Beniash, E. & Stupp, S. I. Self-assembly and mineralization of peptide-amphiphile nanofibers. *Science* **294,** 1684–1688 (2001).
15. Zhang, S. Fabrication of novel biomaterials through molecular self-assembly. *Nat. Biotechnol.* **21,** 1171–1178 (2003).
16. Besenius, P. *et al.* Peptide functionalised discotic amphiphiles and their self-assembly into supramolecular nanofibres. *Soft Matter* **7,** 7980–7983 (2011).
17. Preslar, A. T. *et al.* Gd(III)-Labeled Peptide Nanofibers for Reporting on Biomaterial Localization in Vivo. *ACS Nano* **8,** 7325–7332 (2014).

18. Dankers, P. Y. W., Harmsen, M. C., Brouwer, L. A., Van Luyn, M. J. A. & Meijer, E. W. A modular and supramolecular approach to bioactive scaffolds for tissue engineering. *Nat. Mater.* **4,** 568–574 (2005).
19. Bakota, E. L., Wang, Y., Danesh, F. R. & Hartgerink, J. D. Injectable Multidomain Peptide Nanofiber Hydrogel as a Delivery Agent for Stem Cell Secretome. *Biomacromolecules* **12,** 1651–1657 (2011).
20. Pollino, J. M. & Weck, M. Non-covalent side-chain polymers: design principles, functionalization strategies, and perspectives. *Chem. Soc. Rev.* **34,** 193–207 (2005).
21. You, C. C., Verma, A. & Rotello, V. M. Engineering the nanoparticle–biomacromolecule interface. *Soft Matter* **2,** 190–204 (2006).
22. Stephanopoulos, N., Ortony, J. H. & Stupp, S. I. Self-Assembly for the Synthesis of Functional Biomaterials. *Acta Mater.* **61,** 912–930 (2013).
23. Tran, N. Q., Joung, Y. K., Lih, E., Park, K. M. & Park, K. D. Supramolecular Hydrogels Exhibiting Fast In Situ Gel Forming and Adjustable Degradation Properties. *Biomacromolecules* **11,** 617–625 (2010).
24. Bastings, M. M. C. *et al.* A Fast pH-Switchable and Self-Healing Supramolecular Hydrogel Carrier for Guided, Local Catheter Injection in the Infarcted Myocardium. *Adv. Healthc. Mater.* **3,** 70–78 (2014).
25. Dankers, P. Y. W. *et al.* Bioengineering of living renal membranes consisting of hierarchical, bioactive supramolecular meshes and human tubular cells. *Biomaterials* **32,** 723–733 (2011).
26. Folmer, B. J. B., Sijbesma, R. P., Versteegen, R. M., van der Rijt, J. a. J. & Meijer, E. W. Supramolecular Polymer Materials: Chain Extension of Telechelic Polymers Using a Reactive Hydrogen-Bonding Synthon. *Adv. Mater.* **12,** 874–878 (2000).
27. Dankers, P. Y. W., Adams, P. J. H. M., Löwik, D. W. P. M., van Hest, J. C. M. & Meijer, E. W. Convenient Solid-Phase Synthesis of Ureido-Pyrimidinone Modified Peptides. *Eur. J. Org. Chem.* **2007,** 3622–3632 (2007).
28. Kieltyka, R. E. *et al.* Modular synthesis of supramolecular ureidopyrimidinone–peptide conjugates using an oxime ligation strategy. *Chem. Commun.* **48,** 1452–1454 (2012).
29. Salber, J. *et al.* Influence of different ECM mimetic peptide sequences embedded in a nonfouling environment on the specific adhesion of human-skin keratinocytes and fibroblasts on deformable substrates. *Small Weinh. Bergstr. Ger.* **3,** 1023–1031 (2007).
30. Mizuno, M., Fujisawa, R. & Kuboki, Y. Type I collagen-induced osteoblastic differentiation of bone-marrow cells mediated by collagen-α2β1 integrin interaction. *J. Cell. Physiol.* **184,** 207–213 (2000).
31. Miyamoto, S., Akiyama, S. K. & Yamada, K. M. Synergistic roles for receptor occupancy and aggregation in integrin transmembrane function. *Science* **267,** 883–885 (1995).
32. Geiger, T. & Clarke, S. Deamidation, isomerization, and racemization at asparaginyl and aspartyl residues in peptides. Succinimide-linked reactions that contribute to protein degradation. *J. Biol. Chem.* **262,** 785–794 (1987).
33. Stephenson, R. C. & Clarke, S. Succinimide formation from aspartyl and asparaginyl peptides as a model for the spontaneous degradation of proteins. *J. Biol. Chem.* **264,** 6164–6170 (1989).
34. Pritz, S., Wolf, Y., Klemm, C. & Bienert, M. Modification of guanine residues in PNA-synthesis by PyBOP. *Tetrahedron Lett.* **47,** 5893–5896 (2006).
35. Wan, Z.-K., Binnun, E., Wilson, D. P. & Lee, J. A Highly Facile and Efficient One-Step Synthesis of N6-Adenosine and N6-2'-Deoxyadenosine Derivatives. *Org. Lett.* **7,** 5877–5880 (2005).
36. Feijter, I. de *et al.* Solid-Phase-Based Synthesis of Ureidopyrimidinone–Peptide Conjugates- for Supramolecular Biomaterials. *Synlett* **26,** 2707–2713 (2015).
37. Gilmore, L. *et al.* Arginine functionalization of hydrogels for heparin binding—a supramolecular approach to developing a pro-angiogenic biomaterial. *Biotechnol. Bioeng.* **110,** 296–317 (2013).
38. Ding, H. *et al.* Biologically Derived Soft Conducting Hydrogels Using Heparin-Doped Polymer Networks. *ACS Nano* **8,** 4348–4357 (2014).
39. Fernández-Muiños, T. *et al.* Bimolecular based heparin and self-assembling hydrogel for tissue engineering applications. *Acta Biomater.* **16,** 35–48 (2015).
40. Watarai, A. *et al.* TGFβ functionalized starPEG-heparin hydrogels modulate human dermal fibroblast growth and differentiation. *Acta Biomater.* **25,** 65–75 (2015).
41. Mitchell, A. C., Briquez, P. S., Hubbell, J. A. & Cochran, J. R. Engineering growth factors for regenerative medicine applications. *Acta Biomater.* **30,** 1–12 (2016).
42. Pagel, M. & Beck-Sickinger, A. G. Multifunctional biomaterial coatings: synthetic challenges and biological activity. *Biol. Chem.* **398,** 3–22 (2017).
43. Yang, H. N. *et al.* Differentiation of endothelial progenitor cells into endothelial cells by heparin-modified supramolecular pluronic nanogels encapsulating bFGF and complexed with VEGF165 genes. *Biomaterials* **35,** 4716–4728 (2014).

44.   Li, G., Yang, P., Liao, Y. & Huang, N. Tailoring of the Titanium Surface by Immobilization of Heparin/Fibronectin Complexes for Improving Blood Compatibility and Endothelialization: An in Vitro Study. *Biomacromolecules* **12,** 1155–1168 (2011).

45.   Liu, T. *et al.* Surface Modification with Dopamine and Heparin/Poly-l-Lysine Nanoparticles Provides a Favorable Release Behavior for the Healing of Vascular Stent Lesions. *ACS Appl. Mater. Interfaces* **6,** 8729–8743 (2014).

46.   Gentile, P., Ghione, C., Tonda-Turo, C. & Kalaskar, D. M. Peptide functionalisation of nanocomposite polymer for bone tissue engineering using plasma surface polymerisation. *RSC Adv.* **5,** 80039–80047 (2015).

47.   Rajangam, K. *et al.* Heparin Binding Nanostructures to Promote Growth of Blood Vessels. *Nano Lett.* **6,** 2086–2090 (2006).

48.   Webber, M. J. *et al.* Supramolecular nanostructures that mimic VEGF as a strategy for ischemic tissue repair. *Proc. Natl. Acad. Sci.* **108,** 13438–13443 (2011).

49.   Cardin, A. D. & Weintraub, H. J. Molecular modeling of protein-glycosaminoglycan interactions. *Arterioscler. Thromb. Vasc. Biol.* **9,** 21–32 (1989).

50.   Sijbesma, R. P. *et al.* Reversible polymers formed from self-complementary monomers using quadruple hydrogen bonding. *Science* **278,** 1601–1604 (1997).

51.   Dankers, P. Y. W., Harmsen, M. C., Brouwer, L. A., Van Luyn, M. J. A. & Meijer, E. W. A modular and supramolecular approach to bioactive scaffolds for tissue engineering. *Nat. Mater.* **4,** 568–574 (2005).

52.   van Almen, G. C. *et al.* Development of Non-Cell Adhesive Vascular Grafts Using Supramolecular Building Blocks. *Macromol. Biosci.* **16,** 350–362 (2016).

53.   Muylaert, D. E. P. *et al.* Early in-situ cellularization of a supramolecular vascular graft is modified by synthetic stromal cell-derived factor-1α derived peptides. *Biomaterials* **76,** 187–195 (2016).

54.   Ten Dijke, P., Egorova, A. D., Goumans, M. J. T. H., Poelmann, R. E. & Hierck, B. P. TGF-β signaling in endothelial-to-mesenchymal transition: the role of shear stress and primary cilia. *Sci. Signal.* **5,** pt2 (2012).

55.   Goumans, M. J., van Zonneveld, A. J. & ten Dijke, P. Transforming growth factor beta-induced endothelial-to-mesenchymal transition: a switch to cardiac fibrosis? *Trends Cardiovasc. Med.* **18,** 293–298 (2008).

56.   Mollet, B. B. *et al.* A modular approach to easily processable supramolecular bilayered scaffolds with tailorable properties. *J. Mater. Chem. B* **2,** 2483–2493 (2014).

Cucurbit[8]uril-mediated immobilization of fluorescent proteins on supramolecular biomaterials

Abstract

The reversible introduction of functionality at material surfaces is of interest in the development of functional biomaterials. In particular, the use of supramolecular immobilization strategies facilitates mild reaction and processing conditions, as compared to other covalent analogues. In this chapter, the engineering of multicomponent supramolecular materials, beyond the use of a single supramolecular entity is proposed. Cucurbit[8]uril (Q8) mediated host guest chemistry is combined with hydrogen bonding supramolecular ureido-pyrimidinone (UPy) based materials. The modular incorporation of a UPy-additive that presents one guest to incorporate into the Q8 host allows for selective supramolecular functionalization at the water – polymer material interface. Supramolecular ternary complex formation at the material surface was studied by x-ray photoelectron spectroscopy (XPS), which showed minor changes in surface composition upon complex formation. Surface MALDI-ToF MS measurements revealed useful insights in the formation of complexes, although the ternary complex was not observed. Protein immobilization was monitored using both fluorescence spectroscopy and quartz crystal microbalance with dissipation monitoring (QCM-D), which successfully demonstrated the formation of the ternary complex. Although proteins could selectively be immobilized onto the surfaces, control of the stability of the system remains a challenge as a result of the dynamicity of the host-guest assembly.

4.1 Introduction

The immobilization of proteins on biomaterial surfaces contributes to the range of bioactive functions that can be introduced. [1] Strategies for the controlled immobilization of proteins on biosensor surfaces have made a great contribution in biomarker detection and drug discovery. [2] Biomaterial surfaces that are covered with a layer of functional proteins and growth factors can be used in the field of tissue engineering and regenerative medicine. [3] Upon decoupling of the material processing conditions and functionalization *via* a post-functionalization strategy, a plethora of complex functionalities can be introduced at the material surface. The main challenge is to develop a suitable immobilization approach to introduce surface functionality. Many strategies have been developed to covalently introduce proteins at material surfaces in a chemo- and regioselective fashion. Peptide or imine bonds can be formed upon reaction of *N*-hydroxysuccinimide (NHS) or aldehyde functionalities, which are present at the material surface, with lysines that are present in the protein. Among chemoselective conjugations are native chemical ligation, split- intein mediated trans-splicing and enzyme mediated ligations. [4–6]

An alternative approach to immobilize proteins and growth factors at the material surface is by using supramolecular chemistry, enabling amongst others a mild and reversible protein attachment. [7] Tuning the reversible character of the directional non-covalent interactions allows covering a broad range of dynamics. [8–10] The use of supramolecular host-guest systems facilitates engineering of multicomponent complexes and materials. Supramolecular host-guest assemblies based on cucurbit[*n*]uril have been widely investigated and are able to form stable complexes with different levels of selectivity and reversibility. The specificity as well as the tunability of the interaction strength by selection of the guest, enables eminent control in the design of supramolecular materials based on these host-guest interactions. The cucurbit[8]uril (Q8) based macrocyclic host is able to simultaneously host an electron-deficient methylviologen and an electron-rich indole of the tryptophan amino acid. In a two-step process a ternary complex is formed, in which methylviologen binds first, followed by binding of the indole, both with an individual binding constant of $K_a = 10^5$ M^{-1}. [11–13] The Q8 host is also able to simultaneously host two aromatic guests in its cavity, i.e. two *N*-terminal phenylalanine analogues can incorporate into the Q8 with high affinity in aqueous solution, in a cooperative fashion with an association constant of $K_{ter} = 1.5 \cdot 10^{11}$ M^{-2}. [14–16]

The noncovalent interaction between the Q8 host molecule and hydrophobic guest molecules has been employed as a recognition motif to crosslink polymeric supramolecular biomaterials. [17–19] Q8 mediated complexation on surfaces has widely been studied on gold surfaces [20–22] and glass or silicon nanoparticle substrates [23–25] and as biomimetic networks [26,27], yet examples of the synthesis of supramolecular multicomponent materials are scarce. The engineering of multicomponent supramolecular complexes, i.e. the supramolecular synthesis of materials still remains a challenge, in particular those that go beyond the use of a single supramolecular element. [28–30]

UPy-based supramolecular thermoplastic elastomer (TPE) materials are developed within our group. [31–33] Supramolecular TPE materials can be functionalized *via* a modular approach,

by mixing UPy-functionalized polymers with UPy-functionalized additives. [34] Decoupling of the processing conditions and functionalization strategies allows for selective surface modification with complex proteins and growth factors. An approach to covalently introduce functionality at the surface of supramolecular TPE was developed, which is described in chapter 5. [35]

The combination of a hydrogen bonding UPy-system with a Q8-mediated host-guest assembly to introduce functionality at the water – polymer interface, i.e. proteins is described in this chapter. The combination of these two systems, each with their own self-assembly characteristics and strengths, is orthogonal and allows the assembly of novel biomaterials with the processing and functionalization conditions decoupled. The host-guest system based on Q8, which is able to simultaneously host two phenylalanine guests, was introduced at the surface of supramolecular UPy-based materials (Figure 4.1 E). *Via* a modular approach, FGG-modified UPy-additives (FGGK(UPy)) (Figure 4.1 B) were incorporated into our supramolecular polymer material, based on polycaprolactone (PCL) telechelically modified with a UPy moiety (PCLdiUPy, Figure 4.1 A). Subsequent Q8 (Figure 1 C) complexation allows for ternary complex formation with a yellow fluorescent protein (YFP) featuring an *N*-terminal FGG (Figure 4.1 D). Supramolecular complex formation was studied by surface MALDI-ToF and XPS measurements. The selective immobilization of fluorescent proteins *via* Q8-mediated ternary complex formation were studied both by fluorescence spectroscopy and QCM-D.

A PCLdiUPy

(1)

B FGGK(UPy)

(2)

C   Cucurbit[8]uril (Q8)

(3)

D   FGG-YFP

(4)
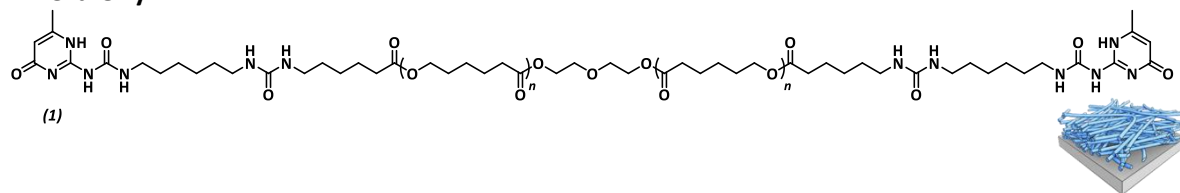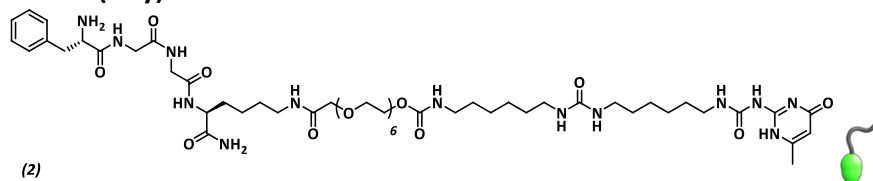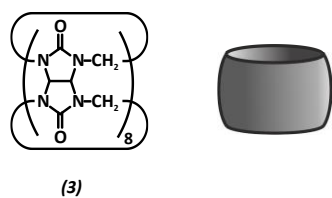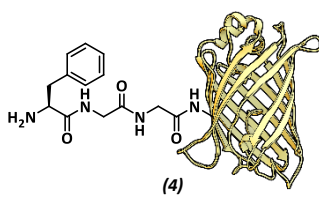
E   Supramolecular system
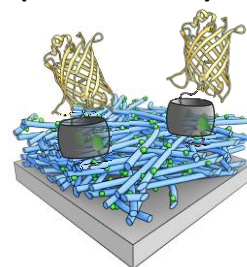
Figure 4.1. Chemical structures and corresponding cartoon representations of the molecules in this study, A) PCLdiUPy (**1**) polymer (M_n= 2000 Da) as the base polymer, B) FGGK(UPy) (**2**) peptide, C) Cucurbit[8]uril (Q8) (**3**), D) FGG-YFP (**4**) model protein and E) Cartoon representation of the supramolecular assembly at the supramolecular thermoplastic elastomer surface, where the FGGK(UPy) is modularly incorporated into the PCLdiUPy polymer film, allowing for subsequent Q8 mediated FGG-YFP complexation.

4.2 Results

4.2.1 Synthesis of FGGK(UPy) additive

A UPy-modified additive with an *N*-terminal FGG peptide motif and an additional lysine for orthogonal UPy-conjugation (FGGK(UPy)) was synthesized, to anchor the supramolecular complex at the surface. The FGGK peptide was orthogonally conjugated to a UPy-carboxylic acid (UPy-COOH) *via* selective deprotection of a *C*-terminal lysine, on the solid support, yielding an *N*-terminal phenylalanine available for complex formation with a Q8 host (Scheme 4.1, 64.6 mg (31%)). In a subsequent step, a fluorescent protein, equipped with an *N*-terminal FGG motif (FGG-YFP, Figure 4.1 D), was introduced at the surface of the supramolecular TPE, enabling the formation of a supramolecular ternary complex (FGGK(UPy)•Q8•FGG-YFP, Figure 4.1 E). The materials were formulated as thin films *via* dropcast or spincoating, either as the pristine polymer (PCLdiUPy) or with 4 mol% UPy-additive incorporated (PCLdiUPy with FGGK(UPy)).
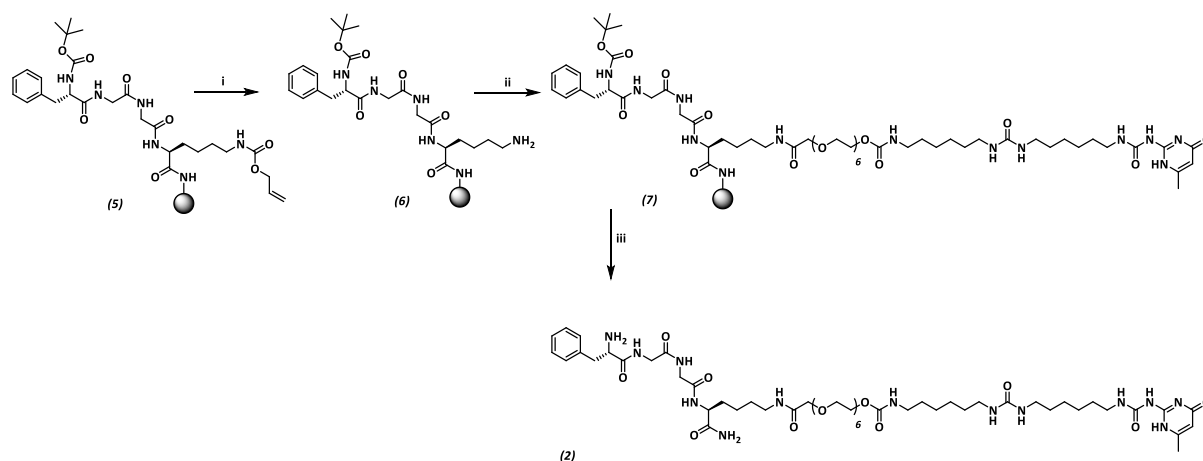
Scheme 4.1: Synthesis of FGGK(UPy) peptide on a Rink-amide resin. The FGGK(Alloc) (**5**) was synthesized on the resin. Subsequent selective alloc deprotection of the K was performed with tetrakis(triphenylphosphine)-palladium(0) (0.1 eq per Alloc moiety) and 1,3-dimethylbarbituric acid (5 eq per Alloc moiety) in DCM for four hours (**i**) as previously described by Hartmann [36] resulting in (**6**). The UPy-COOH derivative was coupled orthogonally to the deprotected K of the FGGK peptide on the resin using PyBOP and DiPEA in DMF overnight (**ii**), resulting in (**7**). Subsequently the protected UPy-peptide was cleaved from the resin using 95% TFA, 2.5% TIS, 2.5% H$_2$O and purified by preparative RP-HLPC (**iii**), yielding (**2**, 64.6 mg, 31%).

4.2.2 Surface composition analysis

The surface composition of dropcast films was investigated using x-ray photoelectron spectroscopy (XPS) (Table 4.1). Upon the incorporation of FGGK(UPy), a decrease in carbon content (72.0 to 69.9 atom%, respectively) and an increase in both oxygen (24.0 to 25.8 atom%, respectively) and nitrogen (4.0 to 4.3 atom%, respectively) content were observed, as was expected based on the molecular structure of the FGGK(UPy). The subsequent introduction of Q8 did not significantly influence the surface composition. Upon the introduction of an FGGG peptide, which serves as the second guest that can incorporate in the Q8 cavity, an increase in both carbon (70.0 to 71.8 atom%, respectively) and nitrogen (4.5 to 4.9 atom%, respectively) content were measured, whereas the oxygen content decreased

Table 4.1. Chemical surface composition of the dropcast films measured by XPS. Atom percentages of carbon (C), oxygen (O) and nitrogen (N) are depicted.

	C [%]	O [%]	N [%]
PCLdiUPy	72.0	24.0	4.0
PCLdiUPy + FGGK(UPy)	69.9	25.8	4.3
PCLdiUPy + FGGK(UPy) + Q8	70.0	25.5	4.5
PCLdiUPy + FGGK(UPy) + Q8 + FGGG-peptide	71.8	23.3	4.9

Table 4.2. Calculated values of chemical surface composition that could be measured by XPS. Atom percentages of carbon (C), oxygen (O) and nitrogen (N) are depicted.

	C [%]	O [%]	N [%]
PCLdiUPy	71.6	22.4	5.9
PCLdiUPy + FGGK(UPy)	71.1	22.2	6.3

(25.5 to 23.3 atom%, respectively). Due to the large overlap in atomic composition of the different material formulations, major changes in the surface composition were not observed. This was supported by the calculated values for the atom composition where homogeneous distribution of the FGGK(UPy) was assumed (Table 4.2). Altogether, the changes in the composition that were observed hint towards presence of the different components at the supramolecular TPE surface.

4.2.3   Surface MALDI-ToF MS measurements

Complex formation at the material surface based on molecular mass was investigated by surface MALDI-ToF measurements. The mass spectrum of the control PCLdiUPy surface did not show any signal, which is proposed to result from the matrix solvent (acetonitrile) that was used to suppress the polymer signals, as the PCLdiUPy is not soluble in this solvent (Figure 4.2 B,v). The incorporation of FGGK(UPy) generated a signal at the corresponding mass (*m/z* 1165) and an additional signal representing an FGGK(UPy) fragment (*m/z* 1014), which results from cleavage of the urea bond next to the UPy-moiety (Figure 4.2 A,i). Upon incubation with Q8, both the PCLdiUPy with FGGK(UPy) (Figure 4.2 A,ii) and PCLdiUPy (Figure 4.2 B,vi) surfaces displayed characteristic Q8 signals (*m/z* 1351 [Q8 + Na$^+$]). Moreover, the PCLdiUPy with FGGK(UPy) surfaces showed a signal that corresponds to the complex of FGGK(UPy) with Q8 (FGGK(UPy)•Q8, *m/z* 2494) and the corresponding signal where the UPy-moiety was cleaved (*m/z* 2343) (Figure 4.2 A,ii). In contrast, at the PCLdiUPy surface, a small signal corresponding to Q8 aggregates (2Q8, *m/z* 2682 [2Q8 + Na$^+$]) were present (Figure 4.2 B,vi). Incubation with an FGGK-peptide (*m/z* 407) showed a signal in both the PCLdiUPy (Figure 4.2 B,vii, *m/z* 407), and the PCLdiUPy with FGGK(UPy) surface (Figure 4.2 A,iii, *m/z* 407). This result indicates that the FGGK-peptide is able to nonspecifically adsorb onto the supramolecular polymer surface. The consecutive incubation of Q8 and subsequently FGGK-peptide (Figure 4 A,iv, Figure 4 B,viii) showed for the PCLdiUPy with FGGK(UPy) surfaces two additional signals,

A

B
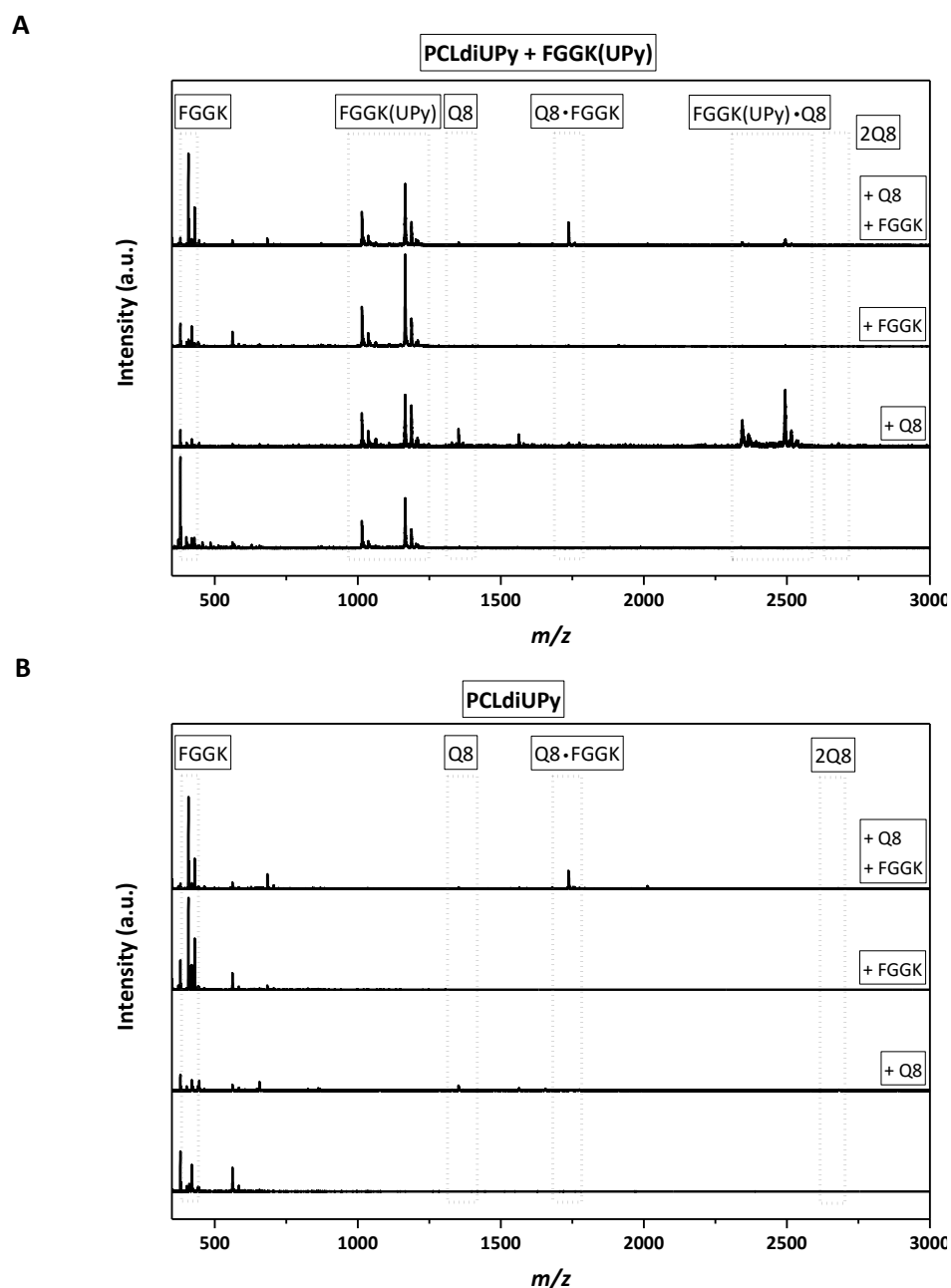
Figure 4.2. Surface MALDI-ToF MS measurements of A) PCLdiUPy with 4 mol% FGGK(UPy) (i), incubated with Q8 (ii), incubated with FGGK-peptide (iii) and subsequently both Q8 and FGGK-peptide (iv) and B) PCLdiUPy (v), incubated with Q8 (vi), incubated with FGGK-peptide (vii) and subsequently both Q8 and FGGK-peptide (viii) surfaces. Relevant observed masses, FGGK-peptide: m/z 407, FGGK(UPy): m/z 1165, FGGK(UPy) with UPy-moiety cleaved off: m/z 1014, $\Delta m/z$ 151, Q8: m/z 1351 [Q8 + Na$^+$], [Q8•FGGK-peptide]: m/z 1736, [FGGK(UPy)•Q8]: m/z 2494, [FGGK(UPy)•Q8] with UPy-moiety cleaved off: m/z 2343, [2Q8]: m/z 2682.

corresponding to the formation of complexes. A signal corresponding to the FGGK(UPy) complex with Q8 (FGGK(UPy)•Q8, m/z 2494) and with the UPy-moiety cleaved (m/z 2343) as well as a signal corresponding to the complex of Q8 with FGGK-peptide (Q8•FGGK, m/z 1736) (Figure 4.2 A,iii) was observed. The latter was also present at the PCLdiUPy surface (Q8•FGGK, m/z 1736) (Figure 4.2 B,viii), indicative for nonspecific interaction of the Q8 with the polymer surface. A signal corresponding to the formation of the ternary complex of the FGGK(UPy)

instability of the ternary complex under surface MALDI-ToF MS conditions. In conclusion, although all molecules were observed and the complexes composed where one guest is incorporated into the Q8 host, the full ternary complex was not obtained during these measurements.

4.2.4 Fluorescent protein expression and analyses

The selective introduction of fluorescent proteins at the surface of the supramolecular material was investigated by fluorescence spectroscopy measurements. A YFP protein featuring an *N*-terminal FGG peptide motif (FGG-YFP) and an MGG-YFP analogue, with an *N*-terminal methionine as a control were expressed, and characterized both by SDS-PAGE (Figure 4.3) and Q-ToF MS (Figure 4.4).

The SPS-PAGE gel showed for all the elution fractions of MGG-YFP and FGG-YFP bands at similar height, indicating the protein was successfully expressed. To assess the exact molecular weight, Q-ToF MS measurements were performed. Q-ToF MS revealed successful expression of both the MGG-YFP analogue, $MW_{calc} = MW_{obs} = 28,630$ Da (Figure 4.4 A) and the FGG-YFP protein, $MW_{calc} = MW_{obs} = 28,646$ Da (Figure 4.4 B). Methionine is unable to incorporate in the cavity of the Q8 host. The surface fluorescence on the different surfaces, i.e. PCLdiUPy, PCLdiUPy with FGGK(UPy), both with and without Q8, after washing, showed a significantly higher surface fluorescence in case the surface was comprised of the combination of FGGK(UPy) with Q8 and FGG-YFP, indicating the ternary complex was successfully assembled at the surface (Figure 4.5). The FGG-YFP fluorescence at the PCLdiUPy with FGGK(UPy) and Q8 surfaces was up to 7 times higher as compared to the MGG-YFP control (Figure 4.5 A). Hardly any fluorescence was detected when FGG-YFP or MGG-YFP were incubated with the control surfaces containing only the polymer or the polymer with the FGGK(UPy). However, the pristine polymer surface incubated with Q8 showed increased fluorescence for FGG-YFP incubation, which was attributed to nonspecific adsorption of the hydrophobic Q8 guest at the polymer surface and subsequent FGG-YFP binding. In time, the
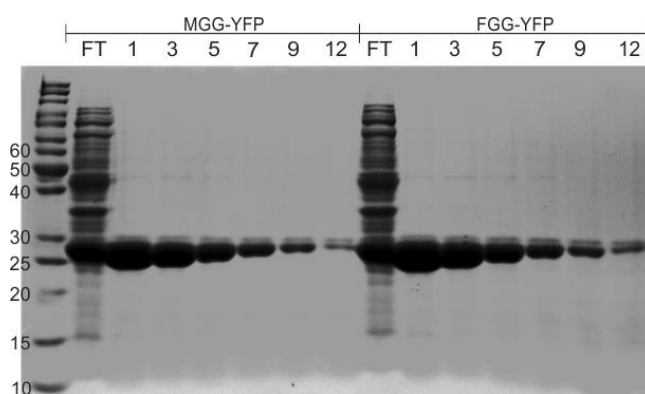
Figure 4.3. Characterization of the MGG-YFP and FGG-YFP protein expression. SDS-PAGE (12%) gel of the different proteins, on the left MGG-YFP (MW 28.6 kDa) and on the right FGG-YFP (MW 28.6 kDa). FT is flow through, numbers represent elution fractions of the chitin column. Elution fractions were combined and concentrated.

A

MGG-YFP
MW$_{Calc}$= 28630 Da
MW$_{obs}$= 28630 Da

B

FGG-YFP
MW$_{Calc}$= 28646 Da
MW$_{obs}$= 28646 Da
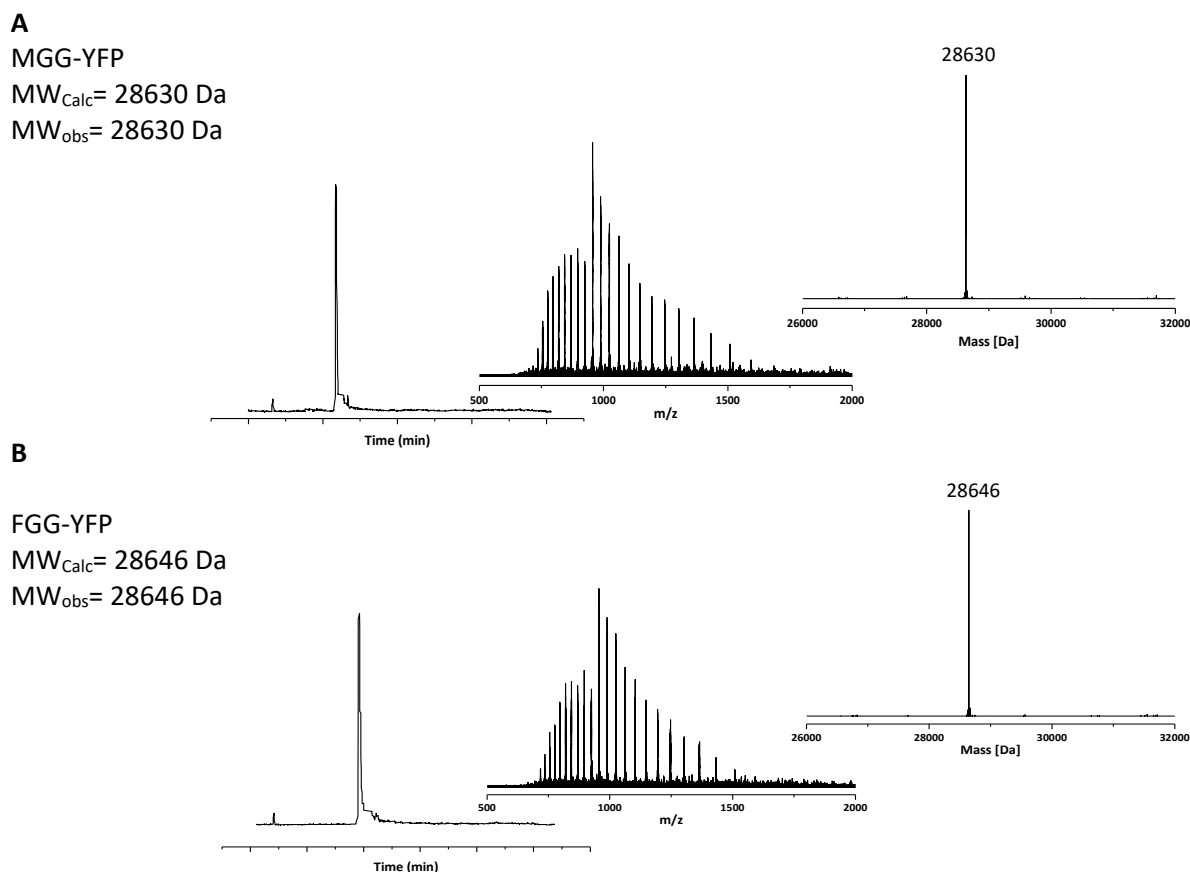
Figure 4.4. QTOF-MS characterization of the concentrated MGG-YFP (A) and FGG-YFP (B) proteins. The left figures represent the total ion count (TIC) chromatogram, the middle graphs show the *m/z* spectra and the right graphs the deconvoluted mass spectra.

A

B
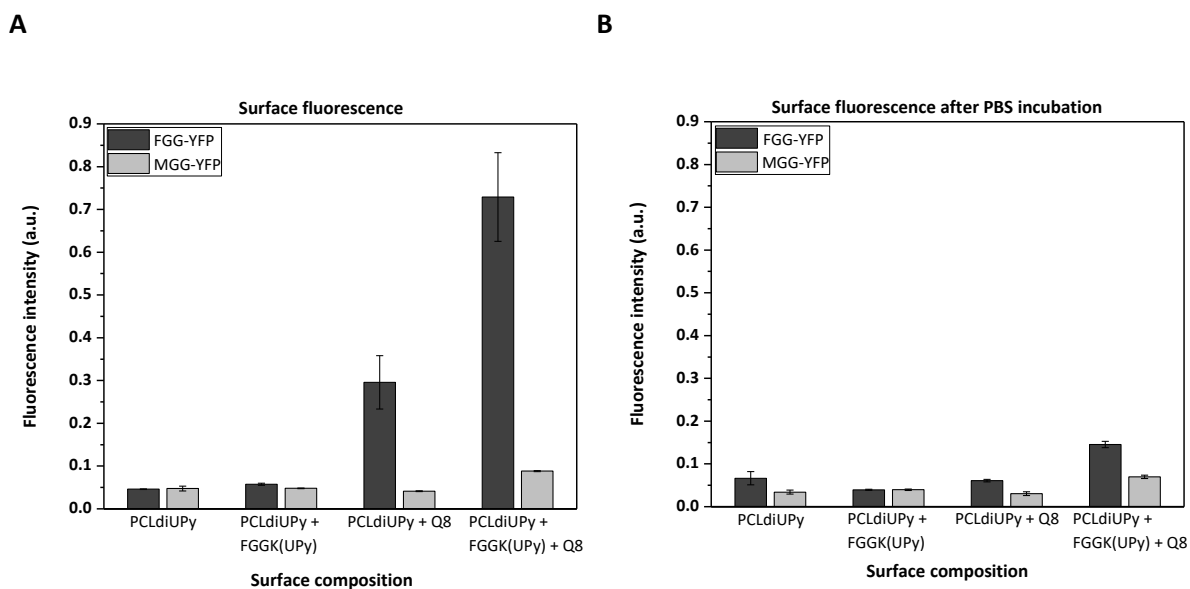
Figure 4.5. Surface fluorescence after complex formation at the surface of supramolecular material films after incubation with FGG-YFP (grey) or MGG-YFP (white). PCLdiUPy, PCLdiUPy with 4 mol% FGGK(UPy), PCLdiUPy incubated with 50 µM Q8 and PCLdiUPy with 4 mol% FGGK(UPy) incubated with 50 µM Q8, a) Surface fluorescence after overnight incubation with 10 µg·mL⁻¹ FGG-YFP or MGG-YFP and b) Surface fluorescence after subsequent incubation with PBS for 2 hours. Average and standard deviations of n = 4 measurements are plotted.

ternary complex was washed off the surface, indicated by a significant decrease in surface fluorescence in both the PCLdiUPy with Q8 and the PCLdiUPy with FGGK(UPy) with Q8 surfaces (Figure 4.5 B). These results demonstrate the Q8 mediated ternary complex is able to reversibly form at the supramolecular surface.

4.2.5 Ternary complex formation investigated by QCM-D measurements

The formation of a Q8 mediated ternary complex at the supramolecular surface, was studied with quartz crystal microbalance with dissipation monitoring (QCM-D). Spincoated films of PCLdiUPy with FGGK(UPy) were prepared and during measurements consecutively Q8 and FGG-YFP were administered at the surface of the material (Figure 4.6 and Figure 4.7). The QCM-D frequency and dissipation response of both the PCLdiUPy (grey lines) surface and the PCLdiUPy with FGGK(UPy) (green and blue lines) were monitored over time (Figure 4.6 A, Figure 4.7). At the first time point, Q8 was administered, resulting in a response of both the PCLdiUPy and the PCLdiUPy with FGGK(UPy) surfaces (I, II, III). At the second time point, FGG-YFP was administered at the PCLdiUPy (grey lines, II) and the PCLdiUPy with FGGK(UPy) surfaces (green lines, I). The PCLdiUPy with FGGK(UPy) surfaces showed a larger decrease in frequency (12 Hz and 18 HZ, respectively), indicative for a higher adsorption at these surfaces (III). The MGG-YFP control surfaces showed a frequency decrease of ~15 Hz, which is lower compared to the FGG-YFP administration. The dissipation values for the different surfaces showed similar values that are within the <5% range of the Δf, indicating that a rigid layer was formed at the surface and there is no need for visco-elastic modeling of the data (Figure 4.7). [37,38] At time point III the surfaces were washed in order remove the non-specifically bound Q8 and proteins. Both the PCLdiUPy and PCLdiUPy with FGGK(UPy) surfaces that were incubated subsequently with Q8 and FGG-YFP showed an increase in frequency, which corresponds to a mass loss at the surface, indicating the disassembly of the ternary complex. The PCLdiUPy with FGGK(UPy) surfaces that were incubated subsequently with Q8 and MGG-YFP showed only a minor increase in the frequency shift, which represents the irreversible non-specific adsorption at the surface. The mass adsorption following the Sauerbrey relation showed the largest mass increase for the FGG-YFP incubation at the PCLdiUPy with FGGK(UPy) surfaces (~ 325 ng cm^{-2}) (Figure 4.6 B), indicative for the formation of the ternary complex. An increase in mass adsorption at the PCLdiUPy with FGGK(UPy) surface incubated with MGG-YFP was observed (~ 260 ng cm^{-2}), yet these values were lower than the PCLdiUPy with FGGK(UPy) surface incubated with Q8 and FGG-YFP. The PCLdiUPy surface that was exposed to the FGG-YFP solution showed a mass increase to ~ 225 ng·cm^{-2}, which is attributed to non-specific interactions of the hydrophobic Q8 with the PCLdiUPy surface and hence the non-specifically adsorbed Q8 can accommodate the immobilization of FGG-YFP. Washing demonstrates disassembly of the ternary complex and the mass that remains at the surfaces represents the non-specific adsorption of both Q8 and the FGG-YFP and MGG-YFP.

In conclusion, the formation of a ternary complex at the surface of a supramolecular material *via* the modular incorporation of an FGG-modified UPy-additive was successful, and demonstrates a reversible character upon washing. Additionally, the hydrophobic character

of both the PCLdiUPy surfaces and the Q8 gives rise to non-specific adsorption at the surface, which yields the differences between supramolecular ternary complex formation and non-specific interactions less pronounced.

A

B
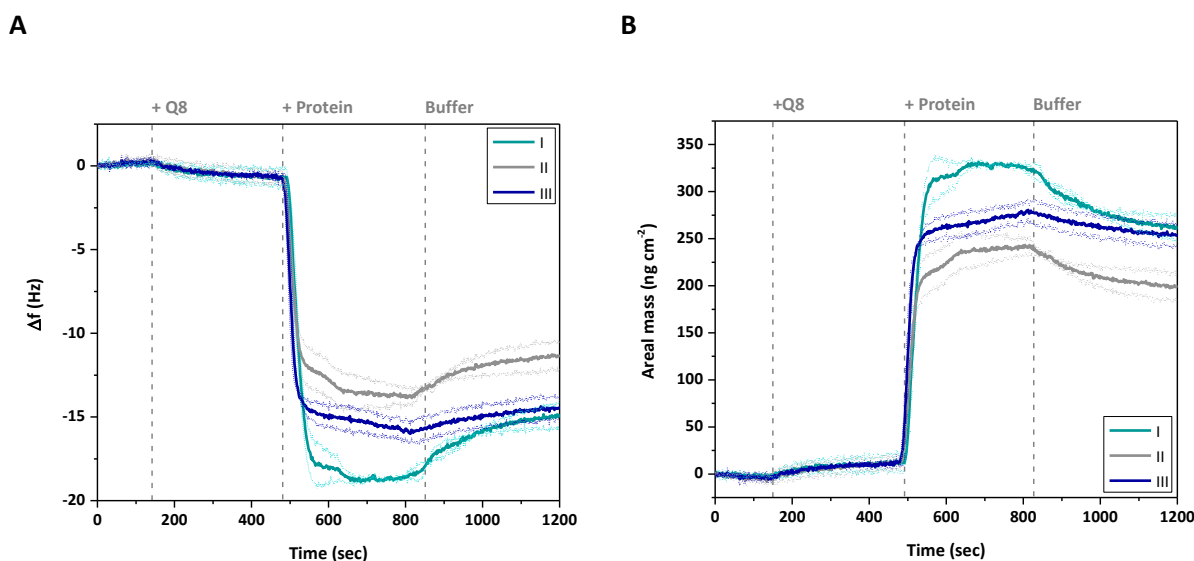
Figure 4.6. Quartz crystal microbalance with dissipation monitoring response after the addition of Q8, fluorescence protein and subsequently buffer, at PCLdiUPy with FGGK(UPy), Q8 and FGG-YFP (green line, I), PCLdiUPy with Q8 and FGG-YFP (grey line, II) and PCLdiUPy with FGGK(UPy), Q8 and MGG-YFP (blue line, III) surfaces, A) Frequency (Δf) response at surfaces and B) Changes in surface response in areal mass (ng·cm^{-2}) is calculated over time. Response of FGG-YFP is investigated on the surfaces with and without FGGK(UPy). Lines represent averages of duplicate measurements. Dotted lines represent standard deviations of n=3 measurements.
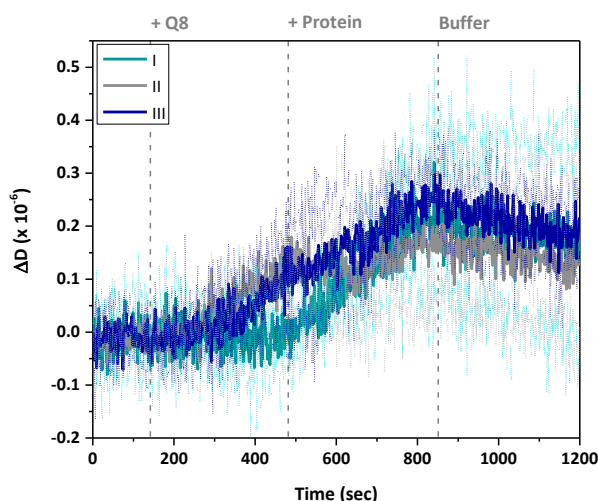
Figure 4.7. QCM-D Dissipation response at the different surfaces after the addition of Q8 (I), fluorescence protein (II) and subsequent washing (III). Response of FGG-YFP is investigated on the surfaces with and without FGGK(UPy). Lines represent averages of duplicate measurements. Dotted lines represent standard deviations of n=3 measurements.

4.3 Discussion and conclusions

A double supramolecular approach based on UPy quadruple hydrogen bond interactions in the bulk of the UPy-polymer materials and Q8-based ternary complex formation at the material – water interface *via* a UPy-additive that also serves as a guest for the Q8 was introduced in this chapter. The materials showed successful ternary complex formation and the ability to supramolecularly immobilize proteins at the supramolecular material surface. *Via* the incorporation of an FGGK(UPy) additive, the complex is proposed to form upon subsequent Q8 and either FGG-peptide or FGG-YFP protein addition at the polymer – water interface.

While MALDI-ToF MS measurements did not reveal the formation of the full ternary complex comprised of the FGGK(UPy), Q8 and an FGGK-peptide at the supramolecular material surface. However, masses of all the individual components as well as the complexes composed of 2 components were present. This might be explained by the instability of the complexes upon exposure to the laser power. Nevertheless, the fact that all masses were observed indicates that all components were present at the materials surface.

Fluorescence spectroscopy measurements showed distinct differences at the material surface, when incubated with FGG-YFP protein and compared to the MGG-YFP control. The increased fluorescence values were measured for the PCLdiUPy with FGGK(UPy) surfaces incubated with Q8 and subsequently with FGG-YFP and the complexes disassemble in time, indicative for the dynamic supramolecular assembly behavior of the Q8-mediated ternary complexes.

QCM-D experiments displayed successful ternary complex formation at the surface, a mass increase was measured first upon Q8 administration and a large mass increase was observed after subsequent fluorescent protein administration. Upon washing, a mass adsorption decrease was observed, which is indicative for disassembly of the complex and shows the reversible nature of the supramolecular host-guest system. In addition, substantial nonspecific adsorption of the Q8 at the PCLdiUPy surface was observed due to hydrophobic interactions, which leaves the differences between the different surfaces rather small.

Altogether, the results depicted in this chapter show that proteins could be successfully immobilized at the water – polymer material interface *via* modular incorporation of an additive that is involved in another supramolecular host-guest assembly. However, due to hydrophobic character of both the PCLdiUPy and the Q8, nonspecific interactions were prone to arise as a result of hydrophobic interactions, which limited the differences that were observed between the different surfaces. The moderate association constants of the ternary complex upon sequential formation, facilitates the disassembly and instability of the complex over time. The presence of both the FGGK(UPy) additive in the polymer film in combination with the administration of Q8 resulted in enhanced protein immobilization as compared to the control experiments where non-specific adsorption was measured. By the use of a heterocomplex, i.e. based on methylviologen and naphtalene [23], more specificity might be introduced to enhance the stability of the complex over longer time periods. The association constants of these complexes outcompete those of the homocomplex, when the system is

sequentially assembled. [11,39,40] The formation of the ternary heterocomplex has successfully been demonstrated at the surface of a lipid bilayers, which in contrast to our supramolecular TPE surfaces display a hydrophilic surface and hence the non-specific adsorption could significantly be reduced.[27] Future developments of these materials may involve the assessment of both the stability as well as the robustness of the systems in the aqueous phase.

4.4 Acknowledgements

4.5 Materials and methods

Materials

Unless stated otherwise, all reagents and chemicals were obtained from commercial sources and used without further purification. Pd/C was purchased from Merck and triethylamine (Et$_3$N) and 1,1,1,3,3,3-Hexafluoroisopropanol (HFIP) were purchased from Acros. PyBOP, HBTU and amino acids for solid phase peptide synthesis were purchased from Novabiochem. The solvents chloroform (CHCl$_3$), dichloromethane (CH$_2$Cl$_2$), tetrahydrofuran (THF), dimethylformamide (DMF), methanol (MeOH), hexane, and ethyl acetate (EtOAc), N-methylpyrrolidone (NMP), N,N-diisopropylethylamine (DIPEA) were purchased from Biosolve and used as received, unless stated otherwise. The PCLdiUPy polymer was synthesized by SyMO-Chem BV (Eindhoven, the Netherlands) [41], 2(6-Isocyanatohexylaminocarbonylamino)-6-methyl-4[1H]pyrimidinone (UPy-C$_6$-NCO) [31], UPy-C$_6$-U-C$_6$-Ut-OEG$_6$-COOH [42] and FGGG [43] were synthesized as described.

General methods

^{1}H-NMR data were recorded on a Bruker Cryomagnet for NMR Spectroscopy (400 MHz) at room temperature. Proton experiments were reported in parts per million (ppm) downfield of TMS. The ^{1}H-NMR data are reported as following: chemical shift, multiplicity (s = singlet, d = doublet, t = triplet, q = quartet, m = multiplet) and integration. Preparative reversed phase liquid chromatography (prep-RPLC) was performed on a system consisting of the following components: Shimadzu LC-8A preparative liquid chromatography pumps (with an Alltima C18 5u (125 x 20 mm) preparative reversed phase column and gradients of water-acetonitrile, supplemented with 0.1% trifluoro acetic acid), a Shimadzu CBM-20A prominence communications bus module and Shimadzu DGU 20A3 prominence degasser, Thermo Finnigan Surveyor PDA detector, Finnigan LCQ Deca XP and Thermo Finnigan surveyor auto sampler. Reversed phase liquid chromatography–mass spectrometry (RPLC-MS) was performed on a system consisting of the following components: Shimadzu SCL-10A VP system controller with Shimadzu LC-10AD VP liquid chromatography pumps (with an Alltima C18 3u (50 mm x 2.1 mm) reversed phase column and gradients of water-acetonitrile supplemented with 0.1% formic acid, a Shimadzu DGU 20A3 prominence degasser, a Thermo Finnigan surveyor auto sampler, a Thermo Finnigan surveyor PDA detector and a Thermo Scientific LCQ Fleet.

Analytical LC-MS. Purity and exact mass of the synthesized compounds were obtained by liquid chromatography – mass spectrometry (LC-MS) using a LCQ Fleet (Thermo Finnigan) ion-trap mass spectrometer equipped with a Surveyor auto sampler and Surveyor PDA detector (Thermo Finnigan). Solvents were pumped with a flowrate of 0.2 mL·min^{-1} using a high-pressure gradient system using two LC-10AD pumps (Shimadzu). Prior to mass analysis, the crude reaction mixture was allowed to separate on a reverse phase C18 column (Grace Smart 2 x 50 mm, Grace) and a 2-90% MeCN linear gradient in water with 0.1 v/v% formic acid (FA) was used to elute products.

MALDI-ToF MS. Matrix-assisted laser desorption ionization time-of-flight mass spectrometry (MALDI-TOF MS) was performed on an Autoflex Speed MALDI-MS (Bruker) using an α-cyano-4-hydroxycinnamic acid (CHCA) matrix. Surface MALDI-TOF MS experiments were performed by casting samples on a MTP 384 target plate polished steel TF and subsequently CHCA in 50/50 MeCN/water v/v% was applied. Measurements were performed both in linear and reflector positive mode.

QToF-MS analysis. Purity and exact mass of the proteins were determined using a Waters ACQUITY UPLC I-Class system coupled to a Xevo G2 Quadrupole Time of Flight (Q-ToF). The system was composed of a Binary Solvent Manager and a Sample Manager with Fixed-Loop (SM-FL). Proteins were separated (0.3 mL·min^{-1}) with an Agilent Polaris C18A reverse phase column (ID 2.0 mm, length 100 mm) using a 15% to 75% water/MeCN gradient with 0.1 v/v% formic acid (FA) prior to analysis in positive mode in the mass spectrometer. Deconvolution of the *m/z* spectra was done using the MaxENT1 algorithm in the Masslynx v4.1 (SCN862) software.

Preparative LC-MS. A preparative LC-MS system composed of a LCQ Deca XP Max (Thermo Finnigan) ion-trap mass spectrometer equipped with a Surveyor auto sampler and Surveyor photodiode detector array (PDA) detector (Thermo Finnigan) was used. Solvents were pumped using a high-pressure gradient system using two LC-8A pumps (Shimadzu) for the preparative system and two LC-20AD pumps (Shimadzu) for the analytical pump. The crude was purified on a reverse-phase C18 column (Alltima HP 125 x 20 mm, Alltech) using a flow rate of 20 mL·min^{-1} and a linear MeCN gradient in water with 0.1 v/v% trifluoracetic acid (TFA). Fractions with the correct mass were collected using a PrepFC fraction collector (Gilson Inc).

Preparation of dropcast surfaces. Samples were prepared by dropcast of 30 μL of a solution of 50 mg·mL^{-1} PCLdiUPy with 0 or 4 mol% FGGK(UPy) from HFIP on glass cover slips with a diameter of 12 mm, yielding a thin solid material film with a thickness in the range of 4-6 μm as was determined by profilometry measurements. Fluorescence assay samples were prepared by dropcast of 25 μL of a solution of 50 mg·mL^{-1} of the PCLdiUPy with 0 or 4 mol% FGGK(UPy) from HFIP in a well of 96-wells plate. Subsequent solvent evaporation yielded a solid, impermeable dropcast film.

Preparation of spin coated films. Samples were prepared by spin coating 50 μL of a solution of 0.5 mg·mL^{-1} of the PCLdiUPy with 0 or 4 mol% FGGK(UPy) from HFIP at 3000 rpm for 30 seconds on gold electrodes with a surface area of 1 cm^2, yielding a thin solid material film on the order of 100-150 nm as was determined with profilometry measurements. Subsequently, the gold electrodes were allowed to dry for 2h at room temperature prior to experiments.

X-ray photoelectron spectroscopy (XPS). XPS was performed on dropcast films that were attached to the sample plate by copper clamps and spectra were recorded using a Thermo Scientific K-Alpha spectrometer equipped with a monochromatic, small-spot X-ray source and a 180° double focusing hemispherical analyzer with a 128-channel detector. Spectra were obtained using an aluminum anode (Al Kα, 1486.6 eV) operating at 72 W. Survey scans were measured at a pass energy of 200 eV and region scans at a pass energy of 50 eV. The background pressure was $2 \cdot 10^{-8}$ mbar and during measurements $3 \cdot 10^{-7}$ mbar argon, because of the charge compensating dual beam source. Analysis and quantification of the spectra were performed using the CasaXPS software version 2.3.16, using C 1s, N 1s and O 1s regions.

Surface MALDI-ToF MS measurements. Matrix-assisted laser desorption ionization time-of-flight mass spectrometry (MALD-ToF MS) was performed on an Autoflex Speed MALDI-MS (Bruker) using an α-cyano-4-hydroxycinnamic acid (CHCA) matrix dissolved in 50/50% MeCN/H$_2$O. Surface MALDI-ToF MS experiments were performed on dropcast samples on a MTP 384 target plate polished steel TF. Dropcast were prepared by 3 μL of 50 mg·mL^{-1} PCLdiUPy with 0 or 4 mol% FGGK(UPy) and directly deposited on the MALDI plate. Subsequently, dropcast spots were incubated with 50 μM Q8 for 1h at room temperature, followed by washing with Milli-Q water. Next, the spots were incubated with 10 μM FGG-peptide for 1 hour at room temperature. After washing, 1 μL CHCA in 49.5/49.5/1 MeCN/water/TFA (v/v/v) was spot on each surface and allowed to dry for 30 minutes. MALDI-ToF MS measurements were performed in positive linear mode (method: 700-2000 Da), 3000 shots per spot and a laser power of 60%.

Fluorescence spectroscopy. Fluorescence assays were performed on a Thermo Scientific Fluoroskan Ascent Microplate Fluorometer. Surfaces were excited at 488 nm and emission was recorded at 538 nm. Surfaces were prepared from 50 mg·mL^{-1} PCLdiUPy +/- 4 mol% FGGK(UPy) in HFIP dropcast into a 96-wells plate. After overnight drying of the surface, wells were incubated with 100 μL 50 μM Q8 solution for 4 hours. Next, the solution was removed and immediately incubated with 100 μL 10 μg·mL^{-1} FGG-YFP or MGG-YFP in PBS overnight. After three washing steps of the surface (with PBS), the fluorescence remaining at the surface was measured.

Quartz Crystal Microbalance with Dissipation monitoring (QCM-D). QCM-D was performed on the Q-Sense E4 instrument (BiolinScientific AB) using gold-coated AT-cut quartz discs with a fundamental frequency of 4.95 MHz (QSX 301 Gold, BiolinScientific AB). Sensors were rinsed with piranha solution and subsequently heated for 10 minutes at 70 °C in a 5:1:1 mixture of ultrapure water, ammonia and 30% hydrogen peroxide (base piranha). Sensors were rinsed with water, acetone and isopropanol and dried with nitrogen. Clean crystals were mounted to record their fundamental frequency in air and subsequently removed for spin coating. All experiments were performed at room temperature (20 °C). After mounting the sensors with the spincoated material, sensors were measured in air. Afterwards, 0.5x PBS was passed over the surface at a flowrate of 0.1 mL·min^{-1} until a stable equilibrium signal was obtained. Subsequently, the 50 μM Q8 solution was passed over the surface at 0.1 mL·min^{-1} flowrate, frequency and dissipation changes were recorded until both signals equilibrated. Thereafter, 1 μM FGG-YFP or MGG-YFP solutions were passed over the surface until equilibration of both the frequency and the dissipation signals, and the sensors were rinsed with 0.5x PBS. After each experiment, the system was cleaned by rinsing with 50 mL a 2 wt% solution of Hellmanex III (Hellma) in ultrapure water, followed by rinsing with 100 mL of ultrapure water. Next, sensors were removed and all components were dried using nitrogen. The Sauerbrey equation was used to analyze the data, since the dissipation values did not exceed a 5 % margin of the frequency shift.

MGG-YFP

MGGASWSHPQFEKSAMVSKGEELFTGVVPILVELDGDVNGHKFSVSGEGEGDATYGKLTLKFICTTGKLPVPWPTLVTTFGYG
LQCFARYPDHMKQHDFFKSAMPEGYVQERTIFFKDDGNYKTRAEVKFEGDTLVNRIELKGIDFKEDGNILGHKLEYNYNSHNVY
IMADKQKNGIKVNFKIRHNIEDGSVQLADHYQQNTPIGDGPVLLPDNHYLSYQSKLSKDPNEKRDHMVLLEFVTAAGITLGMD
ELYK

FGG-YFP

FGGASWSHPQFEKSAMVSKGEELFTGVVPILVELDGDVNGHKFSVSGEGEGDATYGKLTLKFICTTGKLPVPWPTLVTTFGYGL
QCFARYPDHMKQHDFFKSAMPEGYVQERTIFFKDDGNYKTRAEVKFEGDTLVNRIELKGIDFKEDGNILGHKLEYNYNSHNVYI
MADKQKNGIKVNFKIRHNIEDGSVQLADHYQQNTPIGDGPVLLPDNHYLSYQSKLSKDPNEKRDHMVLLEFVTAAGITLGMD
ELYK

MGG-YFP and FGG-YFP expression and purification. An *N*-terminal methionine and phenylalanine were obtained by making use of intein splicing *via* pTWIN vectors containing the DNA coding for FGG-YFP and MGG-YFP. [44] The pTWIN-1 plasmids were transformed in *E. coli* BL21(DE3) host strain (Novagen). The bacteria were cultured in 2 L LB medium containing 100 μg·mL^{-1} Ampicillin at 37 °C and 180 rpm until an OD$_{600}$ of ~0.7.

Subsequently, protein expression was induced by adding isopropyl-β-D-thiogalactopyranoside (IPTG) to a final concentration of 0.5 mM. Cells were incubated for 7 hours at 25 °C and 180 rpm before being harvested by centrifugation (8000 g for 10 minutes). Bacterial cells were lysed by resuspending the pellet in Bugbuster Protein Extraction Reagent supplemented with benzonase (Novagen) and incubated for 1 hour at room temperature. The insoluble fraction was removed by centrifugation (40,000 g for 30 minutes). The soluble fraction was purified by applying it to a column filled with chitin beads (New England Biolabs) by gravity flow. The column was washed with 10 column volumes buffer (20 mM sodium phosphate, 150 mM sodium chloride, 1 mM ethylenediaminetetraacetic acid (EDTA), pH 7). The on-column intein splicing was incubated overnight at room temperature by closing the column. Cleaved proteins were eluted from the column by washing with the same buffer. Proteins were concentrated using an Amicon Ultra centrifugal filter device (MWCO: 10 kDa) (Millipore). The purity and correct mass were confirmed by SDS-PAGE electrophoresis and LC-ESI-MS. Finally, ~4 mg per liter culture for MGG-YFP and ~5 mg per liter culture for FGG-YFP yield was obtained. Concentrations were determined using the Nanodrop ND-1000 spectrophotometer using the reported extinction coefficient ε_{514} = 83400 $M^{-1} \cdot cm^{-1}$. [44]

Solid Phase Peptide Synthesis. The FGGK peptide was manually synthesized *via* Fmoc solid phase peptide synthesis (SPPS) on a Fmoc-Rink-Amide resin (Novabiochem) at a 400 μmol scale. The resin was allowed to swell for 15 minutes in *N*-methylpyrrolidine (NMP). Fmoc deprotection was done with 5 mL 20 v/v% piperidine in NMP and incubated for 5 minutes, twice. Amino acids (4 eq.) (Novabiochem) were activated with 2-(1H-Benzotriazole-1-yl)-1,1,3,3-Tetramethyluronium hexafluorophosphate (HBTU) (3.9 eq.) in NMP and alkalized with *N,N*-diisopropylethylamine (DIPEA) (8 eq.) in a total volume of 12 mL. Amino acids were coupled once for 30 minutes. The final amino acid (Phe) was Boc-protected. All steps were performed under constant agitation and with washing steps with NMP (4 mL) in between. After the peptide coupling, selective deprotection of the alloc protecting group of the Lys was performed twice using tetrakis(triphenylphosphine)-palladium(0) (0.1 eq per Alloc moiety) and 1,3-dimethylbarbituric acid (5 eq per Alloc moiety) in DCM for 4 hours as previously described by Hartmann.[36] Subsequently, UPy-COOH was orthogonally coupled to the deprotected Lys of the FGGK peptide on the resin using PyBOP and DiPEA in DMF overnight. In a final step, the Boc-protected UPy-peptide was cleaved from the resin using 95% trifluoroacetic acid (TFA), 2.5% triisopropylsilane (TIS) and 2.5% H_2O for 3 hours at room temperature. The cleaved UPy-peptide was precipitated in ice cold diethylether, centrifuged (2000 rpm, 10 minutes) and dissolved in MeCN/H_2O (1:6, v/v%). The cleaved UPy-peptide was purified using a preparative LC-ESI-MS system, equipped with a reversed phase C18 column. After filtration, the UPy-peptide was purified using a linear gradient of 30-35% MeCN/H_2O with 0.1% TFA and a flow of 20 mL·min^{-1}. The final purity of the UPy-peptide was determined with an analytical LCMS using a 5-70% MeCN gradient in H_2O with 0.1% formic acid (FA) in a final yield of 34%. After lyophilization, the purified UPy-peptide was stored at -30 °C.

Synthesis of FGGK(UPy). The procedure was continued by selective removal of the alloc protecting group on the lysine by incubating the peptide on the resin twice with tetrakis(triphenylphosphine)-palladium(0) (0.1 eq.) and 1,3-dimethylbarbituric acid (5 eq.) in DCM for 2 hours while agitating the sample. [36] The deprotected lysine was reacted with UPy-COOH (2 eq.) using PyBOP (2 eq.) and DIPEA (10 eq.) in DMF overnight. The resin was washed three times with alternating DCM and diethyl ether. After removing the ether *in vacuo*, the UPy-peptide conjugate was cleaved from the resin using trifluoroacetic acid (95%), triisopropylsilane (2.5%) and H_2O (2.5%) and precipitated in 10 volumes cold diethyl ether. The FGGK(UPy)-peptide conjugate was purified using preparative LCESI-MS system, equipped with a reverse phase C18 column. After filtration, the FGGK(UPy)-peptide was purified using a linear gradient of 20-45% MeCN/H_2O with 0.1 v/v% TFA and a flow of 20 mL·min^{-1}. The obtained fractions were lyophilized, yielding 64.6 mg of the peptide (31%). The purity of the final product was analyzed by LCMS using a 5-70 MeCN gradient in H2O with 0.1% formic acid.

^{1}H NMR (400 MHz, CDCl$_3$/CD$_3$OD): δ 7.39 – 7.30 (m, 5H), 5.97 (s, 1H), 4.38 – 4.34 (q, 1H), 4.20 – 4.13 (2t, 3H), 4.02 – 3.79 (6s, 6H), 3.72 – 3.56 (m, 22H), 3.26 – 3.23 (m, 5H), 3.12 – 3.06 (m, 7H), 2.27 (s, 3H), 1.89 – 1.32 (m, 22H). ESI-MS (positive mode): *m/z* calcd: 1163.6; found: 583.1 [M+2H]$^{2+}$, 1164.67 [M+H]$^{1+}$, 1186.58 [M+Na]$^{1+}$.

4.6 References

1. Ratner, B. D. New ideas in biomaterials science—a path to engineered biomaterials. *J. Biomed. Mater. Res.* **27,** 837–850 (1993).

2. Jonkheijm, P., Weinrich, D., Schröder, H., Niemeyer, C. M. & Waldmann, H. Chemical Strategies for Generating Protein Biochips. *Angew. Chem. Int. Ed.* **47,** 9618–9647 (2008).

3. Lutolf, M. P. & Hubbell, J. A. Synthetic biomaterials as instructive extracellular microenvironments for morphogenesis in tissue engineering. *Nat. Biotechnol.* **23,** 47–55 (2005).

4. Weinrich, D., Jonkheijm, P., Niemeyer, C. M. & Waldmann, H. Applications of Protein Biochips in Biomedical and Biotechnological Research. *Angew. Chem. Int. Ed.* **48,** 7744–7751 (2009).

5. Chen, Y.-X., Triola, G. & Waldmann, H. Bioorthogonal chemistry for site-specific labeling and surface immobilization of proteins. *Acc. Chem. Res.* **44,** 762–773 (2011).

6. Khan, S. *et al.* Post-assembly functionalization of supramolecular nanostructures with bioactive peptides and fluorescent proteins by native chemical ligation. *Bioconjug. Chem.* **25,** 707–717 (2014).

7. Cabanas-Danés, J., Huskens, J. & Jonkheijm, P. Chemical strategies for the presentation and delivery of growth factors. *J. Mater. Chem. B* **2,** 2381–2394 (2014).

8. Aida, T., Meijer, E. W. & Stupp, S. I. Functional supramolecular polymers. *Science* **335,** 813–817 (2012).

9. Boekhoven, J. & Stupp, S. I. 25th Anniversary Article: Supramolecular Materials for Regenerative Medicine. *Adv. Mater.* **26,** 1642–1659 (2014).

10. Wang, Q., Chen, Y. & Liu, Y. Supramolecular ternary polymer mediated by cucurbituril and cyclodextrin. *Polym. Chem.* **4,** 4192–4198 (2013).

11. Bush, M. E., Bouley, N. D. & Urbach, A. R. Charge-Mediated Recognition of N-Terminal Tryptophan in Aqueous Solution by a Synthetic Host. *J. Am. Chem. Soc.* **127,** 14511–14517 (2005).

12. Reczek, J. J., Kennedy, A. A., Halbert, B. T. & Urbach, A. R. Multivalent Recognition of Peptides by Modular Self-Assembled Receptors. *J. Am. Chem. Soc.* **131,** 2408–2415 (2009).

13. Biedermann, F., Rauwald, U., Zayed, J. M. & Scherman, O. A. A supramolecular route for reversible protein-polymer conjugation. *Chem. Sci.* **2,** 279–286 (2011).

14. Heitmann, L. M., Taylor, A. B., Hart, P. J. & Urbach, A. R. Sequence-Specific Recognition and Cooperative Dimerization of N-Terminal Aromatic Peptides in Aqueous Solution by a Synthetic Host. *J. Am. Chem. Soc.* **128,** 12574–12581 (2006).

15. Dang, D. T., Nguyen, H. D., Merkx, M. & Brunsveld, L. Supramolecular Control of Enzyme Activity through Cucurbit[8]uril-Mediated Dimerization. *Angew. Chem. Int. Ed.* **52,** 2915–2919 (2013).

16. Bosmans, R. P. G. *et al.* Supramolecular Control over Split-Luciferase Complementation. *Angew. Chem. Int. Ed.* **55,** 8899–8903 (2016).

17. Wu, G., Li, P., Feng, H., Zhang, X. & Chu, P. K. Engineering and functionalization of biomaterials via surface modification. *J. Mater. Chem. B* **3,** 2024–2042 (2015).

18. Dumitriu, S. & Popa, V. I. *Polymeric Biomaterials: Structure and function*. (CRC Press, 2013).

19. Barrow, S. J., Kasera, S., Rowland, M. J., del Barrio, J. & Scherman, O. A. Cucurbituril-Based Molecular Recognition. *Chem. Rev.* **115,** 12320–12406 (2015).

20. An, Q. *et al.* A Supramolecular System for the Electrochemically Controlled Release of Cells. *Angew. Chem. Int. Ed.* **51,** 12233–12237 (2012).

21. Hu, C., Lan, Y., West, K. R. & Scherman, O. A. Cucurbit[8]uril-Regulated Nanopatterning of Binary Polymer Brushes via Colloidal Templating. *Adv. Mater.* **27,** 7957–7962 (2015).

22. Zhao, J., Yang, L., Tang, Y., Yang, Y. & Yin, Y. Supramolecular Chemistry-Assisted Electrochemical Method for the Assay of Endogenous Peptidylarginine Deiminases Activities. *ACS Appl. Mater. Interfaces* **9,** 152–158 (2017).

23. González-Campo, A. *et al.* Supramolecularly Oriented Immobilization of Proteins Using Cucurbit[8]uril. *Langmuir* **28,** 16364–16371 (2012).

24. Ren, X. *et al.* Surface-Bound Cucurbit[8]uril Catenanes on Magnetic Nanoparticles Exhibiting Molecular Recognition. *Chem. – Asian J.* **11,** 2382–2386 (2016).

25. Yu, Z. *et al.* Dual-responsive supramolecular colloidal microcapsules from cucurbit[8]uril molecular recognition in microfluidic droplets. *Polym. Chem.* **7,** 5996–6002 (2016).

26. Liu, J. *et al.* Biomimetic Supramolecular Polymer Networks Exhibiting both Toughness and Self-Recovery. *Adv. Mater.* **29,** n/a-n/a (2017).

27. Bosmans, R. P. G. *et al.* Supramolecular Protein Immobilization on Lipid Bilayers. *Chem. Eur. J.* **21,** 18466–18473 (2015).

28. Brizard, A. M., Stuart, M. C. A. & Esch, J. H. van. Self-assembled interpenetrating networks by orthogonal self assembly of surfactants and hydrogelators. *Faraday Discuss.* **143,** 345–357 (2009).

29. Yu, Z. *et al.* Microfluidic Droplet-Facilitated Hierarchical Assembly for Dual Cargo Loading and Synergistic Delivery. *ACS Appl. Mater. Interfaces* **8,** 8811–8820 (2016).

30. de Vink, P. *et al.* Cucurbit[8]uril and 14-3-3 based binary bivalent supramolecular-protein assembly platform and co-crystal structure. *Angew. Chem. Int. Ed.* **56,** 8998-9002 (2017).

31. Folmer, B. J. B., Sijbesma, R. P., Versteegen, R. M., van der Rijt, J. a. J. & Meijer, E. W. Supramolecular Polymer Materials: Chain Extension of Telechelic Polymers Using a Reactive Hydrogen-Bonding Synthon. *Adv. Mater.* **12,** 874–878 (2000).

32. Sijbesma, R. P. *et al.* Reversible polymers formed from self-complementary monomers using quadruple hydrogen bonding. *Science* **278,** 1601–1604 (1997).

33. Beijer, F. H., Sijbesma, R. P., Kooijman, H., Spek, A. L. & Meijer, E. W. Strong Dimerization of Ureidopyrimidones via Quadruple Hydrogen Bonding. *J. Am. Chem. Soc.* **120,** 6761–6769 (1998).

34. Dankers, P. Y. W., Harmsen, M. C., Brouwer, L. A., Van Luyn, M. J. A. & Meijer, E. W. A modular and supramolecular approach to bioactive scaffolds for tissue engineering. *Nat. Mater.* **4,** 568–574 (2005).

35. Goor, O. J. G. M. *et al.* Efficient Functionalization of Additives at Supramolecular Material Surfaces. *Adv. Mater.* **29,** 1604652 (2017).

36. Wojcik, F., Mosca, S. & Hartmann, L. Solid-Phase Synthesis of Asymmetrically Branched Sequence-Defined Poly/Oligo(amidoamines). *J. Org. Chem.* **77,** 4226–4234 (2012).

37. Voinova, M. V., Rodahl, M., Jonson, M. & Kasemo, B. Viscoelastic Acoustic Response of Layered Polymer Films at Fluid-Solid Interfaces: Continuum Mechanics Approach. *Phys. Scr.* **59,** 391 (1999).

38. Doliška, A., Ribitsch, V., Stana Kleinschek, K. & Strnad, S. Viscoelastic properties of fibrinogen adsorbed onto poly(ethylene terephthalate) surfaces by QCM-D. *Carbohydr. Polym.* **93,** 246–255 (2013).

39. Cziferszky, M., Biedermann, F., Kalberer, M. & Scherman, O. A. Probing the stability of multicomponent self-assembled architectures based on cucurbit[8]uril in the gas phase. *Org. Biomol. Chem.* **10,** 2447–2452 (2012).

40. Liu, Y., Yang, H., Wang, Z. & Zhang, X. Cucurbit[8]uril-based supramolecular polymers. *Chem. Asian J.* **8,** 1626–1632 (2013).

41. Mollet, B. B. *et al.* A modular approach to easily processable supramolecular bilayered scaffolds with tailorable properties. *J. Mater. Chem. B* **2,** 2483–2493 (2014).

42. de Feijter, I. *et al.* Solid-Phase-Based Synthesis of Ureidopyrimidinone–Peptide Conjugates for Supramolecular Biomaterials. *Synlett* **26,** 2707–2713 (2015).

43. Ramaekers, M., Wijnands, S. P. W., Dongen, J. L. J. van, Brunsveld, L. & Dankers, P. Y. W. Cucurbit[8]uril templated supramolecular ring structure formation and protein assembly modulation. *Chem. Commun.* **51,** 3147–3150 (2015).

44. Nguyen, H. D., Dang, D. T., van Dongen, J. L. J. & Brunsveld, L. Protein Dimerization Induced by Supramolecular Interactions with Cucurbit[8]uril. *Angew. Chem. Int. Ed.* **49,** 895–898 (2010).

CHAPTER 5

Efficient functionalization of additives at supramolecular material surfaces

Abstract

Via covalent post-modification of supramolecular additives on supramolecular polymeric material surfaces, selective surface functionalization is shown. With advanced depth profiling using 3D ToF-SIMS the complex material composition of both surface and bulk were revealed. A supramolecular material consisting of ureido-pyrimidinone (UPy) end-functionalized polyesters and supramolecular UPy-modified tetrazine additives that induce reactivity at the surface towards trans-cyclooctene modified molecules were developed. High resolution depth profiling by ToF-SIMS clearly shows distinct differences in surface and bulk material composition, which culminates understanding of design criteria and control of supramolecular materials and surfaces. Moreover, electrospun supramolecular materials were functionalized with fluorescent dyes and proteins as model reactions for bioactive molecules and functional proteins, respectively. This paves the way for new generation biomaterial development; *en route* to meet nature's complexity.

5.1 Introduction

Supramolecular polymeric materials are formed by molecular building blocks that are connected through directed non-covalent interactions such as hydrogen bonding, electrostatic, metal-ligand or π-π interactions. [1,2] The supramolecular interactions give the materials their dynamic nature in a similar way as living systems for example control the complex process of extracellular matrix assembly, remodeling and bioactivation. [3] This dynamic nature results in synthetic supramolecular materials with extraordinary mechanical, processable, responsive, modular and tunable properties that cannot be achieved with conventional macromolecules. [4] Seminal contributions of supramolecular polymers have been reported, showing applicability as strong thermoplastic elastomers [5,6], functional biomaterials [7,8], drug delivery vehicles [9], self-healing materials [10–12], light-emitting diodes and molecular electronics. [13–15]

Via a modular approach through co-assembly of several supramolecular constituents, complexity and functionality can be introduced into supramolecular aggregates and polymeric structures. [4] This modular approach allows for the mixing-and-matching of functional additives with various chemical, physical and/or biological properties. Intrinsically these modified additives influence the assembly, and therefore properties, of the base supramolecular constituents. Only a few examples are disclosed in which functional additives are incorporated in solid-like supramolecular materials, such as the incorporation of supramolecular reinforcement fillers in supramolecular thermoplastic elastomers (TPE). [16]

In our group we showed that supramolecular TPE can be made using a four-fold hydrogen bonding 2-ureido-4-pyrimidinone (UPy) motif. [5,17–19] These supramolecular TPE materials could be functionalized via a modular approach by mixing with UPy-functionalized additives. [20,21] Recent developments show applicability of this approach as anti-fouling agents [22] and bioactive peptides. [23,24] The additives have been simply mixed with the supramolecular TPE to provide the material with functionality [21], resulting in anti-fouling materials and cell-adhesive scaffolds. Strikingly, in almost all of these materials, the exact distribution of the supramolecular additive as well as specific surface enhancement cannot be fully controlled, whilst in several applications solely surface function is required. Moreover, in biomaterials science, the surface functionality is frequently provided by complex bioactive modules, that are often highly incompatible with the material preparation and processing conditions. Decoupling of processing and functionalization strategies offers flexibility in the choice of processing method, and allows for exclusive surface modification.

Many examples have been reported using several chemoselective reaction strategies. [25–36] Covalent post-modification via such a chemoselective reaction is an elegant approach to introduce surface functionality on solid materials. Although functionality can be conveniently introduced on these materials, they are not inherently dynamic in comparison to supramolecular materials. In order to benefit both from the dynamic nature of supramolecular polymers, and the advantageous and wide applicability of post-modification strategies on material surfaces, covalent modification of supramolecular additives in supramolecular polymeric materials is described in this chapter.
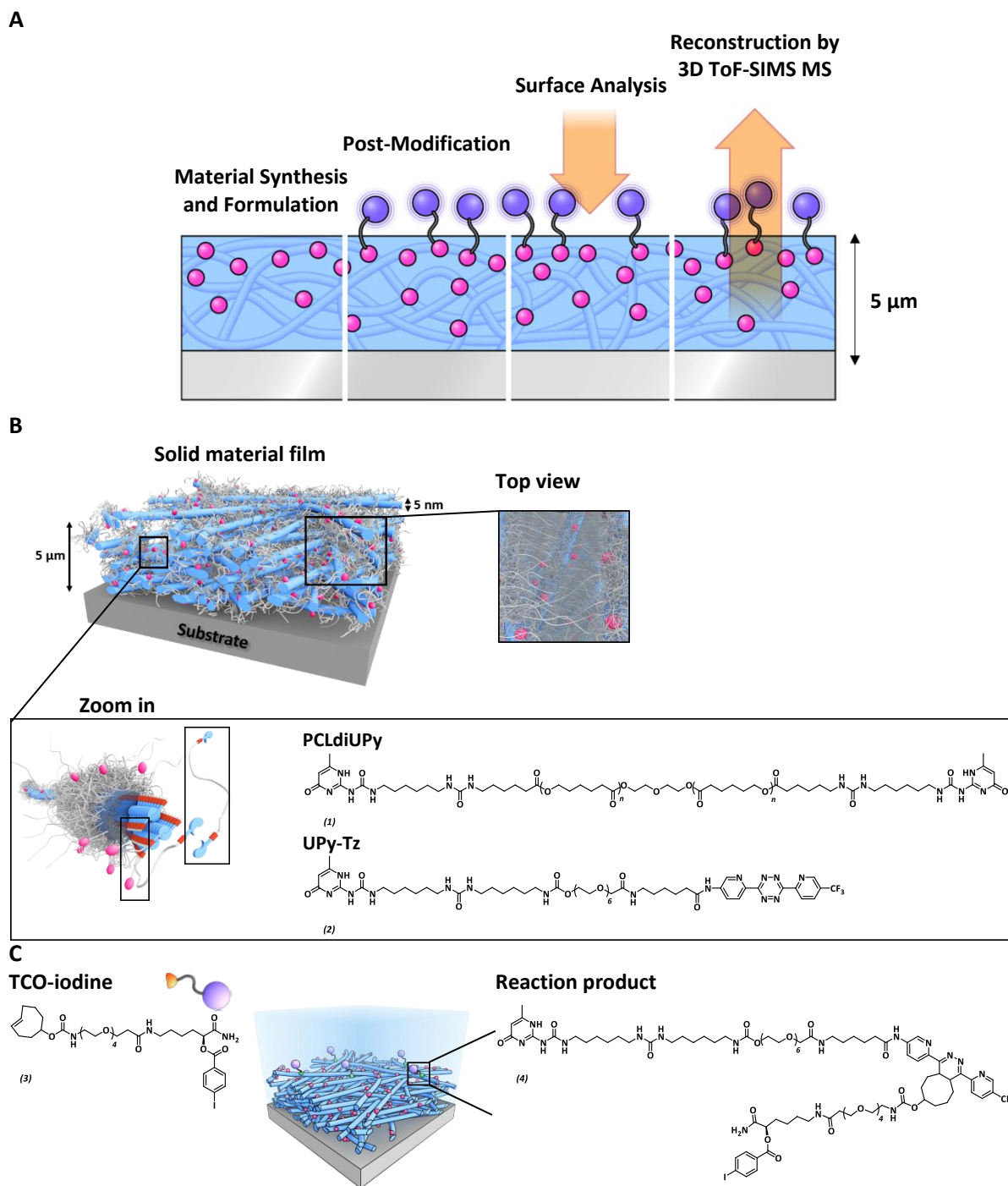
Scheme 5.1. Schematic representations of the surface modified supramolecular materials, A) Representation of the subsequent steps we take: i. supramolecular material synthesis and formulation, ii. surface post-modification, iii. surface analysis, and iv. surface and bulk depth profiling by 3D ToF-SIMS combined with sequential reconstruction. The dropcast supramolecular TPE material films are typically 5 µm in thickness, B) Representation of the self-assembled structure of the solid supramolecular film. The fibers within this solid network (depicted in blue) are composed of bundles of stacked UPy-UPy moieties in the lateral direction, forming a hard phase of ~ 5 nm in diameter. The soft phase is composed of the PCL polymer chains (depicted in grey) filling up the total space in between the hard phase (as is common for traditional thermoplastic elastomers). In a modular fashion, UPy-functionalized tetrazine guest moieties (UPy-Tz, (**2**), pink dots) can be incorporated in the core of these nanofibers formed by the PCLdiUPy (**1**) molecules. The top view provides an overview of the solid film from above, demonstrating the dense characteristic of the films and C) Chemical structure of a TCO-iodine (**3**) with an I atom for detection with XPS (TCO-iodine) that can react at the surface of the supramolecular film resulting in the corresponding reaction product (**4**).

Bioorthogonal reactions have grown interest in recent years, ever since the first reports on azide/alkyne 1,3-dipolar cycloaddition at high temperature and in organic solvent by Huisgen in 1963. [37,38] In 2001, Sharpless et al. reported on the realization of this reaction under mild conditions in aqueous environment with a Cu(I) catalyst. [39] Henceforth, click reactions received considerable attention in diverse areas such as bioconjugation, drug discovery and materials science as a result of its modular character, wide applicability and straightforward reaction conditions. [32,33,40] Bioorthogonal ligations of tetrazines with conformationally strained *trans*-cyclooctene are the fastest reported today, with a rate constant (k_2) exceeding 10^6 M^{-1}s^{-1}. [41–43] General characteristics of click chemistry (*i.e.* modular scope, mild reaction conditions and stereospecificity) show great overlap for reactions to be performed on surfaces. [14] To this end, the inverse electron demand Diels-Alder (iEDDA) cycloaddition [37–39,44–46] reaction which has been reported to be the fastest bioorthogonal reaction in aqueous environment [47,48] is used as a post-modification strategy. Therefore, a supramolecular TPE material in which a reactive UPy-modified tetrazine (UPy-Tz) additive is incorporated is designed, providing a handle for selective surface post-modification via iEDDA (Scheme 5.1 A). Using trans-cyclooctene (TCO) moieties, functionalities are introduced at this supramolecular TPE material surface (Scheme 5.1 C). In conjunction with advanced analysis techniques, the UPy-modified additive distribution and concomitant surface modification is shown. Although materials have been analyzed providing detailed chemical analysis in 2D [49] and 3D [50–52], here the surface and bulk composition of a supramolecular material using secondary ion mass spectrometry with depth profiling (3D ToF-SIMS) are revealed. Moreover, decoupling of the processing conditions and post-modification strategy of the materials by first electrospinning the materials and subsequently introducing functionalization via covalent post-modification is shown.

5.2 Results and discussion

5.2.1 Supramolecular material design

In order to achieve selective surface reaction, analysis and detailed depth profiling, a supramolecular UPy-Tz additive was carefully designed and synthesized in close collaboration with SyMO-Chem BV, Eindhoven, the Netherlands (Scheme 5.1 B, Scheme 5.2). These additives provide supramolecular intercalations into the TPE [53] and which proved to be stable up to at least 7 months. The UPy-Tz additive consists of a hydrophilic oligo (ethylene glycol) (OEG) spacer which is proposed to facilitate surface exposure via extension into water. Furthermore, the UPy-Tz molecule is equipped with a CF_3 group that allows easy detection. Supramolecular TPE polycaprolactone (PCL) (M_n=2 kDa) telechelically modified with UPy-units was used as the base material (PCLdiUPy, Scheme 5.1 B). [54] An iodinated TCO-moiety (TCO-iodine) is synthesized to perform the cycloaddition at the surface-liquid interface of the material (Scheme 5.1 C, Scheme 5.3). Moreover, the generality of this approach is shown by the reaction of a TCO-conjugated fluorescent protein reacted at the supramolecular TPE

surface as well as the translation to different length scales and processing strategies using electrospinning.

5.2.2 Surface analysis of dropcast supramolecular polymers with a supramolecular additive

The influence of UPy-Tz addition to PCLdiUPy dropcast films with respect to surface morphology was investigated with AFM (Figure 5.1). Fibrous structures were observed up to 5 mol% of UPy-Tz, whereas introduction of 10 mol% UPy-Tz showed the formation of hard domains among the fibrous structures. An increase of the UPy-Tz content to 25 mol% resulted in a fully covered surface with crystalline domains (Figure 5.1 D). The presence of fibers in the 5 mol% UPy-Tz phase image indicates the UPy-Tz is completely mixed with the PCLdiUPy (Figure 5.1 B), while the hard domains at 10 and 25 mol% are proposed to be phase separated, crystalline domains of the UPy-Tz (Figure 5.1 D). In contrast, AFM phase images of spin coated material films showed fibrous structures up to 10 mol% UPy-Tz incorporation, and phase separation at 25 mol% UPy-Tz incorporation (Figure 5.1 E-H). Moreover, the fibers are both thinner and shorter in length in the spin coated samples, which is possibly explained by faster solvent drying during spin coating which reduces assembly time.

On a macroscopic level, water contact angle measurements on air dried dropcast films showed an increase in contact angle from 68±1.1° for PCLdiUPy to 84±1.2° for PCLdiUPy with 25 mol% UPy-Tz (Table 5.1), indicative for an increase in surface hydrophobicity. Surfaces of 100% UPy-Tz did not result in a smooth film, hence these contact angles were not determined.
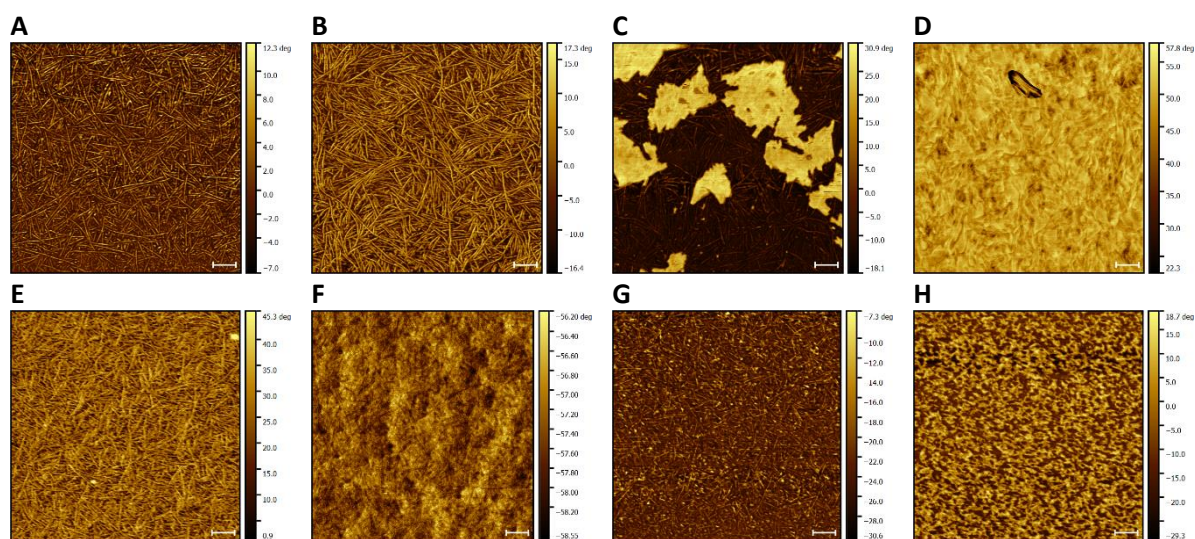
Figure 5.1. Surface analysis of drop-cast (A-D) and spincoated (E-H) films by AFM, 1 μm x 1 μm, A+E) AFM micrograph of a pristine supramolecular polymer film in which the fibers represent the UPy-dimers that stack upon each other in the lateral direction forming the hard phase of the PCLdiUPy supramolecular thermoplastic elastomer. AFM micrographs of films consisting 5 mol% UPy-Tz (B+F), 10 mol% UPy-Tz (C+G) and 25 mol with UPy-Tz (D+H), respectively, are depicted as well. Scale bars represent 100 nm.

Table 5.1. Water contact angle measurements of PCLdiUPy, PCLdiUPy + 5 mol% UPy-Tz, PCLdiUPy + 10 mol% UPy-Tz and PCLdiUPy + 25 mol% UPy-Tz drop-cast films (first column), after post-modification with a TCO-iodine (second column) and after post-modification with a TCO-Protein (third column), measurements were performed on three different samples per condition, *n* = 3 per sample and standard deviations are depicted.

Surface	Water Contact Angle (°)		
	Dropcast	TCO-iodine	TCO-EYFP
PCLdiUPy	68 ± 1.1	63 ± 5.0	78 ± 2.0
PCLdiUPy + 5 mol% UPy-Tz	72 ± 2.5	68 ± 4.0	80 ± 3.3
PCLdiUPy + 10 mol% UPy-Tz	80 ± 1.0	69 ± 1.3	82 ± 6.2
PCLdiUPy + 25 mol% UPy-Tz	84 ± 1.2	76 ± 1.1	84 ± 7.4

XPS measurements revealed fluorine intensities of 0.5 atom%, 4.1 atom% and 7.4 atom% for PCLdiUPy with 5, 10 and 25 mol% UPy-Tz, respectively. Concomitantly an increase in nitrogen intensities was detected: 4.8 atom% for PCLdiUPy, and 5.1 atom%, 8.9 atom% and
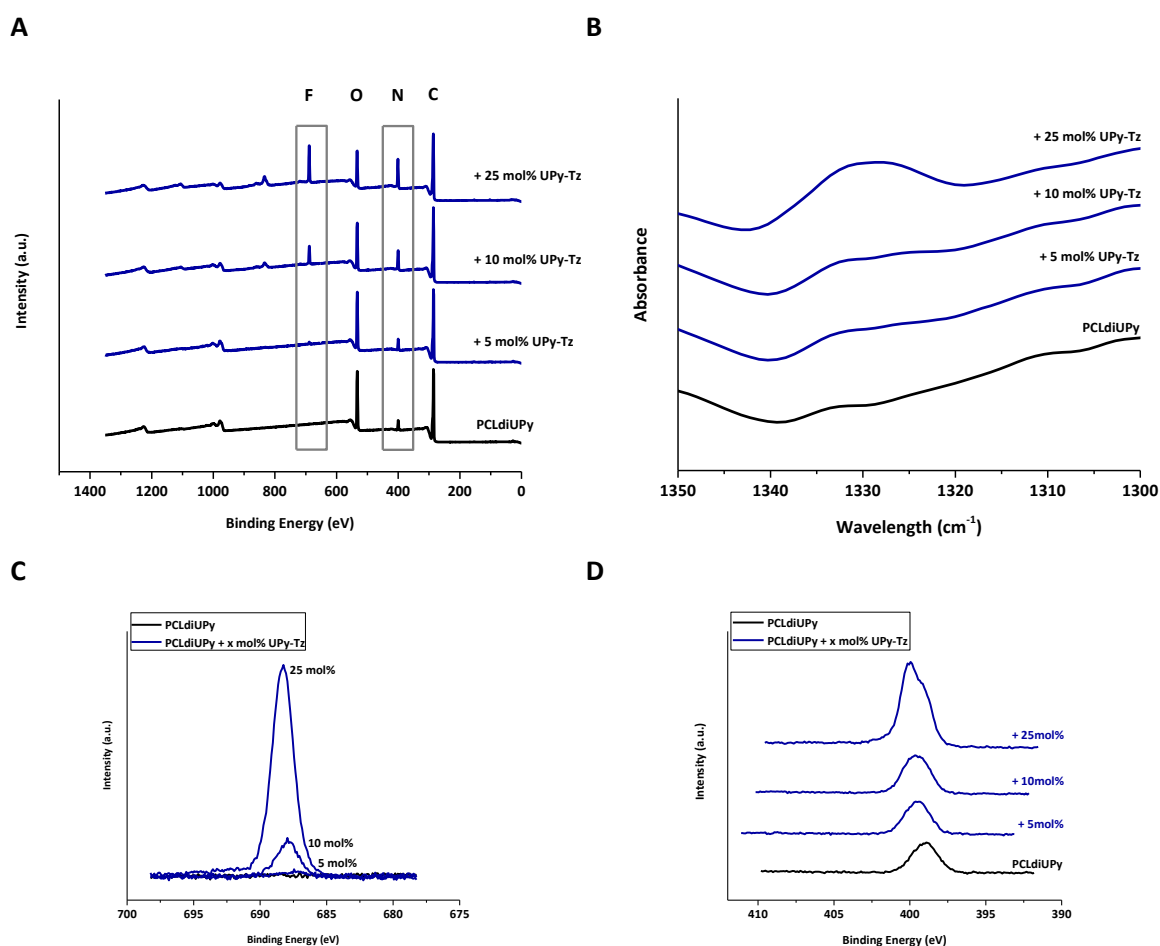
Figure 5.2. Surface analyses of the supramolecular dropcast films with UPy-Tz additive and subsequent post-modification with TCO-iodine, A) XPS results of the different films. Increase in F and N peaks are highlighted, B) FTIR zoom in of the characteristic C-F vibration stretch for the different films C) XPS zoom of the characteristic F binding energy area for the different films and D) XPS zoom of the characteristic N binding energy area for the different films.

12.9 atom% for 5, 10 and 25 mol% UPy-Tz, respectively (Figure 5.2 A,C,D, Figure 5.3 B). These results demonstrate that surfaces of the supramolecular films are gradually enriched in both fluorine and nitrogen upon addition of higher amount of UPy-Tz. In addition, also angle resolved XPS (ARXPS) measurements, with angle increments of 15° to a maximum angle of 75°, pleasingly confirm an increase in the fluorine to carbon (F:C) ratio from 0.1 to 0.2 upon increasing resolving angle. Upon increasing resolving angle, the relative surface area that is measured is increased, while the penetration depth of the X-ray beam decreases. Thus an increase in F:C ratio indicates fluorine enrichment at the surface of the supramolecular material film (Figure 5.3 C,D).

Since the iEDDA cycloaddition post-modification reactions are performed in aqueous solution, it was of interest to investigate the surface composition after water annealing. XPS

A

B

Air dried	Surface Composition (%)				Ratio
Surface	C	O	N	F	F:C
PCLdiUPy	74.0	21.3	4.75	-	-
PCLdiUPy + 5 mol% UPy-Tz	73.5	20.9	5.14	0.49	0.007
PCLdiUPy + 10 mol% UPy-Tz	69.2	16.9	8.92	4.07	0.06
PCLdiUPy + 25 mol% UPy-Tz	63.9	14.0	12.9	7.43	0.12
Water Annealing	Surface Composition (%)				Ratio
Surface	C	O	N	F	F:C
PCLdiUPy	73.8	21.4	4.82	-	-
PCLdiUPy + 5 mol% UPy-Tz	68.3	17.0	9.15	4.36	0.06
PCLdiUPy + 10 mol% UPy-Tz	63.5	14.3	12.9	7.54	0.12
PCLdiUPy + 25 mol% UPy-Tz	60.1	11.3	16.2	9.65	0.16

C

D

Tilt angle (°)	0	15	30	45	60	75
F:C ratio	0.13	0.12	0.13	0.15	0.18	0.22

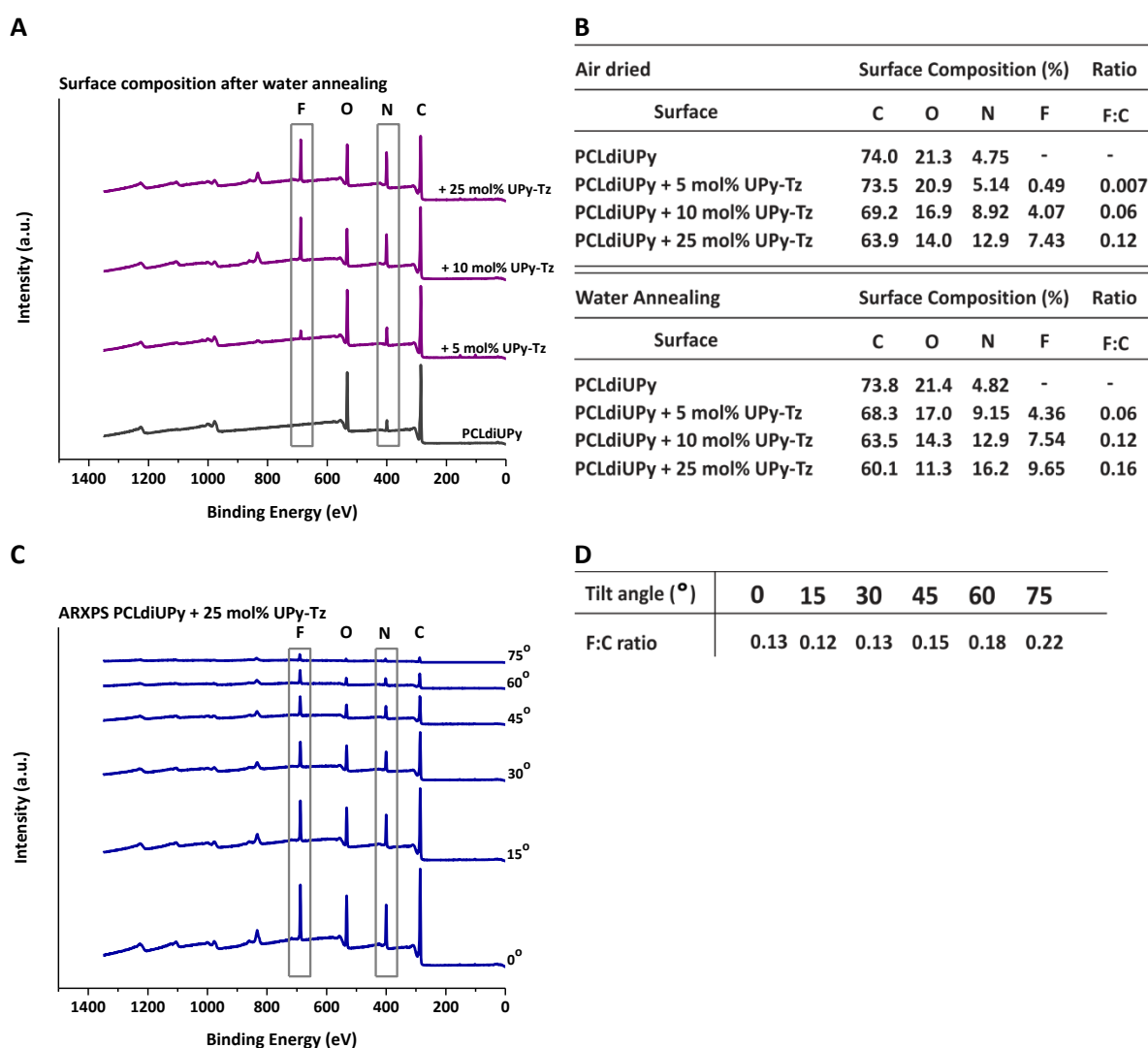**Figure 5.3.** Surface analysis of drop-cast films by XPS, A) Survey of PCLdiUPy + 0, 5, 10 and 25 mol% UPy-Tz after 48 hours water annealing, B) Atom composition of the air dried and water annealed surfaces, C) Development of PCLdiUPy + 25 mol% UPy-Tz surface survey at different tilt angles (0, 15, 30, 45, 60 and 75°, respectively) and D) F:C ratio at the different tilt angles of the PCLdiUPy + 25 mol% UPy-Tz surface.

measurements after 48 hours of water annealing show an increase in fluorine intensity from 4.4 atom% (PCLdiUPy with 5 mol% UPy-Tz) up to 9.7 atom% (PCLdiUPy with 25 mol% UPy-Tz) as well as nitrogen from 4.8 atom% for PCLdiUPy to 16.2 atom% for PCLdiUPy with 25 mol% UPy-Tz (Figure 5.3 B) compared to air dried samples. It is hypothesized that this enhanced stratification might favor the reaction of the TCO-moiety at the surface-water interface. Investigation of the dropcast films with FTIR reveals a gradual increase in stretch vibration around 1330 cm^{-1} upon increasing amounts of UPy-Tz incorporation, which is attributed to the typical C-F bond vibration found in the 1400 - 1100 cm^{-1} region [55], confirming the presence of UPy-Tz at the surface of the material film (Figure 5.2 B).

In conclusion, surface analysis both on a macroscopic level as well as on the molecular level reveal UPy-Tz presence at the material surface and moreover demonstrate further enrichment after water annealing. Additionally, it is shown that the UPy-Tz module is mixed into the supramolecular TPE, and that the material properties are tunable, i.e. accessibility of UPy-Tz for reaction, based on the amount that is mixed in. Therefore, it is proposed that these moieties are perfectly suitable for selective surface functionalization of supramolecular materials.

5.2.3 Selective surface modifications of dropcast supramolecular TPE films

The presence of the UPy-Tz at the surface of the films, suggests convenient surface modification using a TCO-modified molecule as reagent (Scheme 5.1 C). Upon reaction of the TCO-iodine with the UPy-Tz the pink color of the tetrazine significantly decreases. This corresponds to a decrease in the characteristic tetrazine absorption band at 540 nm, after the 1,2-diazine click product has been formed (**7** and **8**, Figure 5.4 B) and N$_2$ is released from **6** (Figure 5.4 B) [56], indicative for the reaction to have occurred and the enhanced presence of the UPy-Tz at the material surface (Figure 5.4). Furthermore, after reaction with TCO-iodine, water contact angle measurements reveal increased surface hydrophobicity upon incorporation of higher amounts of UPy-Tz with angles of 63.4±5.0° for PCLdiUPy up to 75.8±1.1° for PCLdiUPy containing 25 mol% UPy-Tz (Table 5.1).

Importantly, XPS measurements are expected to show an increase of an additional iodine peak in line with the increase in fluorine peak intensity upon the addition of higher amounts of UPy-Tz (Figure 5.5 A,C,D). The spectrum of the reference surface, i.e. pristine PCLdiUPy, shows an iodine signal of 0.12 atom% suggesting nonspecific adsorption of the TCO-iodine, which is attributed to the hydrophobic nature of the surface (Figure 5.5 C). Upon the incorporation of 5 and 10 mol% UPy-Tz, an increase in iodine intensity to 0.3 atom% is observed in both cases, indicative for a successful reaction at the surface. The incorporation of 25 mol% UPy-Tz shows a further increase to 0.7 atom% iodine, indicating more TCO-iodine is reacted at this materials surface.
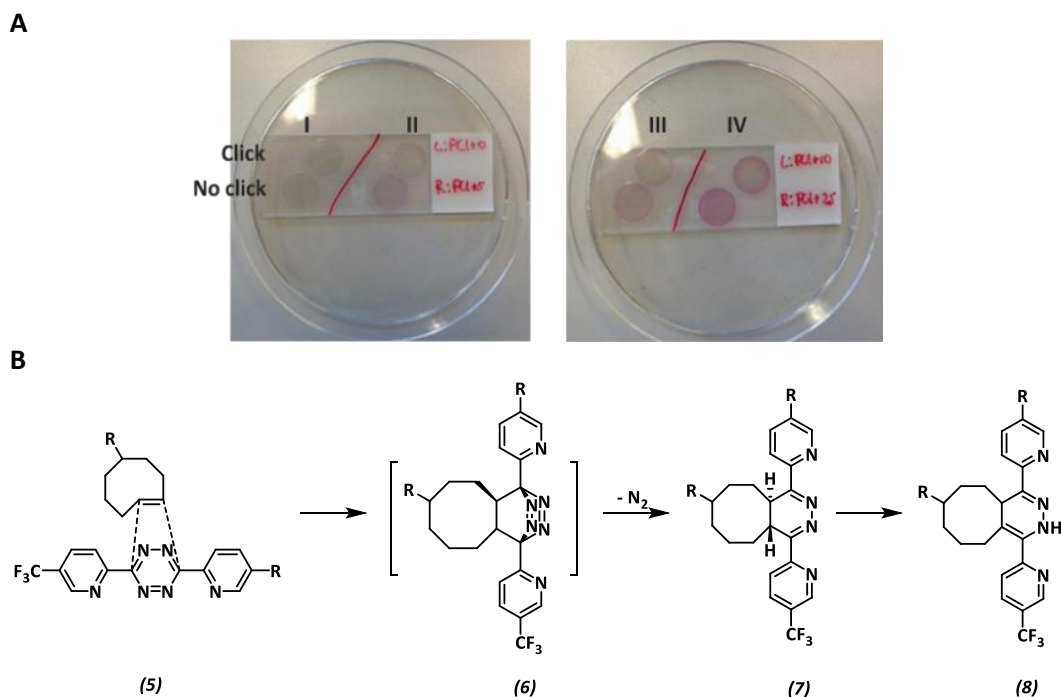
A

B

(5)   (6)   (7)   (8)

Figure 5.4. Pictures of drop-cast films incubated with and without TCO-iodine compound, A) PCLdiUPy (left, **I**) and PCLdiUPy + 5 mol% UPy-Tz (right, **II**), upper row samples show color change after TCO-iodine incubation, lower row samples show unreacted films and PCLdiUPy + 10 mol% UPy-Tz (left, **III**) and PCLdiUPy + 25 mol% UPy-Tz (right, **IV**), upper row samples show color change after TCO-iodine incubation, lower row samples show unreacted films and B) reaction mechanism of the iEDDA cycloaddition between tetrazine and TCO.

Surface MALDI-ToF MS studies are performed to directly confirm the presence of the reaction product (Figure 5.5 B). The mass spectrum of the control PCLdiUPy surface without TCO-iodine (Figure 5.5 D; black spectrum) does not show any signal, which is proposed to result from the matrix solvent (acetonitrile) that is used to suppress polymer signals. PCLdiUPy incubated with TCO-iodine (Figure 5.5 B; grey spectrum) shows the TCO-iodine mass (m/z 798.0) and a cleaved TCO-iodine adduct which corresponds to a fragment from which CO_2 is released (m/z 624.5). The surface of PCLdiUPy with 10 mol% UPy-Tz incorporated that is not incubated with TCO-iodine (Figure 5.5 B; blue spectrum) presents a few matrix peaks in the TCO region. Additionally, in the UPy-Tz region the UPy-Tz mass (m/z 1193.3) and the corresponding salt adducts are visible. Besides that, a UPy-Tz fragment resulting from cleavage of the urea bond next to the UPy-moiety (m/z 1042.8) is present as well. The surface of PCLdiUPy with 10 mol% UPy-Tz incorporated that was incubated with TCO-iodine (Figure 5.5 B; red spectrum) clearly presents the cycloaddition click product (m/z 1937.6) with the corresponding salt adducts. Moreover, the cycloaddition product where the UPy-moiety is cleaved (m/z 1787.4) is observed. Furthermore, two additional peaks are present that correspond to the mass of the cycloaddition product after release of CO_2 from the TCO-iodine (Figure 5.5 B; left peaks, cleaved UPy, m/z 1121.7; right peaks, intact UPy, m/z 1272.2), indicating that all UPy-Tz has reacted. The chemical structures and their corresponding masses of the adducts that are observed in the surface MALDI-ToF MS experiments, UPy-Tz – TCO-I (**4**), UPy-Tz – TCO-I with the UPy-moiety cleaved (**9**), UPy-Tz – TCO-I with CO_2 released

from the TCO-I (**10**) and UPy-Tz – TCO-I with both the UPy-moiety cleaved and CO_2 release from TCO-I (**11**), respectively (Figure 5.6). Surface MALDI-ToF MS of PCLdiUPy with 5 and 25 mol% UPy-Tz show similar trends (Figure 5.7). Moreover, the shift of the peaks in the UPy-Tz region (Figure 5.5 B) demonstrates the efficiency of the surface modification, as no unreacted UPy-Tz was observed after the reaction. Accordingly, surface MALDI-ToF MS measurements reveal indisputable evidence for the successful click reaction at the surface of the supramolecular material surface.
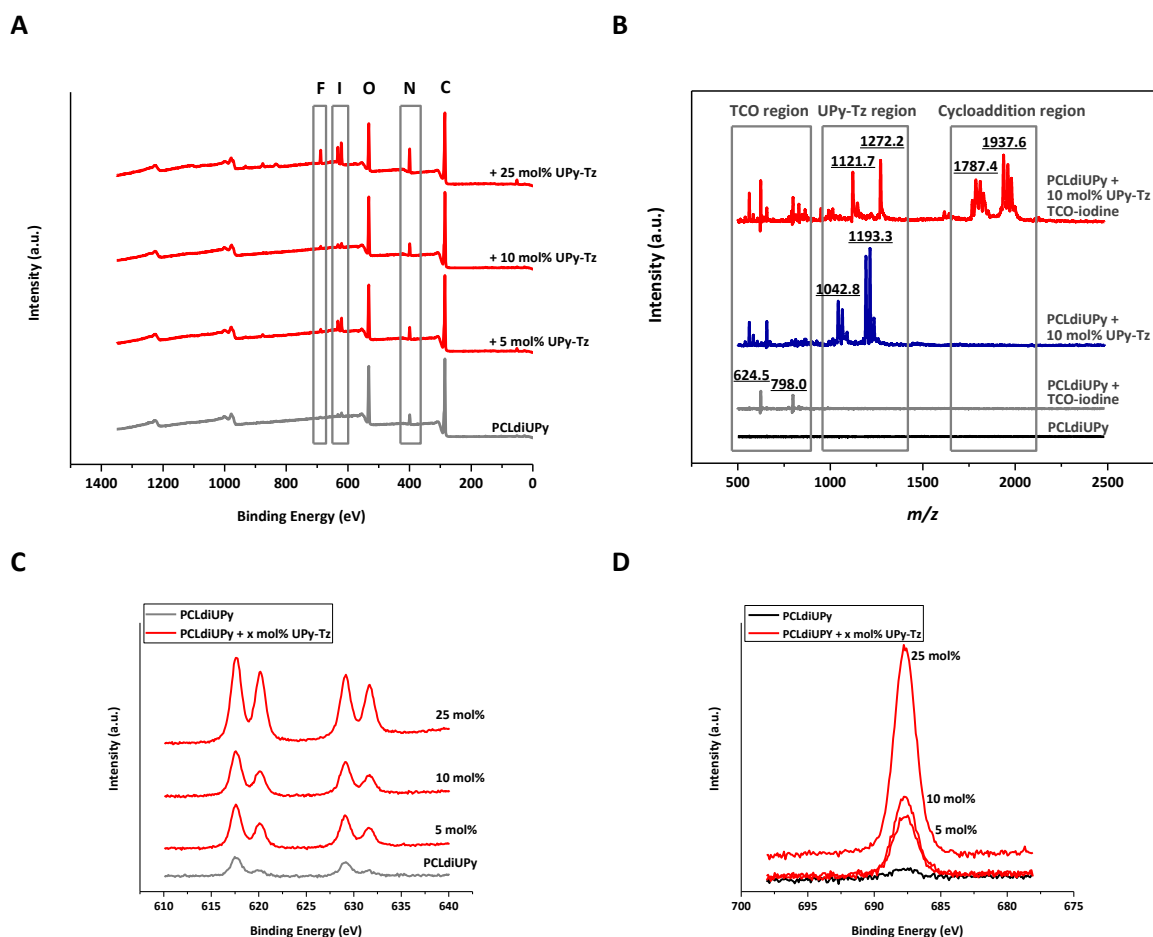
Figure 5.5. Surface analyses of the supramolecular dropcast films with UPy-Tz additive after post-modification with TCO-iodine, A) XPS overview of the different films after post-modification with TCO-iodine. Increase in F, I and N peaks are highlighted, B) Surface MALDI-ToF MS analysis of PCLdiUPy (black line), PCLdiUPy incubated with TCO-iodine (grey line), PCLdiUPy with 10 mol% UPy-Tz (blue line) and PCLdiUPy with 10 mol% UPy-Tz incubated with TCO-iodine (red line), C) XPS zoom of the characteristic I binding energy area for the different films and D) XPS zoom of the characteristic F binding energy area for the different films.

Figure 5.6. Molecular structures and corresponding masses of the products that are detected with surface MALDI-ToF measurements, a) full length UPy-Tz TCO-iodine click product, MW 1936.8 g·mol^{-1}, b) UPy-Tz TCO-iodine click product with UPy-moiety cleaved, MW 1785.8 g·mol^{-1}, c) UPy-Tz TCO-iodine click product after elimination of the carbamate moiety, MW 1269.7 g·mol^{-1} and d) UPy-Tz TCO-iodine click product after elimination of the UPy and carbamate moiety, MW 1118.7 g·mol^{-1}.
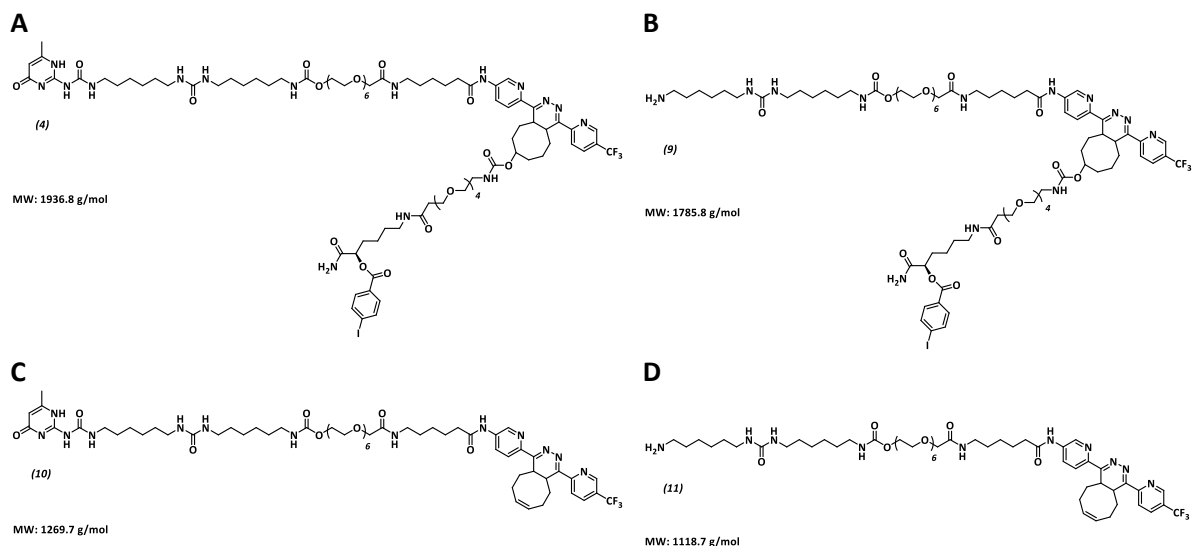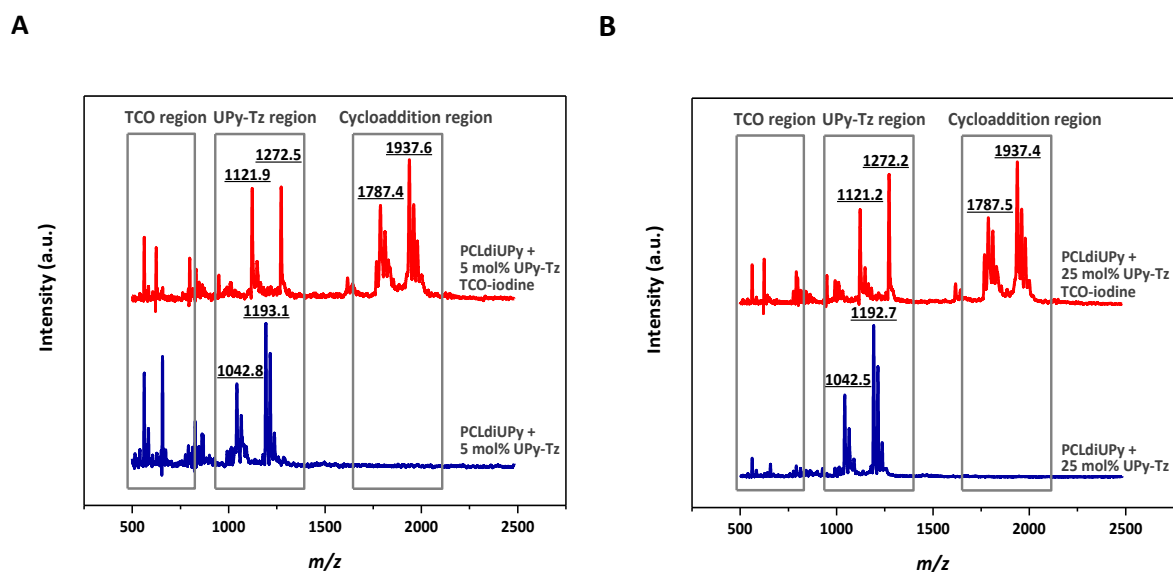

Figure 5.7. Surface analysis of click chemistry with a TCO-iodine at the surface of drop-cast films analyzed by MALDI-ToF MS and corresponding chemical structures, A) PCLdiUPy + 5 mol% UPy-Tz (blue line), PCLdiUPy + 5 mol% UPy-Tz incubated with TCO-iodine (red line) and B) PCLdiUPy + 25 mol% UPy-Tz (blue line) and PCLdiUPy + 25 mol% UPy-Tz incubated with TCO-iodine (red line).

5.2.4 Surface and bulk depth profiling of supramolecular TPE films using 3D ToF-SIMS

The spatial characterization of the surface and bulk composition of supramolecular spincoated polymer films is demonstrated here for the first time, using a series of 50 subsequent surface analyses and sputter events in negative ion mode. Chemical structures of the mass fragments that are discussed are depicted in Figure 5.8. 3D reconstruction

convincingly shows a gradual increase in fluorine content throughout the material film upon increasing amounts of UPy-Tz (Figure 5.9 A-D, mass spectra of the surface are depicted in Figure 5.10). For relatively low amounts of UPy-Tz (i.e. 1 and 5 mol%) the fluorine predominantly appears at the surface of the material film, whereas at high amounts (i.e. 10 and 25 mol%) the fluorine is also distributed throughout the bulk of the material. 3D reconstruction concomitantly reveals an increase in iodine content at the material surface (Figure 5.9 A-D) demonstrating occurrence of the reaction at the surface. Distribution profiles of UPy-fragments (m/z 124 and 150, respectively) and monomers of the PCL (m/z 113) show a homogeneous distribution throughout the films (Figure 5.9 E-H). Upon detailed total-ion-count analyses of the different conditions (1, 5, 10 and 25 mol% UPy-Tz, respectively) both at the surface and in the bulk (Figure 5.9 I) total ion counts of both fluorine and iodine decreased in bulk as compared to the surface in all cases. Additionally, a general trend in the increase of the fluorine and the iodine content at the surface upon higher UPy-Tz amounts is measured, whereas both UPy and PCL ion counts remain constant (Figure 5.9 I).

Interestingly, principal component analysis (PCA) of the surface of PCLdiUPy with 1 and 5 mol% UPy-Tz, respectively, reacted with TCO-iodine showed a correlation between fluorine and iodine (+1 principal component), and between the UPy-fragments and the PCL-fragments (-1 principal component). [57]
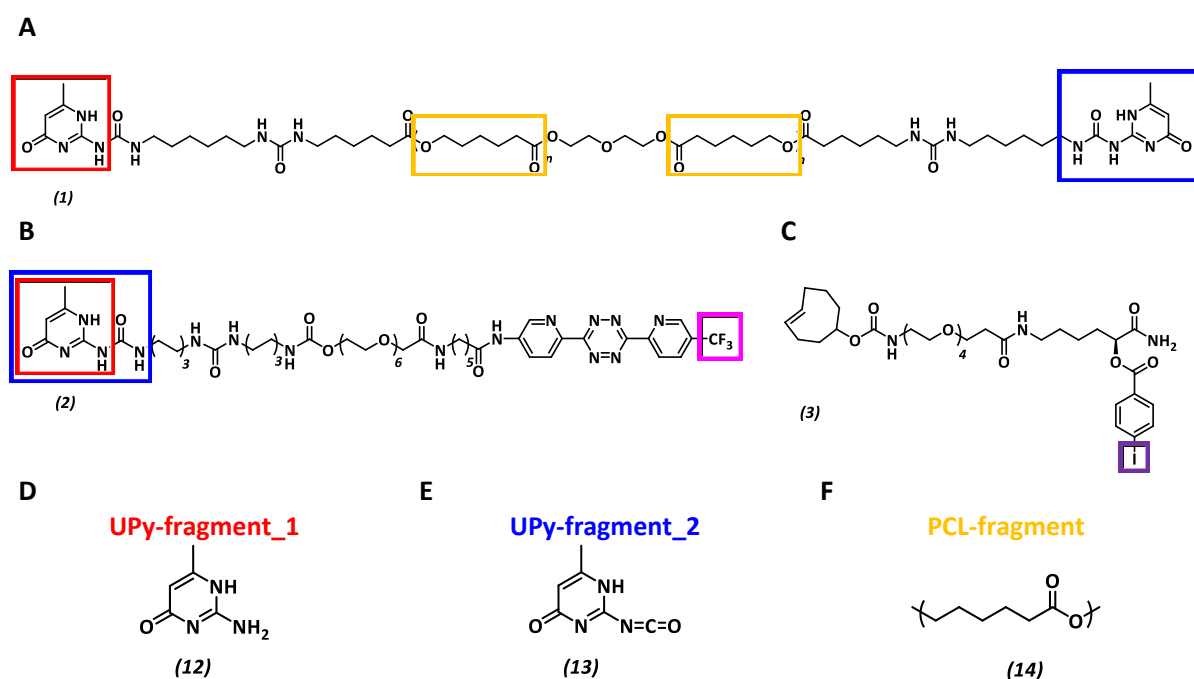
Figure 5.8. Chemical structures of the main masses observed with ToF-SIMS MS, A) Chemical formula of PCLdiUPy with the UPy-fragment_1 (m/z = 125 Da, in red), UPy-fragment_2 (m/z = 151 Da, in blue) and the PCL-fragment (m/z = 114 Da, in yellow) highlighted, B) Chemical formula of the UPy-tetrzine with the UPy-fragment_1 (m/z = 125 Da, in red), UPy-fragment_2 (m/z = 151 Da, in blue) and the fluorine (m/z = 19 Da, in pink) highlighted, C) Chemical formula of the TCO-iodine, with the iodine (m/z = 127, purple) highlighted, D) Chemical structure corresponding to UPy-fragment_1, observed m/z = 124 Da, E) Chemical structure corresponding to UPy-fragment_2, observed m/z = 150 Da and F) Chemical structure corresponding to PCL-fragment, observed m/z = 113 Da.

Pleasingly, 3D ToF-SIMS imaging with C_{60}^+ depth profiling has provided useful and detailed insight into the chemical composition of the supramolecular materials, both at the surface and in bulk. Due to the high depth resolution, this technique holds immense promise in a variety of material science developments, where control and understanding of the polymer structures is extremely important for their function. This technique now paves the way for high resolution analysis of materials in 3D and thereby allows for specific molecular design in order to meet material requirements for a variety of applications.
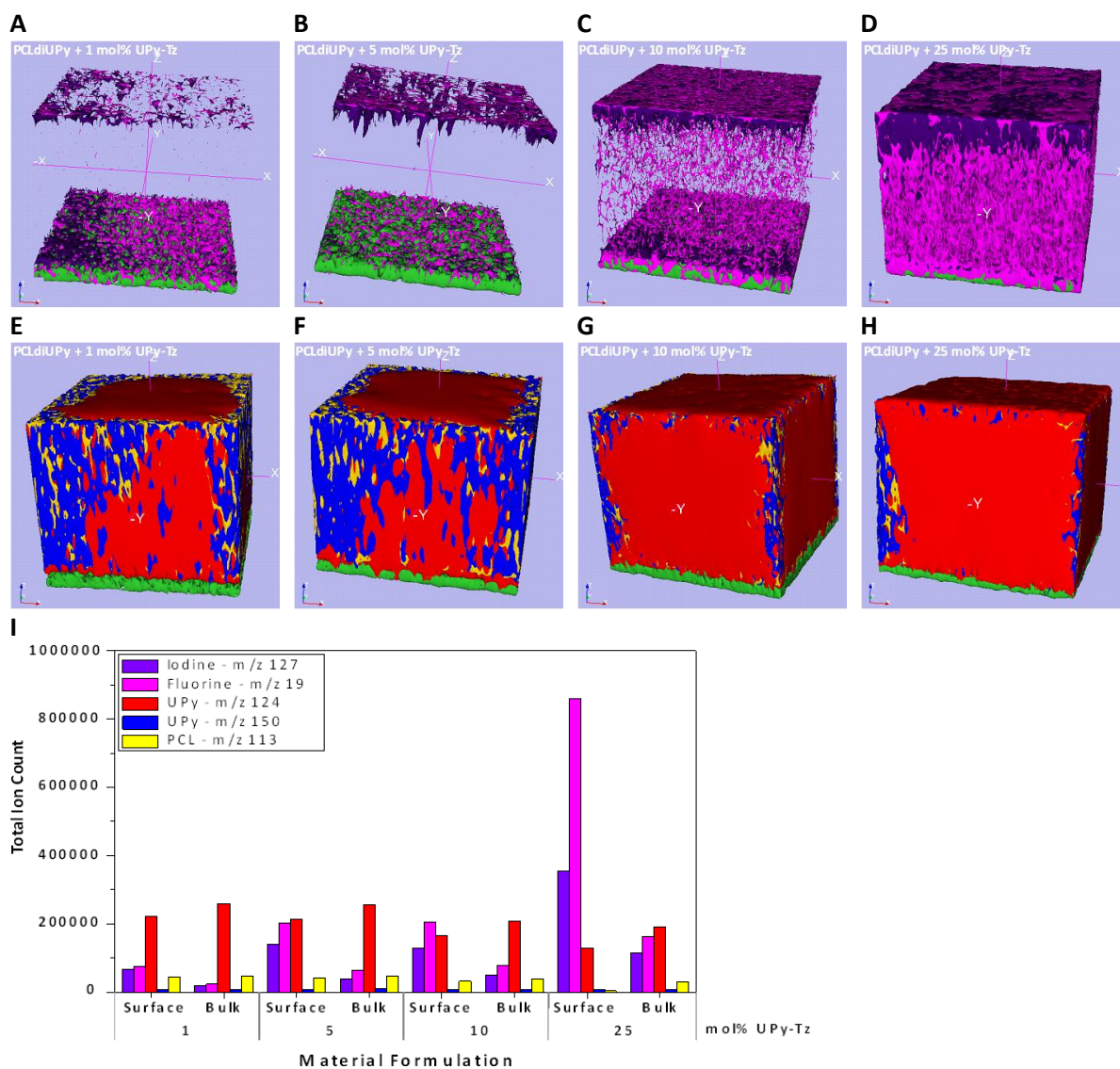
Figure 5.9. 3D Depth profile of supramolecular spincoated films after post-modification using ToF-SIMS. The films have a thickness of 100-150 nm. Relevant mass fragments are depicted in different colors: iodine = purple, fluorine = pink, UPy-fragment m/z 124 = red, UPy-fragment m/z 150 = blue, PCL-fragment = yellow, ITO = green. Dimensions of depth profile area are 100 x 100 µm. Reconstructions were made after 50 sputter cycles of 1 min with 20 keV C_{60}^+ sputter beam and subsequent surface analysis of 4 frames (2.13 min) using a 30 keV Bi_3^{++} beam. Spatial distribution of I and F ions, and ITO fragment in films of PCLdiUPy with A) 1 mol% UPy-Tz, B) 5 mol% UPy-Tz, C) 10 mol% UPy-Tz, and D) 25 mol% UPy-Tz. Spatial distribution of two UPy-fragments, PCL-fragment, and ITO fragment in films of PCLdiUPy with E) 1 mol% UPy-Tz, F) 5 mol% UPy-Tz, G) 10 mol% UPy-Tz, and H) 25 mol% UPy-Tz and I) Total ion count plot of all masses of interest, analyzed for both the surface and the bulk.

A

B

C

D

E
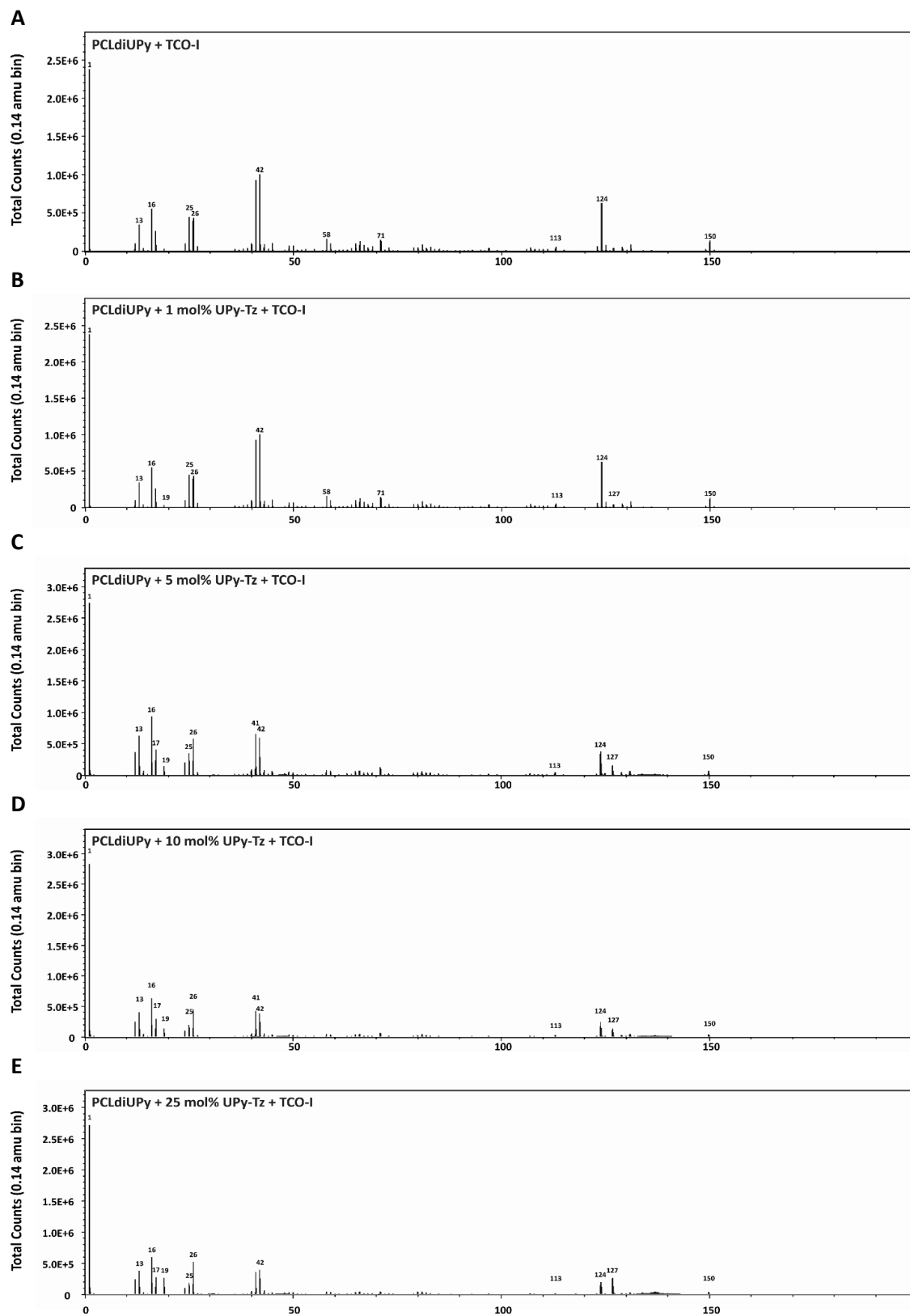
Figure 5.10. ToF-SIMS mass spectra of the different surfaces measured in negative mode with Bi$_3^{++}$, A) PCLdiUPy, B) PCLdiUPy + 1 mol% UPy-Tz, C) PCLdiUPy + 5 mol% UPy-Tz, D) PCLdiUPy + 10 mol% UPy-Tz and E) PCLdiUPy + 25 mol% UPy-Tz.

5.2.5 Conjugation of proteins onto dropcast supramolecular material films

Post-modification of the supramolecular material surfaces with more complex molecules, such as proteins, demonstrates the generality of this covalent modification approach. Therefore, the cycloaddition reaction of enhanced yellow fluorescent protein (EYFP) to UPy-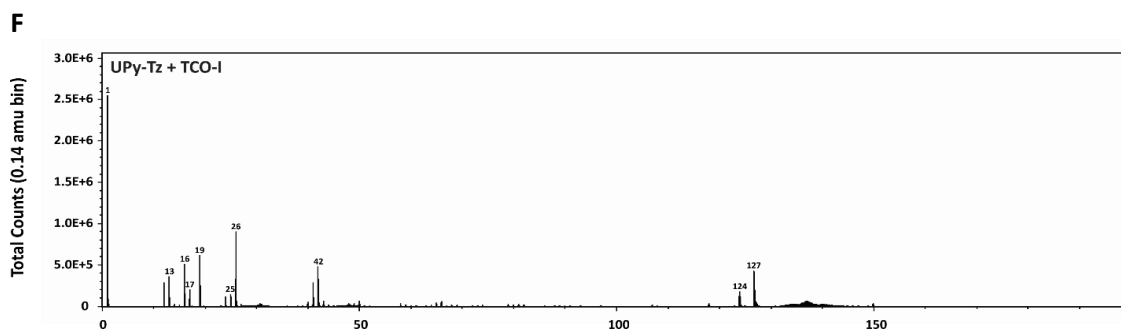Tz by fluorescence spectroscopy (Figure 5.11) is investigated. EYFP is non-specifically functionalized with TCO-moieties (TCO-EYFP, Figure 5.14). Incorporation of 1 and 5 mol% UPy-Tz showed a 9 times increase in surface fluorescence after TCO-EYFP incubation, whereas for both 10 and 25 mol% UPy-Tz 4 times and 2 times increase, respectively, is observed. This moderate increase for larger mol% of UPy-Tz can be explained by differences in morphology of the different mixtures, i.e. the occurrence of phase separated domains at the surface (Figure 5.1). It is proposed that in these cases tetrazine moieties are less available for reaction. An additional explanation might be that a higher amount of protein is reacted on the PCLdiUPy with 10 and 25 mol% UPy-Tz surfaces, thereby inducing quenching of the fluorophores. Surfaces incubated with non-functionalized EYFP do not show any fluorescence
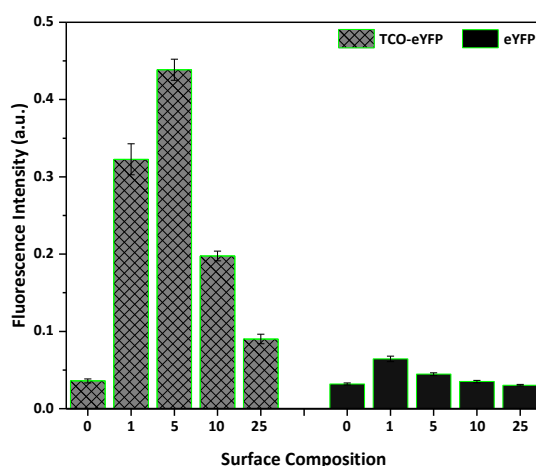
Figure 5.11. Surface analysis of post-modification with a TCO-EYFP and a non-functionalized control at the surface of drop-cast films of PCLdiUPy with various mol% UPy-Tz by fluorescence spectroscopy, PCLdiUPy (**0**), PCLdiUPy + 1 mol% UPy-Tz (**1**), PCLdiUPy + 5 mol% UPy-Tz (**5**), PCLdiUPy + 10 mol% UPy-Tz (**10**) and PCLdiUPy + 25 mol% UPy-Tz (**25**) incubated with TCO-EYFP or EYFP for 2 hours and subsequent 3 washing steps. Error bars represent standard deviations of triplicate measurements per condition, n = 4 per condition.

indicating the EYFP is washed off. In conclusion, these protein conjugation experiments show the versatility of our strategy towards more complex surface modifications.

5.2.6   Decoupling of material processing and functionalization

Electrospun meshes of PCLdiUPy with 5 mol% UPy-Tz are prepared (Figure 5.12), and PCLdiUPy as control. After electrospinning the materials were incubated with either a TCO-conjugated Cy5 dye (Figure 5.12 B, Scheme 5.4) or a TCO-EYFP protein (Figure 5.12 C).
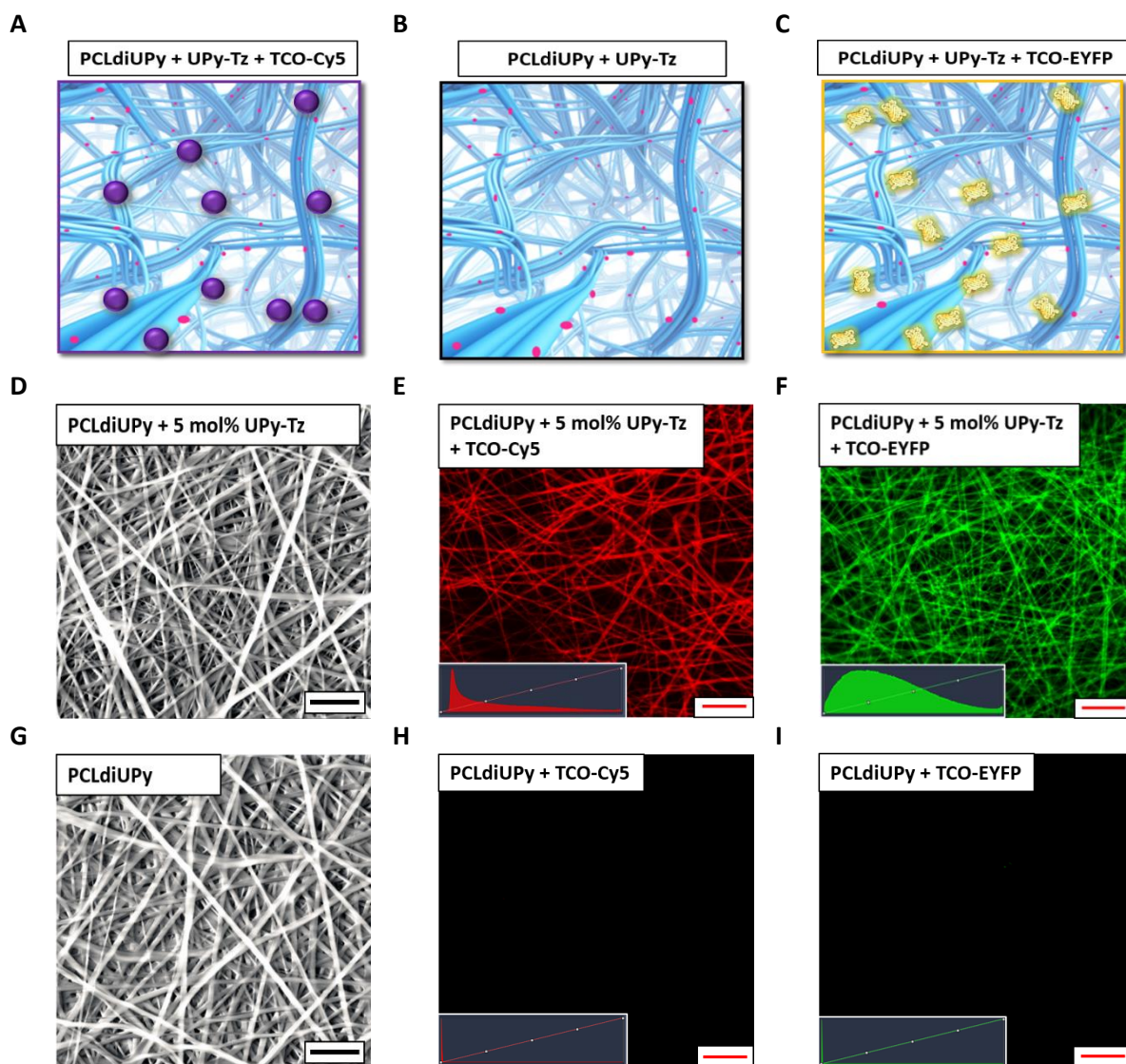
Figure 5.12. Decoupling processing and functionalization of electrospun supramolecular polymer materials, A) Cartoon representation of the electrospun supramolecular materials consisting of PCLdiUPy as the base polymer and UPy-Tz (pink dots) incorporated to facilitate selective surface reaction, B) reacted with the TCO-Cy5 dye or C) reacted with the TCO-EYFP model protein, D) SEM picture of electrospun fibers of PCLdiUPy with 5 mol% UPy-Tz incorporated, diameters 0.6 ± 0.24 µm, and the control elctrospun fibers of PCLdiUPy (G), diameters 0.8 ± 0.36 µm, scale bars represent 10 µm, E) Confocal image of electrospun fibers of PCLdiUPy with 5 mol% UPy-Tz incorporated and the PCLdiUPy control (H), incubated with 1 mg·mL^{-1} TCO-Cy5, fibers show a clear red color, scale bar represents 20 µm, inset shows the fluorescence intensity plot, F) Confocal image of electrospun fibers of PCLdiUPy with 5 mol% UPy-Tz incorporated and the PCLdiUPy control (I), incubated with 1 mg·mL^{-1} TCO-EYFP, fibers show a clear green color, scale bar represents 20 µm, inset shows the fluorescence intensity plot.

Scanning electron microscopy images shows fiber formation for both the PCLdiUPy with 5 mol% UPy-Tz (Figure 5.12 D) and the PCLdiUPy (Figure 5.12 G) with fiber diameters of 0.6 ± 0.24 µm and 0.8 ± 0.36 µm, respectively. Functionalization with the TCO-Cy5 dye shows clear red fluorescence appearance of the fibers (Figure 5.12 E) for the PCLdiUPy with 5 mol% UPy-Tz materials whereas the PCLdiUPy (Figure 5.12 H) materials do not show any fluorescence. A similar trend is observed after incubation with the TCO-EYFP, the PCLdiUPy with 5 mol% UPy-Tz (Figure 5.12 F) shows green fluorescent fiber morphology while the PCLdiUPy materials do not yield any fluorescence (Figure 5.12 I). Moreover, higher magnification images (Figure 5.13) clearly show enhanced fluorescence at the surface of the electrospun fibers, indicative for the reaction to have occurred at the surface. This approach shows decoupling of the material processing conditions and subsequent material functionalization via a post-modification approach.
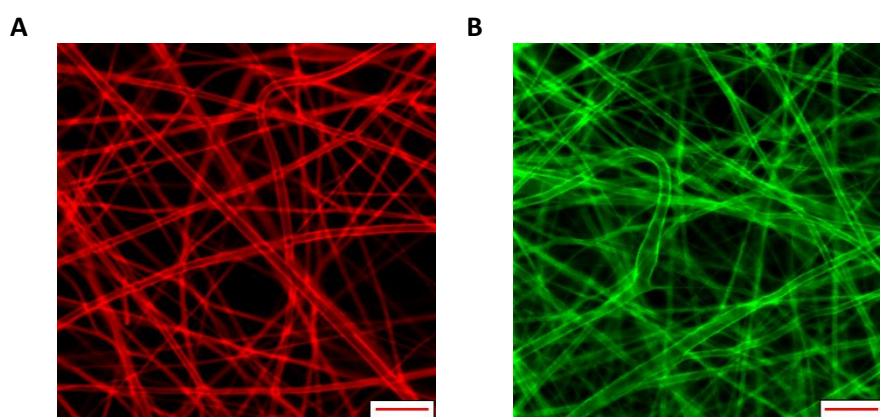
Figure 5.13. CLSM zoomed in images of electrospun fibers of PCLdiUPy with 5 mol% UPy-Tz incorporated after surface post-modification with A) TCO-Cy5 and B) TCO-EYFP. Scale bars represent 10 µm.

5.3 Conclusions

This chapter describes that selective modification reactions can be performed on additives that are supramolecularly incorporated into supramolecular materials. Careful design and synthesis of the additive facilitates control on the assembly process within the material and allows for selective surface post-modification in aqueous environment. Importantly, in this way processing of the material, that regularly requires harsh processing conditions (i.e. the use of organic solvents and/or high temperatures), and functionalization can be decoupled. Along these lines this approach endorses various material preparation methods (i.e. 3D-printing, melt spinning, electrospinning), whereby bulk material properties can easily be tuned and yet the material surfaces can be functionalized via covalent post-modification. The feasibility of this approach is shown by decoupling of material processing by electrospinning and post-modification of the supramolecular additive via selective orthogonal surface reactions. In conjunction with advanced ToF-SIMS depth profiling of bulk and surface the distribution of additive and reactant are revealed. At a supramolecular chemistry level these results allow for further exploration of these selective reactions on

inherently more dynamic systems, such as aggregates in solution and supramolecular hydrogels, yielding complex assemblies with various functionalities. This post-modification strategy of supramolecular systems might accommodate for better control on the assembled structure, when specific functionality is introduced after assembly. Additionally, the accurate depth resolution of ToF-SIMS is proposed to aid in elucidating the complex structures of such hierarchical assemblies.

Finally, this bioorthogonal functionalization and characterization strategy holds great promise in the field of regenerative medicine, in which design and detailed analysis of bioactive, functional biomaterials is important for the ultimate interaction with cells and tissues, and the essential performance. As a result of the bioorthogonal nature, the supramolecular thermoplastic elastomeric materials might as well be suitable for *in vivo* functionalization. In the next chapter the introduction of functionality at the supramolecular material surface via this covalent modification approach will be addressed.

5.4 Acknowledgements

Dr.ir. Henk Janssen and dr.ir. Henk Keizer are acknowledged for their help with both synthesis as well as scientific discussions on the results. Also, I would like to thank Joost van Dongen and dr. Xiawen Lou for helpful discussions regarding analyses, Tiny Verhoeven and dr. ir. Remco Lancee for XPS collaboration, prof. dr. Ron Heeren, Anne Bruinen, Msc, and Gert Eijkel (Maastricht University (M4i)) for assistance with ToF-SIMS depth profiling experiments, Dirk-Jan Mulder, Msc, for assistance with FTIR, dr.ir. Ralph Bosmans for collaboration during protein expression and the ICMS Animation Studio for careful design of cartoons.

5.5 Materials and methods

Instrumentation

^{1}H NMR and ^{13}C NMR spectra were recorded on a 400 MHz NMR (Varian Mercury Vx or Varian 400MR) operating at 400 MHz for ^{1}H NMR and 100 MHz for ^{13}C NMR. Proton chemical shifts are reported in ppm downfield from tetramethylsilane (TMS) and carbon chemical shifts in ppm downfield from TMS using the resonance of the deuterated solvent as internal standard. Abbreviations used are s: singlet, d: doublet, t: triplet, q: quartet, m: multiplet. IR spectra were acquired on a Perkin-Elmer spectrum Two equipped with a UATR Two sample stage.

Synthesis of compounds and materials

PCLdiUPy was synthesized by SyMO-Chem BV (Eindhoven, The Netherlands). [23] 1, 1, 1, 3, 3, 3-Hexafluoroisopropanol (HFIP) was obtained from Sigma-Aldrich (Zwijndrecht, The Netherlands). TCO-OEG$_4$-NHS ester (equatorial isomer) was obtained from Kerafast (Boston, MA, USA). Water was deionized prior to use. 2(6-Isocyanatohexylaminocarbony-lamino)-6-methyl-4[1H]pyrimidinone (UPy-C$_6$-NCO) was synthesized as described. [5] The synthesis of UPy-Tz (**2**) and TCO-iodine (**3**) are described in the synthesis section of this chapter.

Preparation of polymer solutions for dropcast and spincoated supramolecular TPE material films. Solutions of PCLdiUPy were prepared at a concentration of 50 mg·mL^{-1} in HFIP. For mixtures, the calculated amounts to obtain 1, 5, 10 or 25 mol% of the UPy-Tz additive were weighed and subsequently added to resp. 99, 95, 90 and 75 mol% solution of PCLdiUPy. After thorough mixing by vortexing, to allow the in solution mixing and assembly of the PCLdiUPy and the UPy-Tz, the solutions were ready to be dropcast or spincoated into supramolecular TPE

solid films. Upon increasing mol% UPy-Tz additive incorporation, an increase in pink color of the solutions was observed.

Preparation of drop-cast surfaces. Samples were prepared by dropcast 30 µL of a solution of 50 mg·mL-1 of the PCLdiUPy + 1, 5, 10 or 25 mol% UPy-Tz from HFIP on glass coverslips with a diameter of 12 mm, yielding a thin solid material film with a thickness in the range of 4-6 µm as was determined by profilometry measurements. Fluorescence assay samples were prepared by dropcast 25 µL of a solution of 50 mg·mL-1 of the PCLdiUPy + 0, 5, 10 or 25 mol% UPy-Tz from HFIP in a well of a 96-wells plate. Subsequent evaporation of the HFIP yielded the solid, impermeable dropcast films.

Preparation of spin coated surfaces. Samples were prepared by spin coating 50 µL of a solution of 50 mg·mL^{-1} of the PCLdiUPy + 1, 5, 10 or 25 mol% UPy-Tz from HFIP at 2000 rpm for 60 seconds on glass coverslips with a diameter of 12 mm, yielding a thin solid material film in the order of 100-150 nm as was determined by profilometry measurements. The samples were allowed to dry for 2 hours at room temperature before continuing experiments.

Performance of the click reaction at the material surface. Drop cast or spin coated samples were prepared as described. After overnight drying of the samples, the MALDI-TOF MS surfaces were incubated with 4 µL of a 1 µM TCO-iodine solution for 70 minutes, after which the reaction solution was discarded from the MALDI plate and the spots were washed 5 times with 5 µL milli-Q water. After the final washing step, the surfaces were dried under nitrogen flow.

In a similar fashion, the ToF-SIMS MS samples were prepared, here the surfaces were incubated with 100 µL of a 20 mg·mL^{-1} (25.8 mM) TCO-iodine solution for 2 hours. Afterwards, the TCO-iodine solution was taken off, and subsequently the spin coated films were washed 5 times with Milli-Q water in order to remove excess of the nonspecifically adsorbed TCO-iodine. Subsequently, the surfaces were dried under nitrogen flow.

For the fluorescence spectroscopy assay, the wells of the 96-wells plate were incubated with 100 µL of 200 µg·mL^{-1} TCO-EYFP or 200 µg·mL^{-1} EYFP as a control for 2 hours. Fluorescence was measured directly after 2 hours of incubation. Supernatant was removed and surface fluorescence was measured. Subsequently, surfaces were washed 5 times with 100 µL milli-Q water and after each washing step, surface fluorescence was measured. The reported spectra in Figure 5.11 were obtained after the fifth washing step.

The electrospun fibers were incubated at room temperature with 100 µL of a solution of 0.1 mg·mL^{-1} TCO-Cy5 in Milli-Q water for 20 minutes or with 100 µL of 1 mg·mL^{-1} TCO-EYFP in 10 mM sodium phosphate buffer of pH 7.4 for 2 hours. Afterwards, the electrospun fibers on the glass substrate were washed extensively with Milli-Q water. First, 1 mL of Milli-Q water was added and subsequently removed in order to remove the residual TCO-Cy5. Afterwards, the samples were submerged in 10 mL for 2 minutes. This was repeated 3 times. In the final washing step, the samples were placed on a 300 rpm shaking plate for 1 hour. Afterwards, the samples were dried under nitrogen flow.

X-ray photoelectron spectroscopy (XPS). XPS was performed on drop-cast films that were attached to the sample plate by copper clamps and spectra were recorded using a Thermo Scientific K-Alpha spectrometer equipped with a monochromatic, small-spot X-ray source and a 180° double focusing hemispherical analyzer with a 128-channel detector. Spectra were obtained using an aluminum anode (Al Kα, 1486.6 eV) operating at 72 W. Survey scans were measured at a pass energy of 200 eV and region scans at a pass energy of 50 eV. The background pressure was 2 x 10-8 mbar and during measurement 3 x 10^{-7} mbar argon, because of the charge compensating dual beam source. For angle-resolved XPS, the samples were mounted with conducting carbon tape to the sample holder and spectra were measured at 0°, 15°, 30°, 45°, 60° and 75°. Analysis and quantification of the spectra were performed using the CasaXPS software version 2.3.16, using the C 1s, N 1s, O 1s and F 1s regions.

FTIR measurements. IR spectra were recorded using a Varian 670-IR FTIR spectrometer / 610-IR FTIR Microscope setup equipped with a germanium slide-on ATR accessory. Spectra were recorded with a resolution of 2 cm^{-1}

with 50 scans per spectrum for the samples and 100 scans per spectrum for the background. Spectra were analyzed using Spekwin32 version 1.71.6.1.

Atomic force microscopy (AFM). AFM images were recorded at room temperature in air using a Digital Instrument Multimode Nanoscope IV operating in tapping regime mode using silicon cantilever tips (PPP-NCH-50, 204-497 kHz, 10-130 N·m^{-1}). Surface roughness has been measured and images have been processed using Gwyddion software (version 2.39, hhtp://www.gwyddion.net).

Water contact angle measurements. Water contact angles were measured at room temperature on an OCA30 (DataPhysics). Water droplets (5 µL) were applied on the drop-cast films on glass and the angle at the polymer-air-water interface was determined after 5 seconds using an automatic fitting routine (SCA20 software). The mean and the standard deviation of three to five samples are reported.

Surface fluorescence experiments. Fluorescence assays were performed on a Thermo Scientific Fluoroskan Ascent Microplate Fluorometer and analyzed with Ascent Software for Fluoroskan Ascent FL. Surfaces were excited at 488 nm and emission was recorded at 538 nm. Samples were prepared by 25 µL dropcast of 50 mg·mL^{-1} PCLdiUPy + 0, 1, 5, 10 or 25 mol% UPy-Tz in HFIP into a 96-wells plate. After overnight drying of the surface, wells were incubated with 200 µg·mL^{-1} TCO-EYFP or 200 µg·mL^{-1} EYFP for 2 hours. Fluorescence was measured directly after 2 hours of incubation. Supernatant was removed and surface fluorescence was measured. Subsequently, surfaces were washed 5 times with milli-Q water and after each washing step, surface fluorescence was measured.

Surface MALDI-ToF MS measurements. Matrix-assisted laser desorption ionization time-of-flight mass spectrometry (MALDI-ToF MS) was performed on an Autoflex Speed MALDI-MS (Bruker) using an α-cyano-4-hydroxycinnamic acid (CHCA) matrix. Surface MALDI-ToF MS experiments were performed on drop-cast samples on a MTP 384 target plate polished steel TF. Dropcast were prepared by 5 µL 50 mg·mL^{-1} PCLdiUPy + 0, 5, 10 or 25 mol% UPy-Tz and directly deposited on the MALDI plate. Next, drop-cast spots were incubated with 4µL 1 µM TCO-iodine solution for 70 minutes, after which the reaction solution was discarded from the MALDI plate and the spots were washed 3 times with 5 µL milli-Q water. Subsequently 1 µL CHCA in 49.5/49.5/1 MeCN/water/TFA (v/v/v%) was spotted on each surface and allowed to dry for 30 minutes. MALDI-ToF MS measurements were performed in positive linear mode (method: 700-2000 Da), 1500 shots per spot and a laser power of 50%.

3D ToF-SIMS measurements. The in depth ToF-SIMS experiments were performed using a PHI *nanoToF* II TRIFT mass spectrometer (Physical Electronics, Minnesota, USA) equipped with a 30 kV bismuth liquid metal ion gun (LMIG) and a 20 kV C$_{60}$ ion gun (Ionoptika, Hampshire, UK). A pulsed Bi$_3^{++}$ cluster ion beam was used for analysis and a continuous C$_{60}^+$ cluster ion beam was used for sputtering in the described depth profiling measurements. 50 cycles of alternating between sputtering and analyzing were executed, each cycle consisted of 4 frames (512x512 pixel density, 2.13 minutes) LMIG analysis and 1 minute of sputtering with the C$_{60}$ ion beam (1.47 x 10^{17} ions·cm^{-2}) while the sample is kept at ground potential. The analytical area was 100x100 µm, the sputter area was 400x400 µm. On each sample, an in depth experiment was performed in both positive and negative ion mode, with a mass range of *m/z* 0-1850.
All raw data was produced using PHI SmartSoft-ToF and was subsequently processed into 3D visualizations of ion distributions and spectra with PHI ToF-DR (both Physical Electronics, Minnesota, USA).

Principal Component Analysis (PCA). PCA is a statistical tool that is often used to inspect large mass spectrometry imaging data sets. PCA optimizes the variance that is described in each principal component (PC) in descending order of magnitude. The first PC contains the maximum variance direction, the second one the next maximum, etcetera. Therefore, each PC will contain different percentages of the variance originating from multiple analytes and the PC score images reveal the distribution and relative concentrations of this mixture. A PCA was done on the first two analysis layers from each depth profiling ToF-SIMS data set. The analyses were

performed using the ChemomeTricks toolbox for MATLAB version R2014a (The Math-Works, Natick, MA, USA) developed at the FOM Institute AMOLF.

Preparation of the electrospun samples. Two different electrospinning solutions were prepared in glass vials. 20 wt/wt% PCLdiUPy was dissolved in 80 wt/wt% 1,1,1,3,3,3-hexafluoro-2-propanol (HFIP, 147545000, Acros) as a control sample. The solution containing the 5 mol% UPy-Tz for post-modification was composed of 17.5 wt/wt% PCLdiUPy in 82.5 wt/wt% HFIP and 5 mol% UPy-Tz. The solutions were stirred overnight at room temperature and then transferred into separate 2.5 mL glass syringes (Hamilton). Approximately 1 mL of the solution was fed at 0.02 mL min^{-1} using a syringe pump (KR analytical) at the outside of the electrospinning cabinet *via* 35 cm long 1 mm I.D. PTFE tube connected to a flat-tip stainless-steel 23 g needle (Intertronics, United Kingdom). Inside the cabinet, the solution was spun with an in-house built electrospin setup by applying 18.5 kV with a collector distance of 12 cm. Fibers were collected on a 12 x 12 cm grounded collector plate. To enable facile removal of the non-woven electrospun membrane, the collector plate was covered with a thin sheet of polyethylene (PE) film. Round 12 mm Ø cover glasses were placed to collect the fibers. Short electrospinning times of around 1 minute were applied in order to allow electrospinning of a thin layer. The electrospun samples were dried overnight *in vacuo* at room temperature to remove any residual solvent.

Environmental scanning electron microscopy (ESEM). Environmental scanning electron microscopy (ESEM) imaging was performed using FEI Quanta 600 and Xt Microscope Control software. The fiber samples on the round cover glasses were mounted with fiber side up to a metal stub by using double sided carbon tape. The samples were visualized under low vacuum with an accelerating voltage of 10 kV, a spot size of 4 and a working distance of 10 mm. Images were recorded at a resolution of 2048 x 1768, a dwell time of 10 μs and magnifications between 1000 and 10,000 times. Both backscattering electrons (BSEs) and secondary electrons (SEs) were detected. The fiber diameters were determined from multiple high magnification images using ImageJ software and expressed as average ± standard deviation.

Confocal laser scanning microscopy (CLSM). Electrospun samples that were reacted with either the TCO-Cy5 dye or the TCO-EYFP model protein, were mounted between a microscope glass slide and a cover glass using Mowiol. The samples were analyzed with a confocal laser scanning microscope (CLSM), Zeiss LSM510 META NLO and ZEN software. The TCO-Cy5 samples were excited with a Helium-Neon laser at 633 nm, 5% laser power and fluorescence was collected via HFT 488/543/633 main dichroics, NFT 545 secondary dichroics and BP 650-710 IR filter. A Plan-Apochromat 63x/1.4 Oil objective was used with 1 AU (132 μm) pinhole. Images were recorded with a master gain of 719, 1024 x 1024 resolution, line average of 8, pixel dwell of 51.2 μs and zoom up to 4.5 times. The TCO-EYFP samples were excited with an Argon laser at 488 nm, 5% laser power and fluorescence was collected via HFT 488/543 main dichroics, NFT 490 secondary dichroics and BP 500-530 IR filter. A Plan-Apochromat 63x/1.4 Oil objective was used with 1 AU (94 μm) pinhole. Images were recorded with a master gain of 808, 1024 x 1024 resolution, line average of 8, pixel dwell of 51.2 μs and zoom up to 2 times.

Synthesis of UPy-C$_6$-U-C$_6$-OEG$_6$-C$_5$-Tz-CF$_3$ (2)
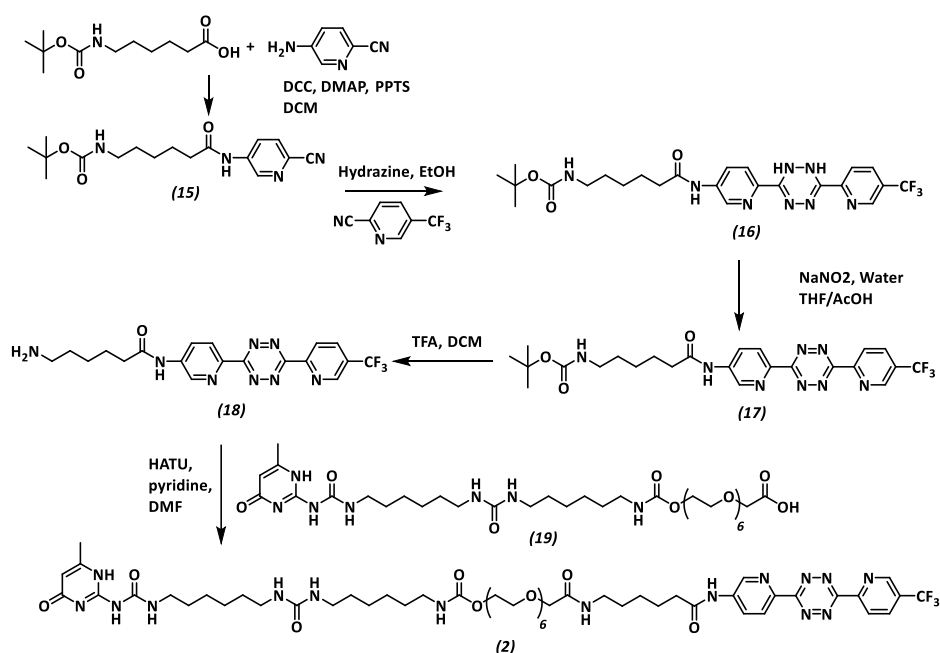
Scheme 5.2. Synthesis of the UPy-OEG$_6$-Tz (**2**), MW 1190.29 g·mol^{-1}.

***tert*-Butyl (6-((6-cyanopyridin-3-yl)amino)-6-oxohexyl)carbamate (15)**

6-((Tert-butoxycarbonyl)amino)hexanoic acid (5.18 g, 22.39 mmol), EDC (6.44 g, 33.6 mmol), DMAP (4.10 g, 33.6 mmol), and PPTS (0.56 g, 2.24 mmol) were dissolved in 50 mL DCM. After stirring for 30 minutes 5-aminopicolinonitrile (4.0 g, 33.6 mmol) was added. The reaction mixture was stirred for 1 hour, after which 50 mL chloroform was added. The organic phase was washed twice with 40 mL 0.5 M citric acid, saturated sodium hydrogen carbonate, and brine, followed by drying with Na$_2$SO$_4$ and evaporating to dryness yielding 7.5 g of the crude product. Eluting over silica with chloroform containing 2.5% methanol afforded 5.9 g (79%) of the pure product.

^{1}H NMR (399 MHz, CDCl$_3$) δ 8.90 (s, 1H), 8.68 (s, 1H), 8.46 (d, 1H), 7.65 (d, *J* = 8.6 Hz, 1H), 4.74 (t, *J* = 6.1 Hz, 1H), 3.10 (q, *J* = 6.7 Hz, 2H), 2.42 (t, *J* = 7.5 Hz, 2H), 1.74 (p, *J* = 7.5 Hz, 2H), 1.59 – 1.29 (m, 13H). ^{13}C NMR (100 MHz, CDCl$_3$) δ 172.69, 156.43, 141.94, 138.51, 129.14, 127.17, 126.08, 117.44, 79.48, 40.13, 37.15, 29.61, 28.40, 26.10, 24.67. LC-MS(ESI) R$_t$= 6.52 min *m/z* calcd (C$_{17}$H$_{24}$N$_4$O$_3$) 332.4; found 233.3 [M-*t*Bu (degraded on MS) + H$^+$]$^+$,277.2 [M-*t*Bu +HCOOH]$^+$, 355.3 [M+Na]$^+$, 687.2 [2M+Na]$^+$.

***tert*-Butyl (6-oxo-6-((6-(6-(5-(trifluoromethyl)pyridin-2-yl)-1,2-dihydro-1,2,4,5-tetrazin-3-yl)pyridin-3-yl)amino)hexyl)carbamate (16)**

5-(Trifluoromethyl)picolinonitrile (0.93 g, 5.42 mmol) and **15** (1.5 g, 4.51 mmol) were dissolved in EtOH (3 mL) and heated to 70 °C. Hydrazine hydrate (50-60% sol, 0.89 mL, ~18 mmol) was added and this solution was stirred overnight at 70 °C under argon. To the yellow/brown precipitate water (30 mL was added) and the suspension was centrifuged. The yellow solution was decanted off and water 50 mL was added. This was repeated until the filtrate was colorless. The yellow/brown residue was redissolved in CHCl$_3$/MeOH 1:1 v/v%, which was removed *in vacuo* yielding 2.2 g of the crude product. Eluting over silica with chloroform containing 5-20% acetone afforded 0.4 g (17%) of the pure product.

^{1}H NMR (399 MHz, CDCl$_3$) δ 8.78 (s, 1H), 8.66 (s, 1H), 8.57 (s, 1H), 8.39 (s, 1H), 8.18 – 8.07 (m, 2H), 8.01 – 7.81 (m, 2H), 5.00 (s, 1H), 3.32 (s, 1H), 3.03 (q, *J* = 6.7 Hz, 2H), 2.33 (t, *J* = 7.5 Hz, 2H), 1.67 (t, *J* = 7.5 Hz, 2H), 1.53 – 1.22 (m, 13H). ^{13}C NMR (100 MHz, CDCl$_3$) δ 173.05, 156.61, 150.48, 146.30, 145.73, 145.37, 141.45, 139.46, 137.06, 133.89, 127.50, 127.13, 124.52, 121.60, 120.99, 79.36, 77.38, 77.26, 77.06, 76.74, 39.96, 36.75, 29.33,

28.20, 25.97, 24.83. LC-MS (ESI) R_t= 8.31 min, m/z calcd ($C_{24}H_{29}F_3N_8O_3$) 534.5; found 535.2 [M+H]$^+$. MS (MALDI-ToF, m/z): Calcd for $C_{24}H_{29}F_3N_8O_3Na^+$, ([M+Na]$^+$): 557.2207, Found: 557.2384. FT-IR (ATR): υ (cm^{-1}) = 3372, 3330, 3297, 2985, 2941, 2857, 1685, 1667, 1603, 1573, 1528, 1466, 1414, 1389, 1368, 1330, 1279, 1249, 1237, 1160, 1132, 1087, 1049, 1016, 990, 958, 942, 914, 899, 862, 777, 758, 707, 662, 651, 636, 623, 577, 516, 472.

tert-Butyl(6-oxo-6-((6-(6-(5-(trifluoromethyl)pyridin-2-yl)-1,2,4,5-tetrazin-3-yl)pyridin-3-yl)amino)hexyl)carbamate (17)

Dihydrotetrazine **16** (0.4 g, 0.75 mmol) was dissolved in 6 mL THF and cooled to 0 °C, followed by the addition of AcOH (6 mL). A solution of $NaNO_2$ (0.21 g, 3.0 mmol in 6 mL water) was added dropwise over 10 min, a clear color change was observed from orange/brown to purple. This solution was stirred for another 5 min. Then it was poured in a separation funnel containing 30 mL water, 10 mL MeOH and chloroform 40 mL, subsequently the organic phase was washed with saturated sodium hydrogen carbonate (twice), water and brine. The organic phase was dried *in vacuo*, yielding a purple powder (0.39 g, 98%).

^{1}H NMR (400 MHz, CDCl$_3$/CD$_3$OD) δ 9.14 (d, J = 2.2 Hz, 1H), 8.85 (d, J = 8.2 Hz, 1H), 8.79 (s, 1H), 8.72 (dd, J = 8.7, 0.7 Hz, 1H), 8.63 (d, J = 9.0 Hz, 1H), 8.26 (dd, J = 8.5, 2.3 Hz, 1H), 3.04 (t, J = 6.8 Hz, 2H), 2.41 (t, J = 7.5 Hz, 2H), 1.71 (p, J = 7.6 Hz, 2H), 1.49 (p, J = 7.0 Hz, 2H), 1.38 (s, 13H).^{13}C NMR (100 MHz, CDCl$_3$/CD$_3$OD) δ 173.45, 163.16, 162.71, 153.02, 147.51, 143.05, 141.67, 139.07, 135.02, 126.88, 125.52, 123.82, 120.58, 79.35, 40.02, 36.86, 29.57, 29.40, 28.22, 27.85, 26.07, 24.87, 24.79. LC-MS (ESI) R_t= 6.72 min, m/z calcd ($C_{24}H_{27}F_3N_8O_3$) 532.5; found 533.0 [M+H]$^+$.]$^+$. MS (MALDI-ToF, m/z): Calcd for $C_{24}H_{27}F_3N_8O_3Na^+$, ([M+Na]$^+$): 555.2050, Found: 555.2412. FT-IR (ATR): υ (cm^{-1}) = 3351, 3320, 3099, 3082, 3048, 3001, 2941, 2865, 2490, 1676, 1661 1596, 1575, 1542, 1522, 1483, 1466, 1449, 1429, 1403, 1381, 1370, 1330, 1283, 1257, 1231, 1161, 1131, 1081, 1052, 1013 982, 942, 924, 882, 862, 801, 776, 728, 706, 665, 649, 620, 583, 533, 490, 473.

6-Amino-N-(6-(6-(5-(trifluoromethyl)pyridin-2-yl)-1,2,4,5-tetrazin-3-yl)pyridin-3-yl)hexanamide (18)

Tetrazine **17** (0.2 g, 0.374 mmol) was dissolved in 2 mL DCM and 2 mL of TFA was added. The solution was stirred for 1 hour at room temperature under Argon. The solvent was removed under reduced pressure and co-evaporated twice with toluene. After redissolving in MeOH/CHCl$_3$ and precipitating in ether (2x) a solid was filtered off. Drying yielded **18** as a pink solid (170 mg, quant.)

^{1}H NMR (399 MHz, CD$_3$OD) δ 9.20 (s, 1H), 9.06 (d, J = 2.5 Hz, 1H), 8.94 (d, J = 8.4 Hz, 1H), 8.78 (d, J = 8.7 Hz, 1H), 8.49 (t, J = 9.6 Hz, 2H), 2.96 (t, J = 7.6 Hz, 2H), 2.54 (t, J = 7.3 Hz, 2H), 1.76 (dp, J = 23.4, 7.6 Hz, 4H), 1.52 (q, J = 7.9 Hz, 2H). ^{13}C NMR (100 MHz, DMSO-d_6) δ 172.79, 163.18, 162.86, 154.23, 147.62, 143.96, 141.81, 139.12, 135.93, 126.55, 125.60, 125.24, 124.58, 122.53, 39.19, 36.54, 27.30, 25.91, 24.74. LC-MS (ESI) R_t= 6.72 min, m/z calcd ($C_{19}H_{19}F_3N_8O$) 432.4; found 433.0 [M+H]$^+$. MS (MALDI-ToF, m/z): Calcd for $C_{19}H_{20}F_3N_8O^+$, ([M+H]$^+$): 433.1707, Found: 433.2352. FT-IR (ATR): υ (cm^{-1}) = 3263, 3171, 3095, 3048, 2962, 1705, 1672, 1601, 1580, 1541, 1439, 1404, 1329, 1261, 1229, 1202, 1172, 1129, 1082, 1021, 927, 864, 799, 722, 621, 585, 479.

UPy-C$_6$-U-C$_6$-Ut-OEG$_6$-C$_5$-Tz-CF$_3$ (2)

UPy-C$_6$-U-C$_6$-Ut-OEG$_6$-COOH [58] **19** (169 mg, 0.22 mmol) was dissolved in DMF (3 mL) and HATU (87 mg, 2.23 mmol) and pyridine (0.11 mL, 2.18 mmol) were added. The solution was stirred for 30 minutes under argon. Thereafter, tetrazine **18** (170 mg, 0.39 mmol) dissolved in 3 mL DMF was added. The reaction mixture was stirred overnight and subsequently poured into 2% FA water solution and centrifuged (2x). Eluting over silica with FA/MeOH/CHCl$_3$ 1:5:94 (v/v/v%) afforded **2** (230 mg, 88%) as a pink solid.

^{1}H NMR (399 MHz, CDCl$_3$/CD$_3$OD) δ 9.21 (s, 1H), 9.02 − 8.83 (m, 2H), 8.83 − 8.61 (m, 2H), 8.38 − 8.19 (m, 1H), 5.84 (s, 1H), 4.17 (t, J = 4.7 Hz, 2H), 3.98 (s, 2H), 3.65 (t, J = 4.6 Hz, 22H), 3.32 − 3.01 (m, 10H), 2.48 (t, J = 7.5 Hz, 2H), 2.26 (s, 3H), 1.79 (p, J = 7.6 Hz, 2H), 1.70 − 1.23 (m, 20H). ^{13}C NMR (100 MHz, CDCl$_3$/CD$_3$OD) δ 173.68, 173.68, 173.55, 170.76, 163.43, 162.92, 159.43, 157.03, 156.22, 154.48, 153.29, 148.98, 147.68, 143.37, 142.04, 139.26, 135.18, 129.30, 128.96, 126.97, 125.68, 124.55, 124.02, 121.83, 106.48, 70.99, 70.62, 70.55, 70.33, 70.27, 69.70, 63.88, 40.73, 40.08, 40.01, 39.76, 38.70, 37.03, 30.10, 30.00, 29.77, 29.31, 29.16, 26.54, 26.46, 26.40, 26.35, 24.95, 18.84. LC-MS (ESI) R_t= 5.75 min, m/z calcd ($C_{53}H_{78}F_3N_{15}O_{13}$) 1189.6; found 595.8 [M+2H]$^{2+}$,606.7 [M+Na+H]$^+$ 1190.3 [M+H]$^+$, 1212.4 [M+Na]$^+$. MS (MALDI-ToF, m/z): Calcd for $C_{53}H_{78}F_3N_{15}O_{13}Na^+$, ([M+Na]$^+$):

1212.5748, Found: 1212.6470. FT-IR (ATR): υ (cm^{-1}) = 3299, 2930, 2857, 1701, 1667, 1616, 1580, 1526, 1462, 1440 1405, 1382, 1331, 1257, 1119, 1081, 1014, 941, 923, 878, 854, 768, 741, 621, 602, 583, 526, 481.

Synthesis of TCO-OEG$_4$-Lys-I (3)
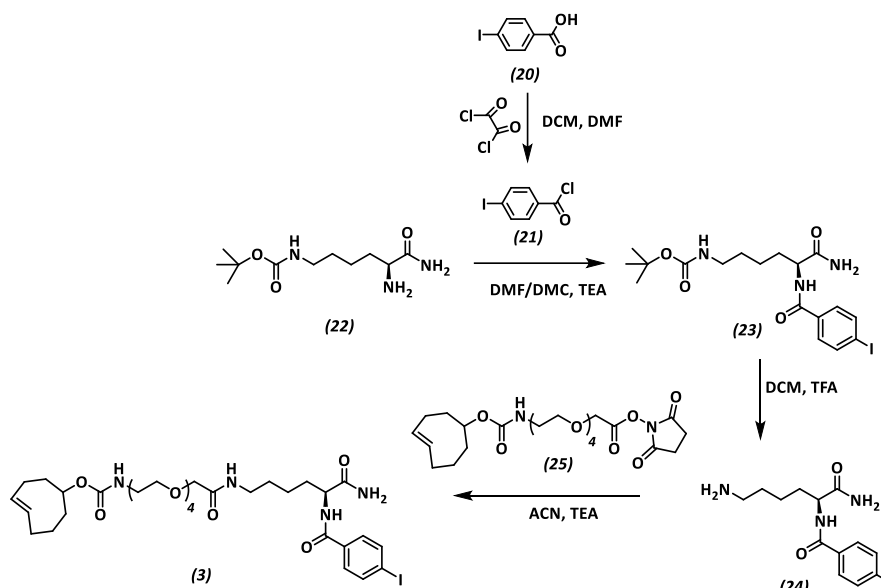
Scheme 5.3. Synthesis scheme for TCO-OEG$_4$-Lys-I (**3**) , MW 774.30 g·mol^{-1}.

4-Iodobenzoyl chloride (21)

To a suspension of **20** (0.5 g, 2.02 mmol) in DCM (8 mL) oxalylic chloride (0.31 mL, 3.63 mmol) was added, followed by 2 drops of DMF. The reaction mixture was stirred for 30 minutes. The solvent was removed under reduced pressure and co-evaporated twice with toluene and ether. A light yellow solid **21** (0.52 g, 97%) was obtained, which was used without further purification.

^{1}H NMR (200 MHz, CDCl$_3$) δ 7.98 – 7.72 (m, 4H). FT-IR (ATR): υ (cm^{-1}) = 3085, 1765, 1720, 1577, 1560, 1476, 1392, 1199, 1174, 1057, 1008, 865, 826, 713, 690,641, 625, 527, 458.

4-Iodobenzamide-Lys(Boc)-NH$_2$ (23)

H-Lys(Boc)-NH$_2$ **22** (0.1 g, 0.36 mmol) was suspended in DMF (0.5 mL), triethylamine (0.20 mL, 1.42 mmol) and iodobenzoyl chloride **21** (0.12 g, 0.44 mmol) were added. The suspension was stirred for 2 hours. Then, the solvent was removed under reduced pressure and co-evaporated twice with toluene. After dissolving in CHCl$_3$/MeOH 1:0.05 the solution was washed with 0.1 M HCl (2x) and saturated NaHCO$_3$ and dried over Na$_2$SO$_4$. Re-crystallization from CHCl$_3$ resulted in a slightly yellow crystalline solid **23** (110 mg, 65%).

^{1}H NMR (399 MHz, CDCl$_3$) δ 7.80 (d, J = 8.1 Hz, 2H), 7.58 (d, J = 8.0 Hz, 2H), 4.58 (s, 1H), 3.41 (d, J = 29.8 Hz, 1H), 3.07 (p, J = 6.4 Hz, 2H), 1.83 (d, J = 51.5 Hz, 2H), 1.52 (p, J = 7.0 Hz, 2H), 1.42 (s, 11H). ^{13}C NMR (100 MHz, CDCl$_3$/CD$_3$OD) δ 174.99, 167.43, 156.84, 137.91, 133.21, 129.02, 99.02, 79.50, 53.11, 40.01, 32.08, 29.51, 28.43, 22.79. LC-MS (ESI) R$_t$= 5.84 min, m/z calcd (C$_{18}$H$_{26}$IN$_3$O$_4$) 475.3; found 376.1 [M-NBoc]$^+$,419.9 [M-tBu]$^+$ 475.8 [M+H]$^+$, 498.1 [M+Na]$^+$, 972.5 [2M+Na]$^+$. FT-IR (ATR): υ (cm^{-1}) = 3366, 3302, 2979, 2945, 2928, 2857, 2499, 2383, 1678, 1652, 1631, 1587, 1527, 1479, 1461, 1427, 1389, 1366, 1333, 1296, 1281, 1249, 1167, 1113, 1047, 1007, 990, 975, 880, 838, 754, 707, 673, 666, 625, 585, 474.

4-Iodobenzamide-Lys(H)-NH$_2$ (24)

4-Iodobenzamide-Lys(Boc)-NH$_2$ **23** (40 mg, 0.084 mmol) was dissolved in 2 mL DCM and 2 mL of TFA was added. The solution was stirred for 2 hours at room temperature under Argon. The solvent was removed under reduced

pressure and co-evaporated twice with toluene. After redissolving in MeCN and precipitating in ether (2x) the solid was centrifuged off. Drying yielded **24** as a light yellow solid (41 mg, quant.).

^{1}H NMR (399 MHz, CD$_3$OD) δ 7.85 (d, J = 8.1 Hz, 2H), 7.63 (d, J = 8.1 Hz, 2H), 4.55 (dd, J = 9.2, 5.2 Hz, 1H), 3.31 (s, 0H), 2.97 – 2.88 (m, 2H), 2.03 – 1.90 (m, 1H), 1.83 (dtd, J = 14.0, 9.2, 5.3 Hz, 1H), 1.78 – 1.62 (m, 2H), 1.52 (th, J = 14.6, 7.1 Hz, 2H). ^{13}C NMR (100 MHz, CD$_3$OD) δ 176.72, 169.43, 138.92, 134.69, 130.23, 99.49, 54.71, 49.28, 40.53, 32.51, 28.12, 24.01. LC-MS (ESI) R$_t$= 3.53 min, m/z calcd (C$_{13}$H$_{18}$IN$_3$O$_2$) 375.0; found 376.0 [M+H]$^+$. FT-IR (ATR): υ (cm^{-1}) = 3288, 3060, 2943, 2866, 2459, 2072, 1666, 1635, 1588, 1535, 1480, 1427, 1390, 1314, 1200, 1180, 1133, 1059, 1025, 978, 838, 799, 752, 722, 683, 667, 625, 592, 555, 517.

4-Iodobenzamide-Lys(OEG$_4$-TCO)-NH$_2$ (3)

4-Iodobenzamide-Lys(H)-NH$_2$ **24** (11.4 mg, 0.023 mmol) was dissolved in DMF (0.5 mL), triethylamine (10.8 ☐L, 0.078 mmol) and TCO-OEG$_4$-NHS (equatorial isomer) **25** (10.0 mg, 0.019 mmol) were added. The solution was stirred for 1 hour at room temperature under Argon. The solvent was removed under reduced pressure and co-evaporated twice with toluene. Ether was added, stirred and decanted off 2x, then MeCN was added, stirred and decanted off 2x. Drying resulted in a slightly yellow solid **3** (12 mg, 80%).

^{1}H NMR (399 MHz, CDCl$_3$) δ 7.76 (d, J = 8.1 Hz, 2H), 7.61 (d, J = 8.0 Hz, 2H), 7.45 (d, J = 6.9 Hz, 1H), 6.81 (d, J = 33.1 Hz, 2H), 5.95 (s, 1H), 5.64 – 5.34 (m, 3H), 4.58 (q, J = 6.9 Hz, 1H), 4.40 – 4.22 (m, 1H), 3.85 – 3.43 (m, 16H), 3.39 – 3.17 (m, 4H), 2.38 (dt, J = 38.7, 5.3 Hz, 5H), 2.07 – 1.82 (m, 6H), 1.71 (s, 2H), 1.64 – 1.37 (m, 6H), 1.25 (s, 1H). LC-MS (ESI) R$_t$= 6.09 min, m/z calcd (C$_{33}$H$_{51}$IN$_4$O$_9$) 774.3; found 775.1 [M+H]$^+$, 797.3 [M+Na]$^+$.

Synthesis of TCO-EG3-Cy5 (4)
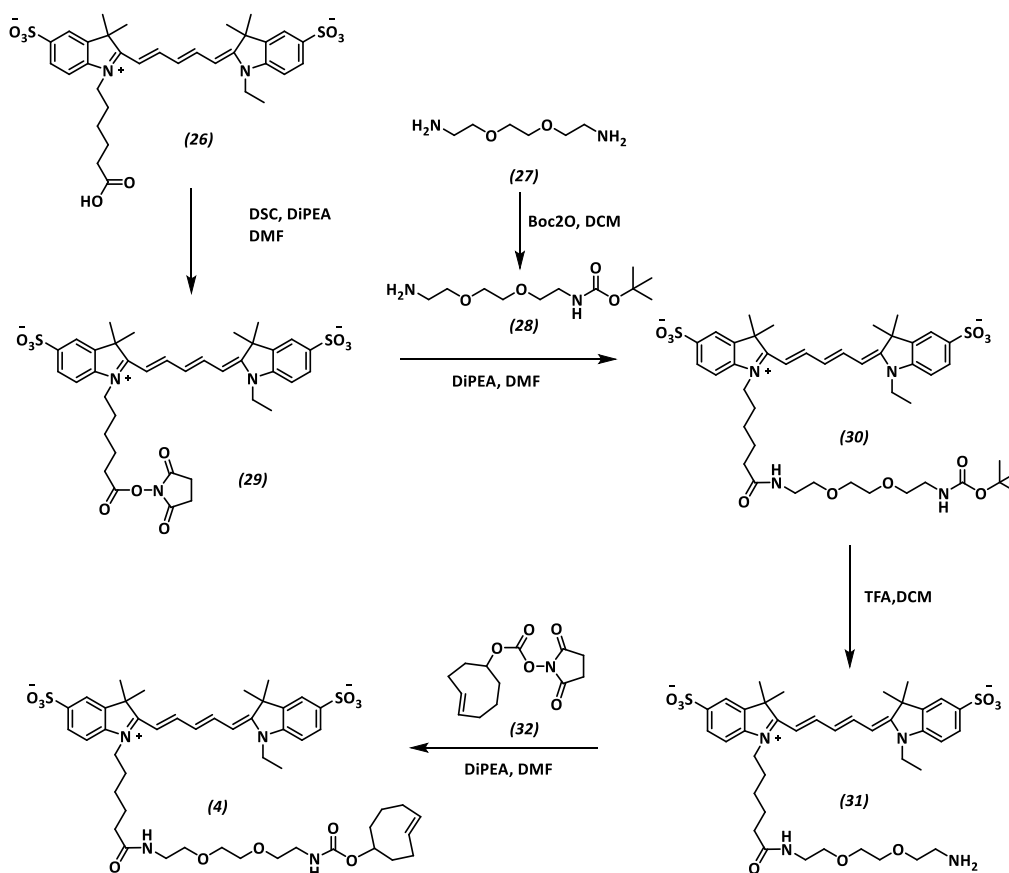
Scheme 5.4. Synthesis of the TCO-EG$_3$-Cy5 (**4**), MW 938.20 g·mol^{-1}.

Cy5-NHS (29)

Cy5 **26** was synthesized according to literature procedure. [59] Cy5 **26** (29.8 mg, 0.045 mmol) was dissolved in DMF (1.0 mL), DiPEA (79.0 µl, 0.45 mmol) and N,N'-disuccinimidylcarbonate (DSC) (46.6 mg, 0.182 mmol) were added. The solution was stirred for 1 hour at 55 °C under argon. The reaction mixture was cooled to room temperature. Ethyl acetate was added, stirred and centrifuged. The precipitate was dissolved in little MeCN and ethyl acetate was added, stirred and centrifuged. Drying resulted in a dark blue solid **30** (34 mg, 99%).

LC-MS (ESI) R_t= 4.48 min, m/z calcd ($C_{37}H_{42}N_3O_{10}S_2$) 752.9; found 754.4 [M+H]$^+$, 776.4 [M+Na]$^+$.

N-Boc- 2,2'-(ethylenedioxy)diethylamine (28)

Mono-protected **28** was synthesized according to an adapted literature procedure. [60] 2,2'-(ethylenedioxy)diethylamine **27** (5 g, 33.6 mmol) was dissolved in 150 ml DCM and cooled to 0 °C. Boc-Anhydride (1.25 mL, 5.38 mmol) was dissolved in 50 ml DCM and added dropwise. The reaction mixture was left stirring for 2 hours at room temperature under argon. Then, the reaction mixture was washed with water (twice), followed by extraction with 0.5 M citric acid (pH ~2) (twice). The pH of the water phase was adjusted from pH ~2 to pH ~12 by addition of 6M NaOH (aq). The product was back extracted from the water phase with CHCl$_3$. The organic phase was dried with Na$_2$SO$_4$ and evaporation yielded a clear oil (1 g, 11.9%).

^{1}H NMR (200 MHz, CDCl$_3$) δ 5.25 (s, 1H), 3.62 (s, 4H), 3.60 – 3.44 (m, 4H), 3.32 (q, J = 5.4 Hz, 2H), 2.88 (t, J = 5.2 Hz, 2H), 1.70 – 1.51 (m, 2H), 1.45 (s, 9H). ^{13}C NMR (50 MHz, CDCl$_3$) δ 155.96, 79.08, 73.39, 70.14, 41.67, 40.29, 28.36. LC-MS (ESI) R_t= 3.37 min, m/z calcd ($C_{11}H_{24}N_2O_4$) 248.3; found 249.1 [M+H]$^+$, 193.2 [M-tBu]$^+$.

Cy5-EG3-N-Boc (30)

Cy5-NHS **29** (34 mg, 0.045 mmol) was dissolved in DMF (1.5 mL), DiPEA (32.0 µL 0.181 mmol) and **28** (22.4 mg, 0.090 mmol) dissolved in 0.5 mL DMF were added. The solution was stirred over night at room temperature under argon. The reaction mixture was coevaporated three times with toluene, then ethyl acetate was added, stirred and centrifuged. The precipitate was redissolved in little MeCN and ethyl acetate was added, stirred and centrifuged. Reversed phase column chromatography (Biotage SNAP C18, 60 g) MeCN/water gradient 5-40% resulted in a dark blue solid (25 mg, 62.5 %).

^{1}H NMR (200 MHz, D$_2$O) δ 8.32 (t, J = 13.0 Hz, 2H), 7.88 (dd, J = 6.9, 1.9 Hz, 4H), 7.34 (d, J = 8.1 Hz, 2H), 6.68 (t, J = 12.4 Hz, 1H), 6.35 (dd, J = 13.7, 3.4 Hz, 2H), 4.16 (p, J = 7.0 Hz, 4H), 3.78 – 3.41 (m, 8H), 3.41 – 3.00 (m, 4H), 2.22 (t, J = 7.2 Hz, 2H), 1.75 (s, 16H), 1.42 (d, J = 3.9 Hz, 14H). LC-MS (ESI) R_t= 4.80 min, m/z calcd ($C_{44}H_{61}N_4O_{11}S_2$) 886.1; found 909.4 [M+Na]$^+$, 887.3 [M+H]$^+$, 787.50 [M-boc]$^+$, 394.3 [M-Boc+2H]$^{2+}$.

Cy5-EG3-amine (31)

To Cy5-EG3-N-Boc **30** (28 mg, 0.032 mmol) 2 mL DCM and 2 mL TFA were added. The mixture was stirred for 2 hours at room temperature under argon. The solvent was removed under reduced pressure and co-evaporated three times with toluene. Ethyl acetate was added, stirred and centrifuged two times. Drying resulted in a dark blue solid **31** (32 mg, quant).

^{1}H NMR (200 MHz, CD$_3$OD) δ 8.44 – 8.18 (m, 2H), 7.97 – 7.80 (m, 4H), 7.45 – 7.28 (m, 2H), 6.67 (t, J = 12.4 Hz, 1H), 6.34 (dd, J = 13.7, 6.3 Hz, 2H), 4.28 – 4.00 (m, 4H), 3.77 – 3.54 (m, 6H), 3.55 – 3.38 (m, 4H), 3.11 (d, J = 5.5 Hz, 2H), 2.18 (t, J = 7.0 Hz, 2H), 1.75 (s, 16H), 1.39 (t, J = 7.0 Hz, 5H). LC-MS (ESI) R_t= 4.08 min, m/z calcd ($C_{39}H_{53}N_4O_9S_2$) 786.0; found 787.50 [M+H]$^+$, 394.3 [M+2H]$^{2+}$.

Cy5-EG3-TCO (4)

Cy5-EG3-amine **31** (32 mg, 0.041 mmol) was dissolved in DMF (1.0 mL), DiPEA (28.0 µL, 0.163 mmol) and **32** (13.1 mg, 0.049 mmol) were added. The solution was stirred over night at room temperature under argon. The solvent was removed under reduced pressure and co-evaporated three times with toluene. Ethyl acetate was added, stirred and centrifuged 2x. Reversed phase column chromatography (Biotage SNAP C18, 12 g) MecN/water gradient 5-34% resulted in a dark blue solid (25 mg, 65.5 %).

^{1}H NMR (399 MHz, CD$_3$OD) δ 8.32 (td, J = 13.1, 2.9 Hz, 2H), 7.98 – 7.81 (m, 4H), 7.34 (dd, J = 8.1, 3.2 Hz, 2H), 6.67 (t, J = 12.4 Hz, 1H), 6.34 (dd, J = 13.7, 7.0 Hz, 2H), 5.68 – 5.34 (m, 2H), 4.29 (s, 1H), 4.15 (dt, J = 24.8, 7.1 Hz, 4H),

3.58 (s, 4H), 3.50 (q, J = 5.8 Hz, 4H), 3.23 (t, J = 5.8 Hz, 4H), 2.21 (t, J = 7.3 Hz, 2H), 2.03 – 1.63 (m, 24H), 1.52 (dt, J = 48.7, 6.8 Hz, 4H), 1.37 (dd, J = 7.9, 5.7 Hz, 5H). LC-MS (ESI) R_t= 5.21 min, *m/z* calcd ($C_{48}H_{65}N_4O_{11}S_2$) 938.20; found 939.33 [M+H]$^+$, 961.42 [M+Na]$^+$, 470.08 [M+2H]$^{2+}$.

Sequence of EYFP

MVSKGEELFTGVVPILVELDGDVNGHKFSVSGEGEGDATYGKLTLKFICTTGKLPVPWPTLVTTFGYGLQCFARYPDHMKQHD
FFKSAMPEGYVQERTIFFKDDGNYKTRAEVKFEGDTLVNRIELKGIDFKEDGNILGHKLEYNYNSHNVYIMADKQKNGIKVNFKI
RHNIEDGSVQLADHYQQNTPIGDGPVLLPDNHYLSYQSALSKDPNEKRDHMVLLEFVTAAGITLGMDELYKKAAALELPETGG
HHHHHH

Expression of EYFP protein in *E. coli*. The pET29a plasmids were transformed in *E. coli* BL21(DE3) host strain (Novagen). The bacteria were cultured in 2 L LB medium containing 100 μg·mL^{-1} kanamycin at 37 °C in a 180 rpm shaking incubator until an OD$_{600}$ of ~0.7 was reached. Subsequently, protein expression was induced by adding isopropyl-β-D-thiogalactopyranoside (IPTG) to a final concentration of 0.5 mM. Cells were incubated for 7 hours at 25 °C and 180 rpm before being harvested by centrifugation (8000 g for 10 minutes). Bacterial cells were lysed by resuspending the pellet in Bugbuster Protein Extraction Reagent supplemented with benzonase (Novagen) and incubated for 1 hour at room temperature. The insoluble fraction was removed by centrifugation (40000 g for 30 minutes). The soluble fraction was further purified by using Ni affinity chromatography. Proteins were concentrated using an Amicon Ultra centrifugal filter device (MWCO: 10 kDa) (Millipore). The purity and correct mass were confirmed by SDS-PAGE electrophoresis and LC-ESI-MS. Finally, ~4 mg per liter culture for eYFP yield was obtained. Concentrations were determined using the Nanodrop ND-1000 spectrophotometer using the reported extinction coefficient ε_{514} 83400 M^{-1} cm^{-1}. [61]

Conjugation of TCO-NHS ester to EYFP. TCO-OEG$_4$-NHS ester was reacted with YFP in order to functionalize the protein with TCO-moieties via non-specific ligation with lysines. 1.72 μL (MW: 514.57 Da, 0.086 mg, 3 eq) TCO-OEG$_4$-NHS ester was added to 100 μL 558 μM of YFP (MW: 28952.6 Da) (1 eq) and allowed to react at 20 °C and 550 rpm in the dark for 2 hours. Afterwards, the mixture was purified using 500 μL 10,000 MWCO Amicon filters, by diluting the reaction mixture with up to 500 μL NaPi pH 7.4 buffer and spinning down at 13.4 k rpm for 5 minutes, repeated 5 times. The conjugated protein remained in the filter and was obtained by inverted spinning and analyzed using LC-ESI-MS to confirm 0-3 times conjugated protein on average.

HPLC-ESI-MS analysis. Purity and exact mass of the proteins were determined using a Waters Xevo G2 Quadrupole Time of Flight (Q-ToF) Liquid Chromatography – Mass Spectrometry equipped with an Agilent Polaris C18A reverse phase column (ID 2.0 mm, length 100 mm). Proteins were flowed (0.3 ml min^{-1}) over the column using a 15% to 75% water/MeCN gradient with 0.1 v/v% formic acid prior to analysis in positive mode in the mass spectrometer. Deconvolution of the m/z spectra was done using the MaxENT1 algorithm in the MassLynx software.
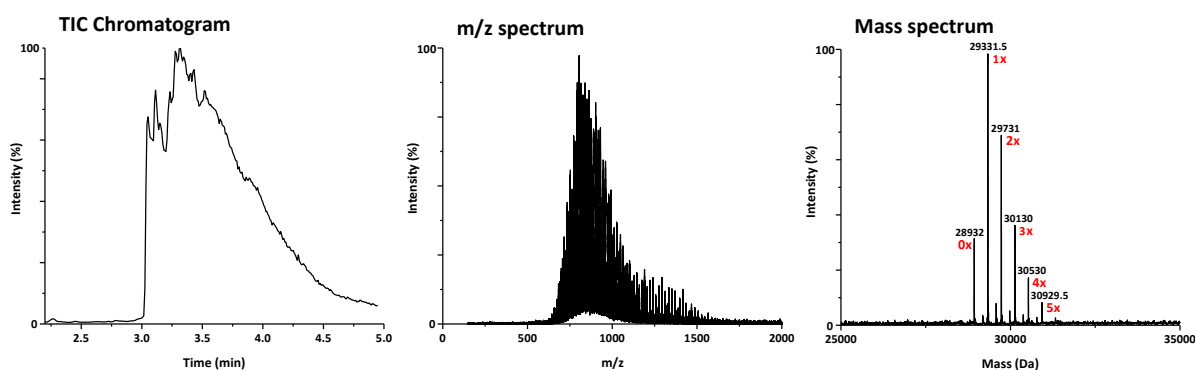
A

TCO-OEG₄-NHS ester	EYFP	TCO-OEG₄-EYFP
MW: 514.57 g·mol⁻¹	MW: 28,932 g·mol⁻¹	MW: 29,331.5
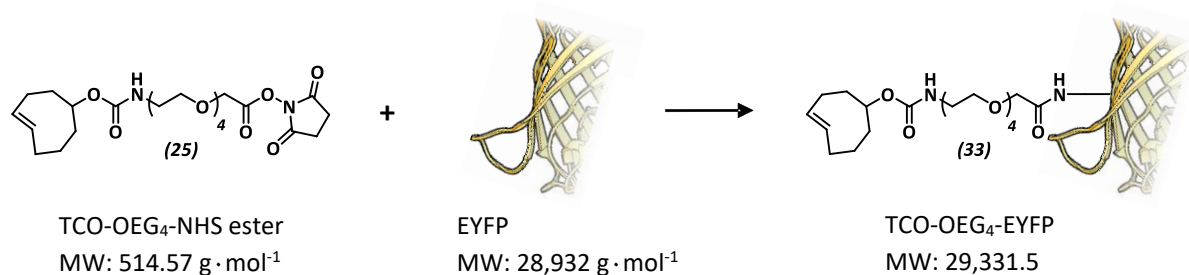
B

Figure 5.14. Protein labeling with TCO-moieties, A) Conjugation scheme of TCO-OEG₄-NHS ester (equatorial isomer) conjugation to peripheral Lysines of the eYFP and B) Q-ToF MS analysis of the conjugated protein, total ion count chromatogram, *m/z* spectrum as well as the deconvoluted mass spectrum are shown.

5.6 References

1. Lehn, J. M. Supramolecular polymer chemistry—scope and perspectives. *Polym. Int.* **51,** 825–839 (2002).
2. Whitesides, G. M. & Grzybowski, B. Self-assembly at all scales. *Science* **295,** 2418–2421 (2002).
3. Epstein, R. J. *Human Molecular Biology: An Introduction to the Molecular Basis of Health and Disease*. (Cambridge University Press, 2003).
4. Aida, T., Meijer, E. W. & Stupp, S. I. Functional supramolecular polymers. *Science* **335,** 813–817 (2012).
5. Folmer, B. J. B., Sijbesma, R. P., Versteegen, R. M., van der Rijt, J. a. J. & Meijer, E. W. Supramolecular Polymer Materials: Chain Extension of Telechelic Polymers Using a Reactive Hydrogen-Bonding Synthon. *Adv. Mater.* **12,** 874–878 (2000).
6. Bosman, A. W., Sijbesma, R. P. & Meijer, E. W. Supramolecular polymers at work. *Mater. Today* **7,** 34–39 (2004).
7. Rajangam, K. *et al.* Heparin binding nanostructures to promote growth of blood vessels. *Nano Lett.* **6,** 2086–2090 (2006).
8. Tysseling-Mattiace, V. M. *et al.* Self-assembling nanofibers inhibit glial scar formation and promote axon elongation after spinal cord injury. *J. Neurosci. Off. J. Soc. Neurosci.* **28,** 3814–3823 (2008).
9. Bae, Y., Fukushima, S., Harada, A. & Kataoka, K. Design of Environment-Sensitive Supramolecular Assemblies for Intracellular Drug Delivery: Polymeric Micelles that are Responsive to Intracellular pH Change. *Angew. Chem. Int. Ed.* **42,** 4640–4643 (2003).
10. Cordier, P., Tournilhac, F., Soulié-Ziakovic, C. & Leibler, L. Self-healing and thermoreversible rubber from supramolecular assembly. *Nature* **451,** 977–980 (2008).
11. Burnworth, M. *et al.* Optically healable supramolecular polymers. *Nature* **472,** 334–337 (2011).
12. Wei, Q. *et al.* Supramolecular Polymers as Surface Coatings: Rapid Fabrication of Healable Superhydrophobic and Slippery Surfaces. *Adv. Mater.* **26,** 7358–7364 (2014).
13. Hill, J. P. *et al.* Self-assembled hexa-peri-hexabenzocoronene graphitic nanotube. *Science* **304,** 1481–1483 (2004).

14. Lucas, L. N., Jong, J. J. D. de, Esch, J. H. van, Kellogg, R. M. & Feringa, B. L. Syntheses of Dithienylcyclopentene Optical Molecular Switches. *Eur. J. Org. Chem.* **2003,** 155–166 (2003).

15. Abbel, R. *et al.* White-Light Emitting Hydrogen-Bonded Supramolecular Copolymers Based on π-Conjugated Oligomers. *J. Am. Chem. Soc.* **131,** 833–843 (2009).

16. Wisse, E., Govaert, L. E., Meijer, H. E. H. & Meijer, E. W. Unusual Tuning of Mechanical Properties of Thermoplastic Elastomers Using Supramolecular Fillers. *Macromolecules* **39,** 7425–7432 (2006).

17. Sijbesma, R. P. *et al.* Reversible polymers formed from self-complementary monomers using quadruple hydrogen bonding. *Science* **278,** 1601–1604 (1997).

18. Beijer, F. H., Sijbesma, R. P., Kooijman, H., Spek, A. L. & Meijer, E. W. Strong Dimerization of Ureidopyrimidones via Quadruple Hydrogen Bonding. *J. Am. Chem. Soc.* **120,** 6761–6769 (1998).

19. Kieltyka, R. E. *et al.* Mesoscale Modulation of Supramolecular Ureidopyrimidinone-Based Poly(ethylene glycol) Transient Networks in Water. *J. Am. Chem. Soc.* **135,** 11159–11164 (2013).

20. Dankers, P. Y. W., Harmsen, M. C., Brouwer, L. A., Van Luyn, M. J. A. & Meijer, E. W. A modular and supramolecular approach to bioactive scaffolds for tissue engineering. *Nat. Mater.* **4,** 568–574 (2005).

21. Wisse, E. *et al.* Multicomponent supramolecular thermoplastic elastomer with peptide-modified nanofibers. *J. Polym. Sci. Part Polym. Chem.* **49,** 1764–1771 (2011).

22. van Almen, G. C. *et al.* Development of Non-Cell Adhesive Vascular Grafts Using Supramolecular Building Blocks. *Macromol. Biosci.* **16,** 350-362 (2016).

23. Mollet, B. B. *et al.* A modular approach to easily processable supramolecular bilayered scaffolds with tailorable properties. *J. Mater. Chem. B* **2,** 2483–2493 (2014).

24. Muylaert, D. E. P. *et al.* Early in-situ cellularization of a supramolecular vascular graft is modified by synthetic stromal cell-derived factor-1α derived peptides. *Biomaterials* **76,** 187–195 (2016).

25. Tolstyka, Z. P. *et al.* Chemoselective Immobilization of Proteins by Microcontact Printing and Bioorthogonal Click Reactions. *Chembiochem.* **14,** 2464–2471 (2013).

26. Zheng, J., Liu, K., Reneker, D. H. & Becker, M. L. Post-Assembly Derivatization of Electrospun Nanofibers via Strain-Promoted Azide Alkyne Cycloaddition. *J. Am. Chem. Soc.* **134,** 17274–17277 (2012).

27. Imbesi, P. M., Fidge, C., Raymond, J. E., Cauët, S. I. & Wooley, K. L. Model Diels–Alder Studies for the Creation of Amphiphilic Cross-Linked Networks as Healable, Antibiofouling Coatings. *ACS Macro Lett.* **1,** 473–477 (2012).

28. Gevrek, T. N., Bilgic, T., Klok, H.-A. & Sanyal, A. Maleimide-Functionalized Thiol Reactive Copolymer Brushes: Fabrication and Post-Polymerization Modification. *Macromolecules* **47,** 7842–7851 (2014).

29. Hansell, C. F. *et al.* Additive-Free Clicking for Polymer Functionalization and Coupling by Tetrazine–Norbornene Chemistry. *J. Am. Chem. Soc.* **133,** 13828–13831 (2011).

30. Williams, R. J., Barker, I. A., O'Reilly, R. K. & Dove, A. P. Orthogonal Modification of Norbornene-Functional Degradable Polymers. *ACS Macro Lett.* **1,** 1285–1290 (2012).

31. Liu, S. *et al.* Meter-Long Multiblock Copolymer Microfibers Via Interfacial Bioorthogonal Polymerization. *Adv. Mater.* **27,** 2783–2790 (2015).

32. Devaraj, N. K. & Weissleder, R. Biomedical Applications of Tetrazine Cycloadditions. *Acc. Chem. Res.* **44,** 816–827 (2011).

33. Devaraj, N. K., Weissleder, R. & Hilderbrand, S. A. Tetrazine-Based Cycloadditions: Application to Pretargeted Live Cell Imaging. *Bioconjug. Chem.* **19,** 2297–2299 (2008).

34. Lin, F. *et al.* Postelectrospinning 'Click' Modification of Degradable Amino Acid-Based Poly(ester urea) Nanofibers. *Macromolecules* **46,** 9515–9525 (2013).

35. Zheng, J. *et al.* Post-Electrospinning 'Triclick' Functionalization of Degradable Polymer Nanofibers. *ACS Macro Lett.* **4,** 207–213 (2015).

36. Mahmoud, Z. N., Gunnoo, S. B., Thomson, A. R., Fletcher, J. M. & Woolfson, D. N. Bioorthogonal dual functionalization of self-assembling peptide fibers. *Biomaterials* **32,** 3712–3720 (2011).

37. Huisgen, R. Kinetics and Mechanism of 1,3-Dipolar Cycloadditions. *Angew. Chem. Int. Ed.* **2,** 633–645 (1963).

38. Huisgen, R. 1,3-Dipolar Cycloadditions. Past and Future. *Angew. Chem. Int. Ed.* **2,** 565–598 (1963).

39. Kolb, H. C., Finn, M. G. & Sharpless, K. B. Click Chemistry: Diverse Chemical Function from a Few Good Reactions. *Angew. Chem. Int. Ed.* **40,** 2004–2021 (2001).

40. Blackman, M. L., Royzen, M. & Fox, J. M. Tetrazine Ligation: Fast Bioconjugation Based on Inverse-Electron-Demand Diels–Alder Reactivity. *J. Am. Chem. Soc.* **130,** 13518–13519 (2008).

41. Lang, K. *et al.* Genetic Encoding of Bicyclononynes and trans-Cyclooctenes for Site-Specific Protein Labeling in Vitro and in Live Mammalian Cells via Rapid Fluorogenic Diels–Alder Reactions. *J. Am. Chem. Soc.* **134,** 10317–10320 (2012).

42. Selvaraj, R. & Fox, J. M. trans-Cyclooctene — a stable, voracious dienophile for bioorthogonal labeling. *Curr. Opin. Chem. Biol.* **17,** 753–760 (2013).

43. Darko, A. *et al.* Conformationally strained trans-cyclooctene with improved stability and excellent reactivity in tetrazine ligation. *Chem. Sci.* **5,** 3770–3776 (2014).

44. Rossin, R., van Duijnhoven, S. M. J., Läppchen, T., van den Bosch, S. M. & Robillard, M. S. Trans-Cyclooctene Tag with Improved Properties for Tumor Pretargeting with the Diels–Alder Reaction. *Mol. Pharm.* **11,** 3090–3096 (2014).

45. Blackman, M. L., Royzen, M. & Fox, J. M. Tetrazine Ligation: Fast Bioconjugation Based on Inverse-Electron-Demand Diels–Alder Reactivity. *J. Am. Chem. Soc.* **130,** 13518–13519 (2008).

46. Barker, I. A. *et al.* Tetrazine-Norbornene Click Reactions to Functionalize Degradable Polymers Derived from Lactide. *Macromol. Rapid Commun.* **32,** 1362–1366 (2011).

47. Thalhammer, F., Wallfahrer, U. & Sauer, J. Reaktivität einfacher offenkettiger und cyclischer dienophile bei Diels-Alder-reaktionen mit inversem elektronenbedarf. *Tetrahedron Lett.* **31,** 6851–6854 (1990).

48. Taylor, M. T., Blackman, M. L., Dmitrenko, O. & Fox, J. M. Design and Synthesis of Highly Reactive Dienophiles for the Tetrazine–trans-Cyclooctene Ligation. *J. Am. Chem. Soc.* **133,** 9646–9649 (2011).

49. Yang, F. *et al.* Nanodomain analysis with cluster-SIMS: application to the characterization of macromolecular brush architecture. *Surf. Interface Anal.* **47,** 1051–1055 (2015).

50. Taylor, M. *et al.* 3D chemical characterization of frozen hydrated hydrogels using ToF-SIMS with argon cluster sputter depth profiling. *Biointerphases* **11,** 02A301 (2016).

51. Bailey, J. *et al.* 3D ToF-SIMS Imaging of Polymer Multilayer Films Using Argon Cluster Sputter Depth Profiling. *ACS Appl. Mater. Interfaces* **7,** 2654–2659 (2015).

52. Claus, T. K. *et al.* Simultaneous Dual Encoding of Three-Dimensional Structures by Light-Induced Modular Ligation. *Angew. Chem. Int. Ed.* **55,** 3817–3822 (2016).

53. Kautz, H., van Beek, D. J. M., Sijbesma, R. P. & Meijer, E. W. Cooperative End-to-End and Lateral Hydrogen-Bonding Motifs in Supramolecular Thermoplastic Elastomers. *Macromolecules* **39,** 4265–4267 (2006).

54. Appel, W. P. J., Portale, G., Wisse, E., Dankers, P. Y. W. & Meijer, E. W. Aggregation of Ureido-Pyrimidinone Supramolecular Thermoplastic Elastomers into Nanofibers: A Kinetic Analysis. *Macromolecules* **44,** 6776–6784 (2011).

55. Socrates, G. *Infrared and Raman Characteristic Group Frequencies: Tables and Charts*. (John Wiley & Sons, 2004).

56. Chen, W., Wang, D., Dai, C., Hamelberg, D. & Wang, B. Clicking 1,2,4,5-tetrazine and cyclooctynes with tunable reaction rates. *Chem. Commun.* **48,** 1736–1738 (2012).

57. Goor, O. J. G. M. *et al.* Efficient Functionalization of Additives at Supramolecular Material Surfaces. *Adv. Mater.* **29,** 1604652 (2017).

58. de Feijter, I. *et al.* Solid-Phase-Based Synthesis of Ureidopyrimidinone–Peptide Conjugates- for Supramolecular Biomaterials. *Synlett* **26,** 2707–2713 (2015).

59. Chipon, B. *et al.* Synthesis and post-synthetic derivatization of a cyanine-based amino acid. Application to the preparation of a novel water-soluble NIR dye. *Tetrahedron Lett.* **47,** 8279–8284 (2006).

60. Favre, A., Grugier, J., Brans, A., Joris, B. & Marchand-Brynaert, J. 6-Aminopenicillanic acid (6-APA) derivatives equipped with anchoring arms. *Tetrahedron* **68,** 10818–10826 (2012).

61. Newman, R. H., Fosbrink, M. D. & Zhang, J. Genetically Encodable Fluorescent Biosensors for Tracking Signaling Dynamics in Living Cells. *Chem. Rev.* **111,** 3614–3666 (2011).

Exploring the material surface *via* supramolecular additives: introduction of anti-fouling properties and the influence of additive design

Abstract

Protein repellent coatings have been extensively studied to introduce anti-fouling behavior at material surfaces. A covalent anti-fouling coating at the surface of supramolecular UPy-based materials is introduced *via* post-modification of reactive UPy-functionalized tetrazine additives incorporated into the supramolecular polymer material. After material formulation, bicyclononyne (BCN) functionalized poly(ethylene glycol) (PEG) was reacted, and thereby covalently attached at the surface *via* a highly selective electron-demand Diels-Alder cycloaddition between tetrazine and BCN. The anti-fouling properties of three different BCN-PEG polymers, monofunctional-PEG-BCN, bifunctional-PEG-BCN and star-PEG-BCN, respectively, were systematically studied. The monofunctional-PEG-BCN showed minor reduction in protein adsorption and cell adhesion, whereas the bifunctional-PEG-BCN and the star-PEG-BCN polymer coating demonstrated complete anti-fouling performance, both towards protein adhesion and cell adhesion. The bioorthogonal ligation strategy was performed in culture medium in the presence of cells and showed similar behavior for the three anti-fouling coatings, which indicates this strategy can be applied for post-modification reactions in complex environment. Additionally, the influence of the supramolecular additive design on the surface distribution and reactivity was investigated.

6.1 Introduction

Surface interactions play an important role upon implantation of a biomaterial, as the surface of the material is the first to interact with the *in vivo* environment. [1] Therefore, control on surface composition and activity are important factors in the design of biomaterials. Surface modifications to introduce surface functionality can be achieved following a broad scope of different strategies, i.e. physical adsorption, covalent modification and the incorporation of biomimetic cues. [2] However, biofouling of the materials surface is of great concern due to its impact on the availability of activity and functionality as a result of nonspecific protein adsorption. [3]

Upon implantation of a biomaterial, a tissue response is initiated with the non-specific adsorption of proteins at the materials surface, [4] which could ultimately lead to biomaterial failure. [5] High mobility proteins, such as albumin, are the first to adsorb. Subsequently, displacement by less abundant proteins with higher affinity occurs, starting with globulin and fibrinogen, which are then later replaced by high molecular weight kininogen. This process is called the Vroman effect. [6]

The inhibition of protein adsorption is therefore critical in order to prevent biomaterial failure. [7,8] To this end, hydrophilic and zwitterionic polymers are widely applied in the design of anti-fouling materials, to allow the formation of an hydration layer at the surface which in turn prevents adsorption onto the surface. [9] Surface functionalization strategies based on the use of poly(ethylene glycol) (PEG) polymers are extensively studied to impart adhesion resistance. [10–14] Among these are self-assembling monolayers (SAMs) [5,12,15], polymer brushes based on PEG and zwitterionic moieties immobilized on different substrates [16–20] and the covalent introduction of PEG polymers based on click chemistry. [21,22] Moreover, PEG polymers can be anchored at different materials and substrates *via* the introduction of triblock copolymers, [23–25] in a supramolecular fashion by the post-modification of polymeric membranes based on cyclodextrin host-guest chemistry [26] or introduced at the surface of electrospun polyurethane (PU) fibers. [27] Additionally, multi-armed PEG polymers can be introduced at substrate surfaces to yield anti-fouling behavior. [28,29] Another elegant approach is the anchoring of PEG polymers at surfaces *via* dopamine or catechol moieties. [30,31]

In our group, supramolecular biomaterials based on the ureido-pyrimidinone (UPy) motif are developed that yield supramolecular thermoplastic elastomer materials upon pre-polymer end-functionalization. [32,33] The modularity of this approach, allows for the incorporation of bioactive functionality into these materials, giving rise to a platform of material functionalization. [34,35] The incorporation of anti-fouling UPy-based polymers and additives have previously been reported in the development of functional biomaterials. [36,37] Moreover, anti-fouling biomaterials could be reactivated upon the incorporation of only small amounts of UPy-functionalized peptides. [38] Nevertheless, this anti-fouling behavior showed only short-term functionality both in *in vitro* and *in* vivo studies and displayed minor protein adsorption prevention. [37] The strategy based on covalent post-modification of the supramolecular thermoplastic elastomers surface *via* the modular incorporation of a reactive additive was more recently proposed, as discussed in chapter 5. This approach allows for

solely surface modification and yet provides a method to decouple the material processing conditions and the post-functionalization. [39]

The introduction of anti-fouling functionality at the surface of supramolecular materials (Figure 6.1 A) *via* the selective modification of a reactive UPy-modified tetrazine (UPy-Tz) additive (Figure 6.1 C, **2**) is discussed in this chapter. UPy-Tz is incorporated in telechelically UPy-modified polycaprolactone (PCLdiUPy) (Figure 6.1 B, **1**), which provides a handle for selective surface post-modification *via* an inverse electron demand Diels-Alder cycloaddition, as was shown in chapter 5. [40,41] Three different poly(ethylene glycol) (PEG) polymers modified

A

B PCLdiUPy

(1)

C UPy-Tz

(2)
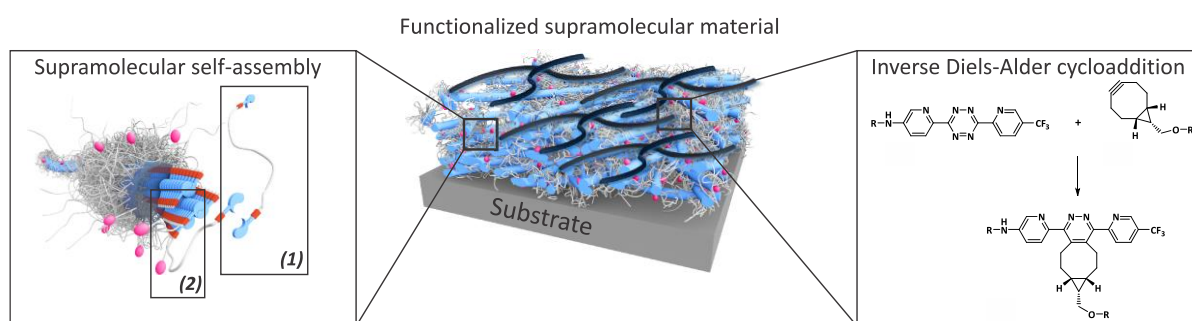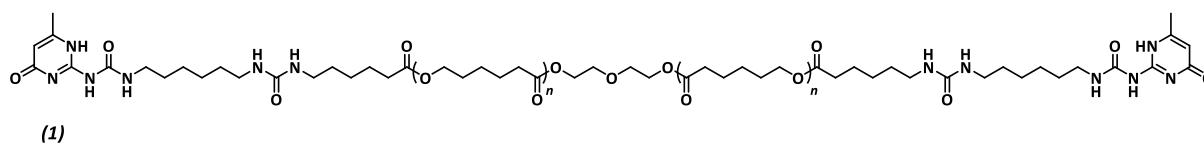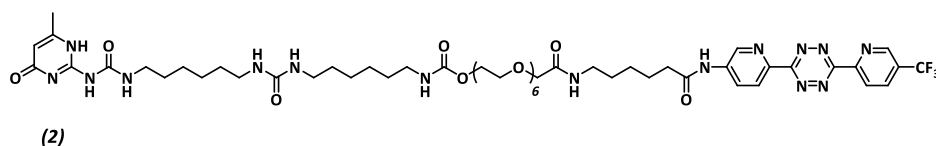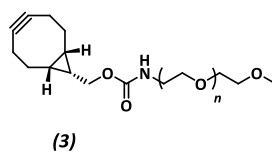
D Monofunctional-PEG-BCN   **E   Bifunctional-PEG-BCN**   **F   Star-PEG-BCN**

(3)   *(4)*

(5)
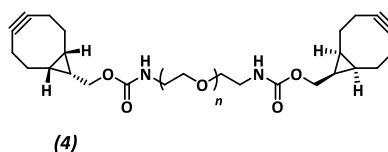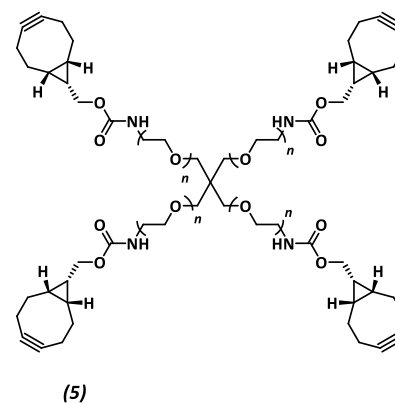
Figure 6.1. Functionalization of supramolecular materials with an anti-fouling coating, A) Schematic representation of the functionalization, with on the left the supramolecular self-assembly of the UPy-functionalized polymer (PCLdiUPy, **1**) with the UPy-additive (UPy-Tz, **2**) and the highly selective inverse Diels-Alder cycloaddition (iEDDA) on the right. Chemical structures of the B) PCL$_{2k}$diUPy (**1**), C) UPy-Tz additive (**2**), D) Monofunctional-PEG$_{2k}$-BCN, E) Bifunctional-PEG$_{5k}$-BCN and F) Star-PEG$_{10k}$-BCN are shown.

with bicyclononyne (BCN) moieties, monofunctional-PEG$_{2k}$-BCN (Figure 6.1 D, **3**), bifunctional-PEG$_{5k}$-BCN (Figure 6.1 E, **4**) and star-PEG$_{10k}$-BCN (Figure 6.1 F, **5**), respectively, were synthesized and introduced to facilitate the anti-fouling function. It is hypothesized that the bifunctional-PEG-BCN and the star-PEG-BCN polymer coatings display excellent anti-fouling properties as a result of their ability to form cyclic loops at the material interface. [42] The monofunctional-PEG-BCN has one anchor point at the supramolecular material surface, whereas the bifunctional-PEG-BCN is in theory able to anchor both ends of the polymer onto the surface. The star-PEG-BCN not only contains four anchor points, the molecular weight of the PEG in this polymer is higher as well, while at the same time the BCN:PEG ratio is kept constant for all three conjugates. The tunability as well as the functionality of the anti-fouling coating were assessed both by protein adsorption examination by quartz crystal microbalance with dissipation monitoring (QCM-D) as well as cell attachment studies. Moreover, the bioorthogonal ligation strategy was performed in complex medium, in the presence of cells.

6.1.2 Material characterization

The surface morphology of the spincoated films of PCLdiUPy, PCLdiUPy with UPy-Tz (10 mol%) before and after functionalization with star-PEG-BCN (**5**) were assessed using AFM (Figure 6.2 A-C). A nanofiber morphology is observed, indicating the UPy-Tz is incorporated into the PCLdiUPy nanofibers (Figure 6.2 A,B). After reaction with the star-PEG-BCN (Figure 6.2 C) the fibrous structures are still present, however in a less defined fashion.

The surface composition of the spincoated materials both before and after modification with an anti-fouling PEG-BCN polymer was investigated using XPS (Figure 6.2 D). Upon the introduction of the monofunctional-PEG-BCN (**2**) and bifunctional-PEG-BCN (**4**) polymers, the carbon content (73.5 atom% and 72.6 atom%, respectively) decreases compared to the PCLdiUPy (74.4 atom%) and the PCLdiUPy with UPy-Tz (74.0 atom%) surfaces. Concomitantly, an increase in oxygen content is observed after modification of the surface with the hydrophilic PEG polymers and this increase is in line with a higher molecular weight PEG and more BCN functionalities (20.5 atom% for monofunctional-PEG-BCN, 20.8 atom% for bifunctional-PEG-BCN and 22.1 atom% for star-PEG BCN, respectively). The oxygen content of the PCLdiUPy surface with UPy-Tz decreases compared to the bare PCLdiUPy surface (20.0 atom% compared to 20.1 atom%), which is explained by an increase in nitrogen and fluorine content in the tetrazine moiety. This result indicates that UPy-Tz is enhanced at the surface of the material. [39] A decrease in nitrogen content is observed after modification of the surface with bifunctional-PEG-BCN (**4**) and star-PEG-BCN (**5**) (4.8 atom% and 5.1 atom%, respectively) compared to the bare PCLdiUPy surface (5.5 atom%). An increase of fluorine to 0.2 atom% was detected after surface modification with the hydrophilic PEG polymers, which could be an effect of the incubation in aqueous medium that results from the rearrangement UPy-Tz at the supramolecular material surface. [39]

The wettability of the modified surfaces was investigated by static water contact angle measurements. No major changes were observed for the bare PCLdiUPy surface and the PCLdiUPy surfaces after incubation with the monofunctional-PEG-BCN (**3**), bifunctional-PEG-

BCN (**4**) and the star-PEG-BCN (**5**) polymers (68.0°, 67.7°, 69.7° and 66.5°, respectively). In contrast, the PCLdiUPy with 10 mol% UPy-Tz prior to and after modification with the monofunctional-PEG-BCN (**3**), bifunctional-PEG-BCN (**4**) and the star-PEG-BCN (**5**) polymers show a clear drop in contact angle values (70.1°, 63.1°, 58.2° and 48.6°, respectively) (Figure 6.2 E). These results indicate that the PEG-BCN polymers show minor non-specific interactions with the PCLdiUPy surfaces, whereas an increased hydrophilicity of the surfaces is observed after modification of the PCLdiUPy with UPy-Tz surfaces. Interestingly, the hydrophilicity of the surfaces increases by increasing the molecular weight of the PEG polymer, accounting for tunable surface properties depending on the polymer architecture.

In conclusion, the supramolecular surfaces show a fibrous morphology, and the UPy-Tz was successfully incorporated into the supramolecular nanofibers, thereby not changing the fiber morphology. Upon introduction of the PEG-BCN polymers, differences in the chemical composition of the surfaces were observed, indicative for effective surface modification. On a macroscopic scale, an increase in the hydrophilicity of the surfaces was measured after introduction of the PEG-BCN polymers at the PCLdiUPy with 10 mol% UPy-Tz surfaces.
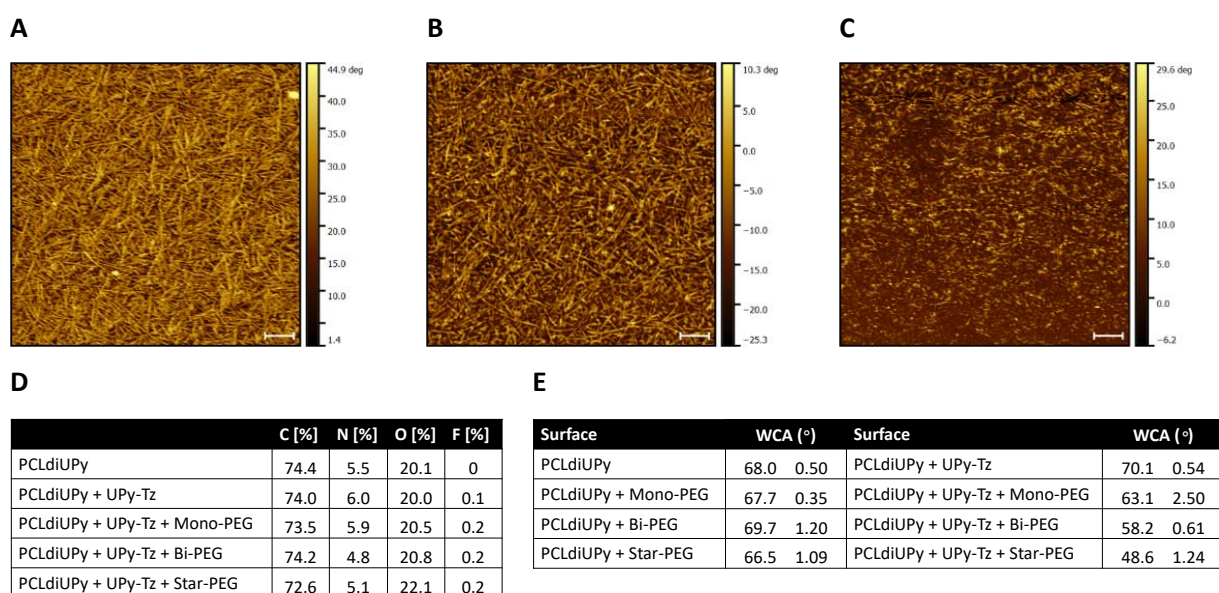
A

B

C

D

	C [%]	N [%]	O [%]	F [%]
PCLdiUPy	74.4	5.5	20.1	0
PCLdiUPy + UPy-Tz	74.0	6.0	20.0	0.1
PCLdiUPy + UPy-Tz + Mono-PEG	73.5	5.9	20.5	0.2
PCLdiUPy + UPy-Tz + Bi-PEG	74.2	4.8	20.8	0.2
PCLdiUPy + UPy-Tz + Star-PEG	72.6	5.1	22.1	0.2

E

Surface	WCA (°)		Surface	WCA (°)	
PCLdiUPy	68.0	0.50	PCLdiUPy + UPy-Tz	70.1	0.54
PCLdiUPy + Mono-PEG	67.7	0.35	PCLdiUPy + UPy-Tz + Mono-PEG	63.1	2.50
PCLdiUPy + Bi-PEG	69.7	1.20	PCLdiUPy + UPy-Tz + Bi-PEG	58.2	0.61
PCLdiUPy + Star-PEG	66.5	1.09	PCLdiUPy + UPy-Tz + Star-PEG	48.6	1.24

Figure 6.2. Surface characterization of the different material films with AFM, XPS and water contact angle. AFM phase micrographs of PCLdiUPy (A), PCLdiUPy with 10 mol% UPy-Tz (B) and after star-PEG-BCN functionalization (C), D) XPS compositional table of the different surfaces and E) Water contact angles of the respective surfaces. 5 Measurements were performed per surface and standard deviations are plotted.

6.1.3   Protein adsorption measurements

Next, the functionality of the modified materials was investigated. The intrinsic fouling properties of our supramolecular materials modified with the PEG-BCN polymers, were examined using QCM-D, by administering the first three proteins of the Vroman series (bovine serum albumin (BSA, 30 mg·mL^{-1}), γ-globulin (10 mg·mL^{-1}) and fibrinogen (3 mg·mL^{-1})).

First, the fouling properties towards BSA adsorption of pristine supramolecular PCLdiUPy and the PCLdiUPy with 10 mol% UPy-Tz surfaces were studied (Figure 6.3). After equilibration,

the BSA is flowed for 30 minutes and subsequently the surfaces are rinsed to remove all the non-adsorbed BSA. The PCLdiUPy with UPy-Tz incorporated shows a decrease in BSA adsorption compared to the PCLdiUPy surface, which is attributed to the presence of the UPy-Tz at the material surface that is composed of a polar tetrazine moiety and a hydrophilic oligo(ethylene glycol) spacer, which might give rise to a slightly more hydrophilic supramolecular surface. Moreover, in order to optimize the extent of anti-fouling behavior upon BSA administration, various star-PEG-BCN (**5**) concentrations were conjugated at the surface of PCLdiUPy with UPy-Tz (Figure 6.3). These results show tunability of the anti-fouling behavior and modulation based on the star-PEG-BCN concentration that was applied. The 0.5 mg·mL^{-1} star-PEG-BCN concentration was chosen to continue experiments with.
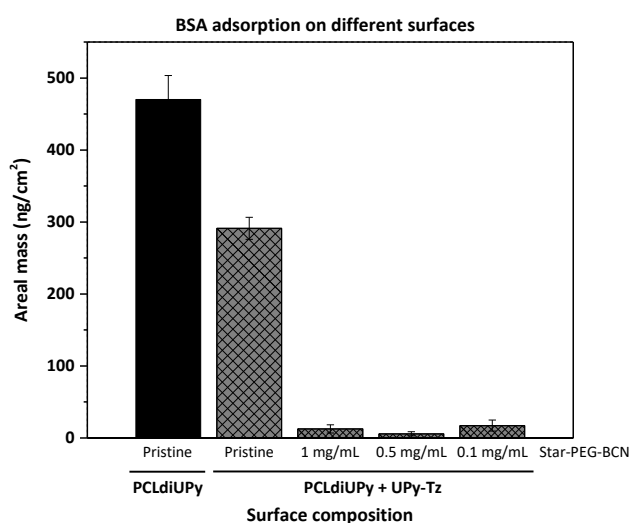

Figure 6.3. Overview of the modelled mass adsorption of BSA (30 mg·mL^{-1}) as determined by QCM-D using a Voigt-Voinova viscoelastic model on the different surfaces, pristine PCLdiUPy and PCLdiUPy with 10 mol% UPy-Tz. Different star-PEG-BCN (**5**) concentrations (1 mg·mL^{1}, 0.5 mg·mL^{-1} and 0.1 mg·mL^{-1} were immobilized on the PCLdiUPy with 10 mol% UPy-Tz surfaces to tune surface properties. Adsorption is represented as mean ± SD (n ≥ 4).

QCM-D measurements were performed to quantify the amount of proteins adsorbed onto the supramolecular surfaces under physiologically relevant conditions. The Vroman series was applied on the different surfaces, PCLdiUPy and PCLdiUPy with 10 mol% UPy-Tz, that were modified with either monofunctional-PEG-BCN (**3**), bifunctional-PEG-BCN (**4**) or star-PEG-BCN (**5**). Both the change in frequency (Δf) and dissipation (ΔD) were monitored over time. After equilibration of the signal, the protein mixture was applied and after 30 minutes the surfaces were rinsed to remove all non-adsorbed proteins. It was hypothesized that the PCLdiUPy surfaces show the largest Δf, indicative for a higher mass adsorption. The increase in molecular mass of the PEG polymers and the additional BCN moieties that are available for surface reaction of the monofunctional-PEG-BCN, bifunctional-PEG-BCN and star-PEG-BCN, respectively, are envisioned to increase the anti-fouling properties of the surface alongside. Upon monofunctional-PEG-BCN modification, the remaining frequency and dissipation shifts

A

B

C

D
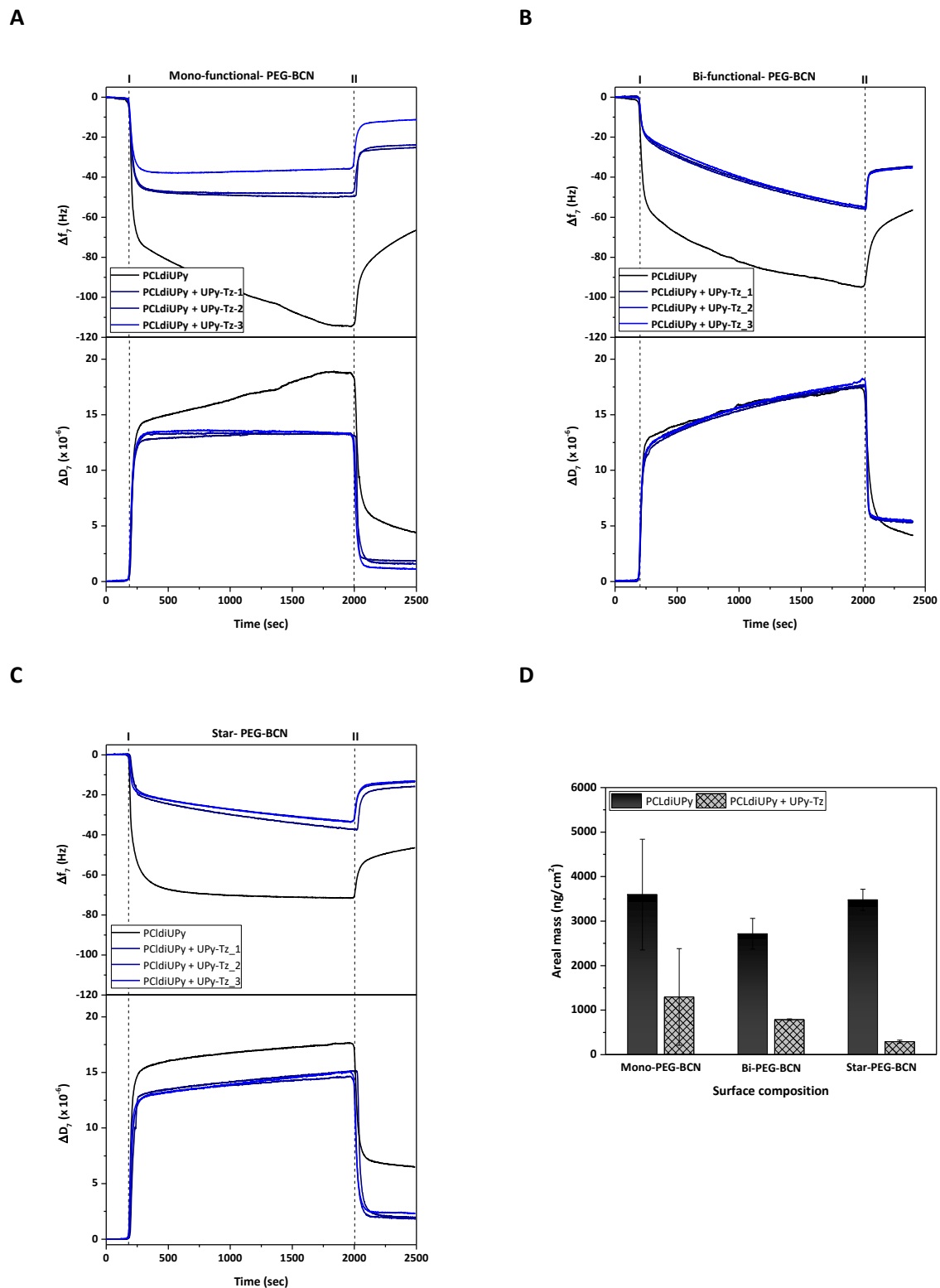
Figure 6.4. Quartz crystal microbalance with dissipation monitoring (QCM-D) results after Vroman series adsorption (30 mg·mL^{-1} BSA, 10 mg·mL^{-1} γ-Globulin and 3 mg·mL^{-1} Fibrinogen) onto PCLdiUPy or PCLdiUPy with 10 mol% UPy-Tz surfaces, at I the protein solution is administered and at II the surfaces are exposed to PBS, A) Frequency and Dissipation response at surfaces modified with 0.5 mg·mL^{-1} monofunctional-PEG-BCN (**3**), B) Frequency and Dissipation response at surfaces modified with 0.5 mg·mL^{-1} bifunctional-PEG-BCN (**4**), C) Frequency and Dissipation response at surfaces modified with 0.5 mg·mL^{-1} star-PEG-BCN (**5**) and D) Corresponding graph that plots the mass adsorption (ng·cm^{-2}) on the modified surfaces. All the data represented in the graphs results from visco-elastic modeling using a Voigt-Voinova model. Averages of n =3 measurements are plotted with the corresponding standard deviations.

for the PCLdiUPy surface are larger than for the PCLdiUPy with UPy-Tz surfaces (-65 Hz, 5·10^{-6} and -30 Hz and 2·10^{-6}, respectively), which indicates a reduction in mass adsorption at the surfaces that were covalently modified with monofunctional-PEG-BCN (Figure 6.4 A). For the bifunctional-PEG-BCN a similar trend is observed for the frequency and dissipation values for the PCLdiUPy and PCLdiUPy with UPy-Tz surfaces (-55 Hz, 4·10^{-6} and -35 Hz and 5·10^{-6}, respectively) (Figure 6.4 B). The dissipation shifts at the modified surfaces are higher compared to the monofunctional-PEG-BCN functionalized surfaces. This might be explained by a different packing of the PEG-BCN polymer coating at the surfaces. The higher dissipation values at the bifunctional-PEG-BCN surfaces indicate a more visco-elastic layer is formed. For the star-PEG-BCN functionalization (Figure 6.4 C), both the frequency and dissipation shifts of the PCLdiUPy surfaces are larger than the PCLdiUPy with UPy-Tz surfaces (-45 Hz, 7·10^{-6} and -15 Hz and 2·10^{-6}, respectively), which indicates that the star-PEG-BCN coating successfully decreases protein adsorption. Since the dissipation values for all the different experiments are >5-10% of the Δf, a Voigt-Voinova visco-elastic model was applied to analyze the datasets. A summary of all the results shows the areal mass adsorption (ng·cm^{-2}) for the different surfaces (Figure 6.4 D). No significant differences were observed for the PCLdiUPy surfaces that were incubated with the different PEG-BCN polymers. Upon the incorporation of 10 mol% UPy-Tz, a significant reduction in protein adsorption can be appreciated. In addition, the protein adsorption gradually decreases in the series monofunctional-PEG-BCN (**3**), bifunctional-PEG-BCN (**4**) and star-PEG-BCN (**5**) polymers, respectively.

Mass adsorption on the PCLdiUPy with UPy-Tz surfaces modified with star-PEG-BCN for the individual proteins as well as the mixture is provided, which clearly shows the excellent anti-fouling properties of the modified surfaces for the individual proteins as well as the mixture of the Vroman series (Figure 6.5).
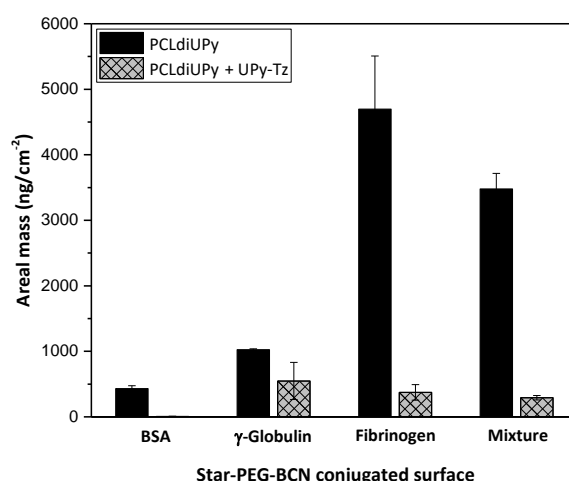
Figure 6.5. Overview of the modelled mass adsorption as determined by QCM-D using a Voigt-Voinova viscoelastic model. BSA (30 mg·mL^{-1}), γ-globulin (10 mg·mL^{-1}), fibrinogen (3 mg·mL^{-1}) and the corresponding protein mixture (Vroman series) on both PCLdiUPy and PCLdiUPy with 10 mol% UPy-Tz spin coated supramolecular surfaces conjugated with star-PEG BCN. Adsorption is represented as mean ± SD (n ≥ 2).

In conclusion, all three different PEG-BCN coatings were able to reduce protein adsorption at the material surface, however star-PEG-BCN significantly outperforms the monofunctional-PEG-BCN and bifunctional-PEG-BCN polymer in its ability to prevent protein adsorption.

6.1.4 Cell adhesion studies

The ability to prevent cell adhesion was studied on the modified supramolecular biomaterials. A strong correlation exists between protein adsorption with both adhesion and spreading of cells. Cells recognize protein structures at the biomaterial surface and along with the surface properties of the material, the initial cell behavior on the biomaterial surface is affected.[43] Cells bind to ECM components adsorbed at the material surface through integrin receptors, which upon clustering form focal adhesions that represent a structural link between the cytoskeleton and the biomaterial surface. [44] The cell adhesion and spreading of human kidney (HK-2) cells was studied on the different supramolecular surfaces prior to and after modification with the PEG-BCN hydrophilic polymers, 24 h after seeding (Figure 6.6). Moreover, the adhesion of the cells on the pristine surfaces (PCLdiUPy and PCLdiUPy with 10 mol% UPy-Tz) clearly shows the vinculin-rich focal adhesions after 72h of culture, indicating the cells adhered on these biomaterial surfaces (Figure 6.7). The PCLdiUPy and PCLdiUPy with UPy-Tz surfaces show cell attachment and spreading. The incubation of the PCLdiUPy surfaces with the monofunctional-PEG-BCN and bifunctional-PEG-BCN does not have any influence on the cell adhesion and morphology, whereas the incubation with star-PEG-BCN shows a reduction in the amount of cells adhered at the surface. The PCLdiUPy with UPy-Tz surfaces that were modified with monofunctional-PEG-BCN show only a minor reduction in cell adhesion and spreading, indicating that the monofunctional-PEG-BCN is not able to

Figure 6.6. Fluorescence microscopy graphs of HK-2 cells on spincoated surfaces after 24 hours of culture. Upper row represents images of PCLdiUPy (A) the pristine material or incubated with either monofunctional-PEG-BCN, bifunctional-PEG-BCN or star-PEG-BCN (from left to right). Lower row represents Images of PCLdiUPy with 10 mol% UPy-Tz incorporated (B) the pristine material or incubated with either monofunctional-PEG-BCN, bifunctional-PEG-BCN or star-PEG-BCN (from left to right). The actin skeleton is stained with Phalloidin (green), the nuclei are stained with DAPI (blue). Scale bars represent 100 µm.

completely cover the surface and thereby prevent cell attachment. In contrast, the modification of the PCLdiUPy with UPy-Tz surfaces with bifunctional-PEG-BCN and star-PEG-BCN show a significant reduction in the amount of cells present at the surface. Additionally, the cells adapt a round morphology, indicating they were not able to adhere or spread on these surfaces. Both the bifunctional-PEG-BCN and the star-PEG-BCN were able to effectively create a cell-repellent material surface.

Figure 6.7. Fluorescence microscopy graphs of HK-2 cells on spincoated surfaces after 72 hours of culture on A) PCLdiUPy and B) PCLdiUPy with 10 mol% UPy-Tz. The actin skeleton is stained with Phalloidin (green), the nuclei are stained with DAPI (blue) and the focal adhesions were stained with Atto-555 (red). Scale bars represent 20 μm.

In order to investigate the development of these coatings in time, cell morphology and spreading were studied after 7 days of culture (Figure 6.8). The pristine PCLdiUPy and PCLdiUPy with UPy-Tz surfaces show a confluent layer at the material surface. For both monofunctional-PEG-BCN and bifunctional-PEG-BCN incubation on the PCLdiUPy surfaces, the cell adhesion and morphology were not affected. However, the star-PEG-BCN incubation on the PCLdiUPy surface shows a reduction in cell adhesion, which suggests the star-PEG-BCN non-specifically interacts with the PCLdiUPy surface. In contrast to the 24 h culture period, the monofunctional-PEG-BCN functionalization of the PCLdiUPy with UPy-Tz surface shows a reduction in cell adhesion and spreading at the surface, however no complete anti-fouling effect was observed. The bifunctional-PEG-BCN and star-PEG-BCN modified PCLdiUPy with UPy-Tz surfaces, show complete prevention of cell attachment 7 days after cell seeding, demonstrating the effective introduction of an anti-fouling coating.

Another interesting examination was to address the effectiveness of the post-modification reaction in the presence of cells in cell culture medium. To this end, the PEG-BCN polymers were diluted in complex medium and mixed with the cells prior to administration on the PCLdiUPy and PCLdiUPy with UPy-Tz surfaces. Cell adhesion and morphology were studied 24 h (Figure 6.9) after seeding. For the pristine PCLdiUPy and PCLdiUPy with UPy-Tz surfaces and the PCLdiUPy surfaces with monofunctional-PEG-BCN, bifunctional-PEG-BCN or star-PEG-BCN present in the culture medium, cell adhesion and spreading was observed despite the presence of the PEG-BCN polymers in the culture
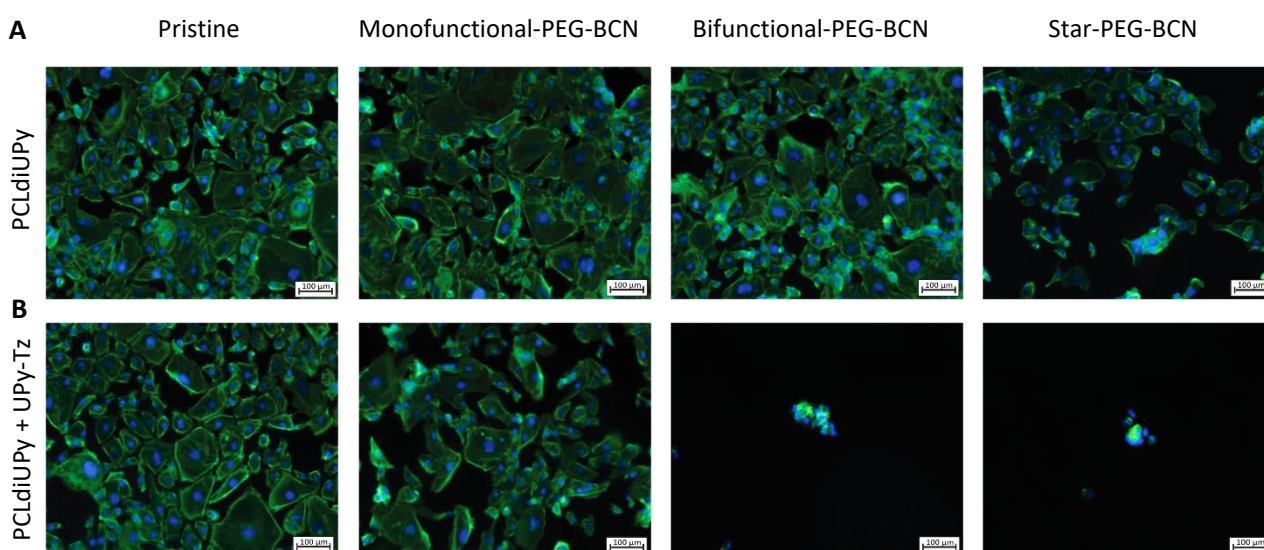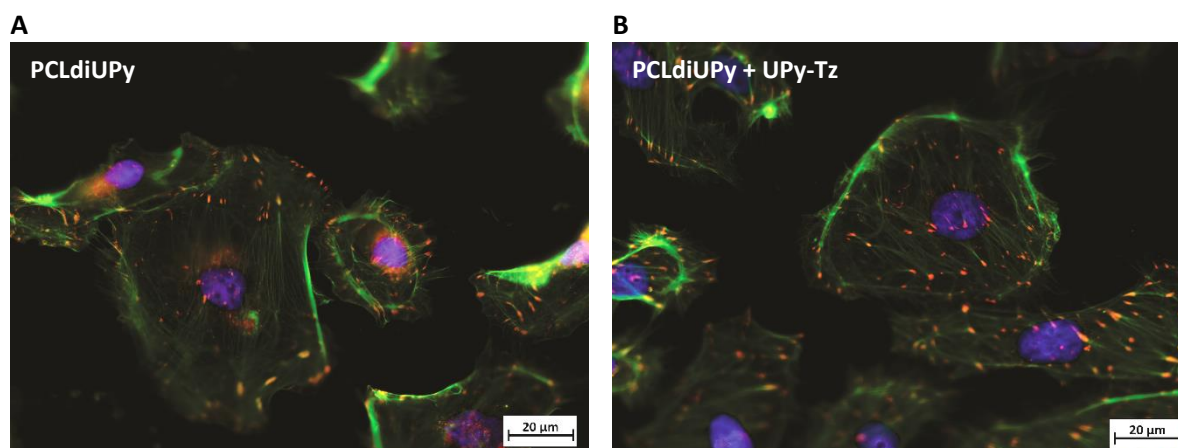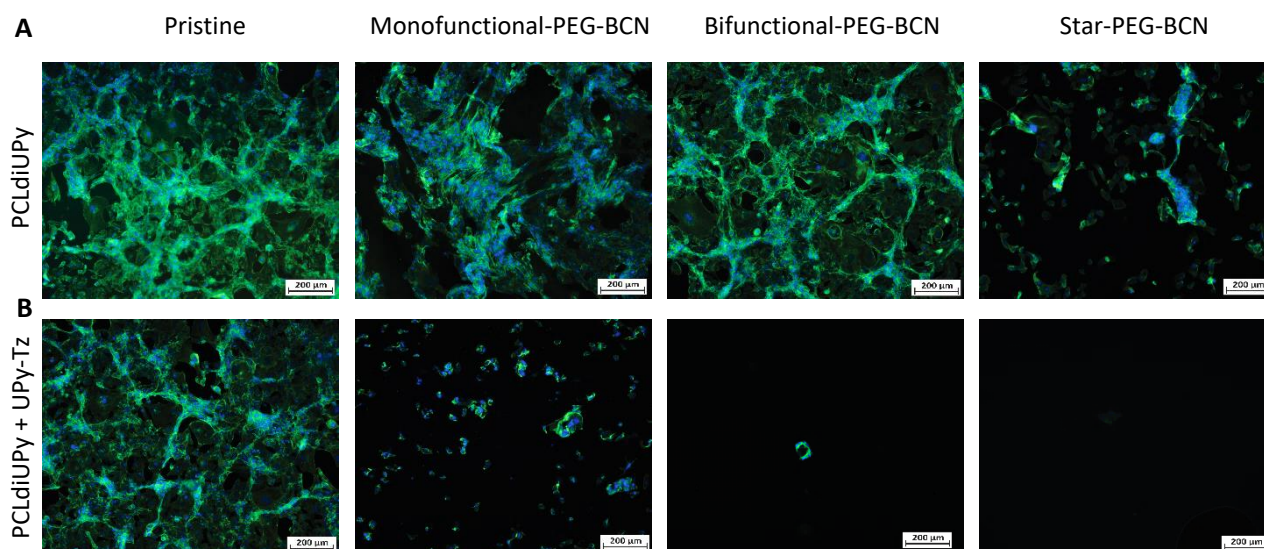
Figure 6.8. Fluorescence microscopy graphs of HK-2 cells on spincoated surfaces after 7 days of culture. Upper row represents images of PCLdiUPy (A), the pristine material or incubated with either monofunctional-PEG-BCN, bifunctional-PEG-BCN or star-PEG-BCN (from left to right). Lower row represents Images of PCLdiUPy with 10 mol% UPy-Tz incorporated (B) the pristine material or incubated with either monofunctional-PEG-BCN, bifunctional-PEG-BCN or star-PEG-BCN (from left to right). The actin skeleton is stained with Phalloidin (green), the nuclei are stained with DAPI (blue). Scale bars represent 200 μm.

Medium. On the PCLdiUPy surfaces that were incubated with the monofunctional-PEG-BCN and the bifunctional-PEG-BCN in the culture medium, a near confluent layer of cells was observed. These results indicate that the presence of the hydrophilic PEG-BCN polymers did not change the adhesion and spreading properties of the cells.

The PCLdiUPy with UPy-Tz surfaces with monofunctional-PEG-BCN, bifunctional-PEG-BCN or star-PEG-BCN present in the culture medium with the cells were hypothesized to display anti-fouling properties due to the effective click reaction between the reactive UPy-Tz additive and the BCN-functionality on the PEG polymers, which was reported to be performed in complex medium and living systems. [41,45–47] The PCLdiUPy with UPy-Tz surfaces incubated with monofunctional-PEG-BCN present in the culture medium with the cells, a reduction of cell attachment was observed (Figure 6.9), hence the surface did not display complete anti-fouling behavior. For the PCLdiUPy with UPy-Tz surfaces that were incubated with bifunctional-PEG-BCN or star-PEG-BCN present in the culture medium with the cells, no cells were observed, indicating that the surfaces were completely anti-fouling and thereby prevent cell adhesion (Figure 6.9).

In conclusion, the presence of the bi-functional-PEG-BCN and the star-PEG-BCN in the culture medium with the cells could completely prevent cell adhesion at the PCLdiUPy with UPy-Tz surfaces, which demonstrate the high efficiency of the reaction between the UPy-Tz and the BCN-modified PEG polymers, even in the presence of complex medium and cells.
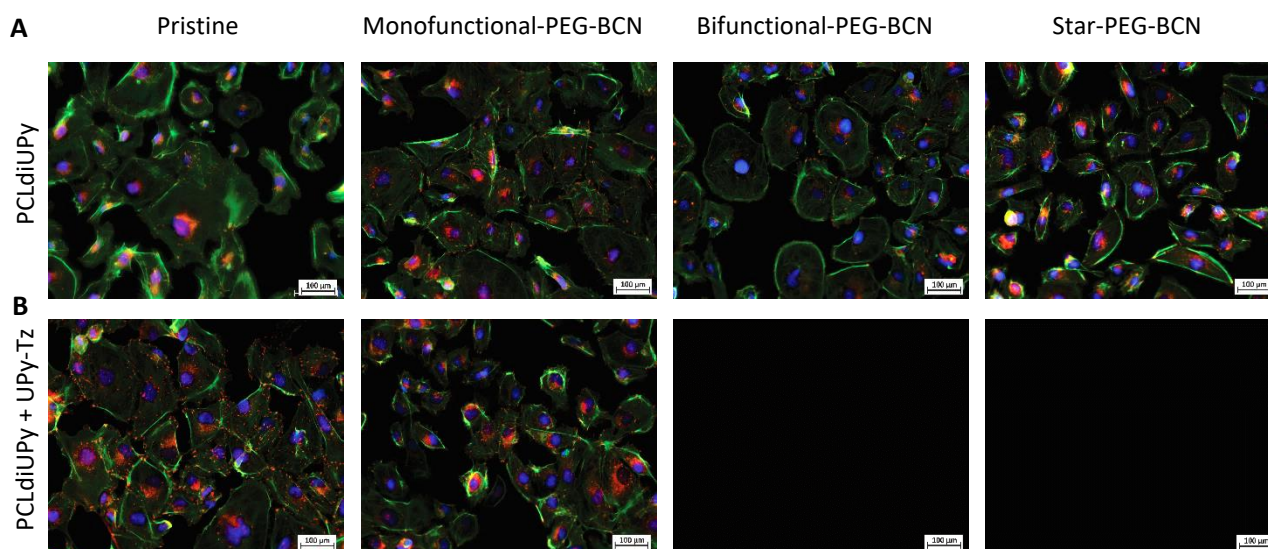
Figure 6.9. Fluorescence microscopy graphs of the cycloaddition reaction in complex medium in the presence of HK-2 cells on spincoated surfaces after 24 hours of culture. Upper row represents images of PCLdiUPy (A), the pristine material or incubated with either monofunctional-PEG-BCN, bifunctional-PEG-BCN or star-PEG-BCN (from left to right). Lower row represents Images of PCLdiUPy with 10 mol% UPy-Tz incorporated (B) the pristine material or incubated with either monofunctional-PEG-BCN, bifunctional-PEG-BCN or star-PEG-BCN (from left to right). The actin skeleton is stained with Phalloidin (green), the nuclei are stained with DAPI (blue) and the focal adhesions were stained with Atto-555 (red). Scale bars represent 100 μm.

6.1.5 Conclusions

In a modular fashion, UPy-modified tetrazine additives were incorporated into a PCLdiUPy polymer. *Via* an inverse Diels-Alder cycloaddition between the UPy-Tz and a BCN-modified PEG-polymer, the surface of the material was selectively functionalized, thereby creating a completely anti-fouling material surface. Moreover, it was shown that the extent of anti-fouling behavior is strongly dependent on the type of PEG-BCN polymer that was reacted, i.e. a monofunctional-PEG-BCN displayed less efficient anti-fouling properties as compared to bifunctional-PEG-BCN and the best performing star-PEG-BCN. The star-PEG-BCN showed excellent resistance to both protein adsorption and cell adhesion, which is attributed to the architecture of the polymer that is able to react up to four times at the material surface.

These results hold great promise in the development of functional supramolecular biomaterials that exhibit selective surface functionality. The introduction of anti-fouling coatings at surfaces has been widely investigated in literature, [30,48–54] however examples where the covalent attachment of such coatings at supramolecular surfaces is investigated are scarce. Upon the introduction of the anti-fouling coating, the materials are prevented from nonspecific protein and cell adhesion. Next steps in material functionalization involve the selective introduction of bioactive cues, which enables the modification of the materials with desired bioactive functionality towards specific regenerative medicine applications.

Moreover, from a fundamental material development point of view, the molecular design of the supramolecular additive might play an important role in the ultimate surface performance of the materials. To this end, a series of different UPy-Tz additives were synthesized and their surface arrangement and surface reactivity were investigated, which is discussed in the next part of this chapter.

6.2 The influence of molecular additive design on the spatial resolution and reactivity

The incorporation of the reactive UPy-modified tetrazine additive (UPy-Tz, **2**) was described and analyzed in chapter 5 and functionalized to introduce an anti-fouling coating in this chapter. The UPy-Tz is enhanced at the material surface and hence facilitates efficient surface modification *via* an inverse Diels-Alder cycloaddition. The UPy-Tz (**2**) was designed to enable incorporation into the supramolecular PCLdiUPy nanofibers and equipped with an oligo(ethylene glycol) (OEG) spacer to extent the tetrazine functionality and allow for reaction in the aqueous phase. From a fundamental point of view, it is of interest to investigate the molecular design of the UPy-Tz additive in more detail, to obtain insight in the effect of the hydrophilic OEG spacer on the material properties. The material morphology, surface hydrophobicity, surface composition and reactivity are assessed in this section (Figure 6.10A).

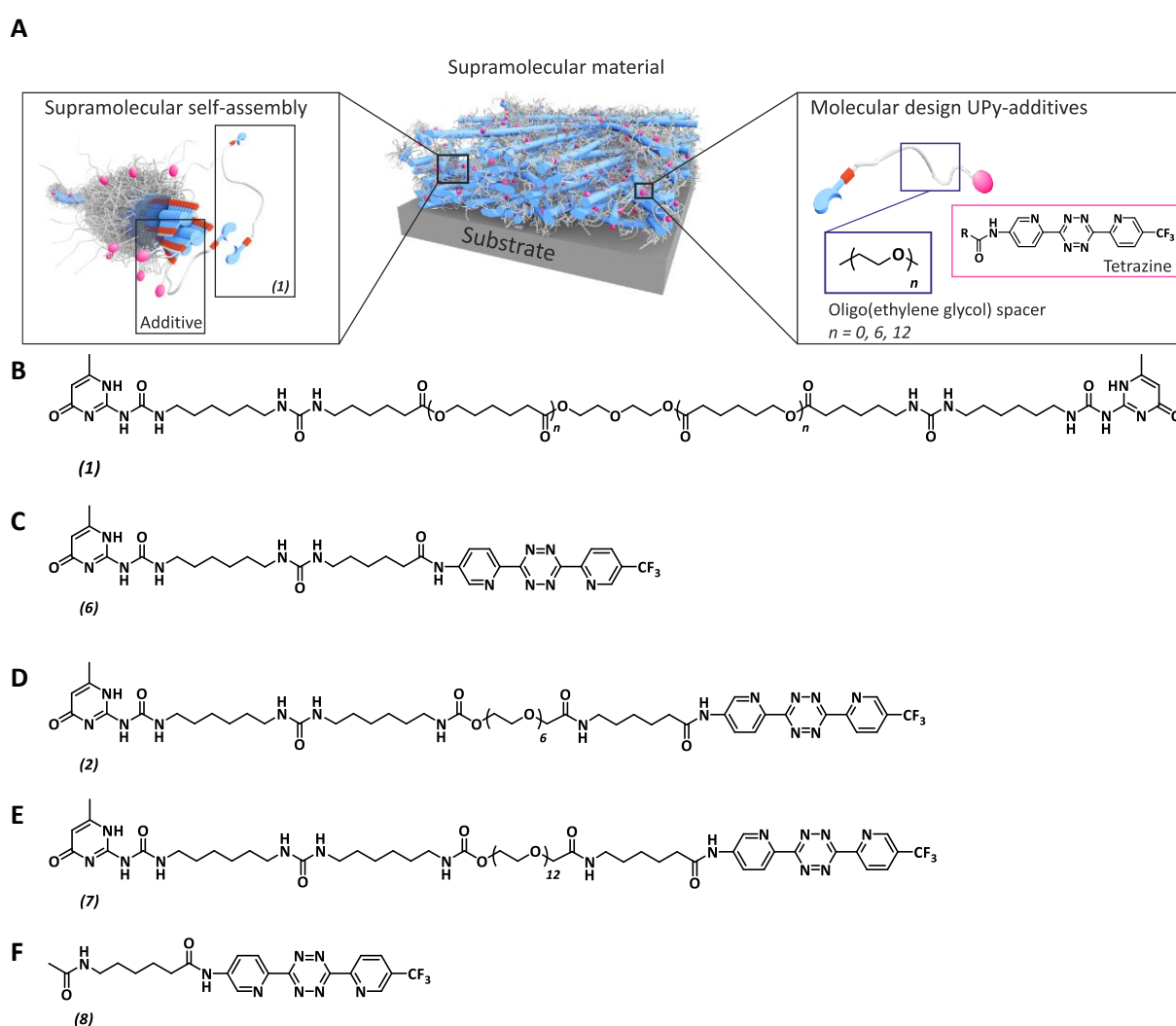**Figure 6.10.** Supramolecular system and corresponding chemical structures, A) Cartoon representation of the supramolecular material, the assembly and the concept that is investigated in this chapter, B) Chemical structure of the PCLdiUPy (**1**) polymer and chemical structures of the UPy-additives, C) UPy-OEG$_0$-Tz (**6**), D) UPy-OEG$_6$-Tz (**2**), E) UPy-OEG$_{12}$-Tz (**7**) and F) C$_5$-Tz (**8**) without a UPy-motif.

Via a modular approach, additives are mixed into the supramolecular polymer material, based on PCLdiUPy (**1**, Figure 6.10 B). Four different additives were investigated, a UPy-Tz additive without an OEG spacer, UPy-OEG$_0$-Tz (**6**, Figure 6.10 C), with an OEG-spacer of 6 repeating units, UPy-OEG$_6$-Tz (**2**, Figure 6.10 D) and with 12 repeating units, UPy-OEG$_{12}$-Tz (**7**, Figure 6.10 E). Additionally, an additive without a UPy-moiety and without an OEG-spacer was investigated, C$_5$-Tz (**8**, Figure 6.10 F). It is hypothesized that the OEG spacer enables both flexibility for the tetrazine to arrange at the materials surface and surface reactivity upon post-modification.

6.2.1 Morphology of the supramolecular materials

The influence of the incorporation of the different additives on the surface morphology of the dropcast films was investigated with AFM. Fibrous structures were observed for the pristine PCLdiUPy surfaces (Figure 6.11a). Incorporation of the UPy-OEG$_0$-Tz (**6**) shows fibrous structures up to 5 mol% incorporation (Figure 6.11b,c), indicative for complete mixing with the PCLdiUPy, whereas the introduction of 10 mol% showed the formation of phase separated hard domains (Figure 6.11 D). The incorporation of UPy-OEG$_6$-Tz (**2**) shows fiber morphology for 1 and 5 mol% (Figure 6.11 E,F) and small phase separated domains for the 10 mol% surface (Figure 6.11 G). For the UPy-OEG$_{12}$-Tz (**7**), which is equipped with a larger OEG-spacer, the onset of crystalline domain formation starts at 5 mol% incorporation (Figure 6.11 I) and is further increased at 10 mol% (Figure 6.11 J), whereas the 1 mol% shows fibrous structures (Figure 6.11 H). The incorporation of C$_5$-Tz (**8**), which lacks the UPy-motif, showed complete phase separation at the material surface in all cases, for 1, 5 and 10 mol% (Figure 6.11 K,L,M), indicative for complete demixing.

These results demonstrate that the presence of the UPy-motif facilitates incorporation into the PCLdiUPy polymer material. Moreover, based on the length of the OEG-spacer the onset of phase separation and crystalline domain formation is different, i.e. the longer the OEG-spacer, the earlier the phase separation behavior seem to start.
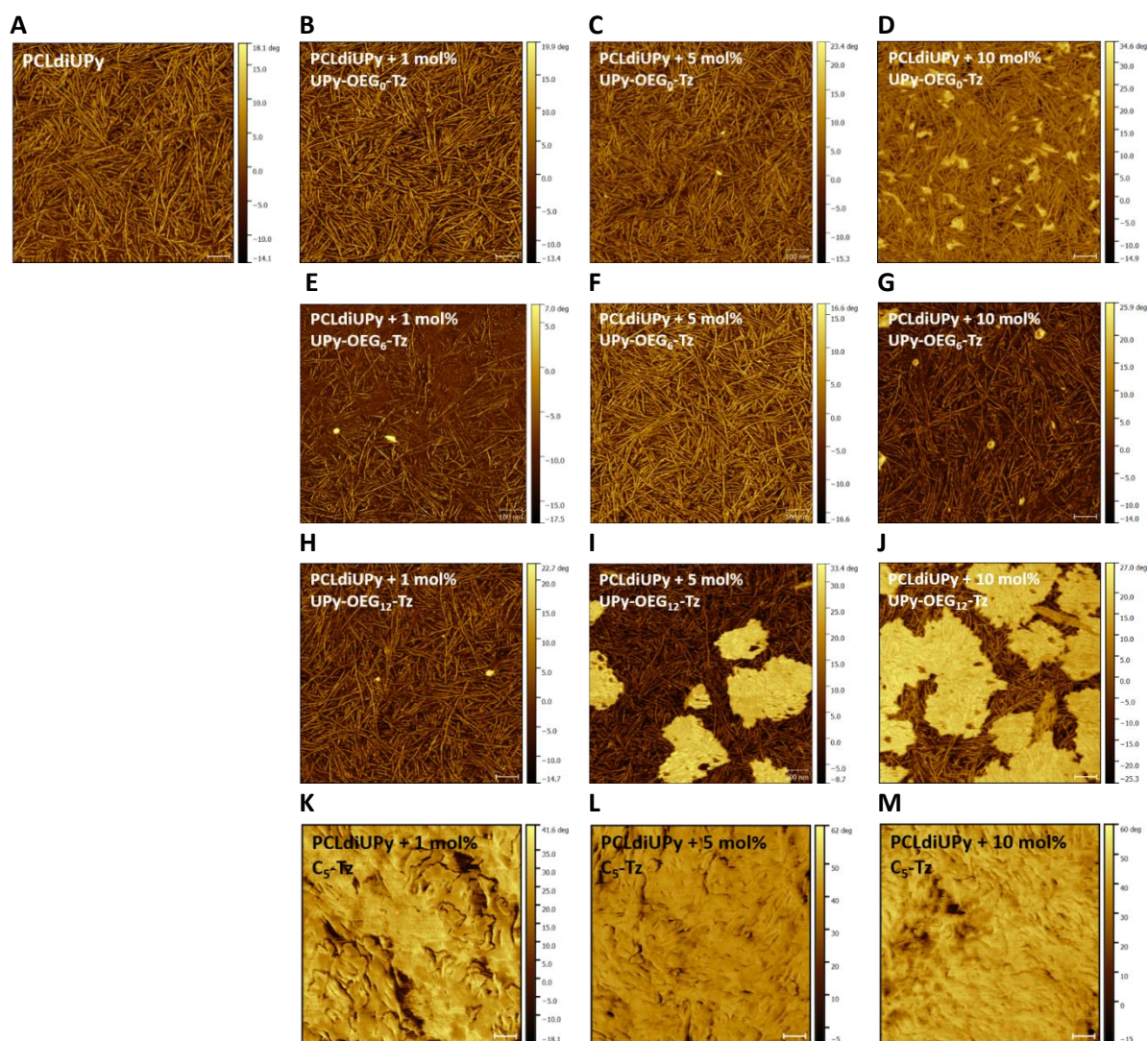
Figure 6.11. Surface analysis of drop-cast films, AFM phase micrograph, 1 μm x 1 μm, pristine PCLdiUPy (a) and PCLdiUPy with 1 (b), 5 (c), 10 (d) mol% UPy-OEG$_0$-Tz (**6**), 1 (e), 5 (f), 10 (g) mol% UPy-OEG$_6$-Tz (**2**), 1 (h), 5 (i), 10 (j) mol% UPy-OEG$_{12}$-Tz (**7**) and 1 (k), 5 (l), 10 (m) mol% C$_5$-Tz (**8**). Scale bar represents 100 nm.

6.2.2 Hydrophobicity analysis of the supramolecular materials

The hydrophobicity of the different dropcast films was assessed by water contact angle measurements (Table 6.1). The water contact angle of 68.5±1.5° of the pristine PCLdiUPy surface showed values in agreement with literature values. [39] The introduction of 1, 5 or 10 mol% of the UPy-OEG$_0$-Tz (**6**) additive did not significantly change the hydrophobicity of the surface, 68.6±1.2°, 69.6±0.9° and 68.6±1.4°, respectively. For the UPy-OEG$_6$-Tz (**2**) a slight increase in water contact angle was observed upon increasing amounts of incorporation, 69.6±1.1°, 70.0±1.2° and 71.5±0.8° for 1, 5 and 10 mol%, respectively. Interestingly, the incorporation of the UPy-OEG$_{12}$-Tz (**7**) with a longer hydrophilic OEG-spacer, results in an increased surface hydrophobicity for 1, 5 and 10 mol% incorporation, 72.9±1.4°, 75.5±0.9° and 78.2±0.5°, respectively. When the C$_5$-Tz (**8**), which lacks the UPy-moiety is incorporated, the hydrophobicity is further increased for the 1 and 5 mol% incorporation, 96.3±1.1° and 96.9±1.5°, respectively. The introduction of 10 mol% C$_5$-Tz shows an increased hydrophobicity

Table 6.1. Surface hydrophobicity analysis by water contact angle measurements. The pristine PCLdiUPy is analyzed as well as PCLdiUPy with 1, 5 and 10 mol% of the different additives, UPy-OEG$_0$-Tz, UPy-OEG$_6$-Tz, UPy-OEG$_{12}$-Tz and C$_5$-Tz, respectively.

	Water Contact Angle (°)		
Surface	**1 mol%**	**5 mol%**	**10 mol%**
PCLdiUPy	68.5 ± 1.5		
PCLdiUPy + UPy-OEG$_0$-Tz	68.6 ± 1.2	69.6 ± 0.9	68.6 ± 1.4
PCLdiUPy + UPy- OEG$_6$-Tz	69.6 ± 1.1	70.0 ± 1.2	71.5 ± 0.8
PCLdiUPy + UPy- OEG$_{12}$-Tz	72.9 ± 1.4	75.5 ± 0.9	78.2 ± 0.5
PCLdiUPy + C$_5$-Tz	96.3 ± 1.1	96.9 ± 1.5	86.1 ± 0.7

compared to the UPy-modified additives, whereas compared to the 1 and 5 mol% C$_5$-Tz a decrease is observed, 86.1±0.7°.

In conclusion, the water contact angle measurements show differences in surface hydrophobicity. Increased water contact angle values were observed for the surfaces that show phase separation behavior as was revealed by AFM. This might indicate that although the OEG-spacer is intrinsically hydrophilic, the crystallization as was observed with AFM, contributes to a more hydrophobic surface character.

6.2.3   Surface composition of the supramolecular materials

The surface composition of the different dropcast surfaces, composed of the PCLdiUPy with 1, 5 or 10 mol% of the respective additives, was investigated by XPS measurements (Figure 6.12). For the pristine PCLdiUPy (Figure 6.12 A) the carbon content was the highest (74.9%) and no fluorine was observed. Upon the incorporation of 1 mol% of the different tetrazine additives, minor changes in surface composition were observed for the UPy-OEG$_0$-Tz (**6**), UPy-OEG$_6$-Tz (**2**) and UPy-OEG$_{12}$-Tz (**7**). However, the C$_5$-Tz (**8**) showed an exorbitant increase in both nitrogen and fluorine content (17.1% and 11.6%, respectively) (Figure 6.12 B), which is proposed to result from the complete demixed morphology (Figure 6.11 K). The incorporation of 10 mol% of the additives clearly showed that UPy-OEG$_{12}$-Tz (**7**) with a longer OEG-spacer results in an enhancement of the tetrazine at the material surface (8.0% nitrogen and 2.7 % fluorine, respectively) compared to UPy-OEG$_6$-Tz (**2**) (5.2% nitrogen and 1.4 % fluorine, respectively) and UPy-OEG$_0$-Tz (**6**) (5.8% nitrogen and 0.6% fluorine, respectively) (Figure 6.12 D). Interestingly, the 5 mol% incorporation shows moderate increase in nitrogen and fluorine content (5.4% and 0.2% for the UPy-OEG$_0$-Tz (**6**), 5.1% and 0.3% for the UPy-OEG$_6$-Tz (**2**) and 6.0% and 0.6% for the UPy-OEG$_{12}$-Tz (**7**), respectively) (Figure 6.12 C). For the 1 mol% UPy-tetrazine incorporation only minor increase in nitrogen and fluorine surface composition were observed (5.2% and 0.1% for UPy-OEG$_0$-Tz (**6**), 4.9% and 0.1% for UPy-OEG$_6$-Tz (**2**) and 5.5% and 0.1% for UPy-OEG$_{12}$-Tz (**7**), respectively) (Figure 6.12 B). For the UPy-tetrazine additives (**6**, **2** and **7**, respectively), a further increase in nitrogen and fluorine content was observed upon 10 mol% incorporation (Figure 6.12 D), whereas this was not

measured for UPy-OEG$_{12}$-Tz (**7**). The C$_5$-Tz (**8**) showed similar values for both 5 mol% and 10 mol% compared to the 1 mol% incorporation. In summary, the incorporation of higher amounts of UPy-tetrazine additives result in increased nitrogen and fluorine content at the materials surface, which is attributed to the presence of the tetrazine at the material surface that is enriched in both nitrogen and fluorine. For the C$_5$-Tz (**8**) this effect was not observed, all incorporation mol% provided similar surface compositions, which is proposed to result from the complete phase separated morphology as was also observed with AFM (Figure 6.11 K,L,M).

Since the post-modification reactions are performed in aqueous environment, it was of interest to investigate the surface composition after water annealing. It was hypothesized that the hydrophilic spacer would allow for exposure into the aqueous phase and hence that the UPy-tetrazine moieties with longer OEG-linkers would display enhanced nitrogen and fluorine content. The incorporation of 10 mol% of the UPy-additives was investigated after 24 h water annealing (Figure 6.12 E), while the water exposure on the 10 mol% C$_5$-Tz (**8**) resulted

A

	C [%]	N [%]	O [%]	F [%]
PCLdiUPy	74.1	4.7	21.2	0.0

B

1 mol% additive	C [%]	N [%]	O [%]	F [%]
PCLdiUPy + UPy-OEG$_0$-Tz	74.5	5.2	20.2	0.1
PCLdiUPy + UPy-OEG$_6$-Tz	74.2	4.9	20.9	0.1
PCLdiUPy + UPy-OEG$_{12}$-Tz	74.6	5.5	19.8	0.1
PCLdiUPy + C$_5$-Tz	64.2	17.1	7.2	11.6

C

5 mol% additive	C [%]	N [%]	O [%]	F [%]
PCLdiUPy + UPy-OEG$_0$-Tz	74.5	5.4	20.0	0.2
PCLdiUPy + UPy-OEG$_6$-Tz	74.2	5.1	20.4	0.3
PCLdiUPy + UPy-OEG$_{12}$-Tz	75.9	6.0	17.6	0.6
PCLdiUPy + C$_5$-Tz	65.5	16.0	8.7	9.8

D

10 mol% additive	C [%]	N [%]	O [%]	F [%]
PCLdiUPy + UPy-OEG$_0$-Tz	73.1	5.8	20.5	0.6
PCLdiUPy + UPy-OEG$_6$-Tz	73.2	5.2	20.2	1.4
PCLdiUPy + UPy-OEG$_{12}$-Tz	73.8	8.0	15.6	2.7
PCLdiUPy + C$_5$-Tz	65.1	16.6	8.6	9.7

E

H$_2$O annealed	C [%]	N [%]	O [%]	F [%]
PCLdiUPy	75.4	4.8	19.8	0.0
10 mol% additive				
PCLdiUPy + UPy-OEG$_0$-Tz	72.8	6.1	19.9	1.2
PCLdiUPy + UPy-OEG$_6$-Tz	69.9	9.3	18.3	2.5
PCLdiUPy + UPy-OEG$_{12}$-Tz	68.0	17.8	10.0	4.2

Figure 6.12. Surface composition analysis by XPS measurements. The pristine PCLdiUPy is analyzed (A) as well as PCLdiUPy with 1 (B), 5 (C) and 10 (D) mol% of the different additives, UPy-OEG$_0$-Tz, UPy-OEG$_6$-Tz, UPy-OEG$_{12}$-Tz and C$_5$-Tz, respectively and E) After 24 h water annealing. The pristine PCLdiUPy is analyzed as well as PCLdiUPy with 10 mol% of the different additives,

in complete disintegration of the material films and hence could not be measured. Compared to the air dried samples, all the UPy-additives showed increased nitrogen and fluorine content at the material surface after water exposure (5.8% to 6.1% and 0.6% to 1.2% for the UPy-OEG$_0$-Tz (**6**), 5.2% to 9.3% and 1.4% to 2.5% for the UPy-OEG$_6$-Tz (**2**) and 8.0% to 17.8% and 2.7% to 4.2% for the UPy-OEG$_{12}$-Tz (**7**), respectively), which indicates that the surfaces have rearranged upon the water exposure. Moreover, the 10 mol% UPy-OEG$_{12}$-Tz (**7**) surface

revealed higher nitrogen and fluorine content compared to the UPy-OEG$_6$-Tz (**2**), which in turn showed an increase as compared to the UPy-OEG$_0$-Tz (**6**) additive. These results indicate that the surface composition after water annealing changes towards an enhanced tetrazine presence indicative for rearrangements at the surface.

6.2.4   Reaction kinetics of the UPy-OEG$_6$-Tz (2) in solution

The inverse electron demand Diels-Alder cycloaddition (IEDDA) between tetrazine and either a bicyclononyne (BCN) or a *trans*-cyclooctene (TCO) has been reported as an extremely efficient bioorthogonal ligation strategy. [45,55–60] The performance of the IEDDA of a TCO-iodine at the material surface was investigated and is was found that the reaction had occurred in chapter 5. The BCN cycloaddition was shown to be successful in this chapter. However, reaction kinetics and speed of the reaction were not investigated.

The kinetics of the reaction between a UPy-OEG$_6$-Tz (**2**) and BCN-NH$_2$ (**9**, Table 6.2) or TCO-iodine (**10**, Table 6.2) in solution were investigated by dr. ir. R.M. Versteegen, SyMO-Chem BV, Eindhoven. First, the aqueous stability of UPy-OEG$_6$-Tz in MeCN/PBS (1:9) was determined by UV-Vis spectroscopy, which provided a calculated half time of 2 h (Figure 6.13). The second order reaction constants of the reaction between UPy-OEG$_6$-Tz (**2**) and BCN-NH$_2$ (**9**) and TCO-iodine (**10**) were determined in MeCN at 20 °C by UV spectroscopy (Table 6.2 and Figure 6.14). It can be observed that the TCO-iodine (**10**) reacts faster than the BCN-NH$_2$ (**9**) (Figure 6.14 A,C). The second-order plot of the data, allowed to determine a k_2 of 150 M^{-1}s^{-1} for the BCN-NH$_2$ (**9**) and a k_2 of 442 M^{-1}s^{-1} was determined for the TCO-iodine (**10**) (Figure 6.14 B,D).
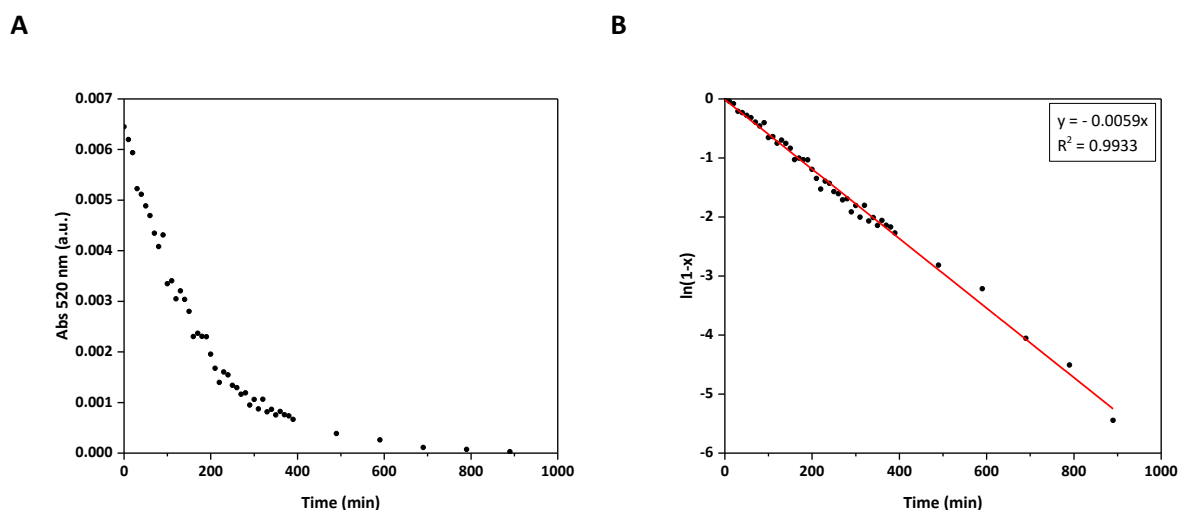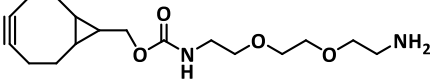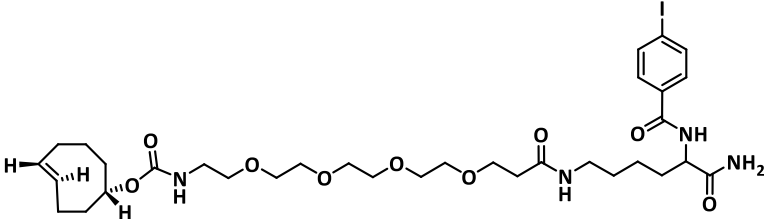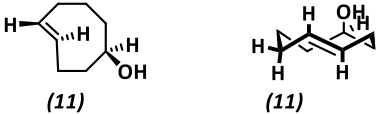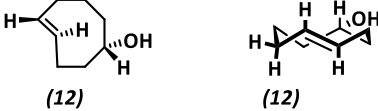

Figure 6.13. Determination of the aqueous stability of the UPy-OEG$_6$-Tz (**2**) in MeCN/PBS 1:9 at 20 °C. a) Decrease of the absorption at 520 nm and b) First-order plot of this data.

Table 6.2. Second order reaction constants of the UPy-OEG$_6$-Tz (**2**) with the BCN-NH$_2$ (**9**), TCO-iodine (**10**), axial TCO isomer (**11**) and equatorial TCO isomer (**12**) dienophile determined in MeCN at 20 °C by UV spectroscopy.

Dienophile	k_2 (M^{-1} s^{-1})
BCN-NH$_2$ *(9)*	**150**
TCO-iodine *(10)*	**442**
(*E*)-cyclooct-4-enol (axial isomer) *(11)* *(11)*	**2724**
(*E*)-cyclooct-4-enol (equatorial isomer) *(12)* *(12)*	**655**

These results show that the k_2 of the TCO-iodine (**10**) is ~ 3 times higher than the BCN-NH$_2$ (**9**) under these reaction conditions, indicating the reaction is 3 times faster. A k_2 of 1.3-3.2·10^4 M^{-1}s^{-1} was reported for the reaction between tetrazine and an equatorial TCO in PBS, whereas the a k_2 for axial isomer is 1.0-2.7·10^5 M^{-1}s^{-1} in PBS, which is ~ 8 times faster. [60] Reaction of the UPy-OEG$_6$-Tz (**2**) with an axial TCO (**11**) provided a k_2 of 2724 M^{-1}s^{-1} and the k_2 for the equatorial TCO (**12**) isomer was 655 M^{-1}s^{-1}, demonstrating that the axial isomer reacts ~ 4 times faster than the equatorial isomer. These values display a similar trend compared to the values reported in literature, given the differences in reaction conditions (PBS and 37 °C vs MeCN and 20 °C). The reactivity for the IEDDA performed in aqueous environment is reported to be ~ 100 times faster compared to organic solvents. [40]

The kinetic data of the UPy-OEG$_6$-Tz (**2**) that was studied for different dienophiles show similar trends in the kinetic behavior as compared to the fastest cycloadditions reported in literature, although the k_2 values are slower. However, the measurements were performed in MeCN whereas the literature values were determined in PBS. Next steps involve the performance of the reactions at the surface of the solid material films in order to investigate if a similar trend can be observed and whether differences can be observed between the different supramolecular additives that are incorporated. As a result of the selective surface

A

B

C

D
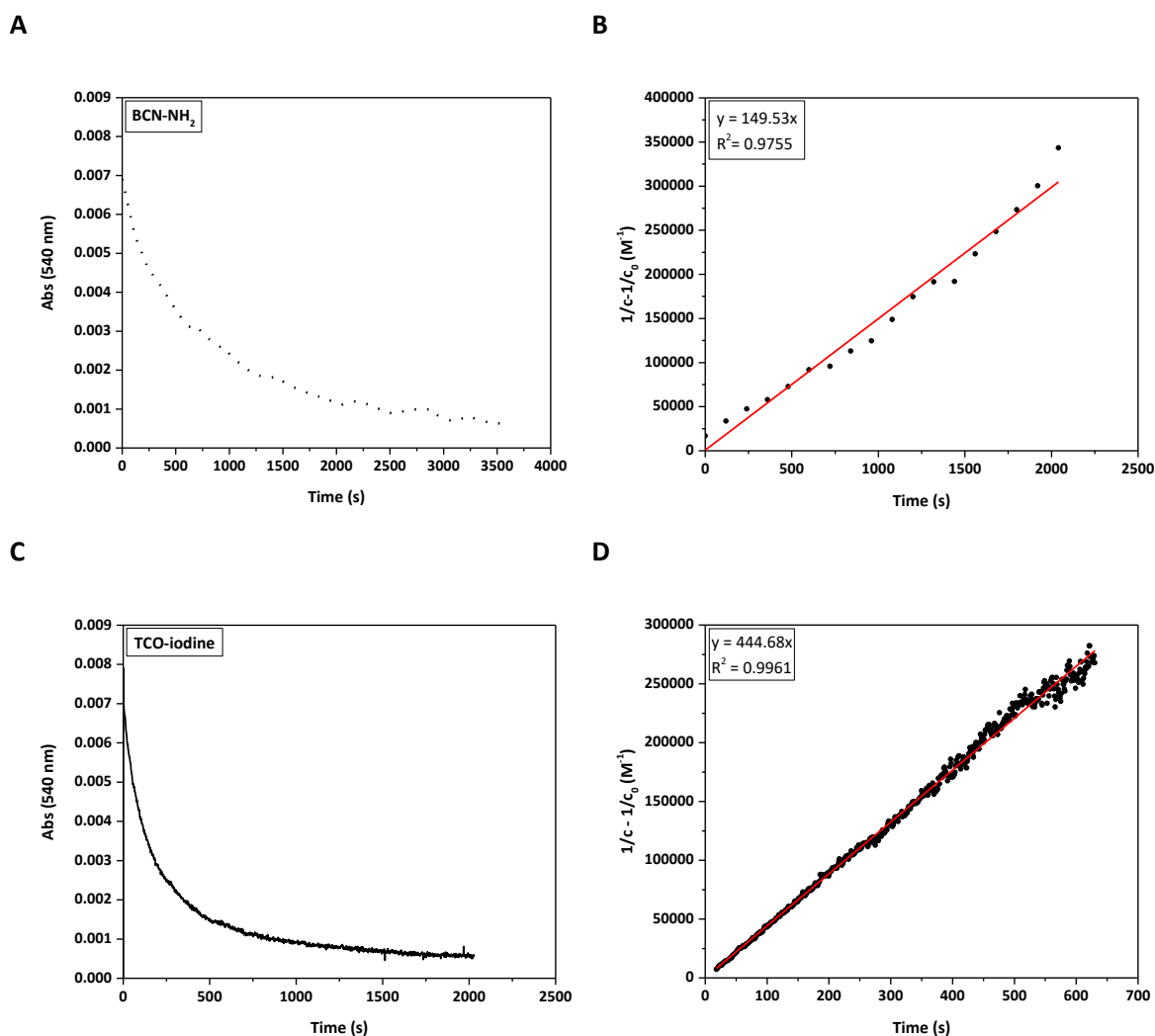
Figure 6.14. Reaction kinetics measured by UV-Vis spectroscopy. Kinetic plots of the reaction of UPy-OEG$_6$-Tz (**2**) with A) BCN-NH$_2$ (**9**), c_0 = 22.0 µM, change in absorption at 540 nm, B) second-order plot of the data, k_2 was calculated to be 150 M^{-1}s^{-1}, C) TCO-iodine (**10**), c_0 = 16.3 µM, change in absorption at 540 nm and D) second-order plot of the data, k_2 was calculated to be 442 M^{-1}s^{-1}. Reactions were performed in MeCN at 20°C.

modification, minor decrease in the specific tetrazine absorption is expected, which conceives these experiments challenging. Additionally, the variations in surface roughness and morphology should be taken into account in order to calculate the amount of tetrazine that has reacted at the material surface.

6.2.5 Discussion and conclusions

The influence of the molecular designs of the tetrazine additives was investigated in order to study differences in surface properties. AFM data showed that 1 mol% incorporation of the different UPy-modified tetrazine additives does not influence the surface morphology. However, from 5 mol% onwards the onset of phase separation is determined by the length of the OEG-linker in the additive design, i.e. longer OEG-linker lengths give rise to earlier onset of phase separation. The C$_5$-Tz additive, which does not have a UPy-motif, was unable to

incorporate into the PCLdiUPy fibers and AFM results showed complete demixing for 1, 5 and 10 mol% incorporation. Water contact angle measurements showed that the longer OEG-linker resulted in more hydrophobic surface properties. The C_5-Tz additive incorporation resulted in the highest water contact angles. XPS measurements revealed higher nitrogen and fluorine content at the surface for the additives with a longer OEG-linker. The C_5-Tz displayed the highest nitrogen and fluorine content, which is proposed to result from the complete demixed morphology. Moreover, upon water annealing the films that contained the C_5-Tz completely disintegrated and could not be analyzed. Water annealing at the PCLdiUPy films in which the UPy-tetrazine additives were incorporated showed an enhanced effect of the nitrogen and fluorine content at the material surface for the longer OEG-linkers. This is proposed to result from rearrangements at the materials surface where the OEG-spacer favors exposure in the aqueous phase.

Kinetic measurements in solution provided useful insights in the reaction kinetics of the UPy-OEG$_6$-Tz (**2**). The kinetics of the reaction with the BCN-NH$_2$ (**9**) was slower compared to the TCO-iodine (**10**) dienophile, which was expected based on literature values. In future experiments, the data that was obtained in solution should be translated to selective surface measurements. These data would then provide understanding on both the reactivity of the surface as well as reaction potential of the different UPy-tetrazine additives. In addition, the results potentially might be valuable when considering applications in a complex biological environment, i.e. the efficiency of the surface functionalization might be additive dependent.

In conclusion, the differences in molecular design of the different additive investigated in this chapter give rise to differences in surface behavior. Longer OEG-linker lengths give rise to earlier onset of phase separation behavior at the surface, result in more hydrophobic surface properties and allow for enhanced surface rearrangements upon exposure in aqueous environment. Future measurements to investigate the reaction behavior at the surface of solid material films will provide fundamental insights in the performance of the UPy-additives at the material surface. These insights can accommodate in the design of materials that can be surface controlled to favor post-modification strategies.

6.3 Acknowledgements

6.4 Materials and methods

Instrumentation

^{1}H NMR and ^{13}C NMR spectra were recorded on a 400 MHz NMR (Varian Mercury Vx or Varian 400MR) operating at 400 MHz for ^{1}H NMR and 100 MHz for ^{13}C NMR. Proton chemical shifts are reported in ppm downfield from tetramethylsilane (TMS) and carbon chemical shifts in ppm downfield from TMS using the resonance of the deuterated solvent as internal standard. Abbreviations used are s: singlet, d: doublet, t: triplet, q: quartet, m: multiplet. Matrix-assisted laser desorption ionization time-of-flight mass spectrometry (MALDI-TOF MS) was performed was performed on a Autoflex Speed MALDI-MS instrument (Bruker, Bremen, Germany) equipped with a 355 nm Nd:YAG smartbeam laser. MALDI-TOF MS experiments were performed by spotting samples on a MTP 384 target ground steel plate using an α-cyano-4-hydroxycinnamic acid (CHCA) (Fluka, Switzerland) matrix. Samples were 1:1 premixed with CHCA in 50/50 MeCN/water supplemented with 0.1 % v/v trifluoracetic acid (TFA). Mass spectra were acquired in reflector positive ion mode by summing spectra from 500 selected laser shots. The MS spectra were calibrated with cesium triiodide of known masses.

Materials

All reagents and solvents were purchased from Sigma Aldrich and used as received, unless stated otherwise. PCLdiUPy and UPy-Tz compounds were synthesized by SyMO-Chem BV (Eindhoven, The Netherlands). [38,39] (1*R*,8*S*,9*s*)-Bicyclo[6.1.0]non-4-yn-9-ylmethyl *N*-succinimidyl carbonate was purchased from Sigma Aldrich (Zwijndrecht, The Netherlands). Methoxy PEG-amine HCL salt and PEG-diamine HCL salt were purchased from Jenkem Technology (Texas, USA). Star-PEG BCN was kindly provided by Maxime Grillaud, Eindhoven University of Technology, Eindhoven, the Netherlands. Monofunctional-PEG BCN and bifunctional-PEG BCN were synthesized as described. Phosphate buffered saline (PBS), 1,1,1,3,3,3-Hexafluoro-2-propanol (HFIP), Triton X-100 buffer and 37 wt.% Formaldehyde solution were purchased from Sigma-Aldrich. Ammonia, hydrogen peroxide and sulphuric acid were obtained from VWR (Amsterdam, The Netherlands). Dulbecco's Modified Eagle Medium (DMEM), trypsin-EDTA (25300, 054), heat inactivated fetal bovine serum (FBS, 26140-079) and penicillin-streptomycin solutions were obtained from Gibco (Thermo Fisher Scientific, USA). Monocolonal IgG1 anti-vinculin mouse antibody, goat anti-mouse IgG1 Alexa 555 antibody, atto-488-conjugated Phalloidin and Hoechst were purchased from Sigma Aldrich. Water was deionized prior to use using a Milli-Q Advantage A-10 equipped with a Q-Guard T2 purification pack. Bovine serum albumin, γ-globulin from bovine blood and fibrinogen from bovine plasma were obtained from Sigma Aldrich as powders and used without further purification.

Synthesis

Synthesis of monofunctional-PEG-BCN (3)
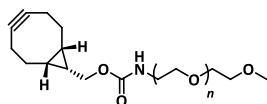
(3)   Methoxy poly (ethylene glycol) amine (359.0 mg, 0.172 mmol) and (1*R*,8*S*,9*s*)-Bicyclo[6.1.0]non-4-yn-9-ylmethyl *N*-succinimidyl carbonate (76.6 mg, 0.343 mmol) was dissolved in 3 mL Dimethylformamide (DMF). 20 equivalents of diisopropylethylamine (DIPEA) (597 μL, 3.43 mmol) were added and the reaction was stirred overnight under argon atmosphere at 50 °C. The reaction mixture was purified using a 2 kDa dialysis membrane in 4L of Milli-Q water and stirred for 24 hours. Water was changed 3 times in total. The reaction mixture was freeze-dried in the lyophilizer for 72 hours, resulting in a white powder **3** (284.2 mg, 0.127 mmol, 79%). The product formation was confirmed by ^{1}H-NMR and MALDI-TOF analysis.

^{1}H-NMR (400 MHz, CDCl$_3$): δ 4.25-4.05 (d, 2H), 3.86-3.45 (m, 184H), 3.42-3.38 (s, 3H), 3.38-3.29 (d, 2H), 2.37-2.11 (m, 4H), 1.26-1.05 (m, 2H), 1.03-0.88 (m, 2H).

Synthesis of bifunctional-PEG-BCN (4)
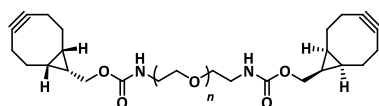
(4)

Poly (ethylene glycol) diamine (442.1 mg, 0.086 mmol) and (1*R*,8*S*,9*s*)-Bicyclo[6.1.0]non-4-yn-9-ylmethyl *N*-succinimidyl carbonate (98.0 mg, 0.343 mmol) was dissolved in 3 mL Dimethylformamide (DMF). 20 equivalents of diisopropylethylamine (DIPEA) (299 µL, 1.72 mmol) were added and the reaction was stirred overnight under argon atmosphere at 50 °C. The reaction mixture purified using a 2kDa dialysis membrane in 4L of Milli-Q water and stirred for 24 hours. Water was changed 3 times in total. The reaction mixture was freeze-dried in the lyophilizer for 72 hours, resulting in a white powder **4** (389.2 mg, 0.072 mmol, 88%). The product formation was confirmed by ^{1}H-NMR and MALDI-TOF analysis.

^{1}H-NMR (400 MHz, CDCl$_3$): δ 4.25-4.08 (d, 4H), 3.87-3.44 (m, 456H), 3.43-3.32 (d, 4H), 2,76-2,66 (s, 2H), 2.38-2.15 (m, 8H), 1.25-1.07 (m, 4H), 1.07-0.83 (m, 4H).

Synthesis of Star-PEG-BCN (5)
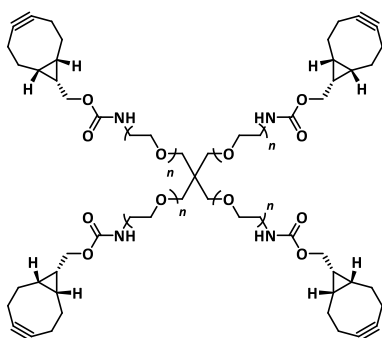
(5)

Four-arm poly (ethylene glycol) tetraamine (Mn ~ 10,000 Da, n ~ 57, 1 g, 0.4 mmol NH2, 1x, Jenkem) and BCN-OSu (175 mg, 0.015 mmol, 1.5x) were dissolved in dimethylformamide (5 mL). N,N-Diisopropylethylamine (277 µL, 207 mg, 1.6 mmol, 4x) was added to the mixture, and the reaction was stirred overnight, concentrated, dissolved in water, dialyzed (molecular weight cutoff ~2 kDa, SpectraPor), and lyophilized to yield a white powder (1.06 g, quantitative yield).

^{1}H NMR (500 MHz, CDCl3) δ 5.27 (s, 4H), 4.13 (d, *J* = 8.0 Hz, 8H), 3.78 – 3.75 (m, 8H), 3.65 – 3.61 (m, 909H), 3.50 – 3.47 (m, 4H), 2.30 – 2.18 (m, 24H), 1.64 – 1.50 (m, 8H), 1.39 – 1.29 (m, 4H), 0.98 – 0.88 (m, 8H). Functionalization was confirmed to be >95% by ^{1}H-NMR by comparing integral values for characteristic BCN peaks (δ 2.24, 1.57, 1.34, 0.92) with those from the PEG backbone (δ 3.63).

Synthesis of UPy-C$_6$-U-C$_6$-OEG$_0$-C$_5$-Tz-CF$_3$ (6)
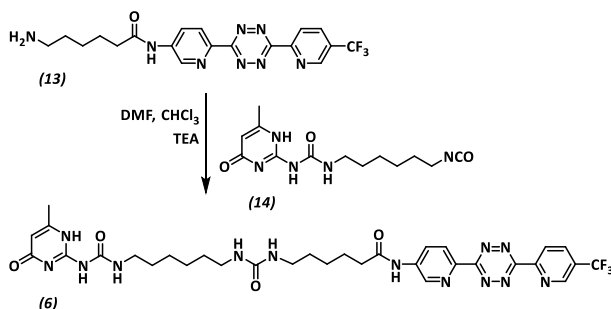
Scheme 6.1. Synthesis of the UPy-OEG$_0$-Tz (**6**), MW 725.74 g·mol^{-1}.

UPy-C6-U-C5-Tz-CF$_3$ (6)

CF$_3$-Tz-C5-NH$_2$ **13** (35.0 mg, 0.81 mmol) was dissolved in DMF (2 mL), UPy-C6-NCO **14** (19.8 mg, 0.067 mmol) in chloroform (2 mL) and triethylamine (0.068 mL, 0.49 mmol) were added. After stirring for 2 hours at room temperature under argon, the solvent was removed. Stirred in MeOH and filtered (2x), affording **2** (35 mg, 71%) as a pink powder.

^{1}H NMR (399 MHz, CDCl$_3$) δ 9.11 (s, 1H), 8.92 (d, J = 8.3 Hz, 1H), 8.86 – 8.73 (m, 2H), 8.49 (d, J = 8.7 Hz, 1H), 8.37 (d, J = 8.3 Hz, 1H), 5.91 (s, 1H), 3.70-3.28. (br, 6H), 3.24 – 3.01 (m, 6H), 2.50 (t, J = 7.5 Hz, 2H), 2.26 (s, 3H), 1.77 (q, J = 7.5 Hz, 2H), 1.62 – 1.19 (m, 12SH). ^{13}C NMR (101 MHz, Chloroform-d) δ 176.25, 176.06, 165.43, 163.60, 163.24, 161.17, 156.89, 154.34, 152.30, 152.21, 147.88, 147.83, 144.44, 142.39, 138.84, 137.33, 130.16, 125.51, 124.73, 122.61, 122.03, 121.70, 106.75, 41.54, 41.12, 40.88, 37.98, 37.79, 29.84, 29.67, 29.63, 26.85, 26.58, 25.54, 18.52.LC-MS(ESI) R$_t$= 5.52 min m/z calcd (C$_{32}$H$_{38}$F$_3$N$_{13}$O$_4$) 725.3; found 363.7 [M + 2H]$^{2+}$, 726.2 [M+H]$^+$.

Synthesis of UPy-C$_6$-U-C$_6$-OEG$_6$-C$_5$-Tz-CF$_3$ (2)

The full synthetic details can be found in Chapter 5 and Ref. [39]
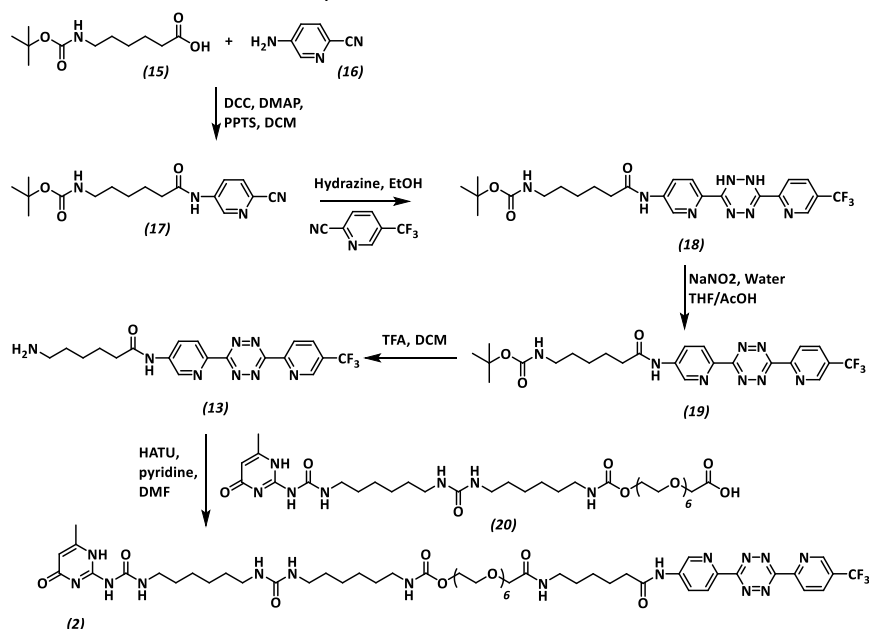
Scheme 6.2. Synthesis of the UPy-OEG$_6$-Tz (**2**), MW 1190.29 g·mol^{-1}.

Synthesis of UPy-C$_6$-U-C$_6$-OEG$_{12}$-C$_5$-Tz-CF$_3$ (7)
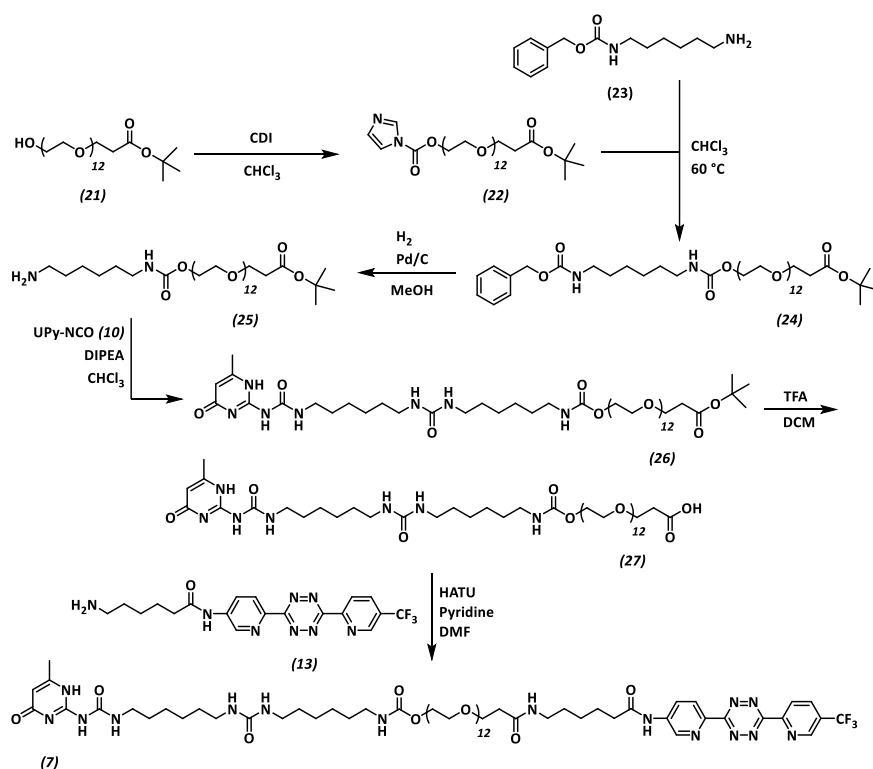
Scheme 6.3. Synthesis of the UPy-OEG$_{12}$-Tz (**7**), MW 1454.61 g·mol^{-1}.

CDI-OEG$_{12}$-COOtBu (22)

OH-OEG$_{12}$-tBu (**21**) (1030 mg, 1.526 mmol) was dissolved in 48 mL chloroform and a solution of N,N-carbonyldiimidazole (272 mg, 1.679 mmol) in 2 mL chloroform was added. The reaction mixture was stirred at room temperature overnight. The reaction mixture was then washed with 10 mL 0.05 M aqueous citric acid. The organic phase was dried with MgSO$_4$ and evaporated to give 1100 mg (97%) of the compound as a viscous oil. LC-MS(ESI) R$_t$= 4.09 min, m/z calcd C$_{35}$H$_{64}$N$_2$O$_{16}$; found 769.33 [M+H]$^+$

Cbz-C$_6$-OEG$_{12}$-COOtBu (24)

The activated CDI-OEG$_{12}$-COOtBu (**22**) (1100 mg, 1.431 mmol) was dissolved in 50 mL chloroform and the Cbz-C$_6$-NH$_2$ (**23**) (430 mg, 1.717 mmol) spacer was added. The reaction was left to stir at reflux while monitoring the reaction with LC-MS. After 4 days the reaction was complete and work-up was performed. The organic phase was washed with 0.5 M citric acid (2 x 50 mL) and brine (50 mL) and dried with MgSO$_4$ to give the crude product as a yellow oil (1202 mg, 88%).

^{1}H NMR (400 MHz, CDCl$_3$): δ = 1.25-1.55 (m, 17 H), 2.50 (t, J = 6 Hz, 2 H), 3.15 (m, 4 H), 3.64 (s, 46 H), 3.70 (t, J = 6 Hz, 2 H), 4.20 (t, 2 H), 5.09 (s, 2 H), 7.35 (m, 5 H). ^{13}C NMR (400 MHz, CDCl$_3$): δ = 170.97, 156.51, 136.76, 128.14, 80.57, 70.70, 70.66, 70.59, 70.45, 69.76, 66.63, 63.91, 40.96, 40.88, 36.36, 29.94, 28.19, 26.33. LC-MS(ESI) R$_t$= 5.49 min, m/z calcd (C$_{46}$H$_{82}$N$_2$O$_{18}$) 950,56; found 951.25 [M+H]$^+$.

NH$_2$-C$_6$-OEG$_{12}$-COOtBu (25)

Cbz-C$_6$-OEG$_{12}$-COOtBu (**24**) (1050 mg, 1.104 mmol) was dissolved in 25 mL MeOH in a thick walled flask and 100 mg 10% wt Pd/C was added. The flask was purged with N$_2$ and then placed in a parr reactor. The reaction vessel was purged three times with H$_2$. The heterogeneous reaction mixture was shaken vigorously overnight at a pressure of 4 mbar. Afterwards the reaction mixture was filtered over Celite and the organic phase was evaporated to give an oily residue. The oily residue was dissolved in 5 mL of DCM and precipitated in 45 mL of

diethyl ether. The supernatant was discarded and the remaining oily precipitate corresponded to pure compound (755 mg, 83%).

^{1}H NMR (400 MHz, CDCl$_3$): δ = 1.25-1.65 (m, 17 H), 2.46 (t, J = 6.54 Hz, 2 H), 2.81 (t, J = 7.21 Hz, 2 H), 3.11 (m, 2 H), 3.55-3.70 (m, 48 H), 4.16 (bs, 2 H). ^{13}C NMR (100 MHz, CDCl$_3$): δ = 170.93, 156.56, 80.3, 70.59, 70.57, 70.54, 70.52, 70.49, 70.39, 69.81, 66.93, 63.99, 40.76, 40.55, 36.31, 29.55, 28.14, 26.16. LC-MS(ESI) R$_t$= 3.55 min, m/z calcd (C$_{38}$H$_{76}$N$_2$O$_{16}$) 816.52; found 817.58 [M+H]$^+$.

UPy-C$_6$-OEG$_{12}$-COOtBu (26)

NH$_2$-C$_6$-OEG$_{12}$-COOtBu (25) (600 mg, 0.734 mmol) was dissolved in 100 mL chloroform and UPy-C6-NCO (10) (215 mg, 0.734 mmol) and DIPEA (0.141 mL, 0.808 mmol) was added. The reaction was stirred overnight. The total volume of chloroform was evaporated to 5 mL. Then the product was precipitated in 45 mL of heptane. The supernatant was discarded and the remaining white solid precipitate corresponded to pure compound (780 mg, 96%).

^{1}H NMR (399 MHz, CDCl$_3$/CD$_3$OD) δ = 1.28-1.62 (m, 25 H), 2.25 (s, 3H), 2.50 (t, J = 6.51 Hz, 2H), 3.13 (m, 6H), 3.23 (m, 2H), 3.60-3.68 (m, 46 H), 3.71 (t, J + 6.52 Hz, 2H), 4.19 (t, J = 4.42 Hz, 2H), 5.84 (s, 1H). ^{13}C NMR (100 MHz, CDCl$_3$/CD$_3$OD) δ = 173.37, 171.00, 158.92, 156.64, 156.21, 154.41, 148.55, 106.40, 80.60, 70.48, 70.45, 70.39, 70.26, 69.55, 66.81, 63.73, 40.64, 40.51, 39.82, 39.50, 36.18, 29.99, 29.80, 29,66, 29.18, 28.01, 26.29, 26.20, 26.12, 18.80. LC-MS(ESI) R$_t$= 4.43 min, m/z calcd (C$_{51}$H$_{95}$N$_7$O$_{19}$) 1109,67; found 566.92 [M+Na]$^+$, 1132.50 [M+Na]$^+$.

UPy-C$_6$-OEG$_{12}$-COOH (27)

UPy-C$_6$-OEG$_{12}$-COOtBu (26) (40 mg, 0.180 mmol) was dissolved in 4 mL DCM/TFA (1:1) and left to stir for three hours. Afterwards the solvents were removed with a flow of N$_2$. Then it was precipitated twice in diisopropyl ether to isolate 35 mg (92%) of the product as a white powder.

^{1}H NMR (399 MHz, CDCl$_3$/CD$_3$OD) δ = 1.18-1.50 (m, 16H), 2.18 (s, 3H), 2.50 (t, J = 6.40 Hz, 2H), 3.03 (m, 6H), 3.15 (t, J = 6.40 Hz, 2H), 3.55-3.61 (m, 46 H), 3.67 (t, J = 6.26 Hz, 2H), 4.10 (bs, 2H), 5.79 (s, 1H). LC-MS(ESI) R$_t$= 3.69 min, m/z calcd (C$_{47}$H$_{87}$N$_7$O$_{19}$) 1053,61; found 527.92 [M+2H]$^{2+}$, 1054.42 [M+H]$^+$.

UPy-C$_6$-OEG$_{12}$-Tz (7)

UPy-C$_6$-OEG$_{12}$-COOH (27) (35 mg, 0.033 mmol) was dissolved in 1 mL DMF in a round bottom flask. HATU (24 mg, 0.063 mmol) was added together with pyridine (0.29 mmol, 23 μL). After 30 minutes of stirring and preactivation, the tetrazine (13) (25 mg, 0.057 mmol) was added and the reaction was stirred overnight. The reaction mixture was stirred overnight and subsequently poured into 2% FA water solution and centrifuged (2x). Eluting over silica with 10/10/80 DME/MeOH/CHCl$_3$ afforded the compound (32 mg, 66%) as a pink solid.

^{1}H NMR (399 MHz, CDCl$_3$/CD$_3$OD) δ = 1.25-1.65 (m, 22H), 2.27 (s, 3H), 3.12 (m, 6H), 2.46 (m, 4 H), 3.24 (t, J = 6.85 Hz, 4H), 3.67-3.7 (m, 40H), 3.72 (t, J = 5.96 Hz, 4H), 4.18 (bs, 2H), 5.89 (s, H), 8.34 (m, H), 8.67 (m, H), 8.76 (m, H), 8.94 (m, 2H), 9.20 (s, H). ^{13}C NMR (101 MHz, CDCl$_3$/CD$_3$OD) δ = 173.52, 172.29, 163.21, 162.74, 159.31, 156.88, 155.79, 153.08, 150.60, 147.54, 147.50, 143.07, 141.83, 139.15, 135.05, 128.89, 126.87, 124.37, 123.89, 121.66, 120.54, 106.07, 70.39, 70.35, 70.33, 70.29, 70.18, 70.04, 69.52, 67.16, 63.70, 40.53, 39.84, 39.54, 38.95, 36.64, 29.89, 29.81, 29.61, 29.58, 29.10, 28.82, 26.15, 24.73. LC-MS(ESI) R$_t$= 4.49 min, m/z calcd (C$_{66}$H$_{104}$F$_3$N$_{15}$O$_{19}$) 1467,76; found 490.33 [M+3H]$^{3+}$, 735.00 [M+2H]$^{2+}$ 1469.42 [M+H]$^+$.

Synthesis of C$_5$-Tz-CF$_3$ (8)
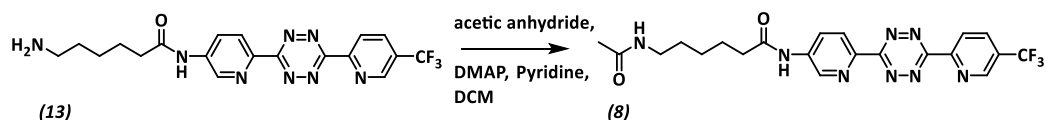
Scheme 6.4. Synthesis of the C$_5$-Tz (8), MW 474.45 g·mol^{-1}.

Acetyl-C5-Tz-CF₃ (8)

CF_3-Tz-C5-NH_2 **13** (100.0 mg, 0.23 mmol) was dissolved in DCM (1.0 mL), pyridine (1.0 mL, 12.4 mmol), DMAP (33.0 mg, 0.27 mmol) and acetic anhydride (0.5 mL, 5.38 mmol) were added. After stirring for 3 hours at room temperature under argon, $CHCl_3$ (5 mL) was added. The resulting precipitate was filtered and washed with $CHCl_3$, affording **5** (81 mg, 74%) as a pink powder.

^{1}H NMR (399 MHz, DMSO-d_6) δ 11.09 (s, 1H), 9.32 (s, 1H), 9.17 (d, J = 2.4 Hz, 1H), 8.76 (d, J = 8.3 Hz, 1H), 8.59 (dd, J = 17.4, 8.6 Hz, 2H), 8.47 (dd, J = 8.7, 2.5 Hz, 1H), 8.06 – 7.76 (m, 1H), 3.00 (q, J = 6.5 Hz, 2H), 2.44 (d, J = 7.4 Hz, 2H), 1.76 (s, 3H), 1.61 (p, J = 7.6 Hz, 2H), 1.53 – 1.24 (m, 4H). ^{13}C NMR (100 MHz, DMSO-d_6) δ 173.10, 169.43, 163.19, 162.84, 154.29, 147.70, 147.63, 143.78, 141.87, 139.38, 135.99, 126.48, 125.56, 124.59, 38.81, 36.72, 29.36, 26.54, 25.09, 23.06. LC-MS(ESI) R_t= 5.22 min m/z calcd ($C_{21}H_{21}F_3N_8O_2$) 474.2; found 238.3 [M + 2H]$^{2+}$, 475.4 [M+H$^+$]$^+$, 949.2 [2M+H]$^+$ 971.3 [2M+Na]$^+$.

Methods

Preparation of polymer solutions. Solutions of PCLdiUPy were prepared at a concentration of 20 or 50 mg·mL^{-1} in 1,1,1,3,3,3-Hexafluoroisopropanol (HFIP). For the mixtures, 1, 5 or 10 mol% UPy-Tz solutions were prepared by adding 1, 5 or 10 mol% UPy-Tz to 99, 95 or 90 mol% PCLdiUPy solutions. PEG solutions were prepared at different concentrations in ultrapure water, obtained using a Milli-Q Advantage A-10 equipped with a Q-Guard T2 purification pack.

Preparation of spin coated surfaces. Spin coated samples were prepared by spin coating 50 μL of a solution of 20 mg·mL^{-1} PCLdiUPy or PCLdiUPy with 10 mol% UPy-Tz at 3000 rpm for 30 seconds on glass coverslips (Ø 12mm, thickness 1 mm) or gold-coated sensors (BiolinScientific AB). Samples conjugated with a BCN functionalized PEG polymer were prepared by incubating spin coated samples with 0.5 or 0.1 mg·mL^{-1} PEG solution for 90 minutes at room temperature. The samples were washed for 10 minutes in Milli-Q water and dried with air before continuing experiments.

Preparation of drop-cast surfaces. Samples were prepared by dropcast 30 μL of a solution of 50 mg·mL-1 of the PCLdiUPy + 0, 1, 5 or 10 mol% of the respective tetrazine additives from HFIP on glass coverslips with a diameter of 12 mm or 65 μL on 15 mm coverslips, yielding a thin solid material film with a thickness in the range of 4-6 μm as was determined by profilometry measurements.

Atomic force microscopy. Atomic force microscopy was performed at room temperature on spincoated films using a Digital Instrument Multimode Nanoscope IV 279 with silicon cantilever tips (PPP-NCH-50, 204-497 kHz, 10-130 N·m^{-1} from Nanosensors) using a tapping regime mode. The roughness of the surface has been measured and images have been processed using Gwyddion software (version 2.39).

X-ray photoelectron spectroscopy. X-ray photoelectron spectroscopy was performed on spincoated coverslips and were recorded using a Thermo Scientific K-alpha spectrometer equipped with a monochromatic, small-spot X261 ray source and a 180° double focusing hemispherical analyzer with a 128-channel detector. The coverslips were mounted on the holder using carbon tape and an Aluminum anode (Al Kα, 1486.6 eV, 72 W) was used to obtain the spectra. Analysis and quantification of the spectra were performed using CasaXPS software version 2.3.16, using the C 1s, N 1s, O 1s and F 1s regions.

Water contact angle measurements. Water contact angles were measured on spincoated surfaces at room temperature in air using an OCA 30 (DataPhysics). Deionized water droplets of 4 μL were applied on the surface of the spincoated coverslips and coverslips conjugated to the BCN functionalized PEG polymers. Images were recorded at a rate of 2.5 frames per second and the angle at the polymer-air-water interface was measured after 5 seconds using an automatic fitting routine (SCA20 software).

Quartz-crystal microbalance with Dissipation monitoring. QCM-D measurements were performed on the Q-Sense E4 instrument (BiolinScientific) using gold-coated AT-cut quartz discs with a fundamental frequency of

4.95 MHZ (QSX 301 Gold, BiolinScientific AB). Before use, sensors were rinsed with piranha solution and subsequently heated for 15 minutes at 70 °C in a 4:1:1 mixture of ultrapure water, ammonia and 30% hydrogen peroxide (base piranha). Subsequently, sensors were rinsed with water and acetone and dried with nitrogen gas. Clean crystals were mounted to record their fundamental frequency in air and subsequently removed for spin coating. All experiments were performed at 37 °C. After equilibration, the frequency and dissipation of the sensors were measured in air for 1 minute. After mounting the sensors with the spincoated material, sensors were again measured in air for 1 minute. The frequency and dissipation changes of the sensor before spincoating and after spincoating were stitched and Sauerbrey was applied to the stitched data to determine the layer thickness. After mounting the PEG-BCN to the sensor surfaces, PBS was passed over the surface at 0.1 mL·min^{-1} until the signal equilibrated. Subsequently, the protein solution was passed over the surface at 0.1 mL·min^{-1}. Frequency and dissipation changes were recorded for 30 minutes, and the sensors were rinsed with PBS. Each experiment was repeated in two-fold, and means and standard errors of the mean are reported. After each experiment, the system was cleaned by rinsing with PBS for 10 minutes, followed by 50 mL a 2 wt% solution of Hellmanex III (Hellma) in ultrapure water, followed by rinsing with ultrapure water for 10 minutes. Next, the sensors were removed and the components were dried using nitrogen.

Visco-elastic modeling of the data. Shifts in frequency and dissipation for overtones 3, 5, 7, 9 and 11 were analyzed using the Voigt-Voinova model and the QTools software (Q-sense). As became evident from the measurements, the viscosity of the protein solutions was higher than the viscosity of PBS. Therefore, the viscosity of the protein solution was accounted in the model by the use of a 1 layer (L1) viscoelastic model with a viscosity of 0.001 Pa s and a fluid density of 1100 kg·m^{-3}. The protein layer density was set to 1145 kg·m^{-3} for all protein layers as found in literature. The minimum and maximum estimate for the fitted parameters of L1 viscosity, L1 shear and L1 thickness were set between 0.0001-0.1, 1000 − 1E8 and 1E-11 − 1E-7 respectively. A 2nd order polynomial model was used to estimate the standard deviation. The data was fitted by using a descending incremental fitting mode with a first row to fit grid mode. The model was optimized by decreasing χ^2 by tuning the selection of overtones.

Aqueous stability of UPy-OEG$_6$-Tz (2). The aqueous stability of UPy-OEG$_6$-Tz (**2**) was assessed in MeCN/PBS 1:9 at 20°C. Therefore, a stock solution of the tetrazine in DMSO (10 mM, 10 μL) was diluted with MeCN (1.5 mL), and subsequently PBS (13.5 mL). The solution was filtered and transferred into a quartz cuvette with a path length of 50 mm, and equilibrated at 20°C. The decrease of the absorption band at 520 nm (characteristic for the tetrazine moiety in water) was monitored using UV spectroscopy. The rate of hydrolysis and half time was derived from the slope of a plot of ln(1-x) versus time. The calculated half time is 2.0 h.

Reaction kinetics between UPy-OEG$_6$-Tz (2) and several dienophiles. The second order reaction constant of the reaction between UPy-OEG$_6$-Tz (**2**) and a dienophile was determined under second order conditions in MeCN at 20 °C by UV spectroscopy. A cuvette was filled with MeCN (3 mL) and equilibrated at 20 °C. The UPy-OEG$_6$-Tz (**2**) was added, followed by a stoichiometric amount of the dienophile, both as stock solutions in DMSO. The concentration of both reactants was identical and approximately 20 μM. The absorption at 540 nm (characteristic for the tetrazine moiety in MeCN) was measured every second for the fastest reaction, or with longer intervals for the slower reactions. From this absorption at 540 nm, the concentration of tetrazine was calculated using a molar absorption coefficient of ε=430 M^{-1}cm^{-1}. The second order rate constant k_2 was obtained from the slope of a plot of ($1/c − 1/c_0$) versus time.

Cell culture

HK-2 cell culture. Human proximal tubule epithelial kidney-2 (HK-2) cells were thawed from liquid N2 tank and cultured on 0.1 % gelatin / PBS pre-coated T75 flask in complete medium. Complete medium consisted of DMEM with 10 v% FBS and 1 v% pencillin-streptomycin solution. Cells were cultured up to 80-90% confluence at 37 °C and 5% CO2 in a humidified atmosphere. Cells were washed with PBS twice and 0.05% trypsin-EDTA was used 2-3 minutes to detach the cells from culture flask. Trypsin was inactivated by addition of complete medium and

cell suspension was transferred to a 15 mL falcon tube and centrifuged at 1000 rpm for 5 minutes. The supernatant was aspirated and the cell pellet was resuspended in complete medium. Cell concentrations were determined *via* cell counting by the use of a hemocytometer.

HK-2 cell seeding on spincoated scaffolds. Transwell inserts were sterilized in 70% ethanol bath and placed in a LAF-cabinet to evaporate the ethanol from the inserts. Spincoated coverslips were placed in the bottom ring of the transwells using sterile forceps. The top of the insert was placed on top of the bottom ring and transferred to a 12-wells plate. The coverslips were sterilized under UV for 30 minutes. Cells were trypsinized and cell concentration was determined *via* cell counting in a hemocytometer. The cells were diluted untill a concentration of 60.000 cells·mL^{-1} and 500 µL of cell suspension was added to each transwell insert. Cells were cultured for 24 h, 72 h or one week at 37 °C and 5% CO_2 in a humidified atmosphere. Cell medium was changed ones for the 72 h culture and twice for the 1-week culture.

HK-2 cell culture procedure in competition assay. Transwell inserts were sterilized in 70% ethanol bath and placed in a LAF-cabinet to evaporate the ethanol from the inserts. Spincoated coverslips were placed in the bottom ring of the transwells using sterile forceps. The top of the insert was placed on top of the bottom ring and transferred to a 12-wells plate. The coverslips were sterilized under UV for 30 minutes. PEG-BCN powder was diluted in complete medium untill a concentration of 0.5 mg·mL^{-1}. Cells were trypsinized and cell concentration was determined *via* cell counting in a hemocytometer. The cells were diluted till a concentration of 60.000 cells · mL^{-1}. The cells were divided in four 15 mL falcon tubes and centrifuged at 1000 rpm for 5 minutes. The supernatant was aspirated and the cell pellet was resuspended in PEG-BCN solutions in complete medium. 500 µL of cell suspension was added to each transwell insert and cells were cultured for 24 h or 72 h at 37 °C and 5% CO_2 in a humidified atmosphere. Cell medium was changed ones for the 72 h culture.

HK-2 cell fixation, staining and visualization. After the culture period, scaffolds were washed three times with PBS. Cells were fixated in 3.7% formaldehyde in PBS and permeabilized in 0.5% Triton-X 100 buffer for 20 minutes. Coverslips were washed three times with PBS and blocked in 500 µL 5 wt/v% BSA solution in PBS for 45 minutes. Coverslips were removed from the transwell inserts and placed cell-side up on a parafilm covered glass plate in a moisturized chamber. Anti-vinculin (monoclonal IgG1 anti-vinculin mouse antibody) was diluted in a 2% BSA in PBS solution at a concentration of 1:400 and 50 µL of solution was incubated at room temperature for 90 minutes. Cells were washed twice with PBS before incubated with goat anti-mouse IgG1 Alexa 555 antibody (1:200) diluted in 2% BSA in PBS solution with phalloidin Atto 488 (1:1000) for 60 minutes at room temperature. Then, cell nuclei were stained with Hoechst (1:1000) for 15 minutes at room temperature. The coverslips were washed five times with PBS and mounted on microscope slides using Mowiol. The samples were visualized by fluorescence microscopy using a 10x and 20x magnifying objective on a Zeiss Axio observer D1 equipped with an AxioCam Mrm camera and Zeiss Axiovision software (Carl Zeiss).

6.5 References

1. Thevenot, P., Hu, W. & Tang, L. Surface Chemistry Influence Implant Biocompatibility. *Curr. Top. Med. Chem.* **8,** 270–280 (2008).
2. Chen, C. *et al.* Research trends in biomimetic medical materials for tissue engineering: 3D bioprinting, surface modification, nano/micro-technology and clinical aspects in tissue engineering of cartilage and bone. *Biomater. Res.* **20,** 10 (2016).
3. Damodaran, V. B. & Murthy, N. S. Bio-inspired strategies for designing antifouling biomaterials. *Biomater. Res.* **20,** 18 (2016).
4. Grainger, D. W. All charged up about implanted biomaterials. *Nat. Biotechnol.* **31,** 507–509 (2013).
5. Wei, Q. *et al.* Protein Interactions with Polymer Coatings and Biomaterials. *Angew. Chem. Int. Ed.* **53,** 8004–8031 (2014).
6. Leonard, E. F. & Vroman, L. Is the Vroman effect of importance in the interaction of blood with artificial materials? *J. Biomater. Sci. Polym. Ed.* **3,** 95–107 (1991).
7. Gittens, J. E., Smith, T. J., Suleiman, R. & Akid, R. Current and emerging environmentally-friendly systems for fouling control in the marine environment. *Biotechnol. Adv.* **31,** 1738–1753 (2013).
8. Banerjee, I., Pangule, R. C. & Kane, R. S. Antifouling coatings: recent developments in the design of surfaces that prevent fouling by proteins, bacteria, and marine organisms. *Adv. Mater.* **23,** 690–718 (2011).
9. Chen, S., Li, L., Zhao, C. & Zheng, J. Surface hydration: Principles and applications toward low-fouling/nonfouling biomaterials. *Polymer* **51,** 5283–5293 (2010).
10. Jeon, S. I., Lee, J. H., Andrade, J. D. & De Gennes, P. G. Protein—surface interactions in the presence of polyethylene oxide. *J. Colloid Interface Sci.* **142,** 149–158 (1991).
11. Fuertges, F. & Abuchowski, A. The clinical efficacy of poly(ethylene glycol)-modified proteins. *J. Controlled Release* **11,** 139–148 (1990).
12. Prime, K. L. & Whitesides, G. M. Adsorption of proteins onto surfaces containing end-attached oligo(ethylene oxide): a model system using self-assembled monolayers. *J. Am. Chem. Soc.* **115,** 10714–10721 (1993).
13. Thalla, P. K. *et al.* A Versatile Star PEG Grafting Method for the Generation of Nonfouling and Nonthrombogenic Surfaces. *BioMed Res. Int.* **2013,** e962376 (2012).
14. Strehmel, C. *et al.* Geometric Control of Cell Alignment and Spreading within the Confinement of Antiadhesive Poly(Ethylene Glycol) Microstructures on Laser-Patterned Surfaces. *ACS Biomater. Sci. Eng.* **1,** 747–752 (2015).
15. Ostuni, E. *et al.* Self-Assembled Monolayers That Resist the Adsorption of Proteins and the Adhesion of Bacterial and Mammalian Cells. *Langmuir* **17,** 6336–6343 (2001).
16. Zhang, Z. *et al.* Surface modification of PDMS by surface-initiated atom transfer radical polymerization of water-soluble dendronized PEG methacrylate. *Colloids Surf. B Biointerfaces* **88,** 85–92 (2011).
17. Yang, W. J., Neoh, K.-G., Kang, E.-T., Teo, S. L.-M. & Rittschof, D. Polymer brush coatings for combating marine biofouling. *Prog. Polym. Sci.* **39,** 1017–1042 (2014).
18. Wang, J. & Li, J. Dopamine-assisted deposition of lubricating and antifouling coatings on polyurethane surfaces by one-pot ATRP and click chemistry. *Mater. Lett.* **186,** 178–181 (2017).
19. Li, L. L., Qi, G.-B., Yu, F., Liu, S.-J. & Wang, H. An Adaptive Biointerface from Self-Assembled Functional Peptides for Tissue Engineering. *Adv. Mater.* **27,** 3181–3188 (2015).
20. Liu, P. *et al.* Zwitterionic modification of polyurethane membranes for enhancing the anti-fouling property. *J. Colloid Interface Sci.* **480,** 91–101 (2016).
21. Yang, W. J. *et al.* Layer-by-Layer Click Deposition of Functional Polymer Coatings for Combating Marine Biofouling. *Biomacromolecules* **13,** 2769–2780 (2012).
22. Laradji, A. M., McNitt, C. D., Yadavalli, N. S., Popik, V. V. & Minko, S. Robust, Solvent-Free, Catalyst-Free Click Chemistry for the Generation of Highly Stable Densely Grafted Poly(ethylene glycol) Polymer Brushes by the Grafting To Method and Their Properties. *Macromolecules* **49,** 7625–7631 (2016).
23. Hu, P. *et al.* Synthesis, characterization and antifouling performance of ABC-type fluorinated amphiphilic triblock copolymer. *Polym. Bull.* **73,** 1405–1426 (2016).
24. Voo, Z. X. *et al.* Antimicrobial/Antifouling Polycarbonate Coatings: Role of Block Copolymer Architecture. *Macromolecules* **48,** 1055–1064 (2015).
25. Chen, K., Zhou, S. & Wu, L. Self-repairing nonfouling polyurethane coatings via 3D-grafting of PEG-b-PHEMA-b-PMPC copolymer. *RSC Adv.* **5,** 104907–104914 (2015).
26. Deng, J. *et al.* Versatile and Rapid Postfunctionalization from Cyclodextrin Modified Host Polymeric Membrane Substrate. *Langmuir* **31,** 9665–9674 (2015).

27. Shi, H. *et al.* Antibacterial and biocompatible properties of polyurethane nanofiber composites with integrated antifouling and bactericidal components. *Compos. Sci. Technol.* **127,** 28–35 (2016).

28. Chen, Y., Zhao, X. & He, C. Dual-mode antifouling ability of PVDF membrane with a surface-anchored amphiphilic polymer. *RSC Adv.* **5,** 68998–69005 (2015).

29. Dang, Y., Quan, M., Xing, C.-M., Wang, Y.-B. & Gong, Y.-K. Biocompatible and antifouling coating of cell membrane phosphorylcholine and mussel catechol modified multi-arm PEGs. *J. Mater. Chem. B* **3,** 2350–2361 (2015).

30. Dalsin, J. L., Hu, B.-H., Lee, B. P. & Messersmith, P. B. Mussel Adhesive Protein Mimetic Polymers for the Preparation of Nonfouling Surfaces. *J. Am. Chem. Soc.* **125,** 4253–4258 (2003).

31. Qun Xu, L. *et al.* Synthesis of catechol and zwitterion-bifunctionalized poly(ethylene glycol) for the construction of antifouling surfaces. *Polym. Chem.* **7,** 493–501 (2016).

32. Sijbesma, R. P. *et al.* Reversible polymers formed from self-complementary monomers using quadruple hydrogen bonding. *Science* **278,** 1601–1604 (1997).

33. Folmer, B. J. B., Sijbesma, R. P., Versteegen, R. M., van der Rijt, J. a. J. & Meijer, E. W. Supramolecular Polymer Materials: Chain Extension of Telechelic Polymers Using a Reactive Hydrogen-Bonding Synthon. *Adv. Mater.* **12,** 874–878 (2000).

34. Dankers, P. Y. W., Harmsen, M. C., Brouwer, L. A., Van Luyn, M. J. A. & Meijer, E. W. A modular and supramolecular approach to bioactive scaffolds for tissue engineering. *Nat. Mater.* **4,** 568–574 (2005).

35. Muylaert, D. E. P. *et al.* Early in-situ cellularization of a supramolecular vascular graft is modified by synthetic stromal cell-derived factor-1α derived peptides. *Biomaterials* **76,** 187–195 (2016).

36. van Almen, G. C. *et al.* Development of Non-Cell Adhesive Vascular Grafts Using Supramolecular Building Blocks. *Macromol. Biosci.* **16,** 350–362 (2016).

37. Pape, A. C. H., Ippel, B. D. & Dankers, P. Y. W. Cell and protein fouling properties of polymeric mixtures containing supramolecular poly(ethylene glycol) additives. *Langmuir* **33,** 4076-4082 (2017).

38. Mollet, B. B. *et al.* A modular approach to easily processable supramolecular bilayered scaffolds with tailorable properties. *J. Mater. Chem. B* **2,** 2483–2493 (2014).

39. Goor, O. J. G. M. *et al.* Efficient Functionalization of Additives at Supramolecular Material Surfaces. *Adv. Mater.* **29,** 1604652 (2017).

40. Blackman, M. L., Royzen, M. & Fox, J. M. Tetrazine Ligation: Fast Bioconjugation Based on Inverse-Electron-Demand Diels–Alder Reactivity. *J. Am. Chem. Soc.* **130,** 13518–13519 (2008).

41. McKay, C. S. & Finn, M. G. Click Chemistry in Complex Mixtures: Bioorthogonal Bioconjugation. *Chem. Biol.* **21,** 1075–1101 (2014).

42. Morgese, G. *et al.* Topological Polymer Chemistry Enters Surface Science: Linear versus Cyclic Polymer Brushes. *Angew. Chem. Int. Ed.* **55,** 15583–15588 (2016).

43. Tagaya, M. In situ QCM-D study of nano-bio interfaces with enhanced biocompatibility. *Polym. J.* **47,** 599–608 (2015).

44. Wang, X. *et al.* Discriminating the Independent Influence of Cell Adhesion and Spreading Area on Stem Cell Fate Determination Using Micropatterned Surfaces. *Sci. Rep.* **6,** 28708 (2016).

45. Rossin, R. *et al.* In vivo chemistry for pretargeted tumor imaging in live mice. *Angew. Chem. Int. Ed.* **49,** 3375–3378 (2010).

46. Devaraj, N. K., Hilderbrand, S., Upadhyay, R., Mazitschek, R. & Weissleder, R. Bioorthogonal Turn-On Probes for Imaging Small Molecules inside Living Cells. *Angew. Chem. Int. Ed.* **49,** 2869–2872 (2010).

47. Lang, K. *et al.* Genetically encoded norbornene directs site-specific cellular protein labelling via a rapid bioorthogonal reaction. *Nat. Chem.* **4,** 298–304 (2012).

48. Flavel, B. S. *et al.* Grafting of Poly(ethylene glycol) on Click Chemistry Modified Si(100) Surfaces. *Langmuir* **29,** 8355–8362 (2013).

49. Wang, C., Ma, C., Mu, C. & Lin, W. A Novel Approach for Synthesis of Zwitterionic Polyurethane Coating with Protein Resistance. *Langmuir* **30,** 12860–12867 (2014).

50. Kostina, N. Y. *et al.* Non-Fouling Biodegradable Poly(ϵ-caprolactone) Nanofibers for Tissue Engineering. *Macromol. Biosci.* **16,** 83–94 (2016).

51. Xu, L. Q. *et al.* Antifouling coatings based on covalently cross-linked agarose film via thermal azide-alkyne cycloaddition. *Colloids Surf. B Biointerfaces* **141,** 65–73 (2016).

52. Felgueiras, H. P. *et al.* Octadecyl Chains Immobilized onto Hyaluronic Acid Coatings by Thiol-ene 'Click Chemistry' Increase the Surface Antimicrobial Properties and Prevent Platelet Adhesion and Activation to Polyurethane. *ACS Appl. Mater. Interfaces* **9,** 7979–7989 (2017).

53. Hui, N., Sun, X., Niu, S. & Luo, X. PEGylated Polyaniline Nanofibers: Antifouling and Conducting Biomaterial for Electrochemical DNA Sensing. *ACS Appl. Mater. Interfaces* **9,** 2914–2923 (2017).

54. Zhi, Z. *et al.* Dual-Functional Polyethylene Glycol-b-polyhexanide Surface Coating with in Vitro and in Vivo Antimicrobial and Antifouling Activities. *ACS Appl. Mater. Interfaces* **9,** 10383–10397 (2017).

55. Lang, K. *et al.* Genetic Encoding of Bicyclononynes and trans-Cyclooctenes for Site-Specific Protein Labeling in Vitro and in Live Mammalian Cells via Rapid Fluorogenic Diels–Alder Reactions. *J. Am. Chem. Soc.* **134,** 10317–10320 (2012).

56. Selvaraj, R. & Fox, J. M. trans-Cyclooctene — a stable, voracious dienophile for bioorthogonal labeling. *Curr. Opin. Chem. Biol.* **17,** 753–760 (2013).

57. Darko, A. *et al.* Conformationally strained trans -cyclooctene with improved stability and excellent reactivity in tetrazine ligation. *Chem. Sci.* **5,** 3770–3776 (2014).

58. Thalhammer, F., Wallfahrer, U. & Sauer, J. Reaktivität einfacher offenkettiger und cyclischer dienophile bei Diels-Alder-reaktionen mit inversem elektronenbedarf. *Tetrahedron Lett.* **31,** 6851–6854 (1990).

59. Taylor, M. T., Blackman, M. L., Dmitrenko, O. & Fox, J. M. Design and Synthesis of Highly Reactive Dienophiles for the Tetrazine–trans-Cyclooctene Ligation. *J. Am. Chem. Soc.* **133,** 9646–9649 (2011).

60. Rossin, R. & Robillard, M. S. Pretargeted imaging using bioorthogonal chemistry in mice. *Curr. Opin. Chem. Biol.* **21,** 161–169 (2014).

EPILOGUE

Towards biomaterials for regenerative medicine applications

Biological systems are exceptionally complex and hence materials science faces an immense challenge in the design and synthesis of materials that are capable of recapitulating the structural and functional complexity found in biological materials. The biological microenvironment is a dynamic interplay between cells and biochemical and biophysical cues and artificial analogues are required to mimic this situation while at the same time being biocompatible, biodegradable and equipped with the desired mechanical properties. [1] Advances in the field of synthetic polymers have increased the use of biomaterials in health care applications. [2] Biomaterials that find their application in regenerative medicine rely on design parameters that emerge from an interdisciplinary interplay of biology, clinical medicine, material science, physics and chemistry. [3] The structural dynamic nature of supramolecular polymer assemblies facilitates advantages over conventional covalent polymers in their biomaterial applications, which arise from the association of monomers *via* noncovalent interactions. As a result of the reversibility of the noncovalent interactions, these polymers are dynamic and yet are able to change in length and structure, giving rise to adaptive properties. Moreover, mechanical properties of these materials can easily be tuned by changing either the supramolecular motif or the polymer that will be modified with a supramolecular motif.

In order to advance towards life-like supramolecular biomaterials, there are many design criteria that should be taken into account when synthesizing supramolecular thermoplastic elastomers. The work described in this dissertation aimed to selectively introduce bioactivity at the supramolecular material surface and four different approaches were investigated. In addition to bioactivity, it is proposed that mechanical properties are important and should be able to meet requirements of the native environment. Moreover, upon implantation the biomaterial not only has to execute a certain function, the material should be able to adapt to the environment, i.e. healing and growth. Herewith responsiveness to the native environment plays a crucial role as well. [4] Altogether, from a material design point of view, these requirements should be taken care of when developing new materials for regenerative medicine. Supramolecular biomaterials can replicate aspects of structural and/or functional features of biological signal transduction. As synthetic scaffolds, supramolecular biomaterials can act as structural mimics of fibrous matrix components. [5]

In order to enable the introduction of surface functionality into supramolecular polymer materials, fundamental understanding on the tunability and molecular design of the materials is a prerequisite. The ureido-pyrimidinone (UPy) quadruple hydrogen bonding motif, which upon polymer functionalization generates supramolecular polymer materials and is extensively studied in biomaterial applications, such as hydrogels[6–9], drug delivery vehicles [10,11] and thermoplastic elastomer materials [12–19].

Implications of the work

Activation of supramolecular biomaterial surfaces using UPy-modified additives *via* post-modification is investigated in this dissertation. To this end, four different approaches have been investigated (Figure 1), based on the incorporation of UPy-functionalized peptides, natural interactions *via* heparin chemistry, a selective supramolecular approach based on cucurbit[8]uril (Q8) host-guest chemistry and a covalent click chemistry approach.
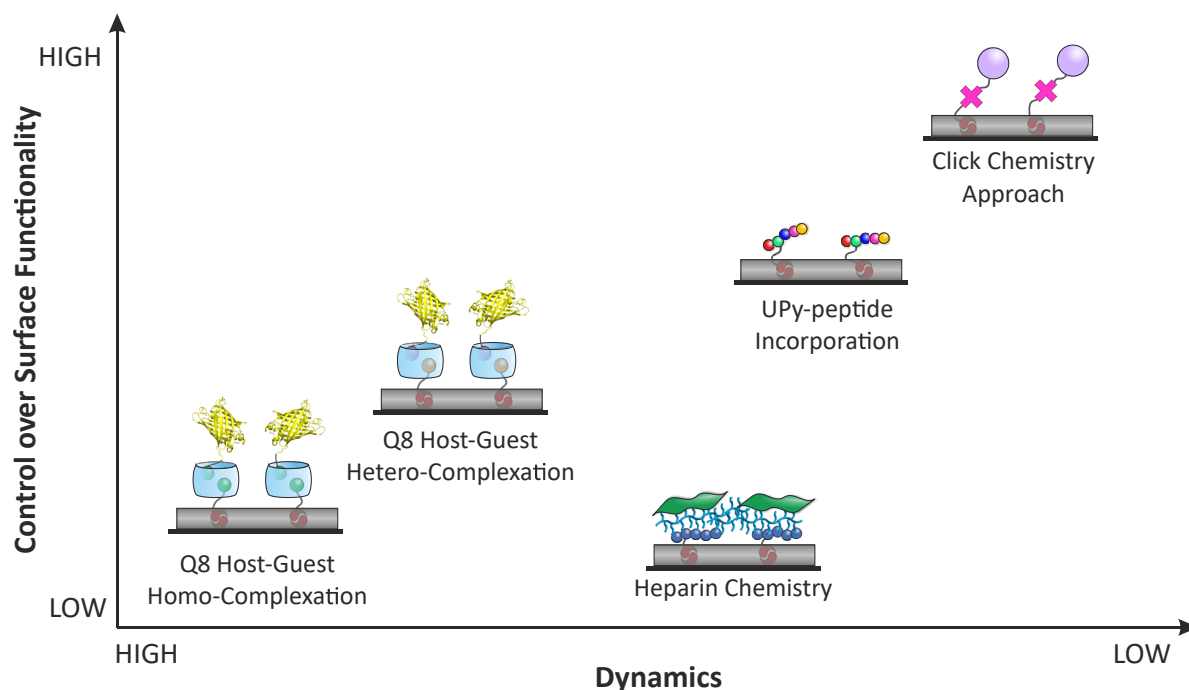
Figure 1. Surface functionalization approaches established on supramolecular UPy-based materials using UPy-additives with regard to the dynamics of the system in relation to the control on surface functionalization.

Modular peptide modification

The introduction of surface functionality can be achieved by the incorporation of bioactive UPy-peptides, which represent mimics of the active domains of proteins. Different synthetic approaches to efficiently synthesize UPy-peptide conjugates were explored in chapter 3. Although synthetically easily accessible, moderate control on surface functionalization and a low level of dynamics, there are limitations in this approach as well. First of all, upon co-assembly of the UPy-peptides and UPy-polymers, the exact surface distribution and enhancement of the UPy-peptides cannot be controlled. Moreover, due to the processing conditions of the UPy-polymers, full length proteins and growth factors cannot be synthesized *via* this approach, as they will denature and lose their activity upon material formulation. However, when combined with other strategies to introduce specific surface functionality, the supramolecular biomaterials can greatly benefit from the incorporation of UPy-peptide conjugates. Upon degradation and surface erosion of the materials, UPy-peptides that are present in the bulk of the material will be exposed to the surroundings and thereby facilitate bioactive function.

Heparin complexation chemistry

Surface modification based on heparin chemistry was investigated in chapter 3. *Via* the modular incorporation of UPy-heparin binding peptides and subsequent heparin immobilization onto the material surface, a platform for growth factor binding was established. The subsequent immobilization of TGF-ß3 onto the heparin or TGF-ß3 supplied into the growth medium of MEEC resulted both in morphological changes as well as gene expression responses of the cells. The ability to endogenously capture growth factors that exhibit a heparin binding domain facilitates a broad scope of bioactive cues that can be immobilized onto the material surface and thereby determine the functionality. However, the extent to which the surface functionality can be controlled is limited. This can be an issue in an *in vivo* situation upon implantation, as due to the reversible nature of the electrostatic interactions also undesirable immobilization might occur. Moreover, it is speculated that heparin exerts a dual role in blood coagulation. [20] Heparin is known to be applied as a potent anticoagulation drug. [21,22] Upon surface immobilization, heparin is known to improve anti-coagulation performance of biomaterials. [23,24] However, heparin is also proposed to play an important role in the intrinsic pathway of blood coagulation due to its dense negative charge. [20]

Supramolecular host-guest complexation

The introduction of surface functionality *via* a bifunctional additive, which is equipped with a UPy-moiety on the one hand, to ensure supramolecular incorporation in the bulk of the material, and an FGG-peptide motif on the other hand to facilitate Q8 mediated host-guest assembly, is described in chapter 4. The immobilization of proteins that were equipped with an *N*-terminal FGG peptide motif was successfully demonstrated. However, as a result of the dynamic nature of the Q8-mediated host-guest assembly, the immobilization was highly reversible and therefore control on surface functionalization is limited. Moreover, the strong hydrophobic interactions of the Q8 with the supramolecular material surface resulted in undesired nonspecific adsorption, which could be overcome by modifying the materials to exhibit an intrinsically more hydrophilic surface. Hetero Q8 mediated ternary complex formation as opposed to the double FGG peptide motif could potentially introduce a more robust modification approach. The reversible nature might be beneficial to induce a burst release from the biomaterial surface upon implantation.

Reactive post-modification

Surface modifications based on efficient covalent post-modification *via* a reactive UPy-tetrazine additive were described in chapter 5. The inverse Diels-Alder cycloaddition between tetrazine and *trans*-cyclooctene turned out to be very accessible at the material surface. Moreover, as a result of the enhanced presence of the UPy-tetrazine additive at the material surface, a platform for selective and efficient functionalization was assessed. The modification *via* this approach results in solely surface functionalization and furthermore facilitates control

on surface modification. As a result of the covalent character of this modification strategy, the functionalization is considered to be more stable as opposed to the supramolecular approaches that were explored in chapter 3 and 4. The results showed that adjacent to small molecules also full length proteins could successfully be introduced at the material surface. The surface functionality of interest can be modified with a reaction partner of the tetrazine and after material formulation the reaction can be performed at the material surface. Translation towards electrospun scaffolds resulted in selective surface modification of the electrospun fibers. Additionally, the detailed analysis of the functionalized materials using different characterization methods has shown to be important to understand the essential material performance.

The post-modification approach *via* the incorporation of a reactive UPy-tetrazine additive was investigated to introduce an anti-fouling surface coating in chapter 6. The cycloaddition between tetrazine and bicyclononyne (BCN) was employed, by functionalization of three different poly(ethylene glycol) (PEG) polymers, i.e. monofunctional, bifunctional and star-shaped, with this BCN moiety. The performance of the anti-fouling coatings was assessed both by protein adsorption studies as well as cell adhesion at the material surface. The bifunctional-PEG-BCN and star-PEG-BCN coatings showed complete anti-fouling performance whereas the monofunctional-PEG-BCN was only able to reduce protein and cell adhesion. These results demonstrated that the degree of material functionalization, in this case the introduction of an anti-fouling coating, greatly determines the ultimate performance. The bifunctional-PEG-BCN and star-PEG-BCN polymers were able to conjugate onto the surface with multiple anchor points, which enhanced the formation of an effective coating. Future developments along these lines involve the introduction of specific bioactive cues to introduce selective bioactive functionality at the material surface.

From a fundamental material development perspective, the molecular design of the tetrazine additive was investigated in chapter 6. Based on the incorporation of oligo(ethylene glycol) (OEG) spacers of different length the surface properties were evaluated. The length of OEG spacer determined the onset of phase separation at the material surface. Moreover, the longer OEG spacer exhibits enhanced ability to induce rearrangements at the surface upon exposure to an aqueous environment. The results provided useful insights which can be of importance in future material design, i.e. the incorporation of additives without an OEG spacer results in sec surface functionalization, whereas a longer OEG spacer allows for enhanced flexibility.

The different approaches that are described in this dissertation rely on thorough characterization of the material surfaces in order to increase the understanding of the material composition and performance. Among the physical characterization methods that were explored, i.e. XPS, 3D ToF-SIMS MS, fluorescence spectroscopy and QCM-D, other characterization techniques are available to study material surfaces. In particular, we were interested to explore super-resolution microscopy to elucidate surface properties as well as patterning to selectively introduce spatial organization at the material surface. Super-resolution microscopy is envisioned to gain surface understanding at the nanometer scale.

Patterning techniques are able to introduce topological control on the functionalization of material surfaces.

Elucidating surface composition and reactivity using super-resolution microscopy

From a fundamental research point of view, it is of interest to investigate the surface properties of the supramolecular biomaterials to improve material development. In recent years, the development of super-resolution fluorescence spectroscopy has proven to be a powerful technique for the direct observation of mechanistic details on the nanoscale. [25] The resolution of high-end fluorescence microscopy is determined by the diffraction limit, which is in the order of 250 nm, whereas new super-resolution technology approaches single-molecule localization, achieving spatial resolution in lateral and axial directions (~20 nm and ~50 nm, respectively). [26,27]

In super-resolution localization microscopy, an image is reconstructed based on the observation of individual fluorescent molecules. Separation of the emission of the fluorophores allows the detection of diffraction-limited fluorescent signals from single molecules, which can be obtained using among others photoswitchable dyes. [28] The use of photoswitchable dyes gives rise to stochastic optical reconstruction microscopy (STORM), which is able to switch between a fluorescent 'on-state' and a non-emissive 'off-state' of the dyes. More specifically, direct STORM (dSTORM) was developed to allow alternations between the dark and the fluorescent states due to chemical modification of the dyes with a primary thiol. [29]

In our group, STORM imaging has been employed to investigate exchange dynamics in supramolecular 1,3,5-benzenetricarboxamide (BTA) polymers to unravel the exchange dynamics of these supramolecular fibers in solution. [30] However, the use of super-resolution microscopy imaging at polymer material films, nanoparticles and gels is scarce. [31–35]

It is proposed that surface compositional understanding is important to tune the design parameters and this can be investigated by the use of super-resolution microscopy to reveal surface properties of the supramolecular material. In collaboration with dr. Daan van der Zwaag and Moniek Schmitz, Msc, we preliminary investigated the ability to determine the UPy-tetrazine distribution at the surface of supramolecular material films using dSTORM. To this end, a TCO-modified Cyanine 5 dye (TCO-Cy5) was synthesized, which in the triplet state reduces fluorescence intensity and blinking. We aimed to localize the UPy-tetrazine moieties at the material surface as a result of the blinking behavior of the TCO-Cy5, i.e. the covalent anchoring of the TCO-Cy5 was hypothesized to induce localized blinking.

The signal of bare glass and bare PCLdiUPy polymer films was investigated prior to the incorporation of UPy-Tz and functionalization with TCO-Cy5 dye. The glass coverslip showed minor blinking, which can be removed when a density filter is applied (Figure 2A). The PCLdiUPy surface presented a large number of blinking spots, which accounted for a large amount background fluorescence (Figure 2B). A zoom of a bright blinking area revealed a high density of the localizations, which are impossible to be filtered out when applying a post-analysis threshold.

Optimization of the background blinking that was observed, resulted in measurement at 50% laser power, to distinguish between background blinks and fluorescent signals. The TCO-Cy5 was introduced both at the PCLdiUPy (Figure 2 C,D) and PCLdiUPy with 1 mol% UPy-Tz (Figure 3 E,F) material surfaces. The results provided highly inconclusive results, as for both the PCLdiUPy and PCLdiUPy with 1 mol% UPy-Tz large variations between the samples were observed. Different washing protocols were employed as well as multiple sample preparation methods, which did not lead to optimized surface behavior.
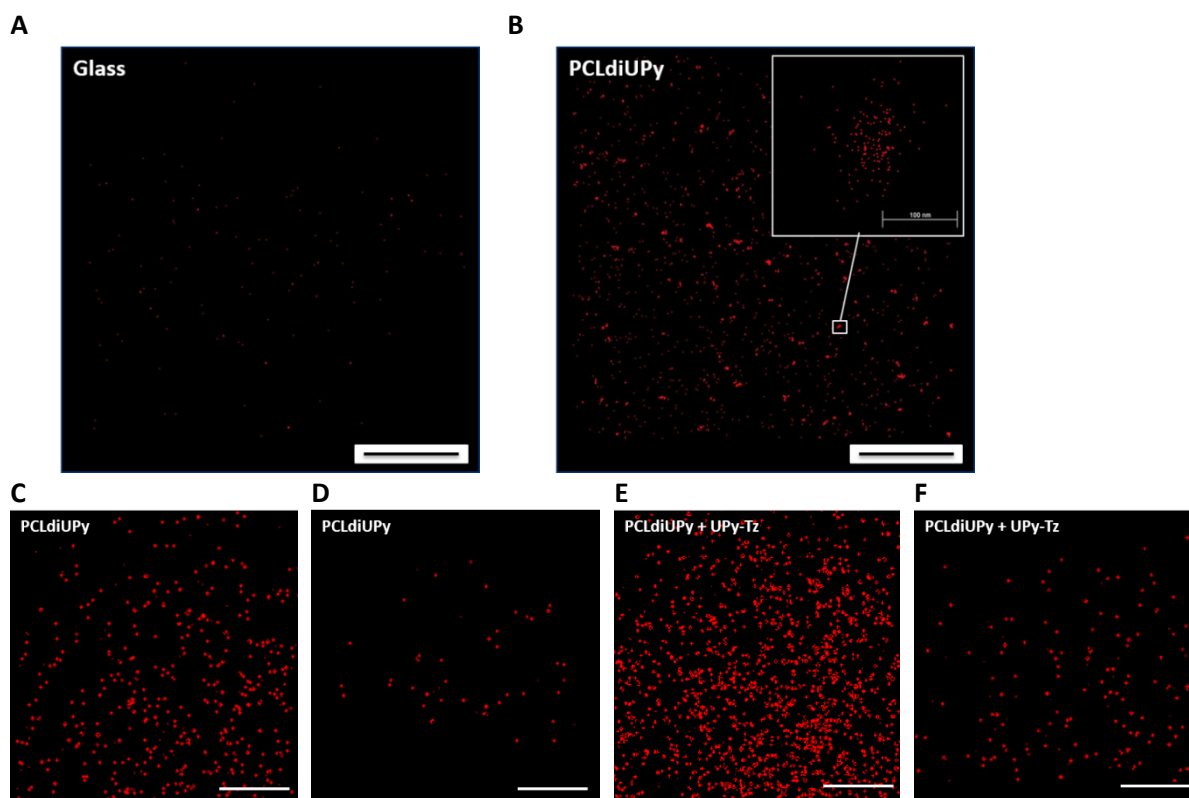

Figure 2. Surface analysis by STORM measurements, A) Glass coverslip that was cleaned with piranha and silanized, B) Spincoated PCLdiUPy polymer film and a zoom of a dense localization, C+D) PCLdiUPy surfaces after TCO-Cy5 introduction and E+F) PCLdiUPy with 1 mol% UPy-Tz surfaces after TCO-Cy5 introduction. The samples were excitation with a laser at 647 nm, scale bars represent 10 μm and 100 nm for the zoom-in. STORM measurements: the spincoated samples were mounted upside down on a microscope glass slide with double sided tape to create a flow chamber. Incubation of the dye molecules was performed, prior to assembly of the flow chamber. The sample were washed with TRIS buffer (twice) and STORM buffer (50 mM Tris pH 8, oxygen scavenging system (glucose oxidase, catalase), glucose and 10 mM 2-aminoethanethiol) (twice). A 2 pM concentration of TCO-Cy5 was used and thoroughly washed after incubation. STORM experiments were performed using a Nikon N-STORM system configured for total internal reflection fluorescence (TIRF) imaging. The excitation inclination was tuned to maximize the signal-to-noise ratio. No activation UV light was employed. Fluorescence was collected with a Nikon 100x, 1.4NA oil immersion objective and passed through a quad-band pass dichroic filter (97335 Nikon). Different time lapses were recorded in 256×256 or 128×128-pixel region of an EMCCD camera (ixon3, Andor). For the 256×256 region 33,000 frames were acquired and for 128×128 region 50,000 frames. The value of the intensity filter was experimentally determined. The amount of localizations over time were analyzed using Matlab and plotted. In experiments with a photon threshold an additional photon filter was used to selectively remove the low intensity blinks.

In conclusion, the surface functionalization analysis of supramolecular material films using super-resolution microscopy at this point does not provide useful insights on the surface composition and UPy-Tz availability at the material surface. The high amount of non-specific

adsorption and irreproducibility of the results leaves room for improvement. Different STORM dyes with a more hydrophilic character might be investigated, as well as the use of beads to ensure proper surface focus. In summary, STORM potentially can provide a correlation between reactive moieties at the material surface correlated to the amount of dyes that can be localized.

Future recommendation in the development of supramolecular biomaterials for regenerative medicine applications

The advantage in the use of supramolecular biomaterials lies in their modular character, i.e. material properties can easily be tuned and depending on the application, specific cues can be incorporated. In addition, the tunable, biomimetic and responsive material behavior, which results from the inherently dynamic and reversible character of the non-covalent interactions, provides supramolecular materials with unique properties across different length scales. However, the translation of supramolecular biomaterials also faces difficulties that need to be overcome. Consequently, the number of supramolecular biomaterials that is in clinical use are limited. Supramolecular systems generally require synthetic procedures that are tedious and result only in small scale quantities, which brings along high costs. Moreover, as compared to their conventional analogues, which can be produced at industrial-scale, efficiency in synthesizing supramolecular materials should be improved. Nevertheless, the ease to customize supramolecular biomaterials by the incorporation of patient-specific cues is considered a great value for future bench to bedside developments.

Future developments should leverage methods to improve the material formulation and processing as well as control the precise surface and bulk definition. Here, it is important to mimic the natural environment of the implantation site in the host, both in terms of structure and function. Supramolecular biomaterials are envisioned to be perfectly suitable to meet the level of complexity that is found in the biological environment, as the complex assemblies can easily be tuned. As a result of this modular approach, functionality and structural features can be controlled. In addition, the spatiotemporal control in the regeneration process with regard to bioactivity, mechanical properties and chemical composition should be taken into account. Ultimately, this will then lead to the engineering of patient-specific tailored materials, *en route* to advance from supramolecular biomaterial design towards regenerative medicine solutions.

References

1. Edalat, F., Sheu, I., Manoucheri, S. & Khademhosseini, A. Material strategies for creating artificial cell-instructive niches. *Curr. Opin. Biotechnol.* **23,** 820–825 (2012).
2. Langer, R. & Tirrell, D. A. Designing materials for biology and medicine. *Nature* **428,** 487–492 (2004).
3. Pashuck, E. T. & Stevens, M. M. Designing regenerative biomaterial therapies for the clinic. *Sci. Transl. Med.* **4,** 160sr4 (2012).
4. Wojtecki, R. J., Meador, M. A. & Rowan, S. J. Using the dynamic bond to access macroscopically responsive structurally dynamic polymers. *Nat. Mater.* **10,** 14–27 (2011).
5. Webber, M. J., Appel, E. A., Meijer, E. W. & Langer, R. Supramolecular biomaterials. *Nat. Mater.* **15,** 13–26 (2016).
6. Guo, M. *et al.* Tough Stimuli-Responsive Supramolecular Hydrogels with Hydrogen-Bonding Network Junctions. *J. Am. Chem. Soc.* **136,** 6969–6977 (2014).
7. Dankers, P. Y. W. *et al.* Hierarchical Formation of Supramolecular Transient Networks in Water: A Modular Injectable Delivery System. *Adv. Mater.* **24,** 2703–2709 (2012).
8. Kieltyka, R. E. *et al.* Mesoscale Modulation of Supramolecular Ureidopyrimidinone-Based Poly(ethylene glycol) Transient Networks in Water. *J. Am. Chem. Soc.* **135,** 11159–11164 (2013).
9. Dankers, P. Y. W. *et al.* Development and in-vivo characterization of supramolecular hydrogels for intrarenal drug delivery. *Biomaterials* **33,** 5144–5155 (2012).
10. Bastings, M. M. C. *et al.* A Fast pH-Switchable and Self-Healing Supramolecular Hydrogel Carrier for Guided, Local Catheter Injection in the Infarcted Myocardium. *Adv. Healthc. Mater.* **3,** 70–78 (2014).
11. Bakker, M. H., Lee, C. C., Meijer, E. W., Dankers, P. Y. W. & Albertazzi, L. Multicomponent Supramolecular Polymers as a Modular Platform for Intracellular Delivery. *ACS Nano* **10,** 1845–1852 (2016).
12. Dankers, P. Y. W., Harmsen, M. C., Brouwer, L. A., Van Luyn, M. J. A. & Meijer, E. W. A modular and supramolecular approach to bioactive scaffolds for tissue engineering. *Nat. Mater.* **4,** 568–574 (2005).
13. Dankers, P. Y. W. *et al.* Chemical and biological properties of supramolecular polymer systems based on oligocaprolactones. *Biomaterials* **27,** 5490–5501 (2006).
14. Dankers, P. Y. W. *et al.* Bioengineering of living renal membranes consisting of hierarchical, bioactive supramolecular meshes and human tubular cells. *Biomaterials* **32,** 723–733 (2011).
15. Bouten, C. V. C. *et al.* Substrates for cardiovascular tissue engineering. *Adv. Drug Deliv. Rev.* **63,** 221–241 (2011).
16. Muylaert, D. E. P. *et al.* Early in-situ cellularization of a supramolecular vascular graft is modified by synthetic stromal cell-derived factor-1α derived peptides. *Biomaterials* **76,** 187–195 (2016).
17. van Almen, G. C. *et al.* Development of Non-Cell Adhesive Vascular Grafts Using Supramolecular Building Blocks. *Macromol. Biosci.* **16,** 350-362 (2016).
18. Mollet, B. B. *et al.* A modular approach to easily processable supramolecular bilayered scaffolds with tailorable properties. *J. Mater. Chem. B* **2,** 2483–2493 (2014).
19. Mollet, B. B., Bogaerts, I. L. J., van Almen, G. C. & Dankers, P. Y. W. A bioartificial environment for kidney epithelial cells based on a supramolecular polymer basement membrane mimic and an organotypical culture system. *J. Tissue Eng. Regen. Med.* **11,** 1820-1834 (2017).
20. Blezer, R., Fouache, B., Willems, G. M. & Lindhout, T. Activation of blood coagulation at heparin-coated surfaces. *J. Biomed. Mater. Res.* **37,** 108–113 (1997).
21. Jaques, L. B. & Mustard, R. A. Some factors influencing the anticoagulant action of heparin. *Biochem. J.* **34,** 153–158 (1940).
22. Gray, E., Hogwood, J. & Mulloy, B. The anticoagulant and antithrombotic mechanisms of heparin. *Handb. Exp. Pharmacol.* 43–61 (2012).
23. Ren, X. *et al.* Immobilized heparin and its anti-coagulation effect on polysulfone membrane surface. *J. Biomater. Sci. Polym. Ed.* **24,** 1707–1720 (2013).
24. Murugesan, S., Xie, J. & Linhardt, R. J. Immobilization of Heparin: Approaches and Applications. *Curr. Top. Med. Chem.* **8,** 80–100 (2008).
25. Schermelleh, L., Heintzmann, R. & Leonhardt, H. A guide to super-resolution fluorescence microscopy. *J. Cell Biol.* **190,** 165–175 (2010).
26. Rust, M. J., Bates, M. & Zhuang, X. Sub-diffraction-limit imaging by stochastic optical reconstruction microscopy (STORM). *Nat. Methods* **3,** 793–796 (2006).
27. Betzig, E. *et al.* Imaging Intracellular Fluorescent Proteins at Nanometer Resolution. *Science* **313,** 1642–1645 (2006).

28.   Bates, M., Huang, B., Dempsey, G. T. & Zhuang, X. Multicolor super-resolution imaging with photo-switchable fluorescent probes. *Science* **317,** 1749–1753 (2007).

29.   Dempsey, G. T. *et al.* Photoswitching Mechanism of Cyanine Dyes. *J. Am. Chem. Soc.* **131,** 18192–18193 (2009).

30.   Albertazzi, L. *et al.* Probing exchange pathways in one-dimensional aggregates with super-resolution microscopy. *Science* **344,** 491–495 (2014).

31.   Urban, B. E. *et al.* Subsurface Super-resolution Imaging of Unstained Polymer Nanostructures. *Sci. Rep.* **6,** 28156 (2016).

32.   Gramlich, M. W., Bae, J., Hayward, R. C. & Ross, J. L. Fluorescence imaging of nanoscale domains in polymer blends using stochastic optical reconstruction microscopy (STORM). *Opt. Express* **22,** 8438–8450 (2014).

33.   Yabiku, Y., Kubo, S., Nakagawa, M., Vacha, M. & Habuchi, S. Super-resolution fluorescence imaging of nanoimprinted polymer patterns by selective fluorophore adsorption combined with redox switching. *AIP Adv.* **3,** 102128 (2013).

34.   Zhu, M.-Q. *et al.* Reversible Fluorescence Switching of Spiropyran-Conjugated Biodegradable Nanoparticles for Super-Resolution Fluorescence Imaging. *Macromolecules* **47,** 1543–1552 (2014).

35.   Conley, G. M., Nöjd, S., Braibanti, M., Schurtenberger, P. & Scheffold, F. Superresolution microscopy of the volume phase transition of pNIPAM microgels. *Colloids and Surfaces A: Physicochem. Eng. Aspects* **499,** 18–23 (2016).

Supramolecular Biomaterials in Action - Bioactivation through Surface Modifications -

The advancement of material science in the design and synthesis of life-like polymeric biomaterials requires understanding of the complexity found in biological materials. When implanted *in vivo*, inevitably the material surface is the first to interact with the biological environment. Therefore, it is important to control both surface composition and the degree of surface modification. Supramolecular materials that are composed of macromers and oligomers that are held together *via* directed, noncovalent interactions, are envisioned to be perfectly suitable to meet requirements to closely mimic the biological environment in a synthetic fashion.

Supramolecular materials based on the quadruple hydrogen bonding motif ureidopyrimidinone (UPy) were developed in our group. Upon end-functionalization of telechelic polymers with UPy-moieties, supramolecular thermoplastic elastomer materials with unique properties can be synthesized. In the development of next generation supramolecular biomaterials, it is of great interest to both study surface and bulk composition of the materials as well as to investigate strategies to introduce function into these materials. The work presented in this dissertation employed UPy-functionalized poly(caprolactone) (PCLdiUPy) supramolecular polymers as the base material. Different approaches were explored that decoupled the material processing conditions and the surface modification strategy *via* the incorporation of different UPy-modified additives. These approaches were systematically studied and allowed for an increasing degree of control on the surface functionalization.

Supramolecular systems based on UPy-modified additives

| UPy-peptide | Heparin chemistry | Cucurbit[8]uril | Click chemistry |
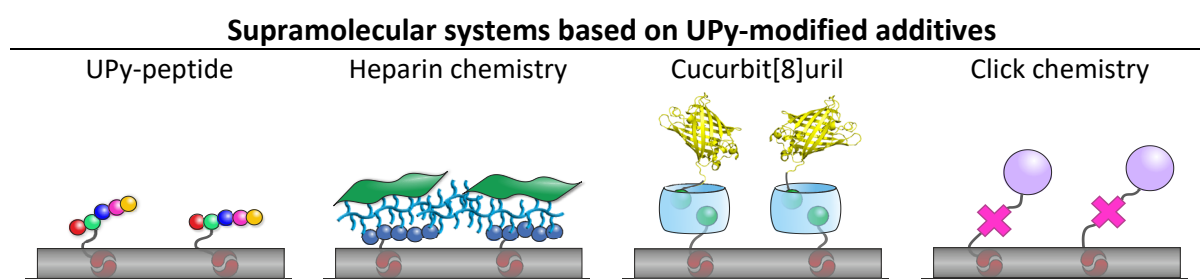
The first approach is based on the modular incorporation of UPy-modified peptide motifs, which provide the material with bioactive cues. In a second approach, specific electrostatic interactions *via* heparin chemistry were introduced, where a UPy-modified heparin binding peptide additive was incorporated, able to bind heparin at the material surface. Subsequently, growth factors that exhibit a heparin binding domain can be introduced and bind to the surface immobilized heparin. A third, truly supramolecular approach based on cucurbit[8]uril (Q8) host-guest chemistry was studied by the incorporation of a UPy additive modified with a specific recognition motif for the Q8 host. Q8 mediated ternary complex formation allowed the introduction of surface functionality in a supramolecular fashion. This approach endorsed functionalization specificity and as a result of the dynamic character of the host-guest complex, the supramolecular assembly was able to reversibly form at the surface. Finally, irreversible surface modification was generated by covalent post-

modification of a UPy additive that was equipped with a reactive tetrazine. Inverse electron demand Diels-Alder (iEDDA) cycloaddition with either *trans*-cyclooctene (TCO) or bicyclononyne (BCN) modified bioactive cues resulted in highly selective and efficient surface functionalization. It was shown that both small molecules, proteins as well as polymeric coatings could be introduced at the surface following this strategy.

In summary, the approaches that were investigated involved the careful design and synthesis of UPy-modified additives that can modularly be incorporated into the supramolecular polymer material. To allow surface modification, a broad scope of dynamics was covered, ranging from truly supramolecular systems to highly selective covalent surface reactions. This work opens up new avenues in the development of UPy-based supramolecular biomaterials that ultimately find their applications in the field of regenerative medicine, *en route* to meet nature's complexity.

Supramoleculaire Biomaterialen in Actie - Bioactivatie door middel van Oppervlakte Modificaties -

Het vakgebied van de materiaalwetenschappen houdt zich onder andere bezig met het ontwikkelen van synthetische materialen met biologische eigenschappen die in het lichaam geïmplanteerd kunnen worden. Om dit soort biomaterialen te ontwerpen is kennis van de complexiteit zoals we die in biologische materialen aantreffen vereist. Wanneer een biomateriaal geïmplanteerd wordt in het lichaam, zal het oppervlak van het materiaal als eerste een interactie aangaan met deze biologische omgeving. Het is daarom uitermate belangrijk om te begrijpen wat de invloed van de chemische samenstelling van het materiaaloppervlak is en hoe het materiaaloppervlak er topologisch uitziet. Wanneer we dit weten, kunnen we de mate van oppervlakte modificatie reguleren en zodanig de gewenste functionaliteit aan het biomateriaal toegevoegen. Op deze manier hopen we intelligente materialen te ontwikkelen die gedecoreerd zijn met de juiste biologische functionaliteiten om zo in het lichaam de regeneratie van het weefsel op de plek van implantatie te sturen. Om de regeneratie te controleren is het belangrijk dat het materiaal adaptief en dynamisch is en in de tijd zal degraderen, zodat het regeneratie proces door het lichaam zelf wordt overgenomen. Een interresante klasse van materialen die hier uitermate geschikt voor is, zijn supramoleculaire polymeren materialen. Deze materialen zijn samengesteld uit macromeren en oligomeren die via specifieke, niet-covalente interacties bij elkaar gehouden worden. Supramoleculaire materialen worden gezien als geschikte analogen om aan de voorwaarden te voldoen om op een synthetische manier de biologische omgeving na te bootsen, vanwege hun dynamische en adaptieve materiaaleigenschappen. Zo kunnen we intelligente plastics ontwerpen die het lichaam aansturen om zichzelf te regenereren.

Supramoleculaire materialen welke gebaseerd zijn op het viervoudige waterstof brug vormende ureidopyrimidinone (UPy) motief worden in onze onderzoeksgroep ontwikkeld en onderzocht. Wanneer de uiteindes van polymeren ketens gefunctionaliseerd worden met een UPy-motief, kunnen supramoleculaire thermoplastische elastomeer materialen gesynthetiseerd worden met unieke materiaaleigenschappen. In de ontwikkeling van nieuwe generatie supramoleculaire biomaterialen is het van belang dat zowel het oppervlak als ook de bulk compositie van het materiaal bestudeerd wordt. Daarnaast is het belangrijk om nieuwe strategieën te onderzoeken om functionaliteit te introduceren in deze materialen.

Het werk dat beschreven wordt in dit proefschrift maakt gebruik van UPy-gefunctionaliseerd poly(caprolactone) (PCLdiUPy) supramoleculaire polymeren als het basis materiaal. Verschillende strategieën die de materiaalverwerking en de oppervlakte modificatie ontkoppelen zijn geëxploreerd via de incorporatie van verschillende UPy-gefunctionaliseerde additieven. Deze verschillende UPy-additieven zijn systematisch onderzocht en hebben ertoe geleid dat er in toenemende mate controle over de oppervlakte functionalisatie verkregen kon worden.

De eerste strategie is gebaseerd op de modulaire incorporatie van UPy-gemodificeerde peptiden, die ervoor zorgen dat het materiaal bioactief wordt. In een tweede benadering, is

Supramoleculaire systemen gebaseerd op UPy-gemodificeerde additieven

UPy-peptide	Heparine chemie	Cucurbit[8]uril	Click chemie
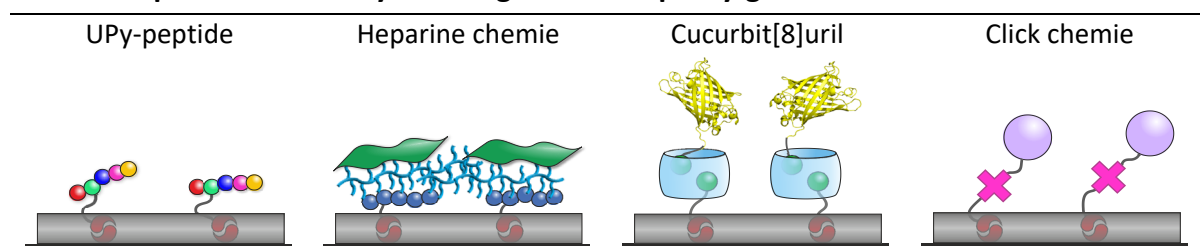
gebruik gemaakt van specifieke electrostatische interacties via heparine chemie. Hierbij is een UPy-heparine bindend peptide (UPy-HBP) additief toegevoegd aan het materiaal, waarna heparine aan het materiaal oppervlak kan binden. Vervolgens kunnen groeifactoren die eenheparine bindend domein bevatten worden geïntroduceerd middels binding aan het oppervlakte gebonden heparine. In een derde, volledig supramoleculaire strategie, gebaseerd op cucurbit[8]uril (Q8) gastheer-gast chemie is een UPy-additieve ingemengd waarbij een N-terminaal phenylalanine-glycine-glycine-lysine (FGGK) peptide als specifiek herkenningsmotief voor de Q8 aanwezig is, FGGK(UPy). De vorming van een ternair complex gebaseerd op Q8 met twee FGG motieven faciliteert in het functionaliseren van het oppervlak op een supramoleculaire wijze. Deze strategie onderschrijft de specifieke functionalisatie van het oppervlak als gevolg van het dynamische karakter van het gastheer-gast complex, waarbij de supramoleculaire assemblage reversibel aan het materiaaloppervlak gevormd kan worden. Tot slot is irreversibele oppervlakte modificatie bewerktstelligd door middel van covalente modificatie van een UPy-additief met een reactieve tetrazine groep (UPy-Tz). Een cycloadditie door middel van een click reactie van de UPy-Tz met ofwel een *tans*-cyclooocteen (TCO) of bicyclononyn (BCN) gemodificeerde bioactieve moleculen maakte het mogelijk het materiaaloppervlak zeer selectief en efficiënt te functionaliseren. Zowel kleine moleculen als ook eiwitten en polymeren coatings zijn succesvol geïntroduceerd aan het materiaaloppervlak met deze strategie.

Samenvattend, in dit proefschrift worden verschillende methodes onderzocht om supramoleculaire polymeer materialen te modificeren. Aan de hand van zorgvuldig ontworpen en gesynthetiseerde UPy-gemodificeerde additieven, die op modulaire wijze kunnen worden geïncorporeerd, is er een platform ontwikkeld waarbij de mate van controle van de modificatie systematisch onderzocht kon worden. Het werk dat hier wordt gepresenteerd opent nieuwe deuren in het ontwikkelen van op UPy-gebaseerde supramoleculaire biomaterialen die uiteindelijk hun toepassing vinden in de regeneratieve geneeskunde, *en route* om de complexiteit van de natuur tegemoet te gaan.

Curriculum Vitae

Olga Goor werd geboren op 22 december 1986 te Geleen. Na het behalen van haar gymnasiumdiploma aan de Trevianum Scholengemeenschap te Sittard (2005) begon zij aan haar studie Technische Bedrijfskunde aan de Technische Universiteit Eindhoven (TU/e). Na twee jaar vervolgde ze haar academische opleiding aan de faculteit Biomedische Technologie. Tijdens haar bachelor heeft ze in 2010 onderzoek gedaan in de groep van prof. dr. Songi Han aan de University of California in Santa Barbara (UCSB) in de Verenigde Staten. Hier heeft ze gewerkt aan het kwantificeren van moleculair transport over liposomale bilagen middels Overhauser Dynamic Nuclear Polarisation (*O*-DNP). Tijdens haar afstudeerstage in de groep van prof. dr. E.W. Meijer onder begeleiding van dr. dr. P.Y.W. Dankers en dr. ir. M.M.C. Bastings onderzocht ze de mogelijkheid meerstapse niet-covalente synthese te gebruiken om supramoleculaire gastheer-gast systemen te assembleren. Ze vervolgde haar opleiding bij het International Institute for Nanotechnology (IIN) onder begeleiding van prof. dr. Chad A. Mirkin aan Northwestern University in Chicago in de VS. Hier deed ze onderzoek naar de sequentie-specifieke cellulaire opname van sferische nucleïne zuur gebaseerde nanodeeltjes. In juni 2013 startte ze haar promotieonderzoek binnen het Instituut voor Complexe Moleculaire Systemen (ICMS) aan de TU/e. Onder begeleiding van prof. dr. E.W. Meijer en dr. dr. P.Y.W. Dankers deed zij onderzoek naar het functionaliseren van oppervlakten van supramoleculaire materialen voor toepassingen in de regeneratieve geneeskunde. De belangrijkste resultaten van dit promotieonderzoek staan beschreven in dit proefschrift.

Olga Goor was born December 22nd, 1986 in Geleen (the Netherlands). After finishing her gymnasium (pre-university) degree at the Trevianum Scholengemeenschap in Sittard (2005), she started her university education at the Eindhoven University of Technology (TU/e) in Industrial Engineering and Management Science. After two years, she continued her education at the de Biomedical Engineering department. The bachelors program included an international research internship in 2010 at the University of California in Santa Barbara (UCSB) in the United States. She investigated quantitative analysis of molecular transport across liposomal bilayers by Overhauser Dynamic Nuclear Polarization (*O*-DNP) in the group of prof. dr. Songi Han. In her master thesis in the group of prof. dr. E.W. Meijer under supervision of dr. dr. P.Y.W. Dankers and dr. M.M.C. Bastings, she investigated multistep non-covalent synthesis in order to develop supramolecular host-guest assemblies. During an internship at the International Institute for Nanotechnology (IIN) at Northwestern University in Chicago, United States, she worked under supervision of prof. dr. Chad A. Mirkin. The research involved investigation of the sequence-specific uptake of spherical nucleic acid nanoparticle conjugates. In June 2013 she started her PhD project at the Institute for Complex Molecular Systems (ICMS) at the TU/e. Supervised by prof. dr. E.W. Meijer and dr. dr. P.Y.W. Dankers, she investigated functionalization strategies to modify supramolecular biomaterial surfaces for regenerative medicine applications. The most important findings of this research are presented in this dissertation.

List of publications

Scientific Journals

José Augusto Berrocal, Joan Teyssandier, Olga J.G.M.Goor, Steven De Feyter, E.W. Meijer, Architectures with tunable Hydrophobicity from the Self-Assembly of Oligodimethylsiloxane-Based Block Molecules on Graphite, *manuscript in preparation (Nature Nanotechnology)*, **2017**.

Valentina Bonito, Anthal I.P.M. Smits, Olga J.G.M.Goor, Tijmen J.A.G. Munker, Anita Driessen-Mol, Tonny W. Bosman, Patricia Y.W. Dankers, Carlijn V.C. Bouten, Heparin-based IL-4 Functionalization of Supramolecular Materials for Immunomodulatory Purposes, *manuscript in preparation (Acta Biomaterialia)*, **2017**.

Olga J.G.M. Goor, Simone I.S. Hendrikse, Patricia Y.W. Dankers, E.W. Meijer, From Supramolecular Polymers to Multi-Component Biomaterials, *Chem. Soc. Rev. (manuscript under review)*, **2017**.

Olga J.G.M. Goor, Ralph P.G. Bosmans, Luc Brunsveld, Patricia Y.W. Dankers, Cucurbituril-Mediated Immobilization of Fluorescent Proteins on Supramolecular Biomaterials, *J. Polym. Sci. Part A: Polym. Chem.*, **2017**, DOI: 10.1002/pola.28743.

Olga J.G.M. Goor, Joyce E.P. Brouns, Patricia Y.W. Dankers, Introduction of Anti-Fouling Coatings at the Surface of Supramolecular Elastomeric Materials via Post-Modification of Reactive Supramolecular Additives, *Polym. Chem.*, **2017**, DOI: 10.1039/C7PY00801E.

Olga J.G.M. Goor, Henk M. Keizer, Anne L. Bruinen, Moniek G.J. Schmitz, Ron M. Versteegen, Henk M. Janssen, Ron M.A. Heeren, Patricia Y.W. Dankers, Efficient Functionalization of Additives at Supramolecular Material Surfaces, *Adv. Mater.*, 29, 1604652, **2017**.

Maria S. Cabrera, Bart Sanders, Olga J.G.M. Goor, Anita Driessen-Mol, Cees W.J. Oomens, F.P.T. Baaijens, Computationally Designed 3D Printed Self-Expandable Polymer Stents with Biodegradation Capacity for Minimally-Invasive Heart Valve Transplantation: A Proof-of-Concept Study, *3D Printing and Additive Manufacturing,* 4, 19-29, **2017**.

Olga J.G.M. Goor, Patricia Y.W. Dankers, Advances in the Development of Supramolecular Polymeric Biomaterials, in Comprehensive Supramolecular Chemistry II, (ed. Atwood, J.L), 255-282, Elsevier, **2017**.

Gerardus M. Bögels, Jody A.M. Lugger, Olga J.G.M. Goor, Rint P. Sijbesma, Size-Selective Binding of Sodium and Potassium Ions in Nanoporous Thin Films of Polymerized Liquid Crystals, *Adv. Funct. Mater.*, 26, 8023-8030, **2016**.

Isja de Feijter[*], Olga J.G.M. Goor[*], Simone I.S. Hendrikse, Marta Comellas-Aragonès, Serge H.M. Söntjens, Sabrina Zaccaria, Peter P.K.H. Fransen, Joris W. Peeters, Lech-Gustav Milroy, Patricia Y.W. Dankers, Solid-Phase-Based Synthesis of Ureidopyrimidinone-Peptide Conjugates for Supramolecular Biomaterials, *Synlett.*, 26, 2707-2713, **2015**.

[*] These authors contributed equally

Suguna P. Narayan, Chung Hang J. Choi, Liangliang Hao, Colin M. Calabrese, Evelyn Auyeung, Chuan Zhang, Olga J.G.M. Goor, Chad A. Mirkin, The Sequence-Specific Cellular Uptake of Spherical Nucleic Acid Nanoparticle Conjugates, *Small*, 11, 4173-4182, **2015**.

Chi-Yuan Cheng, Olga J.G.M. Goor, Songi Han, Quantitative Analysis of Molecular Transport across Liposomal Bilayer by J-Mediated ^{13}C Overhauser Dynamic Nuclear Polarization, *Anal. Chem.*, 84, 8936-8940, **2012**.

Patent

Olga J.G.M. Goor, Henk M. Keizer, Henk M. Janssen, Patricia Y.W. Dankers, Post-Functionalization of Supramolecular Materials, Filing Date May 15 2017, PCT application number PCT/EP2017/061593, **2017**.

Dankwoord / Acknowledgements

Het is zover, mijn proefschrift is af en hiermee komt een hele mooie, leerzame en waardevolle promotieperiode tot een einde. In deze laatste pagina's wil ik graag terugblikken op deze periode en mijn dank uitspreken aan allen die de afgelopen vier jaar een bijdrage hebben geleverd aan het succesvol tot stand komen van dit proefschrift, promoveren doe je immers niet alleen.

Allereerst wil ik graag mijn promotor prof.dr. E.W. Meijer bedanken. Bert, ik heb ontzettend veel bewondering voor de gepassioneerde wijze waarop jij wetenschap op het hoogste niveau beoefent. Daarbij wordt persoonlijke ontwikkeling en het welbevinden van de mensen in de groep nooit uit het oog verloren. Ik ben dankbaar voor de vele mogelijkheden die je me hebt geboden om mezelf te ontwikkelen, van wetenschapsbeoefening als Spinoza student tot een onvergetelijke stage in Santa Barbara en een heel uitdagend verblijf in Chicago in de groep van prof. Chad Mirkin. Daarnaast waardeer ik ook jouw support vanaf de zijlijn tijdens mijn promotie traject, de juiste zetjes in de juiste richting op het juiste moment, veel dank daarvoor. Ik beschouw het als een voorrecht dat ik binnen het FMS nog nauw met jou mag samenwerken, bedankt voor deze mogelijkheid als volgende stap in mijn carrière.

Mijn copromotor, dr.dr. Patricia Dankers wil ik bedanken voor de de onmisbare bijdragen gedurende mijn promotietraject. Patricia, het proefschrift zoals het hier voor ons ligt is het resultaat van een ontzettend fijne samenwerking welke al heel wat jaren geleden begon. Jouw gedrevenheid in de wetenschap en het vermogen elk tegenvallend resultaat een positieve draai te geven werkt aanstekelijk en opbeurend. Ons beider enthousiasme voor UPy-biomaterialen en het fanatisme om mooie resultaten te behalen heeft geresulteerd in een aantal mooie papers. Bedankt voor het vertrouwen, ik ben blij dat ik veel van je heb mogen leren de afgelopen jaren. Na onze vele nachtelijke emailsessies klonken optimistische quotes als 'dat lukt wel, want ik heb dan ook nog een nacht' jou heel herkenbaar in de oren. Ook de niet-wetenschappelijke discussies over allerlei zaken zoals de laatste fashion trends (hoofdzakelijk schoenen) of een goed verhaal onder het genot van een drankje vond ik altijd erg gezellig. Met de resultaten die hier beschreven staan zijn UPy-biomaterialen nu echt '*en route* to meet nature's complexity'. Patricia, heel hartelijk dank voor de ontzettend fijne tijd in jouw groep, ik wens je alle goeds voor de toekomst, zowel op wetenschappelijk gebied, maar zeker ook samen met Igor, Arthur en Rembrand, jouw mannen.

Graag wil ik ook de leden van mijn promotiecommissie bedanken voor hun deelname in mijn commissie en het kritisch beoordelen van mijn werk. Prof.dr Carlijn Bouten, hartelijk dank hiervoor. Carlijn, tijdens mijn promotie hebben we niet heel nauw samengewerkt, maar ik kan me prettige meetings en een leuk congres op Kos nog goed herinneren. Ik kijk uit naar een hele fijne samenwerking binnen het MDR zwaartekracht programma. Prof.dr. Bart Jan Ravoo, hartelijk dank voor uw deelname aan mijn promotiecommissie en het kritisch lezen van het proefschrift. Leuk dat ik afgelopen voorjaar op de ACS in San Francisco al kennis met u heb mogen maken. Prof.dr. Ron Heeren, hartelijk dank voor de samenwerking tijdens mijn promotieperiode en uw deelname aan de promotiecommissie. Mede dankzij de state of the art apparatuur in Maastricht hebben de resultaten van hoofdstuk 5 tot een mooie

gezamenlijke publicatie geleid. Prof.dr.ir. Jan van Hest en prof.dr. Pamela Habibović, dank voor het lezen van mijn proefschrift en uw deelname aan de promotiecommissie.

Graag wil ik iedereen binnen SMO en ICMS bedanken voor de prettige werksfeer. Dr. Anja Palmans, dr. Ilja Voets, prof. Luc Brunsveld, dr. Lech Milroy, dr. Christian Ottmann, prof. Maarten Merkx, prof. Rint Sijbesma, dr. Hans Heuts, prof. René Janssen, dr. Martijn Wienk, dr. Stefan Meskers, dr. Tom de Greef, dr. Marcel van Genderen, hartelijk dank voor het delen van expertise en de wetenschappelijke discussies.

Een werkdag begon pas echt na een straf kopje koffie, Henk hartelijk dank voor de goede zorgen en de hulp bij allerlei zaken. Van fietsreparaties tot het versturen van pakketjes en het custom fit maken van UV-spectrometer houder, jij denkt altijd in oplossingen en bent altijd bereid te helpen. Zonder de support van Nora, Joke, Margot, Marjo, Martina, Cindy, Wendy en Carla zouden veel dingen niet zo soepeltjes verlopen binnen SMO en ICMS, hartelijk dank voor jullie ondersteuning. Sagitta Peters, dank voor de workshops en cursussen die je voor ICMS georganiseerd hebt. Heel erg veel succes met alle nieuwe uitdagingen. Hans Damen, zonder jouw hulp bij het doen van bestellingen en het traceren van pakketjes zat ik nu nog te wachten op sommige compounds. Hartelijk dank voor het meedenken en het verzorgen van alle logistieke orders. Graag wil ik ook het analytische team bedanken voor de hulp op het lab, het uitvoeren van experimenten of het meten van samples. Ralf Bovee, bedankt voor de MALDI-ToF MS metingen en de leuke limburgse conversaties. Xiawen Lou, thanks a lot for all the help regarding GPC measurements and surface MALDI-ToF MS experiments. Joost van Dongen, ik herinner me veel nuttige maar ook soms flauwe discussies aangaande analytische technieken, maar ook iets minder werk gerelateerde gekheid. Fijn dat je altijd bereid bent om mee te denken en te helpen of een goede suggestie hebt wanneer iets onmogelijk lijkt. Voor allerlei zaken in en rondom het lab, maar zeker ook daarbuiten, wil ik Jolanda Spiering hartelijk bedanken. Jolanda, ik mag altijd langs komen met de bekende woorden 'ik heb even een vraagje' en meestal is het probleem dan snel opgelost. Van het nemen van een NMR tot een raadzaam advies, jouw deur (lab) staat altijd open, veel dank en laten we snel weer een lunch of etentje plannen.

Zonder de synthese van een heel aantal moleculen waren veel experimenten niet mogelijk geweest. Hiervoor wil ik iedereen binnen SyMO-Chem, met name Henk Janssen, Henk Keizer, Ron Versteegen en Serge Söntjens heel hartelijk bedanken. Ook veel dank voor de waardevolle discussies en suggesties omtrent de resultaten, de input voor vervolg experimenten en het kritisch lezen van de manuscripten.

Koen Pieterse en Ricky Cornish, ICMS animatie studio toppers, jullie hebben vele mooie cartoons gemaakt gedurende mijn promotietijd, inclusief de mooie cover, heel veel dank. Helaas hebben de unicorns en de regenbogen het niet gehaald, maar wie weet wat er nog in het verschiet ligt.

Tijdens mijn promotieperiode heb ik het voorrecht gehad met veel mensen samen te werken en ik wil iedereen hiervoor hartelijk danken. Anne Bruinen en Gert ten Eijkel, Maastricht University, bedankt voor de fijne samenwerking en een kijkje in de wondere wereld van de massa spectrometrie. Remco Lancee en Tiny Verhoeven, fijn dat ik altijd weer

XPS metingen met jullie mocht doen. Isja, wat begon als een goed idee bleek enorm veel werk, maar we hebben uiteindelijk een mooi paper in SynLett gepubliceerd! Berry, leuk dat ons QCM-D hoogstandje heeft bijgedragen aan een mooi paper. Simone, bedankt voor de fijne samenwerking en natuurlijk gezelligheid in Montreal. Sjors, schandalig dat we niet mee mochten op die vlucht vanuit Brussel! José, it was a pleasure to contribute to your beautiful paper. Valentina, all the best in finishing your PhD thesis, I hope your beautiful paper will be accepted soon. Bas van Genabeek en Mathijs Mabesoone, bedankt voor de UV-Vis tips en tricks en problem solving. Vele discussies, gezelligheid, uit de hand lopende kerstborrels of een welverdiende dosis onzin horen ook bij een prettige werksfeer; Tristan, Tonny, Janus, Gijs, Marcin, René, Simone H, Tim, Chidambar, Balu, Ghislaine, Beatrice, Sabrina, José, Nic, Bram T, Daan, Müge, Lorenzo, Luuk, Isja, Antonio, Neus, Roma, Anneloes, Björne, Bram P, Mellany, Peter-Paul, Geert, Hans, Fallon, Eveline, Samaneh, Jody, Marcos, Sebastian, Seppe, Marcel, Jurgen, Lidia, Brian, Thuur, Sjors, Wouter, Eline, Richard, Loes, Maarten, Martijn, Simone W, Ellen, Lenny, Lenne, Røy, Sam, Bas, Eva, Anniek, Remco, Jeroen, Pim, and many more, thanks a lot. Chan Vinh een speciaal woord voor jou, ik heb diep respect voor de manier waarop je met je ziekte omgaat. Je onverminderde interesse in hoe het met anderen gaat bewonder ik enorm, bedankt.

Gedurende mijn promotietijd heb ik het voorrecht gehad een heel aantal studenten te mogen begeleiden, Rudie, Eline, Tijmen, Jeroen, Frank, Jan Paul, Alex, Daniek en Boris, leuk dat ik met jullie mocht samenwerken en veel succes met het afronden van jullie opleiding, promotie en in jullie verdere loopbaan. Een speciaal woord van dank voor Moniek en Joyce, jullie werk heeft bijgedragen aan twee mooie publicaties en ik wil jullie dan ook hartelijk bedanken voor jullie inzet en de prettige samenwerking. Leuk om te zien dat jullie allebei als promovenda onderzoek gaan doen in de groep van Patricia, heel veel succes dames!

Pauline, Jessica and Xiao, office mates from STO 3.49, thanks for the help when I first started my PhD and all the best for your future careers. Kantoorgenoten van STO 3.27, Peggy, Björne, Stijn, Rens en Daan, hartelijk dank voor de fijne werksfeer en de gezelligheid op kantoor. Een serieus gesprek, een af en toe dichtknallende deur, een peptalk na (weer) een mislukt experiment, hilarische momentjes en ook een schouderklopje waar nodig, bedankt allemaal. Heel veel succes in jullie verdere loopbaan en veel gezondheid en geluk gewenst!

I would also like to thank all the members from the Dankers group, for all the fruitful discussions during the meetings as well as the nice atmosphere during the social events. Geert, Mellany, Björne, Bram, Sabrina, Maxime, Maarten, Peter-Paul, Sergio, Matilde, Bastiaan, Ronald, Giulia, Jiankang, Dan Jing, Renee and Moniek, all the best for your future careers.

Ook een woord van dank voor mijn paranimfen, Anniek en Maarten. Allereerst hartstikke leuk dat jullie me willen bijstaan, zeker gezien de tight scheduldes omtrent de afronding van jullie eigen promoties, heel veel dank! Anniek, je bent inmiddels al vier jaar lang the girl next door in STO 3.28 (en inmiddels ook op de 13^e in Hartje NY) en ik kom nog altijd met veel plezier jullie kantoor even binnen vallen voor een bijklets momentje, een goede dosis gossip, een (bescheiden) klaagzang over het serieuzere promotiewerk of gewoon voor de gezelligheid. Ik

bewonder je positieve instelling en je altijd enthousiaste en vrolijke humeur. Succes met de afronding van jouw promotie in december. Ik wens je samen met Ronald (Ronnieponnie) alle goeds en heel veel geluk! Maarten, Dankerslab buddy, PhD buddy, Helix buddy, Sambuca buddy, Tequila buddy, borrel en speciaalbier buddy. Of je er nou wel of niet op zit te wachten, na elke mislukking, euforisch moment, irritatie, stomme actie, onverwacht resultaat of voor een goed advies storm ik even jouw kantoor binnen. Mooi dat ik altijd even bij je terecht kan en fijn dat je me af en toe even een schop onder mijn kont geeft of me gewoon even uitlacht. Veel succes met de afronding van jouw promotie, ik weet zeker dat je onverstoorbaar naar de eindstreep toewerkt. Voor de toekomst veel geluk samen met Mila!

Marta, I would like to devote a special word of thanks to you as well. It has been a great pleasure working with you and I am looking forward to keep in touch after you leave the FMS. I wish you all the best in your next career step at the Innovation Space and lots of happiness in your personal life together with Erik and Ainara.

De beginjaren van mijn promotie werden aangenaam door het wonen op FFP 116, Daan en Stefan wat heb ik af en toe hoofdpijn gehad op dinsdag, na een 'goeie-ideeën-maandag' maar wat was dat altijd gezellig. Stefan, bedankt voor de het klussen, het koken, de gezelligheid, de fijne gesprekken, het gekibbel over poetsen maar bovenal de mooi tijd samen in hartje Rio. Succes met de laatste loodjes van jouw promotietraject. Daan, grappig dat ik exact een jaar na jou aan mijn promotie begon en exact ook een jaar later op 19 september mijn verdediging gepland staat, goed voorbeeld doet goed volgen ;). Bedankt voor de vele fijne discussies aan het keukenblok, van wetenschap tot drankgerelateerde aangelegenheden. Ik wens je veel succes in je carrière en veel geluk samen met Line.

Voor een serieus, maar vaker nog een minder serieus avondje of weekendje plezier zijn er 'Die Kölscher Kinder', Anniek, Bas, Bjorn, Chantine, Enitia, Marijke, Marloes, Nils, Robbin, Ruben, Stefan, Willeke en Wilma, bedankt voor de gezelligheid en ik ben benieuwd naar het volgende weekende in november!

Als de koers aan is, dan bij voorkeur natuurlijk op de schaats of op de fiets, Theo, Bram, Rico en Eva, Nard en Floor, Gerwin, Wouter, Gerwin, Rik en Eva, bedankt voor al het kopwerk! Ook heb ik met ontzettend veel plezier vele schaats-, loop- en spinninglessen verzorgd in de afgelopen jaren. De B$^+$-selectie van ESSV Isis, elke donderdagavond opnieuw is het weer een mooi festijn op de ijsbaan. Leuk om te zien dat mijn enthousiasme aanslaat en dat de trainingen goed ontvangen worden. Tot in oktober op het ijs! In de categorie we gaan maximaal aan is het spinning theater op het SSCE op de dinsdagavond altijd het toneel van veel gezweet. Ontzettend leuk dat de ESWV Squadra spinning squad wekelijk netjes aansluit, ondanks dat jullie buiten fietsen natuurlijk veel leuker vinden. De SMO-cycling pro's, Bas, Anniek, Ronald, Pim, Remco, Joyce, Sam, Eline, Loes, Anneloes, Lenne, Ardjan, Gijs, Peter-Paul, fantastisch dat jullie altijd present zijn. Wat als een klein geintje begon, werd elke dinsdag serieus zweten. De beweegreden om trouw te komen is mij nog steeds niet geheel duidelijk, gaat het om het spinnen zelf, wellicht een beetje uit medelijden voor mij, of toch vanwege die ontzettend lekkere biertjes achteraf, ik weet het niet, maar ik vind het in ieder geval tof dat jullie er altijd bij waren. Binnenkort beginnen we weer.. ;)!

In en rondom het lab, sportief of met een glaasje in de hand, gelukkig was er ook vaak tijd voor gezelligheid. Anne en Gijs, bedankt voor gezelligheid in en rondom Tilburg. Bram en Michelle, ontzettend gaaf dat jullie zo'n mooie reis aan het maken zijn, van afstand blijf ik op de hoogte. Ik wens jullie nog een hele mooie tijd en tot snel zodra jullie weer in het land zijn. Brian en Anouk, Thuur en Karin, hopelijk staat de volgende date snel weer op de planning. De Venloup 2018 vindt plaats op 25 maart, ik zet hem alvast in de agenda, we zien elkaar bij de start! Nick en Sanne, Jos en Sylvia, Ken en Rianne, Bart en Ilona, Danny en Chantal, Bart en Anita, Anne en Vital, Joan en Mariëlle, Wim en Kristel, Rob en Riny, Sebastiaan en Jody, bedankt voor alle gezelligheid en de vele feestjes. Ilona en ik gaan iets moois van vriendendag 2018 maken! Ruben ('Koos'), sinds onze reis naar China zijn wij een komisch duo in 'Koos-en-Toos' formatie. Wat betreft humor en sterke verhalen zit het altijd wel goed en bij menig anekdote lig ik nu nog vaak hardop in een deuk. Ook voor serieuze aangelegenheden kan ik altijd bij jou terecht, bedankt daarvoor. Heel veel succes bij het afronden van jouw promotie, en veer zeen os gauw weer! Laura en Gaston, Bjel en Johan, Veerle en Ron, Fleur en Bart-Jan, Nina en Joep, Rieky en Luca, bedankt voor jullie betrokkenheid en vriendschap. De vele gezellige avondjes, weekendjes, feestjes, activeiten en dates zijn genieten, dat er daar nog velen van mogen volgen!

Ook een woord van dank voor mijn familie, Magda en Ger, Roger, Ruben en Stella, Frans en Lilian, Cato en Denis, Ben en Marijke, Susan en Rick, Manon en Michiel. Bedankt voor jullie welgemeende interesse en betrokkenheid in de dingen die ik doe. Oma, helaas kan ik u dit boekje niet meer overhandigen, maar ik weet zeker dat u ontzettend trots geweest zou zijn.

Wat is het altijd fijn om naar Hunsel af te reizen, Marga en Jan bedankt voor jullie hartelijkheid en interesse, ik voel me altijd onzettend welkom. Martijn en Jorn, door de hoop onzin en ongein is het altijd gezellig met jullie. Ik wens jullie alle goeds, in jullie carrière maar vooral natuurlijk in de liefde.

Papa en mama, niet in de minste plaats wil ik hier ook jullie bedanken, want jullie staan me altijd met raad en daad bij en hebben me altijd alle mogelijkheden geboden om mezelf te ontwikkelen. Jullie zijn er altijd en onvoorwaardelijk voor me, bedankt. Dankzij jullie ben ik geworden wie ik nu ben. Colette, wat ben ik trots op mijn kleine zus, een fantastisch mens en zo ontzettend fijn dat jij er altijd voor me bent. Aan één woord hebben we genoeg, je bent mijn maatje. Samen met Rik vorm je een superkoppel en ik wens jullie heel erg veel geluk toe voor de toekomst, op naar jullie bruiloft!

Ralph, de laatste woorden zijn voor jou, want het allermooiste wat me tijdens mijn promotieperiode overkomen is ben jij. Met alles kan ik bij jou terecht, en bij jou kan ik helemaal mezelf zijn. Bedankt voor je support en dat je er voor me bent, altijd. Ik kijk uit naar een hele mooie toekomst samen met jou!

Olga